A STUDY OF THE FLOW PROPERTIES AND
PROCESSABILITY OF THERMOPLASTIC POLYESTERS

by

FREDERICK HENRY AXTELL

A Doctoral Thesis

Submitted in partial fulfilment of the requirements
for the award of Doctor of Philosophy of the
Loughborough University of Technology, December 1987.

ACKNOWLEDGEMENTS

ABSTRACT

A Study Of The Flow Properties and Processability Of Thermoplastic Polyesters

Poly(ethylene terephthalate) (PET) has recently gained vast new markets through its ability to be biaxially oriented and/or crystallised rapidly, by 'novel' processing techniques. This investigation aims to provide information enabling theories on these processes to be further developed.

Conventional capillary rheometry has been used to obtain shear flow data on a wide variety of polymers based on PET. The elongational flow characteristics have been derived from two techniques: the first based on the converging flow method developed by Cogswell; and the second based on the Rutherford Elongational Rheometer. Data from these different techniques have been compared and viewed in the context of three industrial processes.

The rheological results showed that the polymers were pseudoplastic in shear and tension thinning in converging flow. Complete shear flow master curves were constructed using a temperature and molecular weight superposition scheme.

The Rutherford Elongational Rheometer was modified to work at temperatures up to 285°C. Although it was not possible to characterise the melt behaviour of PET, the instrument was used to study the viscoelastic behaviour of amorphous PET in the 'rubbery' region. This yielded information on the elongational stress growth function, stress relaxation and strain recovery. PET is tension thinning with respect to elongation rate. The stress growth-time data departs from linear viscoelastic behaviour at a critical strain and strain-induced crystallisation occurs at a higher critical strain, which was relatively independent of temperature and elongation rate.

iii

PETG Copolyester was characterised using the Rutherford Elongational Rheometer. The time-dependent stress growth behaviour obeys the rubber-like network theory up to a critical elongation rate at 110°C and shows tension stiffening behaviour at 170°C, this was opposite to the response found in converging flow.

Practical moulding trials were undertaken to verify the predicted rheological behaviour generated by a computer-aided injection moulding model. The effects of injection rate, mould temperature and polymer melt temperature on cavity pressure/hydraulic pressure have been explored. The simulated model showed good agreement with experimental results for the total pressure drop during mould filling and its dependence on temperature and molecular weight. In contrast, however, it is shown that limitations on predicting cooling times are due to the models reliance on the thermal properties of fast-crystallising PET which are different to those for the amorphous PET polymers studied.

The rheological properties were compared with processing performance in extrusion blow moulding. Good agreement was found between the simulative models for parison sag, and experimental observations.

Commensurate with predictions from free-surface uniaxial elongational flow data, practical stretch blow moulding trials showed evidence of strain hardening in the hoop direction (and increased molecular orientation) with increasing inflation pressure, resulting in higher burst and top load strengths and better control of bottle thickness.

CONTENTS

1. Introduction

1.1 Introduction

The commercial importance of polymers based upon poly(ethylene terephthalate) (PET) has increased with the advent of some relatively recent applications by processes such as injection moulding and thermoforming; specialised grades have been developed for extrusion blow moulding and a new process, injection stretch blow moulding, has been developed for manufacturing biaxially oriented PET containers. The processability of PET is a function of its ability to exist in the amorphous state but remain thermally or strain-induced crystallisable, this unusual property has previously been utilised in the established PET fibre and film applications.

Although these processes are all in use, the rheological characteristics of PET polymers relevant to many of them have only been determined in part, or have not featured equivalent modes of deformation. Currently, design and process development for novel processes has to rely on experience and trial-and-error methods. Also, the flow property approach to equipment design interacts with processing conditions, their optimisation and refinements to the polymer structure to achieve specific mechanical properties in the product. Clearly, in order to expand the technological basis upon which future process developments around PET must rest, the flow and deformation characteristics under strictly-relevant conditions (e.g. elongational flow) must be more exactly characterised.

Rheology of PET melts in shear has been studied and reported by several workers.[1,2,3,4] The data in these works form useful initiation points for further study. The effects of temperature, shear rate, inherent viscosity[1,2,3], molecular weight, shear stress[2], constant shear rate activation energy, entrance pressure drop[3] and thermal degradation[4] have been scrutinised. For example, *Baron*[5] assessed the processability of different PET polymers to avoid parison sagging in extrusion blow moulding, by considering their shear rheology (at low

strain rates). However, extrusion blow moulding (like many other processes mentioned) involves elongational flows and the relevant data has not been available due to practical difficulties in experimentation, or to the absence of directly relevant data-forms.

Cogswell[5] developed a method which determines the elongational flow component from a converging flow geometry. By assuming the elastic deformation response of the melt is finite the interpretation involves approximations similar to those accepted for interpreting simple shear viscosity from a capillary flow. The flow in a tapered die is considered as consisting of three separate components: that due to flow from the reservoir into the die; that due to telescopic shear within the die; and that due to extensional flow within the die. The die-entry pressure drop is measured and the analysis involves a trigonometric approach to determine the three separate components. This method uses a conventional capillary rheometer and provides data relevant to melt flow in injection moulds or extrusion dies. Gibson and Williamson[7,8] applied converging flow data to the injection moulding of short-fibre reinforced thermosets. However, the elongational flow properties of polymers are dependent on the geometry and type of flow, therefore, the converging flow method is not applicable to all situations within PET processes. For direct relevance, the determination of the rheological properties must be carried out in the same mode, using similar geometries to the flow present in the process of interest.

In previous studies on elongational flows at Loughborough University of Technology, Smoker[9] and Arif[10] used the Rutherford Elongational Rheometer to determine the elongational flow properties of some commodity resins. (LDPE and PVC polymers respectively.) This instrument operates using a free-surface uniaxial elongational flow geometry, which (in the context of PET) is applicable to parison sagging in extrusion blow moulding, to the inflation stage of stretch blow moulding and to thermoforming. The instrument was previously limited to a maximum working temperature of 200°C; on the basis of previous suggestions[10], machine uprating was deemed to be necessary in order to enable measurements of other polymers to be carried out

at higher temperatures.

The Rutherford Elongational Rheometer, although essentially designed to study the uniaxial flow of polymer melts, also has the potential to study polymers in the rubbery (thermoelastic) phase, which for amorphous PET, enables data relevant to the stretch blow moulding and thermoforming processes to be determined.

Some flow models of several of the processes mentioned have been derived previously, though not for application to PET. *Barrie*[1] has developed a computer simulation of injection moulding, called SIMPOL, which is based on a theory derived from observations of the non-isothermal mould flow characteristics of general purpose thermoplastics. *Garcia-Rejon et al*[2] derived a model that predicts the parison sagging and swelling of polyolefines in extrusion blow moulding by relating the parison swell and sag effects to previously determined rheological properties such as die swell, shear viscosity and elongational stress growth function. An additional objective to be studied in the programme was to extend the application of existing models to PET resins.

1.2 General Objectives Of The Research Programme

From this background of rheometric methodology and processing, this study was undertaken to determine the rheological behaviour of thermoplastic polyester polymers and to assess the suitability of the data to model several processes for future exploitation. The overall objectives of the study are shown below:

(i) Shear Flow

To characterise several different thermoplastic polyesters of varying molecular structure, (i.e. linear, branched and copolymers.) and to study the shear flow behaviour of the different polymers, thereby producing master curves with respect to structure, temperature and molecular weight.

(ii) Elongational Flow

To characterise and compare the elongational flow behaviour of different thermoplastic polyester melts by the converging flow technique and by the use of the Rutherford Elongational Rheometer. The latter technique necessitates that the Rutherford

Elongational Rheometer be uprated to permit high temperature testing to be carried out. In addition, the free-surface uniaxial elongational deformation properties of PET in the thermoelastic phase has to be exploited.

(iii) Injection Moulding

To apply the shear and converging flow rheological data to the injection moulding process and compare the processability of different polymers under various conditions; to compare computer simulated rheological data with experimental data and to evaluate computer simulated processability results under various conditions with experimentally measured results. To assess the usefulness of, and suggest refinements to enhance the accuracy of the SIMPOL computer simulation on the basis of PET injection moulding.

(iv) Blow Moulding

To investigate various phases of the extrusion blow moulding process, on the basis of the rheological data, for various polyester polymers. Also, to compare the processing characteristics and product properties of PET during stretch blow moulding with the free-surface uniaxial deformation data for PET in the thermoelastic phase. For each of these fundamentally different blow moulding techniques, practical assessment of theoretical concepts and experimental flow data was deemed necessary.

2. Rheology of PET Melts in Shear

2.1 Introduction

2.1.1 Aims Of Chapter

This chapter describes the experimental programme carried out with the objective of characterising several different thermoplastic polyesters of varying molecular structure, i.e. linear, branched and copolymers. The characterisation includes molecular weight determinations and descriptions of the shear rheological behaviour of the different polymers. The aims of the chapter were:

-   to characterise the polymers used in the study;
-   to produce flow curves for the polymers, which allow the data to be applied to process design and control;
-   to apply superposition techniques on the data to generate master curves with respect to temperature and molecular weight.

2.1.2 Shear Rheology[6,13,14]

Rheology is defined as the study of flow behaviour. It provides the basis for defining and evaluating the basic parameters required in designing and controlling plastics processing equipment and the manufacture of industrial products. Two approaches to polymer processing rheology are evident in the literature, the theoretical approach to provide a fundamental description of idealised behaviour, and the practical approach which tackles results from actual practice.

Mechanics Of Shear Flow

The geometry of deformation considered in this chapter is that of simple shear, where the stress is applied tangentially to the sheared body: (see Figure 2.1).

FIGURE 2.1: SIMPLE SHEAR[6]
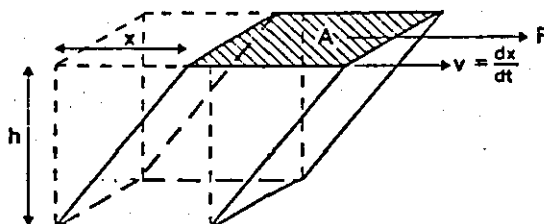
In Figure 2.1 the area A and distance h remain constant during deformation. The equations for stress, strain and rate of strain for the deformation illustrated in Figure 2.1 are shown below:

stress, $\qquad\qquad \tau = F/A$ (2.1)

strain, $\qquad\qquad \gamma = x/h$ (2.2)

rate of strain, $\dot{\gamma} = 1/h.(dx/dt) = v/h$ (2.3)

apparent viscosity, $\qquad \eta = \tau/\dot{\gamma}$ (2.4)

Thermoplastic melts are viscoelastic materials, that is, at some time they have the characteristics of both elastic solids and viscous liquids. Viscoelasticity manifests itself as: strain recovery on removal of an applied stress; stress relaxation, stress decaying with time for a constant strain; creep, deformation increasing with time under an applied load.[15]

A qualitative description of viscoelastic behaviour can be made using idealised 'models'.[13] When a stress is applied to a polymer material there is a resultant deformation (strain). The rheological equations of state relate stress, strain and time mathematically.

In a linear elastic (Hookean) material the stress in a sheared body is proportional to the amount of shear.[16] From this equation (2.5) is derived[15]

$$\tau = G.\gamma \qquad (2.5)$$

where G is the shear modulus. In a Newtonian fluid the shearing stress is proportional to the rate of shear.[16] From this equation (2.6) is derived.[15]

$$\tau = \mu.\dot{\gamma} \qquad (2.6)$$

where μ is the Newtonian viscosity. In viscoelastic materials the effects of both elasticity and viscosity are noticeable. The stress being a function of both strain and time

$$\tau = f(\gamma, t) \qquad (2.7)$$

often simplified to

$$\tau = \gamma.f(t) \qquad (2.8)$$

The mechanical analogue approach to rheology[9,15,16] applies mechanical models consisting of spring and dashpot elements to describe the behaviour. Springs representing idealised elastic behaviour (obeying equation (2.5)) and dashpots representing idealised

viscous behaviour (obeying equation (2.6)). The stress is represented by the total extending force and the strain is represented by the total extension. Spring and dashpot models are used to give a first approximation to equilibrium steady state viscoelastic behaviour such as creep, recovery and stress relaxation.

The Maxwell model (see Figure 2.2) consists of a spring and dashpot in series, whilst the Voigt model (see Figure 2.3) consists of a spring and dashpot in parallel.

FIGURE 2.2: MAXWELL MODEL[15]

RESPONSE OF MAXWELL MODEL.
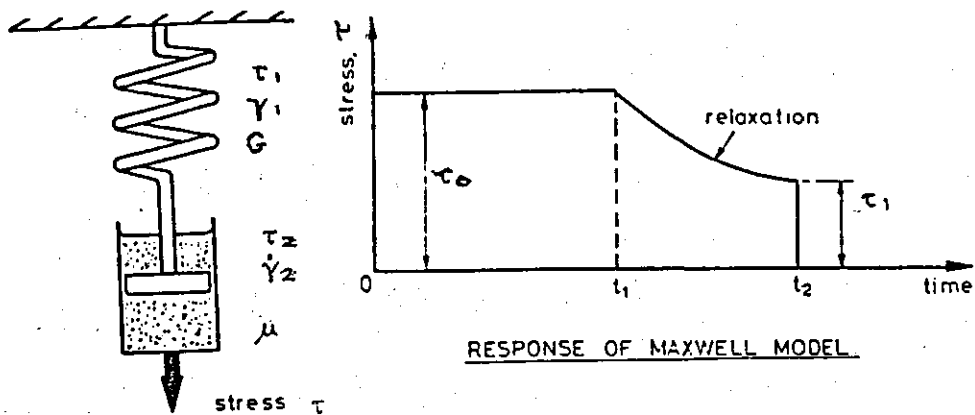
FIGURE 2.3: VOIGT MODEL[15]
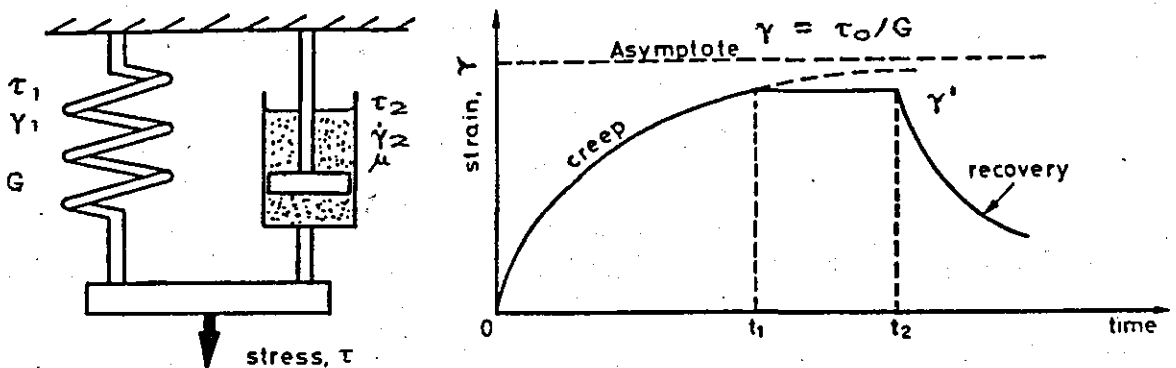
With the Maxwell model, on application of a stress an instantaneous elastic deformation occurs, followed by a Newtonian viscous deformation.[13] The response of the spring can be represented by equation (2.5) and the response of the dashpot can be represented by equation (2.6), under equilibrium conditions the stress acts

equally on both the spring and the dashpot, and the total strain is equal to the sum of the strain of the spring and the dashpot. This leads to the equation governing the Maxwell model.[15]

$$\dot{\gamma} = (1/G).\dot{t} + (1/\mu).\tau \qquad (2.9)$$

The Maxwell model gives an acceptable first approximation for stress relaxation, but not for recovery or creep.

With the Voigt model the dashpot dampens the response of the spring both when strained under an applied load and during recovery on removal of an applied stress. Under equilibrium conditions the total stress is equal to the sum of the stresses acting on spring and the dashpot, whilst the strain is equal for both the spring and the dashpot. This leads to the equation governing the Voigt model.[15]

$$\tau = G.\gamma + \mu.\dot{\gamma} \qquad (2.10)$$

The Voigt model gives an acceptable first approximation for creep and recovery, but not for stress relaxation.

As stress relaxation is of more general concern than creep during processing the Maxwell model is more commonly used. The 'Generalised Maxwell Model', consisting of a number of Maxwell elements in parallel with each other, more closely represents viscoelastic behaviour.[9] A more detailed description of this approach to representing the viscoelastic properties of polymers can be found in *Crawford*.[15]

Polymer Characteristics In Shear

Polymers behave differently to simple fluids primarily because of their long molecular chains. The molecular weight and molecular weight distribution of polymers dictate the role of molecular interactions caused by chain entanglements; the presence of entanglements leads to the non-Newtonian behaviour of polymers.

The network theory approach, based on the concept of rubber-like liquids suggested by *Lodge*[14], proposes that strong interactions between molecules, due to an entanglement network, behave as temporary cross-links formed between molecules which have some physical interaction. This model can explain many viscoelastic phenomena in terms of the long-chain network response to an externally applied deformation or stress.

- The apparent elastic behaviour over short time periods can be explained by the network. The apparent elastic behaviour is caused by deformation of the mobile areas between the temporary cross-links causing orientation of the chains, without breakage of the links that act as fixed points, on removal of the stress, the mobile areas spring back to their original random configuration between the cross-links.

- The decay of positional memory with time and permanent deformation can both be explained by the concept of the network being temporary, new entanglements forming whilst old entanglements are lost.

- Viscosity decreasing with increasing shear rate can be explained by the increase in loss of junctions at high shear rates whilst the rate of creation of new junctions is unaffected. Therefore the resistance to flow is shear rate dependent.

- The time-dependent structure behaviour of the material can be explained by the time taken to reach equilibrium of junction loss and creation.

- The influence on flow behaviour of molecular structure can be explained as the number of junctions that will be affected by the length of the individual molecules and the amount of branching.

These various approaches offer equations that do not necessarily fit the behaviour of some polymer melts, therefore it is often better to use graphical relationships such as flow curves.

Pseudoplasticity

Polymer melts are generally pseudoplastic (shear thinning) in their behaviour, the shear rate increases at a more than linear rate with an increase in shear, as shown by their flow curves. Therefore a constant coefficient of viscosity does not exist, at least not at shear rates relevant to processing, but the concept of an apparent viscosity at a given shear rate is adopted. The apparent viscosity decreases with increasing rate of shear. Exceptions to this behaviour are found with low molecular weight fluids and at low shear rates, where the behaviour tends towards that of a Newtonian fluid.

Pseudoplastic behaviour can be described by molecular

explanations such as the network model or the highly solvated molecule model.[13] The latter proposes that with an increase in shear rate the solvated layers may be sheared away resulting in decreased interaction of molecules, due to their smaller effective size and consequently, a reduction in the apparent viscosity.

The flow curve is a log-log plot of shear stress as a function of shear rate, the plots are almost linear and are derived from the Ostwald-de Waele power law equation:

$$\tau = K(\dot{\gamma})^n \qquad (2.11)$$

rewritten,
$$\dot{\gamma} = A(\tau)^v \qquad (2.12)$$

where $v = 1/n$, and $A = (1/K)^{1/n}$, therefore since $\eta = \tau/\dot{\gamma}$ from equation (2.4),

$$\eta = K(\dot{\gamma})^{n-1} \qquad (2.13)$$

$$\log(\tau) = \log(K) + n.\log(\dot{\gamma}) \qquad (2.14)$$

There are many different types of rheometer which can be used to generate the data for shear flow curves. Several reviews have been published[9,17,18] describing and comparing the different instruments. The more common rheometers can be divided into two groups: rotational rheometers and capillary rheometers. The main disadvantage of using rotational rheometers is that due to edge effects, the resultant data relate to shear rates much lower than those employed in polymer processes such as extrusion and injection moulding. The shear rates obtainable on capillary rheometers approach the practical processing values.

2.1.3 Capillary Rheometry[6,13,19,20]

2.1.3.1 Introduction

Capillary rheometry is primarily designed to measure the apparent viscosity of liquids during simple shear. The history of capillary rheometry was documented by *Philippoff and Gaskins*[19], the first experiments being those of Poiseuille in 1840. A capillary rheometer forces molten thermoplastic from a reservoir through a capillary die whilst temperature, applied force, output rate, and barrel and die dimensions are controlled and accurately measured. The rheometers either work under constant pressure (stress) or constant rate conditions.

The method is sensitive to polymer molecular weight and molecular weight distribution, polymer stability, shear instability, and the presence of even small quantities of additives. Capillary rheometry permits the measurement of melt viscosity, sensitivity and stability with respect to temperature and polymer dwell time in the rheometer, die swell ratio, and shear sensitivity when extruding under constant stress or rate. Other properties that can be estimated from capillary rheometry include viscosity in extension (see Chapter 3), modulus in shear, modulus in extension and rupture stress in tension. The data is useful for correlating with processing conditions.

The Poiseuille law for capillary flow[6,13] yields:

wall shear stress, $\qquad \tau = \Delta Pr/2L$ $\qquad\qquad$ (2.15)

apparent wall shear rate, $\hat{\gamma} = 4Q/\pi r^3$ $\qquad\qquad$ (2.16)

where ΔP is the pressure drop; Q is the volumetric flow rate; r is the capillary radius, and L is the capillary length.

The determination of the relationship between flow rate and pressure drop through the die is the aim of capillary rheometry. The pressure drop measurement should be made directly in the melt just above the die to reduce any errors due to pressure drops associated with the flow in the reservoir and frictional losses between the piston and the reservoir wall.

The equations for flow through a pipe which are used for capillary rheometry assume steady-state viscous flow. However, in the extrusion and injection moulding processes steady-state viscous flow often does not exist, there is a need to take into account the elastic response as well as the viscous response, otherwise large errors will result.[13]

Cogswell[5] stated that the measurement of orifice pressure drop is itself a useful rheological parameter. If plotted as entrance pressure drop against shear stress in fully developed flow the result is largely independent of melt temperature and molecular weight but extremely sensitive to "structural" variations such as, molecular weight distribution, chain branching, fillers, grafting, and particulate nature. The orifice pressure drop may also be used to obtain a qualitative assessment of the elongational flow rheology. (see

Chapter 3).

Measurements of post extrusion swelling can be interpreted as partially-recoverable strain[6]. By making similar assumptions to those assumed in the interpretation of viscosity from capillary flow, recoverable shear strain can be interpreted from post-extrusion swelling. Cogswell[6] reported the relationship

$$B_L{}^2 = 2/3\gamma_R [(1 + 1/\gamma_R{}^2)^{3/2} - 1/\gamma_R{}^3]$$ (2.17)

where B_L is the swelling ratio from a long die and γ_R is the recoverable shear at the die wall. A plot of this relationship is shown in Figure 2.4.

FIGURE 2.4: PLOT OF RECOVERABLE SHEAR AGAINST SWELLING RATIO[6]

Ratio of solidified extrudate to die diameter, B_L

Plot of recoverable shear against swelling ratio
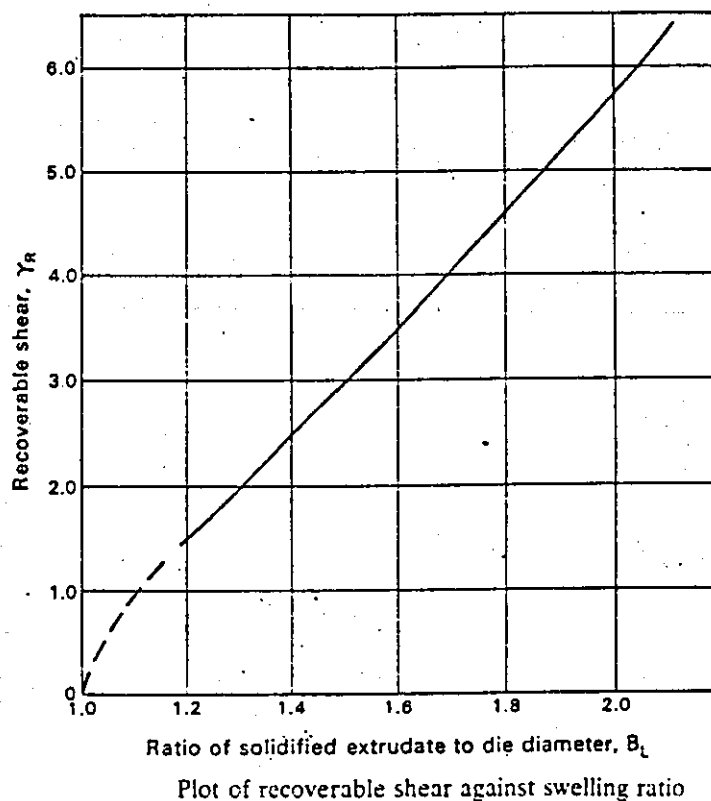
Observations of the extrudate provide information of evidence of non-laminar flow or surface imperfections. When non-laminar flow occurs the equations for deducing the rheological properties are invalid. The extrudate appearance can be used to deduce quality of flow behaviour during processing and evidence of rupture behaviour.

2.1.3.2 Assumptions, Errors And Corrections

The assumptions made in capillary rheometry are discussed by *Brydson*.[13] Most capillary rheometers assume that there is no pressure drop in the reservoir, that the pressure drop in the capillary is linear with axial distance along the capillary and that at the capillary exit the pressure drop is zero. The analysis of flow through a pipe assumes that there is no slip at the wall; that the fluid is time-independent; that the flow pattern is constant along the whole length of the tube; that the flow is isothermal; and that the melt is incompressible. These assumptions do not describe the true situation in extrusion or injection moulding, hence the data must be used bearing in mind this situation.

A capillary rheometer imitates practical flow in moulds and dies and provides an extrudate on which subjective assessments of quality can be made.[6]

The principle sources of error when measuring melt viscosity by capillary rheometry were listed by *Cogswell*[5]:

frictional losses;

ends pressure drop;

non-parabolic velocity profile;

influence of pressure on viscosity;

influence of heat generation;

influence of decompression on temperature;

modification of the material due to work in the die.

Two other shortcomings of capillary rheometry as a process simulator are the pre-heat time being longer than the residence times experienced in processing equipment and the absence of any mixing action in the rheometer compared with that occurring in processing equipment.

Cogswell[5] recommends that corrections for reservoir and frictional losses and for ends pressure drop are made. He states that the others may be larger but are mutually cancelling. Further these effects feature in most practical flows, therefore in engineering calculations they can be ignored. If the data is for comparative purposes then applying a correction will not affect the comparability.

The reservoir and frictional losses can be corrected for by positioning the transducer just above the die. The ends pressure drop correction usually applied is that derived by *Bagley*[21] who observed that at a given shear rate a plot of pressure drop versus die length to radius ratio gave a straight line with an intercept, such that the pressure gradient dP/dL should be used in calculation of the apparent shear stress in place of P/L. The pressure gradient is determined by using dies of different lengths but the same radius. *Cogswell*[5] claims that two dies are adequate, a long die (L/R $\geqslant$ 20 and $\leqslant$ 50) and an orifice die (L/R = 0), as the potential error of not using several dies does not exceed ±2%. The calculation for the Bagley corrected shear stress is shown below:

$$\tau = (\Delta P - \Delta P_o) r / 2L \qquad (2.18)$$

where ΔP is the long die pressure drop, and ΔP_o is the orifice die pressure drop.

2.1.3.3 Factors Affecting Viscosity

Kumar[22] extensively reviewed the literature for both Newtonian and non-Newtonian flows, discussing the theoretical and empirical relationships that attempt to describe the dependence of polymer melt viscosity on molecular weight, molecular weight distribution, temperature, and chain branching. He stated that the most practical utilisation is the approach towards representing the flow behaviour of polymer melts by universal master curves (incorporating molecular weight and its distribution, temperature, and shear rate). *Bowers*[23] agrees that the master curve concept overcomes the need to obtain data for viscosity at various shear rates over the range of temperatures encountered during processing.

Some of the factors affecting the viscosity of polymers are itemised below.

2.1.3.4 The Effect Of Temperature

The zero shear rate shear viscosity is reduced by increasing temperature, provided no structural changes occur. For Newtonian liquids the temperature dependence can be described by an Arrhenius-type equation:

$$\mu = A \cdot \exp(E/R \cdot T) \qquad (2.19)$$

where A is a constant, and E is the activation energy, μ is the coefficient of viscosity for any absolute temperature T. (R is the universal gas constant.)

For polymer melts an empirical relationship is often used:

$$\eta = a.\exp(-b.T) \qquad (2.20)$$

where both a and b are constants.

Williams, Landel and Ferry[24] developed a relationship, known as the WLF equation, that proposes the temperature dependence of the zero shear rate viscosity is purely a function of the melt temperature and the glass transition temperature. The WLF equation is limited in its application as it does not account for the rate dependence of polymer melt viscosity.

Mendelson[25] has reported the successful application of a superposition technique to obtain master curves for HDPE and LDPE polymers. He found that if shear rate-shear stress curves obtained at different temperatures were superimposable along the shear rate axis, then the resultant shift factors were not affected by the Rabinowitsch correction.

The method of superposition *Mendelson*[25] used involved the arbitrary choice of a reference temperature. The flow curves at various temperatures were plotted, (see Figure 2.5). The values of horizontal shift factors a_T at these temperatures were obtained by choosing two low shear rate values on the reference temperature curve and shifting the corresponding points (constant shear stress) on the other flow curves to coincide with these shear rates. The values of a_T were calculated from

$$a_T = \dot{\gamma}_{w(ref)}/\dot{\gamma}_{w(T)} \qquad (2.21)$$

and for each temperature, those corresponding to the two shear rates, were averaged to minimise errors due to reading of the graphs.

FIGURE 2.5: FLOW CURVES AFTER *GREGORY AND WATSON*[1]
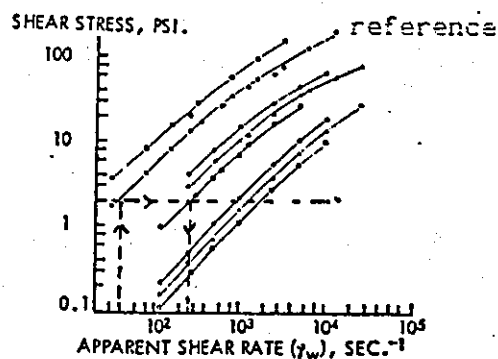
The applicability of the shift factors was confirmed by the good fit of the data at all temperatures on the constructed master flow curves at the reference temperature. The temperature dependence of the shift factors was fitted excellently over the entire temperature range by an Arrhenius-type equation

$$a_T = B.\exp(E/R.T) \qquad (2.22)$$

A linear plot of $\log a_T$ versus $1/T$ confirmed the applicability of equation (2.22). The coefficient B was a function of the reference temperature chosen, while the activation energy E was independent of the reference temperature chosen.

2.1.3.5 The Effect Of Molecular Weight

Kumar[22] reviewed the theories that attempt to describe the dependence of viscosity on molecular weight. For example, the Bueche theory which imagines the polymer molecule to be subdivided into a large number of "submolecules" each of which behaves mathematically like a small mass attached to a linear spring was reported as being not quantitatively exact.

The Graessley molecular entanglement theory[22] imagines entanglement between molecular segments, leading to increased dissipation of energy. In a shear field, as two molecules approach each other, when they are close, entanglements begin to occur at a finite rate. As they pass, disentanglement occurs. An entanglement density for the bulk material may be defined to characterise the number of entanglements which exist at any instant, averaged over the material.

For an entanglement to exist, two molecules must be within a certain distance of each other. Also, the molecules must remain close enough for a certain time or else no entanglement occurs. The greater the shear rate, the more rapidly two molecules move relative to one another. Hence, the entanglement density is reduced by high shear rate, since fewer molecules will remain close enough for a sufficiently long time at a high shear rate. The Graessley theory was reported to predict the general trend but the results do not agree closely with experimental observations.

Brydson[13] reviewed the work published which studied the effect

of molecular weight on viscosity. A common pattern of behaviour was found for linear polymers. The relationship between the zero shear rate viscosity, η_o, and the weight average molecular weight, $\bar{M}_w$, is of the form

$$\eta_o = K.\bar{M}_w{}^a \tag{2.23}$$

Up to a critical value, $\bar{M}_c$, of the molecular weight the relationship is linear, i.e. $a = 1$. Above $\bar{M}_c$, for many linear polymers, the dependence of the zero shear rate viscosity and $\bar{M}_w$ is found to be in the range 3.4-3.5. The value of the exponent is independent of temperature. The critical molecular weight value varies for different polymers. It is believed to coincide with the molecular size at which molecular entanglements begin to exert a significant effect on viscosity.

The Bueche expressions were further developed by *Allen and Fox*[26] who expressed the K term in equation (2.23) in terms of molecular features of the molecules.

2.1.3.6 The Effect Of Molecular Weight Distribution

Brydson[13] reviews the factors affecting shear viscosity and reports that a narrower molecular weight distribution will result in a greater temperature dependence of viscosity and a lower melt elasticity. In a broader distribution, the smaller molecules act as "lubricating" molecules lying between the longer molecules and keeping them apart preventing interchain entanglements along the length of two long molecules. The smaller molecules will be entangled but will require less shearing to become completely disentangled than long molecules, also the longer molecules, being held apart by the smaller ones, will be less intimately entangled.

2.1.3.7 The Effect Of Chain Branching

Reported comparisons[22] of viscosity data for branched and linear polymers of the same chemical species show that different types of behaviour can occur.

For some branched systems the zero shear rate viscosity has often been found to be lower than of the linear polymer of the same number of chain elements. The volume occupied by a molecule of a given molecular weight decreases as it becomes more highly branched

which in turn lowers the interchain entanglements, hence viscosity.

An example of this behaviour is given by comparing low-density and high-density polyethylene molecules of similar weight. The linear polymer (HDPE) is more extended and able to entangle than the more compact branched material (LDPE).[13]

For similar reasons, increasing the branching increases the critical entanglement molecular weight. The increased volume which results in a greater distance between the entanglement points stiffens the backbone chain that increases the glass transition temperature. It can be expected that the temperature dependence of the viscosity increases. *Mendelson*[26] reported that the magnitude of the activation energy was determined by the presence of long-chain branching, rather than any other structural feature in polyethylene.

For higher molecular weight branched polymer systems, the zero shear rate viscosity has been found to be higher than the corresponding linear polymer. This is due to the side chains being long enough to form interchain entanglements.

Bearing in mind the sensitivity of viscosity to molecular weight, molecular weight distribution and branching, it can be postulated that "molecular design" for various processes is possible, for many families of plastics.

2.1.4 Shear Rheology Of Thermoplastic Polyesters

Recently there have been many new applications for PET, therefore there is a need for a more complete characterisation than has been reported in the literature to date. The literature does not contain rheological data for relatively low molecular weight PET polymers and there is a possibility these polymers will have rheological differences to the PET polymers that have previously been studied. Also new grades and modified structures of PET polymers are being developed and used for new processes without their full scientific background being known.

Gregory and Watson[1] reported the steady-state flow properties of PET melts as a function of temperature, shear rate and "inherent viscosity" as determined by capillary rheometry. [Eastman Plastics use inherent viscosity, not the more commonly used intrinsic viscosity.

Inherent viscosity = Intrinsic viscosity + 0.041[27] Their study investigated the properties of PET polymers of typical commercial intrinsic viscosities in the temperature and shear rate environments relevant to processing.

The resultant flow curves showed the flow behaviour to be near-Newtonian over the shear rate range 50 to 1000s^{-1} and slightly pseudoplastic over the shear rate range 1000 to 24000s^{-1}. *Gregory and Watson*[1] used the Mendelson shear rate-temperature superposition scheme (see Section 2.1.3.4) with an additional shifting to a single reference "inherent viscosity" level. The following equation was used to relate inherent viscosity and weight-average molecular weight:

$$\text{inherent viscosity} = 1.60 \times 10^{-4} (\bar{M}_w)^{0.76} \qquad (2.24)$$

The results of the double superposition are shown below.

Temperature Superposition

shift factor relationship: $\ln(a_T) = -11.9755 + (6802.1 \div T)$

activation energy, E_a: 13.6kcal/mole (55.8kJ/mole)

Molecular Weight Superposition

shift factor relationship: $B_{DR_{w3}} = 1.49 \times 10^{-16} (\bar{M}_w)^{3.8}$

Gregory and Watson's[1] ability to obtain the master curve for molecular weights led them to conclude that the molecular weight distribution of PET is independent of molecular weight.

Gregory[2] summarised his results by stating that "for PET of 0.60 *IV*, a 0.0025 change in *IV* accounts for about the same change in melt viscosity as a 1°C change in temperature".

Boudreaux and Cuculo[3] reported that PET was only mildly pseudoplastic, the reported viscosity values lay between those of HDPE and PBT, this result is not the general case, the order being molecular weight dependent. At high shear rates stress-induced crystallisation was thought to affect the results. The flow curve for PET through a 180° die entrance is shown as Figure 2.6. Using an equation such as (2.19) *Boudreaux and Cuculo*[3] evaluated the activation energies for the flow curves shown, using the natural logarithmic form of (2.19):

$$\ln(\eta) = a_0 + a_1 (1000/T) \qquad (2.25)$$

The activation energy was calculated from:

$$E_a = (1000)R.a_1 \qquad\qquad (2.26)$$

The resultant activation energies are shown in Table 2.1.

FIGURE 2.6: PET FLOW CURVE AFTER *BOUDREAUX AND CUCULO*[3]

(O) 265°C; (△) 275°C; (□) 285°C.
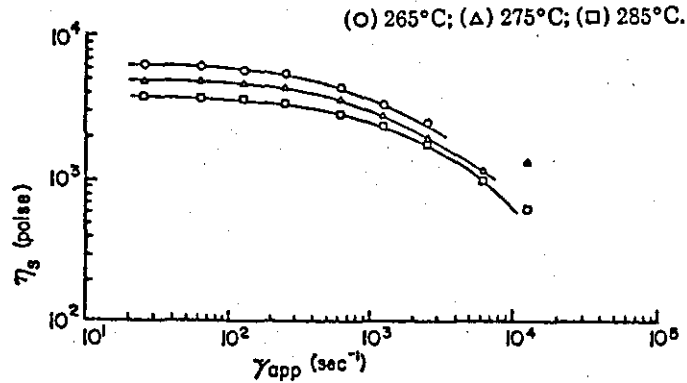
TABLE 2.1: ACTIVATION ENERGIES AFTER *BOUDREAUX AND CUCULO*[3]

Shear Rate (s^{-1})	a_0	E_a (kcal/mole)	E_a (kJ/mole)
63.75	-5.78	15.52	64.98
255	-4.80	14.33	60.00
637.5	-2.78	11.92	49.91
1275	-1.48	10.24	42.87
2550	-1.99	10.46	43.79

Boudreaux and Cuculo[3] also interpreted elastic behaviour from their study, using a simple Maxwell model to describe viscoelasticity, the elastic response is given by a Hooke's law relation of the form

$$\tau_w = G.\gamma_R \qquad\qquad (2.27)$$

where G is the shear modulus of elasticity and γ_R is the recoverable shear strain. The modulus is directly proportional to the absolute temperature and inversely proportional to the molecular weight between entanglements. *Boudreaux and Cuculo*[3] discussed elasticity in terms of the recoverable shear strain, a larger value being obtained from a more elastic material.

The polyesters showed a reversal of the order expected from entanglement theory. *Boudreaux and Cuculo*[3] suggested two alternative reasons

for this behaviour. An increased dipole interaction would increase the shear modulus and decrease the apparent elasticity. The plasticisation effect of oligomers would decrease the coherence of the fluid and hence increase the apparent elasticity.

Effect Of Degradation

Jabarin and Lofgren[28] reviewed the literature on the thermal stability of PET. PET degrades with random chain scission at the ester linkages, with the methylene group being the principle point of weakness. The thermal degradation rate is increased by the presence of oxygen. Moisture causes rapid hydrolytic degradation to occur at melting temperatures. The hydrolysis causes a reduction in the polymer molecular weight.

Jabarin and Lofgren[28] studied the effects of time, temperature, environment of the melt, and drying history, upon the short term PET degradation. They concluded that the time and temperature of melting affect the extent of degradation of PET; the amount of degradation was reduced by melting in an inert environment, or under vacuum, rather than in air; drying conditions of the PET pellets affects the extent of degradation.

Gregory and Wampler[4] discussed the problems of degradation of thermally sensitive polymers during shear measurements. Even after precautions are taken to remove moisture and oxygen from PET samples the problem of thermal degradation remains as a source of error in the results. An equation describing the thermal degradation of PET was proposed[4]

$$IV_t = \{1 \div [1/(IV_0)]1.47 + \exp[26.9 - (17080/T)]t\}^{0.68} \qquad (2.28)$$

where *IV* is the inherent viscosity, *t* is the residence time and *T* is the temperature. *Gregory and Wampler*[4] assumed the PET melt to behave in a Newtonian manner below a shear rate of $850 s^{-1}$. They then used an equation to describe the melt viscosity which accounted for degradation effects:

$$\eta_0 = 0.0979 \exp(6800/T)(IV_t)^{5.1} \qquad (2.29)$$

Other models were proposed by *Gregory and Wampler*[4] to relate melt viscosity as a function of IV_t, residence time and temperature.

From their study, *Gregory and Wampler*[4] suggested procedures to

account for thermal degradation.

    1. Determine the *IV* of the polymer extrudate at each shear rate and correct for the effect of *IV* on melt viscosity.

    2. Use a different polymer sample for each shear rate.

    3. Use a rheometer equipped with a plasticating extruder which operates under steady-state conditions with respect to *IV*, (i.e. constant average residence time and constant average thermal history).

The three procedures seem uneconomic, the *IV* measurements being laborious, of limited accuracy (±5%), and for PET use dangerous solvents. The second procedure would involve the analysis taking typically eight times longer than normal, and use eight times as much sample. The third may require the purchase of a new rheometer.

Buchneva et al.[29] reported a rheological study of some structurally modified PET polymers. By introducing PEO oligomers with an epoxy endgroup (laproxide) during the synthesis of PET at the transesterification stage they obtained a marked intensification of the polycondensation reaction, which resulted in the formation of branched reaction products.

They measured the rheological properties using a cone-and-plate rotary viscometer operating in an dry argon atmosphere. The viscosity was reported to decrease with increasing laproxide content (i.e. higher degree of branching).

Munari, Pilati and Pezzin[30] studied linear and randomly branched polybutylene terephthalate (PBT). After characterisation of the different polymers they studied their melt rheology, by vacuum drying the samples before extrusion, but no precautions were taken to prevent oxidative degradation and no account was made for thermal degradation.

The linear polymers were slightly pseudoplastic over the measured shear rate range; the relationship for Newtonian viscosity and molecular weight for the linear PBT polymers was reported as

$$\eta_o = 2.04 \times 10^{-13} (\bar{M}_w)^{3.2} \qquad (2.30)$$

The branched polymers appeared to be more pseudoplastic than the linear polymers, though this could be an illusion due to the

onset of shear thinning occurring at a lower shear rate with the branched polymers, see Figure 2.7.

FIGURE 2.7: LINEAR AND BRANCHED PBT RHEOLOGY AFTER *MUNARI et al.*[30]
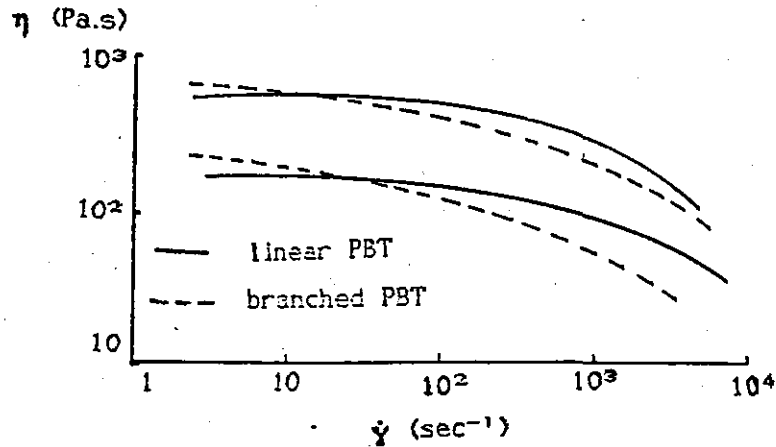
A master curve of the ratio η/η_0 versus $\dot{\gamma}\tau_\eta$ (where τ_η is a characteristic relaxation time introduced by Graessley) is shown as Figure 2.8; the predicted Graessley curve is also shown. The difference in pseudoplasticity between linear and branched PBT is shown to be small by Figure 2.8, whereas the difference from Graessley's prediction is notable.

FIGURE 2.8: MASTER CURVE AFTER *MUNARI, PILATI AND PEZZIN*[30]

Master curve for linear (-○ ⊘ ⊘-) and branched (-➔ ⟿ ◉ ●-) PBTP samples compared with Graessley's theoretical curve (—).
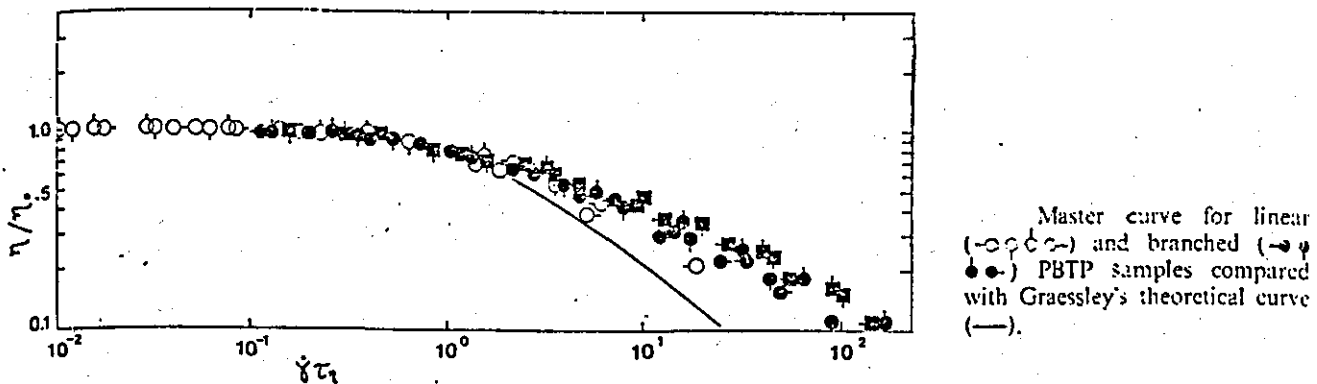
In a later paper *Munari, Pilati and Pezzin*[31] reported the activation energy for melt flow of linear and branched PBT polymers.

The flow activation energy for linear PBT was reported to be about 47 kJ/mole. Whilst the activation energy for the branched PBT was reported to increase with increasing degree of branching for polydisperse PBT samples with long branches.

Mishra and Deopura[32] reported the rheological behaviour of PET and PBT blends, with up to 10% PBT blended into PET. The polymers were only slightly pseudoplastic over the shear rate range used. Blends of increasing PBT content had decreasing viscosities, all lower than PET. The 2% PBT blend showed anomalous behaviour having a higher viscosity than the PET sample.

The viscosity was expressed as a function of temperature by an Arrhenius-type equation, such as equation (2.19). The activation energy increased with increasing PBT content, the 2% and 4% PBT content blends having lower activation energies than the PET sample. None of the blending rules fitted all the samples and no fit was found for the 2% PBT blend. For the blends of low PBT content the increase in viscosity and decrease in activation energy was due to a higher entanglement density. Whilst the reverse trends found with the higher PBT content blends were due to parallel phase segregation.

PET For Extrusion Blow Moulding

Baron, McChesney and Sinker[5] reported a modified PET polymer that could be extrusion blow moulded. A review was made of the approach of using a PET copolymer where the comonomer introduces irregularity in the molecular chain preventing crystallisation. The amorphous polymers being processable in what would otherwise be the thermoelastic region. However, *Baron, McChesney and Sinker*[5] modified the PET via the molecular architecture (branching?). The shear sensitivity of the modified polymer allows it to be extrusion blow moulded, it has a very high melt viscosity at low shear rates, yet a low melt viscosity at high shear rates. This allows a parison to form with sufficient melt strength, whilst not requiring excessive power to extrude the polymer. The rheology of the modified PET was compared with other common extrusion blow moulding polymers, as shown in Figure 2.9. The comparison indicates similar melt strength at low deformation rates and fluidity at high shear rates for all the

extrusion blow moulding polymers. The direct comparison of flow curves of different polymers from Figure 2.9 could be confusing, as different polymers were tested at different temperatures.

The experiments Baron, McChesney and Sinker[s] reported were all carried out in shear. However, parison sag requires a high elongational viscosity at low extension rates. It is not known whether the shear and tensile viscosities will correlate. Without a knowledge of the tensile flow behaviour it is not possible to determine the critical features of flow behaviour required for extrusion blow mouldable polymers, as Baron et al. attempted to in their paper.[s]

FIGURE 2.9: RHEOLOGY OF EXTRUSION BLOW MOULDING POLYMERS
AFTER BARON, McCHESNEY AND SINKER[s]
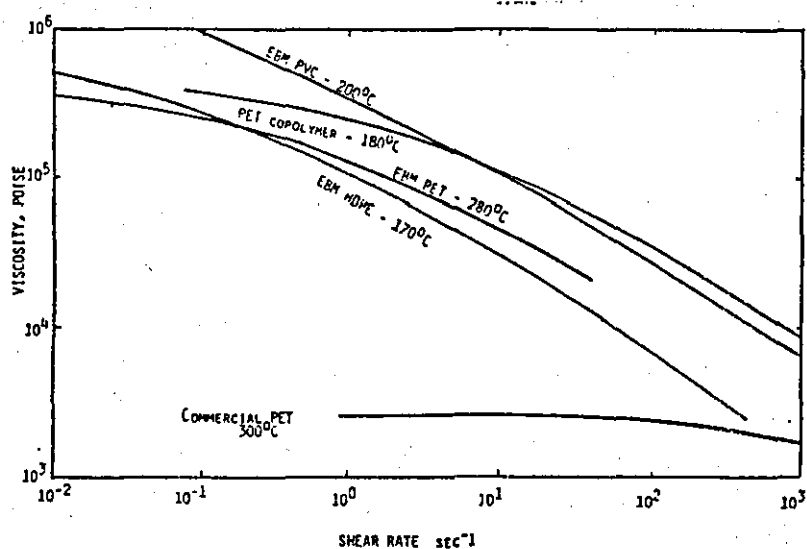
2.1.5 Objectives Of This Chapter

The rest of this chapter describes the polymers used in the experimental exercise. The equipment, procedures, results and discussion of results for the molecular characterisation and the shear rheology. Superposition methods were applied to obtain master curves with respect to temperature, molecular weight and structure. The methods used are described and the resultant master curves reported and discussed.

2.2 Polymer Characterisation

The polymers used in the study are described below, they have been classified into three groups: linear PET polymers, branched PET polymers, and copolyesters.

The linear PET polymers used in the study were 'Melinar' B90S, a standard bottle grade PET polymer (0.74ml/g nominal I.V.) supplied by ICI, a high viscosity (0.9ml/g nominal I.V.) development grade, EX167, supplied by ICI, and a series of four lower viscosity polymers prepared by conditioning B90S in humid environments. The method of conditioning the PET is shown in Appendix 1.

The five branched PET polymers were all development grades supplied by ICI for characterisation by *Mulla and Haworth*[33] and *Robinson and Haworth*[34]. This study expands on their work on these branched PET polymers. *Mulla and Haworth*[33] characterised four of the polymers and *Robinson and Haworth*[34] characterised the fifth polymer (BRAN-5). The intrinsic viscosities for the branched polymers are shown in Table 2.2.

TABLE 2.2: BRANCHED PET POLYMERS

POLYMER	I.V.	$\bar{M}_w/\bar{M}_n$
BRAN-1	0.9ml/g	
BRAN-2	0.85ml/g	
BRAN-3	1.0ml/g	4.35
BRAN-4	1.4ml/g	4.34
BRAN-5	1.1ml/g	

Three copolyesters were used in the study all supplied by Eastman Plastics. They were PETG 6763 a commercial grade developed primarily for extrusion blow moulding. PCCE 9967 a development grade for extrusion blow moulding of medical products. The third copolyester was PCTG 5445 a development grade, due for full commercialisation in April 1987, which was developed as a cheaper substitute for injection moulding grade polycarbonate.[35]

Two of the Eastman copolyesters are polyesters polymerised with isophthalic acid and cyclohexanedimethanol (CHDM) substituted for some of the terephthalic acid and ethylene glycol. PETG 6763 is a low CHDM copolyester, whilst PCTG 5445 is a high CHDM copolyester. PCCE 9967 is a thermoplastic elastomer.[36] Table 2.3 shows some of the

copolyesters properties.

TABLE 2.3: EASTMAN COPOLYESTERS

	PETG_6763[37]	PCCE_9967[38]	PCTG_5445[39]
	amorphous	crystalline	amorphous
inherent viscosity	0.75ml/g	1.28ml/g	0.75ml/g
intrinsic viscosity	0.71ml/g	1.24ml/g	0.71ml/g
$\bar{M}_n$	26000		
T_g	81°C	<0°C	88°C
T_m		200°C	

2.2.1 Solution Viscometry

A convention of quoting a solution viscosity value for different grades of PET polymers has been adopted by the industry. Problems can arise when comparing viscosities quoted by different laboratories due to different solvents being used or different types of viscosity being quoted (e.g. inherent or intrinsic viscosity).

Solution viscometry provides information for the molecular characterisation of polymers. Correlations between dilute solution viscosity and molecular parameters such as molecular weight or chain length have been established. These correlations are not valid for branched polymers as the method determines molecular size and not molecular weight, the correlations exist where there is a unique relationship between the mass and the size of the dissolved polymer molecules.[40]

The Mark-Houwink equation (2.31) describes the relationship between the intrinsic viscosity and the viscosity-average molecular weight.

$$[\eta] = K(\bar{M}_v)^a \qquad (2.31)$$

where $[\eta]$ is the intrinsic viscosity and K and a are constants. The viscosity-average molecular weight is approximately the same as the number-average molecular weight for polymers that have a narrow molecular weight distribution.

The constants in equation (2.31) vary dependent on the solvent and temperature used. *Moore and Sanderson*[41] and *Hergenrother and*

Nelson[42] studied the Mark-Houwink relationship for PET using various solvent systems, determining the constants for equation (2.31). Table 2.4 shows the Mark-Houwink constants for PET in various solvents.

The authors also quote the Mark-Houwink constants from twelve other sources, for the same solvents. The results vary between solvents and temperatures, and between various workers using the same solvents and temperatures.

TABLE 2.4: MARK-HOUWINK CONSTANTS FOR PET AT 25°C

SOLVENT	K X 10^4,dl/g	a	REFERENCE
1:1 P/TCE	2.50	0.73	42
3:2 P/TCE	2.37	0.73	42
OCP	2.25	0.73	42
OCP	1.9	0.81	41
3:2 P/TCE	14.0	0.64	41
Dichloroacetic acid	67.0	0.47	41
Trifluoroacetic acid	14.0	0.64	41

where P/TCE indicates a phenol and tetrachloroethane solvent mixture, by weight ratio. OCP indicates o-chlorophenol.

2.2.1.1 Sample Preparation

The sample preparation for PET polymers, before the solution viscosity can be measured, is a laborious and hazardous procedure. All the solvents for PET are hazardous, hence all the preparation and testing was performed in a fume cupboard.

The solvent system chosen was a 60:40 mixture by weight of phenol and 1,1,2,2-tetrachloroethane. The phenol was dried before use, this involved mixing a molecular sieve with molten phenol for 15 minutes, then after the mixture had settled, decanting the phenol into a stoppered dry container. The tetrachloroethane was distilled before use. The solvents were mixed in a ratio of 60% phenol by weight to 40% tetrachloroethane.

To dissolve the vacuum dried polymer, the granules were soaked in hot solvent at 90°C for three hours, the solvent was stirred continuously. (Higher temperatures could not be used as the phenol tends to oxidise, turning brown, and the resultant solution would be chemically different to the reference solvent used in the viscometry

method.) After the initial soaking in hot solvent the polymer was soaked for a few hours at room temperature, whilst being stirred continuously, until the polymer dissolved.

Solutions of different concentrations were prepared for each polymer sample: the concentrations used were 0.1%, 0.2%, 0.3% and 0.4% by volume. The solutions were filtered before the tests performed.

2.2.1.2 Experimental Procedure

The experimental procedure followed that laid down in British Standard 2782, Part 7, Method 730A:1979.[43] A Ubbelohde viscometer, size 1B, was clamped in position in a constant temperature water bath at 24.7°C. The solutions were kept in the waterbath for 10 minutes before they were tested. The solutions were transferred to the viscometer using a pipette, then left for 3 minutes to thermally stabilise before testing. The efflux times of the solvent and the solutions were determined to within 0.1 seconds and repeated until agreement within 0.1s was obtained for three consecutive readings. The intrinsic viscosity was calculated for each polymer.

2.2.1.3. Results

The intrinsic viscosity (equation (2.32)) is the intercept at zero concentration of a plot of the relative viscosity (equation (2.33)) or the specific viscosity (equation (2.34)) against solution concentration.

$$[\eta] = (\eta_{sp})_{c=0} \div c = \ln ((\eta_r)_{c=0}) \div c \qquad (2.32)$$

where $[\eta]$ is the intrinsic viscosity, and η_r is the relative viscosity (equation (2.33)), η_{sp} is the specific viscosity (equation (2.34)) and c is the solution concentration.

$$\eta_r = t/t_0 \qquad (2.33)$$

$$\eta_{sp} = \eta_r - 1 \qquad (2.34)$$

where t is the average efflux time for the solution, t_0 is the average efflux time for the solvent.

Table 2.5 shows the intrinsic viscosities obtained, also shown are previously reported values for the same polymers using the same solvent system and temperature.

2.2.1.4 Discussion Of Results

Table 2.5 shows that the intrinsic viscosity values obtained agree, within experimental error, with those previously reported. The only difference being with the branched polymers, BRAN-2 was found to have a higher intrinsic viscosity than BRAN-1; whilst *Mulla*[33] reported the reverse order.

The copolyesters were not analysed by this technique.

TABLE 2.5: INTRINSIC VISCOSITY RESULTS

POLYMER	INTRINSIC VISCOSITY (ml/g)	PREVIOUSLY REPORTED INTRINSIC VISCOSITY (ml/g)	REFERENCE
B90S	0.733	0.73	44
EX167	0.951	0.9	34
LIN-A	0.71		
LIN-B	0.665		
LIN-C	0.598		
LIN-D	0.545		
BRAN-1	0.843	0.9	33
BRAN-2	0.964	0.85	33
BRAN-3	0.976	1.0	33
BRAN-4	1.244	1.4	33
BRAN-5	1.062	1.1	34
PETG		0.71	37
PCCE		1.24	38
PCTG		0.71	39

2.2.2 Gel Permeation Chromatography

2.2.2.1 Introduction[45]

Gel permeation chromatography (GPC) is a technique used to determine the molecular size and size distribution of polymers. The molecular size is related to molecular mass for known fractions of polystyrene via the Mark-Houwink equation. The molecular mass of other polymers can then be determined by using the appropriate Mark-Houwink constants. Using this method the molecular weight distribution is determined from the molecular size distribution.

In GPC mixtures of soluble organic species are separated into their different sizes. The separation occurs in the GPC columns. A column is packed with a gel of porous crosslinked polystyrene. The columns are maintained saturated with solvent which flows through

continuously. When a polymer solution passes through the column, the dissolved molecules separate according to their size, as the smaller molecules enter the pores in the gel whilst the larger molecules cannot and hence pass through the column more quickly. Figure 2.10 illustrates the separation of the different sizes of polymer molecules. The residence time of each species in the column is measured, from the injection point and from the quantity of solvent emerging from the column. A more detailed description of the technique can be found in the literature.[45,46,47]

FIGURE 2.10: MOLECULAR SEPARATION IN GPC[45]
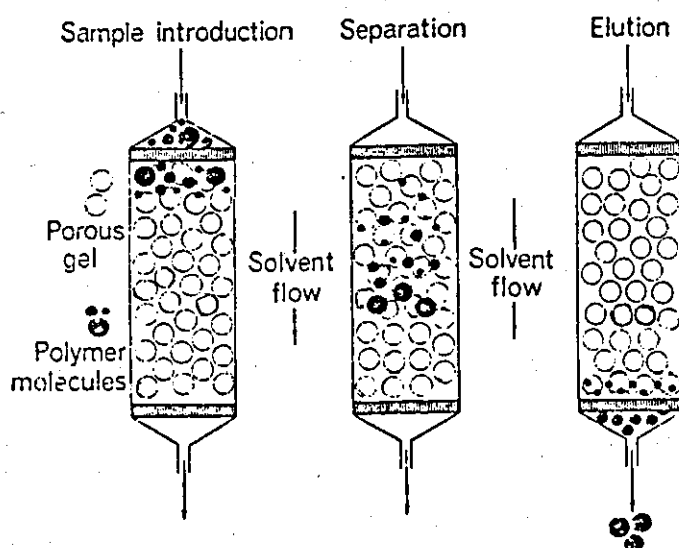
Holding[48] recommends that GPC should only be used as a comparative tool, since variations in results occur between different laboratories and with time in the same laboratory. Also the correction method using a calibrant polymer can lead to large errors. Baseline determination on the chromatograms is a source of operator error, which can lead to large differences in the values of $\bar{M}_n$ and $\bar{M}_z$.

The most common solvent for GPC of PET is m-cresol at 110°-135°C. It has to be used at elevated temperatures because of its high viscosity.[49] However, *Paschke, Bidlingmeyer and Bergmann*[50] reported that m-cresol degrades PET by acid catalysed hydrolysis. This results in a narrower distribution being observed. *Overton and Browning*[49]

reported that, as m-cresol is a polar solvent, in dilute solutions of PET, the PET undergoes intramolecular ester interchange and the resultant equilibrium distribution consists mostly of cyclic species. The presence of these cyclic species leads to a broader distribution being observed.

A summary of the solvent systems that have been used for PET is shown below in Table 2.6.

The solvent system proposed by *Paschke, Bidlingmeyer and Bergmann*[50], 0.5% nitrobenzene-99.5% tetrachloroethane by volume appears to be promising, being a room temperature solvent system for the GPC of PET. *Janca*[53] reviewed GPC of many polymers and concluded that room temperature mixed solvents were preferable for GPC as no degradation occurs. Problems of using this solvent system include the Mark-Houwink constants not having been published and, as *Holding*[48] warns, there can be problems with mixed solvents if the ratio of the mixture changes during the analysis. The safer room temperature operation justifies the choice of this solvent system, despite its potential problems.

2.2.2.2 GPC Experiments

(a) Equipment

The equipment used was a Polymer Laboratories GPC system, consisting of a Knauer HPLC pump, a PL injection unit, a PL column, a Knauer detector, and a BBC computer for datalogging and data interpretation. The GPC system was used in a fume cupboard due to the hazardous nature of the solvent system used. The column, the piping from the column to the detector, the reference sample and the pipes connecting the reference sample reservoir to the detector were all thermally insulated to maintain a horizontal baseline.

The GPC system was used under the following conditions: solvent system used was 0.5% nitrobenzene-99.5% tetrachloroethane; 23°C temperature; 1ml/min nominal flow rate (0.97ml/min measured rate); PL gel column (Polymer Laboratories Ltd) styrene-divinyl benzene packing.

The solvents used were reagent grade tetrachloroethane (TCE) (Fisons Ltd), and analytical grade nitrobenzene (NB) (BDH Chemicals Ltd). The GPC eluant (NB-TCE) was 0.5% NB-99.5% TCE by volume at room

temperature.

TABLE 2.6: PET SOLVENTS CONSIDERED FOR GPC

SOLVENT SYSTEM	ADVANTAGES	DISADVANTAGES	REFERENCES
m-cresol	Mark-Houwink constants known.	degrades PET, high viscosity, hazardous, polar solvent (causes ester interchange).	49,50
o-chlorophenol		degrades PET, hazardous.	50
nitrobenzene		polymer precipitates below 135°C.	50
trifluoroacetic acid		degrades PET	50
hexafluoroacetone		degrades PET	50
hexafluoroisopropanol		degrades PET	50
70:30 methylene chloride: hexafluoro-isopropanol	good resolution (can detect cyclic oligomers)	polar solvent, low boiling point, costly, hazardous.	48,49
25:75 o-chlorophenol: chloroform		hazardous, mixed solvent (ratio can change during analysis).	51,52
0.5:99.5 nitrobenzene: tetrachloro-ethane	room temperature (no degradation)	mixed solvent, Mark-Houwink constants unknown.	50,53
60:40 phenol: tetrachloroethane		too viscous	50
20:80 phenol: tetrachloroethane		too viscous	50
10:90 phenol: tetrachloroethane		too viscous, polymer precipitates at room temperature.	50

The system was prepared for running on the NB-TCE solvent system, in place of the usual tetrahydrafuran (THF) solvent, using the column manufacturers recommended procedure.[54] The system was flushed with toluene at a rate of 1ml/min overnight, then the system was flushed for 24 hours with the NB-TCE solvent system. The system was then ready to use.

The system calibration is described in Appendix 2. The PET distributions are reported in terms of equivalent PS molecular weight, this method was used as the Mark-Houwink constants for the solvent system was unknown for both polystyrene and PET.

The data interpretation was carried out by the software package supplied with the instrument. The software runs on a BBC computer, and the results are printed out as molecular weight distributions. The baseline is arbitrarily selected by the operator, this is a potential source of error.

(b) Sample Preparation

The solvent system used was a mixture of 0.5% nitrobenzene-99.5% tetrachloroethane, by volume. The solution preparation was carried out as reported by *Paschke, Bidlingmeyer and Bergmann.*[50] The PET samples were dissolved in the nitrobenzene at 180°C (an oil bath was used to maintain steady temperature and a cold finger was inserted in the boiling tube), after the PET had dissolved, warm TCE (nearly boiling) was added with vigorous stirring. The warm solution was filtered (Whatman paper #1) into warm (60°C) TCE.

The solutions had a limited stability, precipitation occurred after approximately 48 hours. Therefore fresh samples were made prior to each GPC run.

(c) GPC Results

The results from the GPC analysis carried out as described in section 2.2.2.2 are reported in Table 2.7. Table 2.7 shows the number-average molecular weight $\bar{M}_n$, the weight average molecular weight $\bar{M}_w$, the z-average molecular weight $\bar{M}_z$ and the polydispersity index $\bar{M}_w/\bar{M}_n$.

During the running of these GPC analyses the pump pressure gradually built up to an unacceptable level, due partly to the frit becoming blocked in the column. The cause of the blockage was due

either to insufficient filtering of the solutions, or the solvent system attacking the column packing material.

Samples of all the polymers were sent to RAPRA for analysis on their recently set up GPC system for PET running on a m-cresol solvent system.

TABLE 2.7: GPC RESULTS

Polymer	$\bar{M}_n$	$\bar{M}_w$	$\bar{M}_z$	$\bar{M}_w/\bar{M}_n$
Linear PET				
B90S	38750	24700	410000	6.7
(B90S	30500	107000	422000	3.53)
EX167	53000	412000	658000	7.58
LIN-A	25650	94050	387500	3.6
LIN-B	23400	89900	429000	3.84
LIN-C	22500	78100	395000	3.44
LIN-D	20900	61900	258000	2.96
Branched PET				
BRAN-1	33650	253500	7895000	7.755
BRAN-2	32350	277000	5580000	8.61
BRAN-3	45500	137500	30950000	18.65
BRAN-4	57200	2540000	175000000	44.44
BRAN-5	62900	1730000	56750000	27.42
Copolymer				
PETG	33900	214500	2640000	7.17

2.2.2.3 Discussion Of GPC Results

Comparing Table 2.5 and Table 2.7 it can be seen that the number-average molecular weights follow the same order of increasing molecular weight and intrinsic viscosity for a given structural class (i.e. linear or branched PET).

From Table 2.7 it can be seen that the polydispersity index was higher than the theoretical value for linear PET of 2.0.[49] A higher polydispersity index indicates a broader molecular weight distribution. The very high values reported for the branched polymers were probably due to the experimental problems noted above, though branched polymers will have a different hydrodynamic volume to linear polymers and so a significant difference was expected in these results which are values relative to the hydrodynamic volume of polystyrene.

Overton and Browning[49] reported a broadening of the

distribution due to the presence of cyclic oligomers. If any degradation of the polymer occurred then a broader distribution would be obtained. *Paschke, Bidlingmeyer and Bergmann*[60] reported that this solvent system does not degrade PET, however, they only studied linear grades. If branched PET grades are more sensitive to attack by the solvent system this may account for the broad distributions obtained.

If the polymer has an affinity for the column packing material it will have a longer residence time than its true distribution would, in this case a very broad distribution could be obtained.

Another possibility is that under the pressure in the GPC system precipitation occurred inside the column, blocking the pores of the gel and causing a pressure build-up. However, no precipitate was observed in the solvent eluted.

2.2.2.4 RAPRA GPC Results

RAPRA (Rubber and Plastics Research Association) used a m-cresol solvent system at 120°c, to permit a form of monitoring of any acid catalysed hydrolytic degradation the time spent by the polymer at elevated temperatures in m-cresol has been reported.

The samples were tested in two batches the majority tested in one batch and the PCCE and PCTG copolyesters tested at a later date. The sample preparation technique used was different for the two batches of samples, see Appendix 3 for details of the preparation.

The equipment used included three PL gel columns:

      1 X 500Å   10micron;

      1 X 10(4)Å   10micron;

      1 X 10(6)Å   10micron.

The solvent was m-cresol, at a flow rate of 1.0ml/min, and a temperature of 120°C. The calibration was based on a third order polynomial using polystyrene.

The molecular weights are expressed as "polystyrene equivalent". The RAPRA GPC results are shown in Table 2.8. All the runs are shown and when a decrease in molecular weight corresponds with an increase in heating time, degradation can be assumed to have occurred.

No detector response was detected for the PCCE copolyester

sample, possibly due to some extra affinity of this polymer and the polystyrene packing.

The difference in values for the PETG sample tested in both batches may have been a function of the change in solution preparation method, or it may have been just the general variation observed over a period of time; only runs performed together should be compared.

Comparing Table 2.5, Table 2.7 and Table 2.8 it can be seen that for the linear PET polymers there is agreement in the order of increasing molecular weight (when $\bar{M}_n$ is considered). The molecular weights determined for the branched PET polymers do not show the same trends.

The values reported in Tables 2.7 and 2.8 do not show any correlation, it is a characteristic of GPC data that inter-laboratory results do not always agree.

Comparing the polydispersity index values in Tables 2.7 and 2.8, it can be concluded that the RAPRA results are more consistent and nearer the theoretical value of 2.0. These data will be used for reference purposes in the remainder of this Chapter.

TABLE 2.8: RAPRA GPC RESULTS

POLYMER	TIME IN OVEN (min)	$\bar{M}_w$	$\bar{M}_n$	POLYDISPERSITY INDEX ($\bar{M}_w/\bar{M}_n$)
FIRST BATCH				
B90S	50	62700	38800	1.6
B90S	60	66600	41700	1.6
EX167	40	79600	47700	1.7
EX167	50	71900	43600	1.6
LIN-A	15	54000	32900	1.6
LIN-A	25	52600	33400	1.6
LIN-B	15	56200	30000	1.9
LIN-B	35	61600	37500	1.6
LIN-C	15	61400	30200	2.0
LIN-C	25	55200	31500	1.8
LIN-D	15	41900	25900	1.6
LIN-D	25	39100	24700	1.6
BRAN-1	40	96100	46000	2.1
BRAN-1	50	89100	34600	2.6
BRAN-2	40	92100	37800	2.4
BRAN-2	50	81900	41300	2.0
BRAN-3	42	116000	41700	2.8
BRAN-3	52	128000	45000	2.8
BRAN-4	80	130000	50700	2.6
BRAN-5	50	84300	37800	2.2
BRAN-5	60	92100	35600	2.6
PETG	35	68000	39100	1.7
PETG	45	67800	38400	1.8
SECOND BATCH				
PETG	40	40200	22400	1.8
PETG	45	48400	28500	1.7
PETG	50	54400	28600	1.9
PCTG	40	67900	32600	2.1
PCTG	45	66700	37500	1.8
PCCE	40	*	*	*

* No detected response for PCCE.

2.3 Experimental Shear Rheology

2.3.1 Introduction

A Davenport Extrusion Rheometer was used to obtain rheological data on several PET polymers. The Cogswell and Lamb method[13] was used to calculate the shear data. This method, a modification of the Bagley end-effect correction method, uses data obtained from two dies, a long die (L=20mm) and an orifice die. The rheological values are derived from equations (2.16), (2.18) and (2.4).

$$\text{apparent wall shear rate,} \quad \dot{\gamma} = 4Q/\pi R^3 \qquad (sec^{-1})(2.16)$$

$$\text{apparent wall shear stress,} \quad \tau = (P_L - P_O)R/2L \qquad (Pa)(2.18)$$

$$\text{apparent viscosity,} \quad \eta = \tau/\dot{\gamma} \qquad (Pa.s)(2.4)$$

The Rabinowitsch correction to the shear rate due to the non-Newtonian nature of the flow was neglected because PET was reported[13] as being only mildly pseudoplastic.

2.3.2 Test Procedure

The procedure used for testing PET with a Davenport Extrusion Rheometer was designed, considering the work of *Gregory and Wampler*[4], to prevent hydrolytic or oxidative degradation and to minimise the effect of thermal degradation.

Firstly the material was dried for a minimum of 4 hours (usually longer e.g. overnight) at 140°C in a vacuum oven. On removal from the vacuum oven the material was stored in a desiccator, containing silica gel, until loaded into the rheometer barrel. This procedure prevented moisture being present during extrusion and so prevented hydrolytic degradation.

During the charging of the rheometer barrel with the material, the barrel was flooded with nitrogen gas displacing any oxygen trapped in the material and so oxidative degradation during extrusion was prevented.

The pre-heat time after charging and before extrusion was kept constant and between the limits of incomplete melting of all the crystalline structure and the onset of thermal degradation. A 15 minute pre-heat time was used for crystalline PET granules and a 10 minute pre-heat time was used for amorphous copolyesters. As well as maintaining a constant pre-heat time the extrusion runs were

duplicated using an ascending order and a descending order of piston speeds. The results from the two runs were then averaged to minimise any thermal degradation (due to the residence time in the barrel with respect to the duration of the test) effects on the results.

The rheometer barrel was cleaned between each run to prevent degraded residual material interfering with the next run.

Data from the Davenport Extrusion Rheometer was obtained for various temperatures for each of the polymers listed in Section 2.2. For each temperature, data for two dies fitted in the Davenport were obtained. The dies used had L/D ratios of 20/2 and 0/2, the dies had a capillary radius of 1mm.

2.4 Experimental Shear Rheology Results

The rheological behaviours of the different polymers tested are illustrated by viscosity curves (apparent shear viscosity-shear rate curves). Figures 2.11 and 2.12 show the effect of temperature on the shear rheology of B90S linear PET. Figure 2.11 is an example of a flow curve (shear stress-shear rate curve). In this study viscosity curves such as Figure 2.12 are preferred as they are simpler to compare conceptually. Figures 2.13 and 2.14 show the effect of intrinsic viscosity on the shear rheology of linear PET at 270°C and 280°C respectively.

Figures 2.15 and 2.18 show the effect of the weight-average molecular weight on the near-Newtonian viscosity of the linear and branched PET polymers respectively. The gradient of each plot can be represented as the exponent in equation (2.23). Figure 2.15 relates the apparent shear viscosity at a shear rate of $200s^{-1}$ with $\bar{M}_w$ and was constructed using data from Figures 2.13 and 2.14 and Table 2.8. Figure 2.18 shows the effect of $\bar{M}_w$ on the apparent shear viscosity at a shear rate of $20s^{-1}$ and was constructed using data from Figures 2.16 and 2.17 and Table 2.8.

Figures 2.16 and 2.17 show the effect of intrinsic viscosity on the shear rheology of branched PET polymers at 270°C and 280°C

respectively. Figure 2.19 shows the effect of temperature on the shear rheology of branched PET polymers.

The effects of temperature on the shear rheology of the copolyesters are shown by Figures 2.20-2.22. Figure 2.20 showing the behaviour of PETG, Figure 2.21 showing the behaviour of PCTG and Figure 2.22 showing the behaviour of PCCE.

At low shear rates the viscosity curves approached Newtonian flow behaviour (horizontal curve), the zero shear rate viscosity was estimated by extrapolating the curve to very low shear rates, the estimated values are shown in Table 2.9.

Tables 2.10-2.12 show the power law constants (from equation (2.14)) for various conditions for the linear PET, branched PET and copolyester polymers respectively.

Table 2.13 shows the temperature sensitivity of the apparent viscosity at a shear rate of $100s^{-1}$.

TABLE 2.9: NEAR-NEWTONIAN VISCOSITY

Polymer	Temperature (°C)	n value	Shear Rate (sec^{-1})	η_o estimate (Pa.s)
B90S	270	0.80	10	700
B90S	275	0.98	10	530
B90S	280	0.93	10	360
B90S	285	0.95	10	380
B90S	290	1.00	60	220
EX167	270	0.99	30	1200
LIN-A	270	0.89	25	190
LIN-A	280	1.00	25	140
LIN-B	280	0.87	100	140
LIN-C	280	0.81	100	100
LIN-D	270	1.00	100	57
LIN-D	280	1.00	100	29
BRAN-1	270	0.95	10	760
BRAN-1	280	0.95	10	680
BRAN-2	270	0.96	10	500
BRAN-2	280	0.88	10	480
BRAN-3	270	0.95	10	1100
BRAN-3	280	0.97	10	1000
PETG	200	0.93	10	4900
PETG	220	0.88	10	2500
PETG	240	0.92	10	1400
PETG	260	0.98	10	700
PCCE	245	1.00	100	270

TABLE 2.10: POWER LAW CONSTANTS FOR LINEAR PET

POLYMER	TEMPERATURE (°C)	SHEAR RATE (sec⁻¹)	K	n
B90S	270	100	1.46×10^{-3}	0.80
B90S	270	1000	4.49×10^{-3}	0.61
B90S	275	100	1.11×10^{-3}	0.82
B90S	275	1000	3.00×10^{-3}	0.65
B90S	280	100	4.25×10^{-4}	0.93
B90S	280	1000	7.61×10^{-3}	0.47
B90S	285	100	7.06×10^{-4}	0.90
B90S	285	1000	2.35×10^{-3}	0.68
EX167	270	100	2.89×10^{-3}	0.77
EX167	270	1000	3.90×10^{-2}	0.34
EX167	280	100	1.27×10^{-3}	0.77
EX167	280	1000	3.65×10^{-3}	0.59
LIN-A	270	100	2.85×10^{-4}	0.89
LIN-A	270	1000	2.72×10^{-4}	0.89
LIN-A	280	100	4.57×10^{-5}	1.00
LIN-A	280	1000	2.80×10^{-5}	1.00
LIN-B	270	100	1.09×10^{-3}	0.69
LIN-B	270	1000	1.18×10^{-3}	0.69
LIN-B	270	10000	1.11×10^{-3}	0.69
LIN-B	280	100	2.00×10^{-6}	1.00
LIN-B	280	1000	3.45×10^{-4}	0.87
LIN-B	280	10000	1.68×10^{-2}	0.37
LIN-C	270	100	2.40×10^{-4}	0.77
LIN-C	270	1000	5.96×10^{-4}	0.77
LIN-C	270	10000	2.24×10^{-2}	0.33
LIN-C	280	100	2.68×10^{-4}	0.81
LIN-C	280	1000	2.92×10^{-4}	0.81
LIN-C	280	10000	5.23×10^{-3}	0.47
LIN-D	270	100	1.30×10^{-5}	1.00
LIN-D	270	1000	1.60×10^{-5}	1.00
LIN-D	270	10000	7.30×10^{-4}	0.65
LIN-D	280	100	1.38×10^{-5}	1.00
LIN-D	280	1000	7.00×10^{-5}	0.88
LIN-D	280	10000	7.00×10^{-5}	0.88

TABLE 2.11: POWER LAW CONSTANTS FOR BRANCHED PET

POLYMER	TEMPERATURE (°C)	SHEAR RATE (sec⁻¹)	K	n
BRAN-1	270	100	2.50×10^{-3}	0.70
BRAN-1	270	1000	2.59×10^{-2}	0.32
BRAN-1	280	100	7.81×10^{-4}	0.95
BRAN-1	280	1000	3.00×10^{-3}	0.63
BRAN-2	270	100	5.70×10^{-4}	0.96
BRAN-2	270	1000	1.84×10^{-3}	0.79
BRAN-2	280	100	8.41×10^{-4}	0.88
BRAN-2	280	1000	8.20×10^{-3}	0.49
BRAN-3	270	100	1.60×10^{-3}	0.95
BRAN-3	270	1000	8.60×10^{-3}	0.48
BRAN-3	280	100	1.00×10^{-3}	0.97
BRAN-3	280	1000	8.00×10^{-3}	0.52
BRAN-4	270	100	1.26×10^{-2}	0.58
BRAN-4	270	1000	1.37×10^{-2}	0.58
BRAN-4	280	100	1.35×10^{-2}	0.48
BRAN-4	280	1000	1.31×10^{-2}	0.48
BRAN-5	270	100	1.41×10^{-2}	0.55
BRAN-5	270	1000	1.77×10^{-4}	0.55
BRAN-5	280	100	6.20×10^{-3}	0.62
BRAN-5	280	1000	2.27×10^{-2}	0.40

TABLE 2.12: POWER LAW CONSTANTS FOR COPOLYESTERS

POLYMER	TEMPERATURE (°C)	SHEAR RATE (sec⁻¹)	K	n
PETG	170	100	3.65×10^{-2}	0.62
PETG	170	1000	7.06×10^{-1}	0.14
PETG	200	100	4.60×10^{-2}	0.43
PETG	200	1000	1.48×10^{-1}	0.23
PETG	220	100	5.23×10^{-3}	0.78
PETG	220	1000	6.56×10^{-2}	0.32
PETG	240	100	4.45×10^{-3}	0.72
PETG	240	1000	1.56×10^{-1}	0.16
PETG	260	100	7.17×10^{-4}	0.98
PETG	260	1000	3.10×10^{-3}	0.68
PCTG	240	100	1.35×10^{-2}	0.55
PCTG	240	1000	3.65×10^{-2}	0.37
PCTG	250	100	2.56×10^{-3}	0.75
PCTG	250	1000	7.84×10^{-3}	0.55
PCTG	260	100	2.43×10^{-3}	0.75
PCTG	260	1000	1.04×10^{-2}	0.50
PCCE	230	100	4.02×10^{-3}	0.56
PCCE	230	1000	3.97×10^{-3}	0.56
PCCE	245	100	2.60×10^{-4}	1.00
PCCE	245	1000	4.13×10^{-3}	0.51
PCCE	260	100	9.45×10^{-4}	0.64
PCCE	260	1000	1.20×10^{-3}	0.64

FIGURE 2.11: EFFECT OF TEMPERATURE ON B90S LINEAR PET

SHEAR STRESS (MPa)

Legend:
- 270C
- 275C
- 280C
- 290C

SHEAR STRAIN RATE (sec-1)
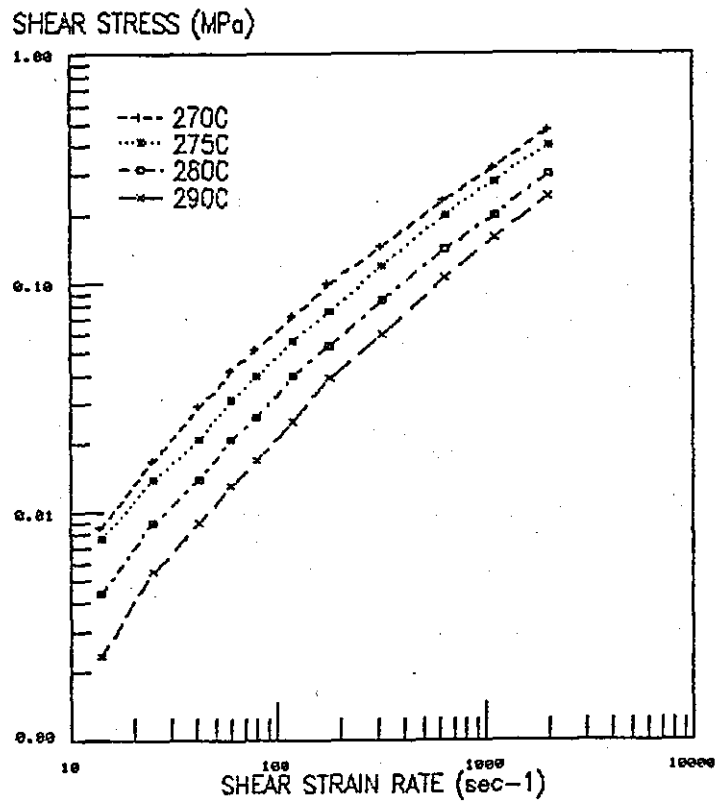
FIGURE 2.12: EFFECT OF TEMPERATURE ON B90S LINEAR PET

SHEAR VISCOSITY (Pa.s)

Legend:
- 270C
- 275C
- 280C
- 290C

SHEAR STRAIN RATE (sec-1)
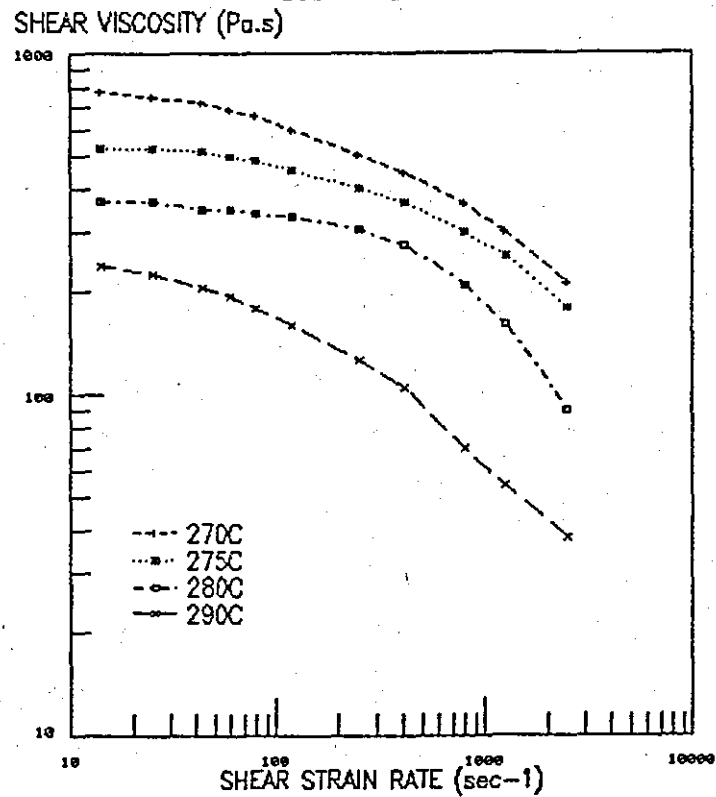
FIGURE 2.13: EFFECT OF I.V. ON THE SHEAR
VISCOSITY OF LINEAR PET AT 270C

SHEAR VISCOSITY (Pa.s)

SHEAR STRAIN RATE (sec-1)
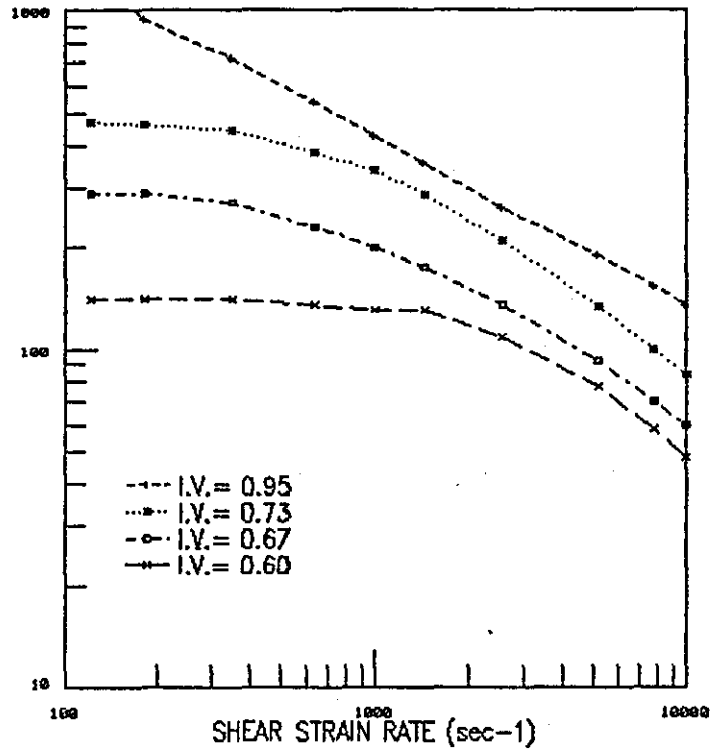
FIGURE 2.14: EFFECT OF I.V. ON THE SHEAR
VISCOSITY OF LINEAR PET AT 280C

SHEAR VISCOSITY (Pa.s)

SHEAR STRAIN RATE (sec-1)
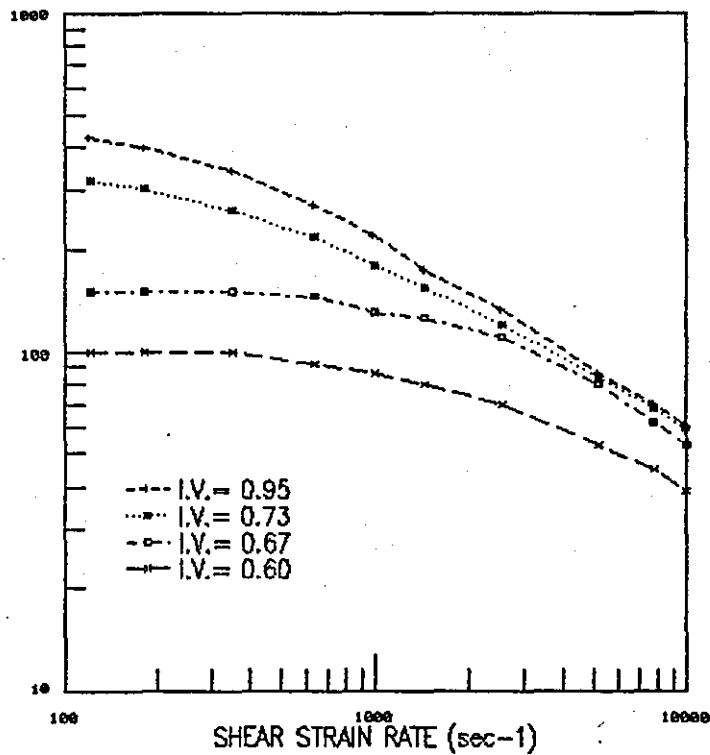
FIGURE 2.15: EFFECT OF $\overline{M}w$ ON THE NEAR-
NEWTONIAN VISCOSITY OF LINEAR PET
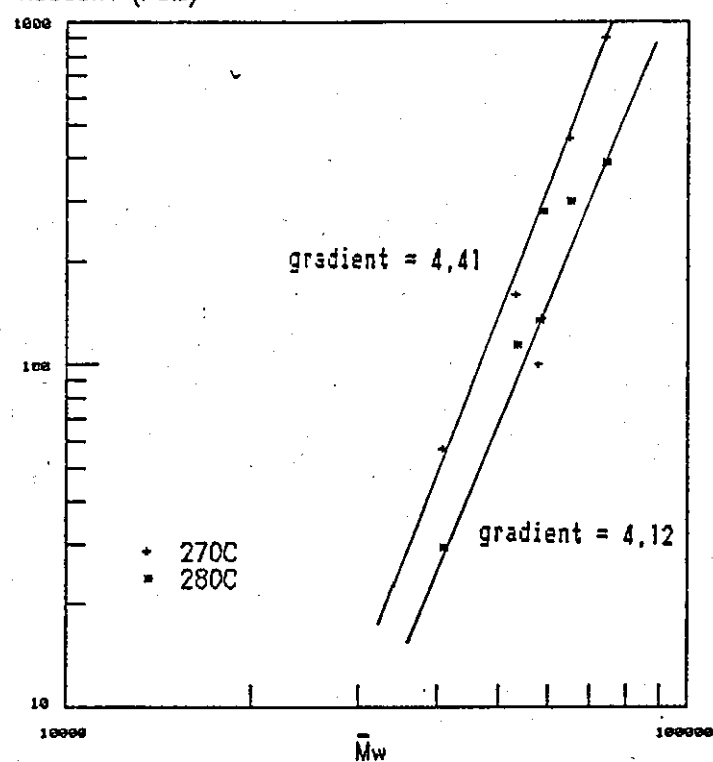
FIGURE 2.16: EFFECT OF I.V. ON THE SHEAR
VISCOSITY OF BRANCHED PET AT 270C

SHEAR VISCOSITY (Pa.s)

	I.V.	M.W.D.
BRAN-1,	0.84	2.35
BRAN-5	1.06	2.40
BRAN-3	0.98	2.80
BRAN-2	0.96	2.20
BRAN-4,	1.24	2.60

SHEAR STRAIN RATE (sec-1)
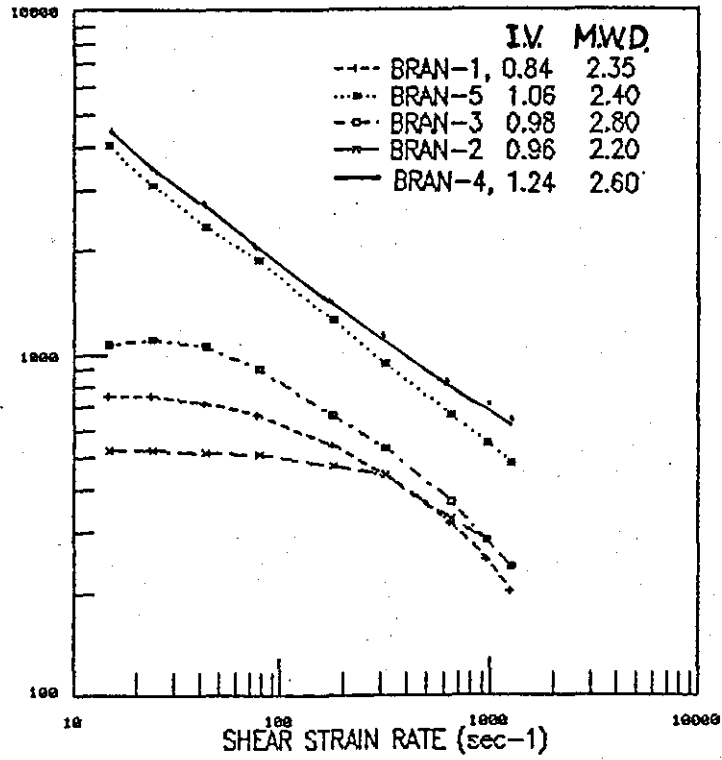
FIGURE 2.17: EFFECT OF I.V. ON THE SHEAR
VISCOSITY OF BRANCHED PET AT 280C

SHEAR VISCOSITY (Pa.s)

	I.V.	M.W.D.
BRAN-4,	1.24	2.60
BRAN-5,	1.06	2.40
BRAN-3,	0.98	2.80
BRAN-1,	0.84	2.35
BRAN-2,	0.96	2.20

SHEAR STRAIN RATE (sec-1)
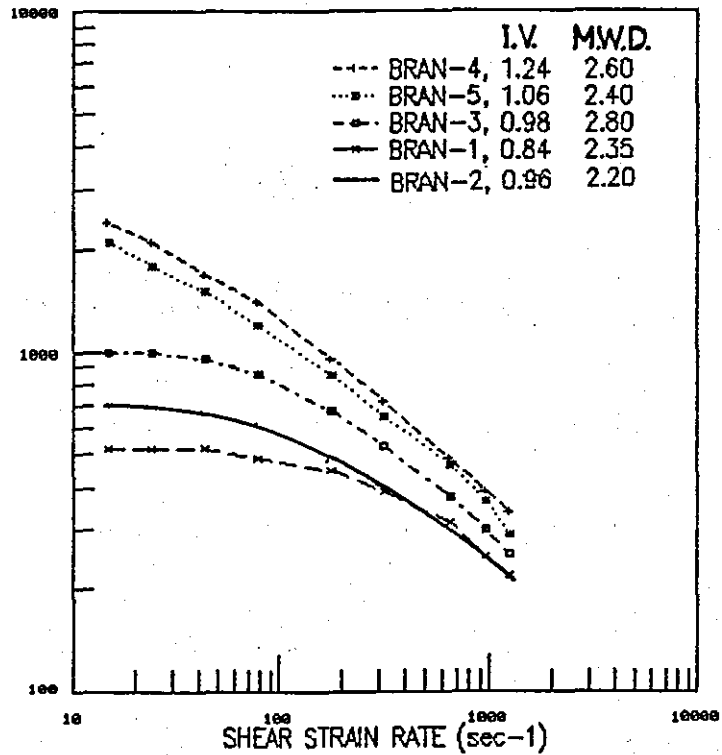
FIGURE 2.18: EFFECT OF M̄w ON THE NEAR-
NEWTONIAN VISCOSITY OF BRANCHED PET

VISCOSITY (Pa.s)

gradient = 3.57

gradient = 4.85

+ 270C
■ 280C

M̄w
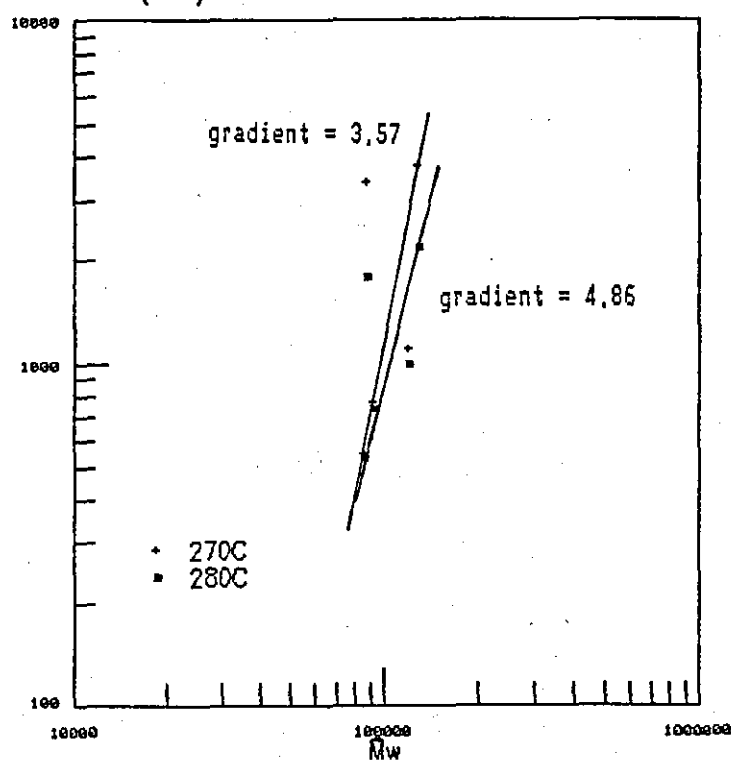
FIGURE 2.19: EFFECT OF TEMPERATURE ON
BRANCHED PET RHEOLOGY

SHEAR VISCOSITY (Pa.s)

--+-- BRAN-4 at 270C
···■·· BRAN-4 at 280C
--●-· BRAN-2 at 270C
--*-- BRAN-2 at 280C

SHEAR STRAIN RATE (sec-1)
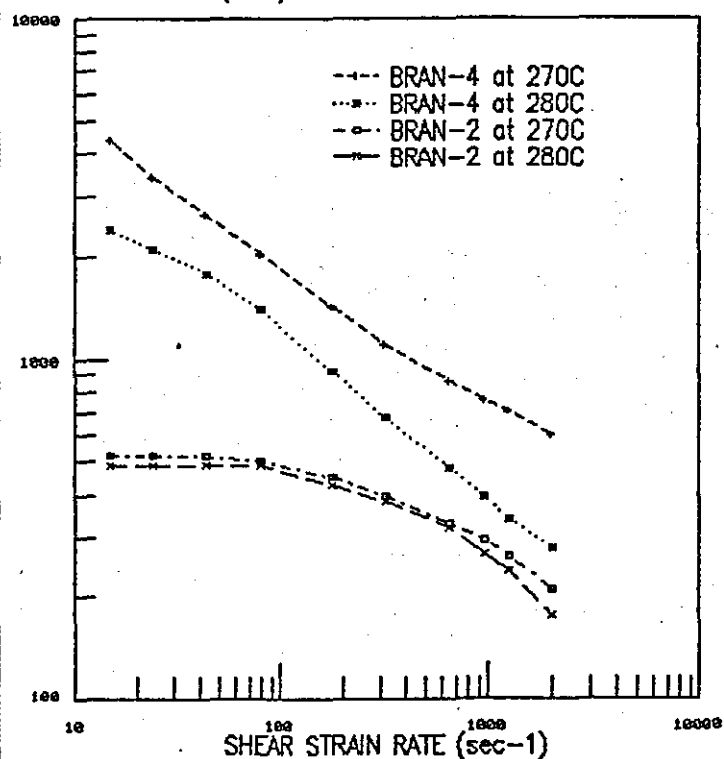
FIGURE 2.20: EFFECT OF TEMPERATURE ON
PETG 6763 COPOLYESTER SHEAR RHEOLOGY
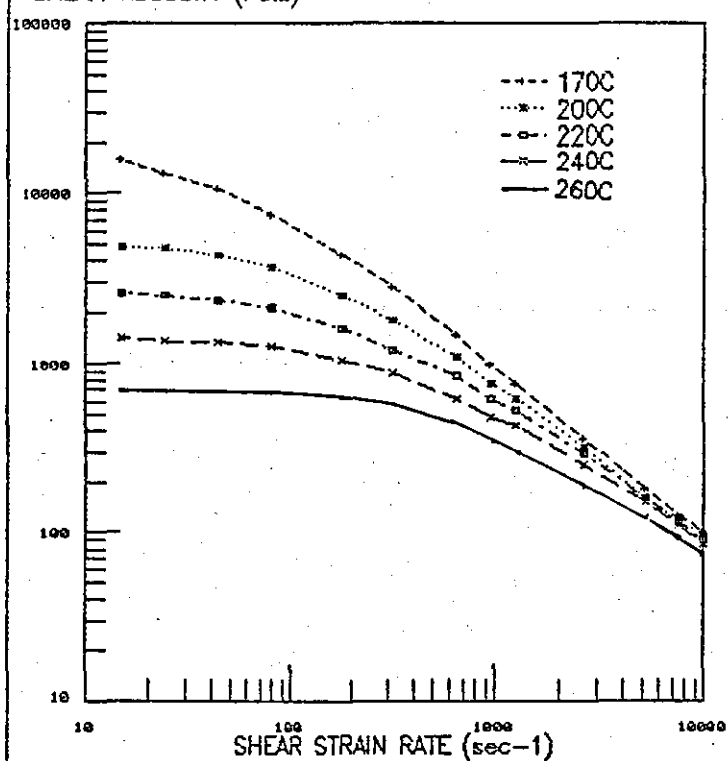
FIGURE 2.21: EFFECT OF TEMPERATURE ON
PCTG 5445 COPOLYESTER SHEAR RHEOLOGY
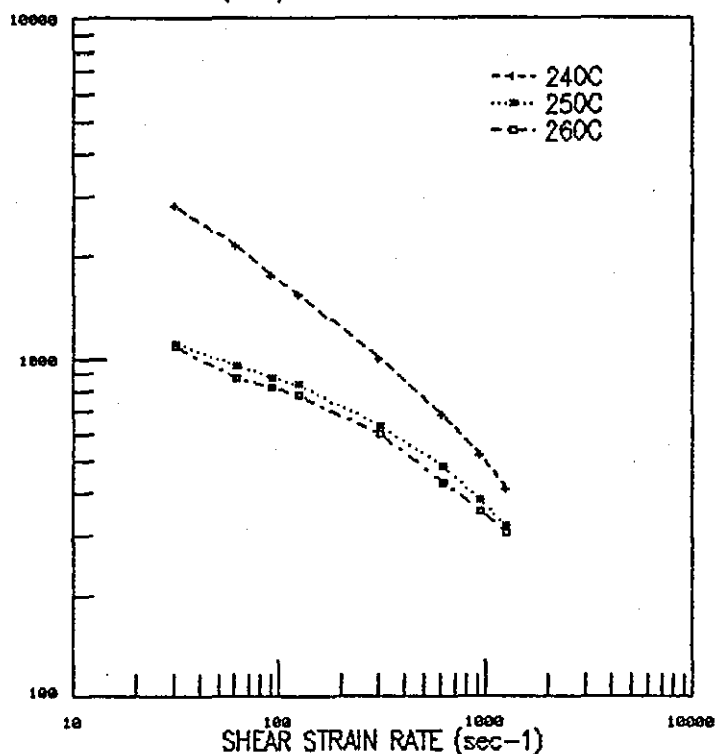
FIGURE 2.22: EFFECT OF TEMPERATURE ON
PCCE 9967 COPOLYESTER SHEAR RHEOLOGY
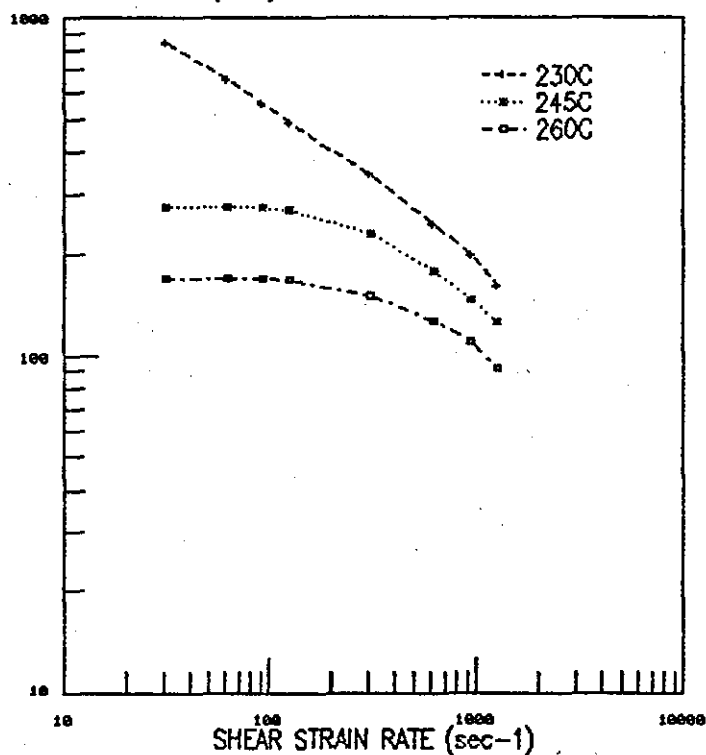
TABLE 2.13: TEMPERATURE SENSITIVITY OF VISCOSITY

POLYMER	(VISCOSITY AT 270°C ÷ VISCOSITY AT 280°C)
B90S	1.91
EX167	2.33
LIN-A	1.36
LIN-B	2.17
LIN-C	1.33
LIN-D	1.97
BRAN-1	1.03
BRAN-2	1.11
BRAN-3	1.02
BRAN-4	1.53
BRAN-5	1.42

2.5 Discussion Of Experimental Shear Rheology Results

2.5.1 Linear PET Polymers

Pseudoplasticity

Figure 2.11 shows that the shear stress increases with increasing shear rate, but the curves are not linear. Therefore the power law relationship (equation (2.14)) is only an approximation of the behaviour over part of the shear rate range, a series of power law relationships can characterise the complete flow curve.

Figures 2.12-2.14 show that the apparent shear viscosity decreases with increasing shear rate (pseudoplastic behaviour). At a shear rate of $100s^{-1}$ the linear PET polymers flow approaches Newtonian flow behaviour; at a shear rate of $1000s^{-1}$ they show mildly pseudoplastic behaviour and at a shear rate of $10000s^{-1}$ they show pseudoplastic behaviour. The power law index (n) values are shown in Table 2.10. No evidence of stress-induced crystallisation was observed (*Boudreaux and Cuculo*[3] reported an increased viscosity at shear rates above 10^4s^{-1} at 275°C, due to stress-induced crystallisation).

Newtonian Viscosity

At low shear rates the viscosity curves approach Newtonian flow behaviour (horizontal curve), the zero shear rate viscosity was estimated by extrapolating the curve to very low shear rates, the

estimated values are shown in Table 2.9. The near—Newtonian viscosity decreases with increasing temperature and decreasing molecular weight.

Temperature Sensitivity

The apparent shear viscosity decreases with increasing temperature. Table 2.13 shows the temperature sensitivity of the different polymers. The viscosities of LIN-A and LIN-C are less sensitive to temperature than the other linear PET polymers.

Effect Of Molecular Weight

Figures 2.13 and 2.14 show the apparent shear viscosity at a given shear rate is higher for polymers with higher molecular weight.

Figure 2.15 correlates melt viscosity data with the weight-average molecular weight. The relationship for linear PET at 270°C is shown as equation (2.35):

$$\eta_{\dot{\gamma}=200s}^{-1} = K(\bar{M}_w)^{4.41} \qquad (2.35)$$

The relationship for linear PET at 280°C is shown as equation (2.36):

$$\eta_{\dot{\gamma}=200s}^{-1} = K(\bar{M}_w)^{4.12} \qquad (2.36)$$

The gradient of the plotted curves in Figure 2.15 (exponent of above relationships) are higher than the "universal" value of 3.4 which has been found to apply to most polymer melts above the critical molecular weight, this maybe due errors caused by estimating the Newtonian viscosity at a shear rate of $200s^{-1}$, alternatively it could be due to entanglements or chain association as a result of PET chemistry such as the molecular polarity.

The convergence of the viscosity curves, in Figures 2.13 and 2.14, at high shear rates indicates that the shear viscosity dependence on molecular weight varies with shear rate.

Table 2.8 shows the linear PET polymers all had similar polydispersity index values, indicating molecular weight distributions of similar breadth. Therefore, no molecular weight distribution effects were observed for the linear PET polymers.

Suitability For Injection Moulding

The low viscosity at high shear rates make these polymers suitable for processing by injection moulding. The absence of stress-induced crystallisation at high shear rates is an attractive polymer

property for the injection moulding of PET bottle preforms. The drop in viscosity observed with the four hydrolysed grades highlights the need for proper drying of the polymers before any melt processing.

2.5.2 Branched PET Polymers

Pseudoplasticity

Figures 2.16 and 2.17 show the molecular weight dependence of the shear rheology of branched PET polymers, the apparent shear viscosity decreases with increasing shear rate (pseudoplastic behaviour) and increases with increasing molecular weight. Figure 2.16 shows that the BRAN-4 and BRAN-5 polymers behaviour can be described by a single power law relationship at 270°C, whilst the other branched polymers require a series of relationships to fully describe them. The power law constants are shown in Table 2.11. The viscosity values are significantly higher than those reported for the linear PET polymers, due to greater interchain entanglement.

The viscosity curves, in Figures 2.16 and 2.17, indicate that the branched PET polymers can be grouped into two sets with respect to flow behaviour: the first set contains BRAN-4 and BRAN-5, which behave in a pseudoplastic manner over the whole range of shear rates studied $(10-1200s^{-1})$; the second set contains BRAN-1, 2 and 3 and at a shear rate of $100s^{-1}$ the flow approaches Newtonian flow behaviour; at a shear rate of $1000s^{-1}$ BRAN-2 shows mildly pseudoplastic behaviour whilst BRAN-1 and BRAN-3 show pseudoplastic behaviour. The power law index (n) values are shown in Table 2.10. As with the linear polymers evidence of stress-induced crystallisation was not observed.

Table 2.11 shows that the power law index values for the branched PET polymers were lower than those for linear PET polymers (Table 2.10), this confirms that the branched polymers are more pseudoplastic. The onset of shear thinning occurs at lower shear rates with the branched PET polymers than with the linear PET polymers. This effect of chain branching is similar to that reported by *Munari, Pilati and Pezzin*[30] for PBT polymers.

Newtonian Viscosity

The first set of branched polymers do not show any near-

Newtonian behaviour in the shear rate range studied.

The Newtonian viscosity values obtained for the second set of branched polymers show that the viscosity decreases with increased temperature and decreased molecular weight. The values were higher than those reported for the linear PET polymers, see Table 2.9.

Effect Of Temperature

Figure 2.19 shows the effect of temperature on the two branched polymers (BRAN-2 and BRAN-4) at either end of the molecular weight range tested, and from each of the two behavioural sets. The shear viscosity decreased with increasing temperature. It can be seen from Figure 2.19 that, the higher molecular weight polymer, BRAN-4 has a greater temperature sensitivity than BRAN-2. Table 2.13 shows that the viscosities of the two sets of branched polymers have different temperature sensitivities, the first (more pseudoplastic) set being more temperature sensitive. A temperature superposition has been attempted and is described later, see Section 2.6. The activation energies are calculated and reported in Section 2.6.

Comparing the BRAN-2 curve in Figures 2.16 and 2.17 with the B90S curves at the same temperature in Figure 2.12 it can be seen that the low shear rate viscosities are very similar for both the branched and linear PET polymers. This infers that either (i) the branches are not long enough to form interchain entanglements; or (ii) there are an insufficient number of branches to form interchain entanglements, otherwise a significant difference in the low shear rate viscosity values would have been observed.[22]

This observation suggests a possible explanation for the existence of the two sets of flow behaviour reported for the branched PET polymers. The possible explanation being that the difference between the two sets is that the more pseudoplastic set (BRAN-4 and BRAN-5) has a higher number of branches, or longer branches, resulting in more effective interchain entanglement than the second set.

Effect Of Molecular Weight

Figure 2.18 correlates melt viscosity data with the weight-average molecular weight. The outlying two datapoints on the curves

in Figure 2.18 are due to inaccuracy in determining the molecular weight of branched polymers from GPC when the degree of branching is unknown. The relationship for branched PET at 270°C is shown as equation (2.37)

$$\eta_{\dot{\gamma}=20s}{}^{-1} = K(\bar{M}_w)^{4.86} \qquad (2.37)$$

The relationship for branched PET at 280°C is shown as equation (2.38):
$$\eta_{\dot{\gamma}=20s}{}^{-1} = K(\bar{M}_w)^{3.57} \qquad (2.38)$$

The exponent value for the 280°C curve is close to the "universal" value of 3.4 quoted by *Brydson*.[13] The higher exponent value obtained for the 270°C curve indicates a high order of chain entanglement or chain association at this temperature.

The convergence of the viscosity curves, in Figures 2.16 and 2.17, at high shear rates indicates that the shear viscosity dependence on molecular weight varies with shear rate.

Effect Of Molecular Weight Distribution

The viscosity increases as the molecular weight distribution broadens. The onset of shear thinning occurs at lower shear rates with the broader molecular weight distribution polymers.

Suitability For Extrusion Blow Moulding

The high viscosity values at low shear rates obtained for BRAN-4 and BRAN-5 were the criteria aimed for when these grades were developed commercially for the extrusion blow moulding process.[33,34] *Baron et al*[35] proposed shear rheological criteria for the suitability of polymers for the extrusion blow moulding process, these being (i) very high shear viscosity at low shear rates; (ii) low viscosity at high shear rates. Applying the criteria proposed by *Baron et al*[35] to the branched polymers tested, BRAN-4 and BRAN-5 would appear to meet the criteria better than the other polymers, but all the branched polymers have much higher shear viscosities at low shear rates than the linear PET polymers (which are known to be unsuitable for extrusion blow moulding). BRAN-4 has viscosity values at a shear rate of 100s[-1] which are four times those of the B90S bottle grade linear PET, meeting criteria (i); whilst at 1000s[-1] the viscosity value are only double those of B90S, meeting criteria (ii). Therefore the branched PET polymers appear suitable for extrusion blow moulding.

However, the criteria should also include melt elasticity and the tensile flow behaviour of the polymers, both of which are important in the extrusion blow moulding process. These properties are studied later in Section 2.6 and Chapter 3.

2.5.3 PETG Copolyester

Pseudoplasticity

Figure 2.20 shows the pseudoplastic nature of the PETG copolyester, the shear viscosity decreases with increasing shear rate and temperature. The values of viscosity are similar to those of the branched PET polymers and higher than the linear PET polymers. At low shear rates the behaviour approaches that of a Newtonian fluid. At a shear rate of $100s^{-1}$ the higher temperature curves approach Newtonian flow behaviour while the lower temperature curves show mildly pseudoplastic behaviour; at a shear rate of $1000s^{-1}$ all the curves show pseudoplastic behaviour, the lower temperature curves being very pseudoplastic. The power law index (n) values are shown in Table 2.12. At higher shear rates the curves for different temperatures converge, showing less temperature sensitivity at the higher rates.

The PETG copolymer has higher viscosity values, at lower temperatures, than the linear PET polymers. This is due to the PETG molecular chain being stiffer, as it contains a cyclic component in the glycol monomer in place of the linear alkane component in the glycol monomer used in the linear PET polymers. The PETG copolymer contains a high cyclohexane dimethanol comonomer content (35%) and being bulkier than linear PET has greater interchain distances and therefore decreased entanglement. Also any residual glycol will act as a plasticiser. The reduced entanglements and _____ plasticisation effects account for the level of pseudoplasticity of PETG.

Newtonian Viscosity

Table 2.9 shows the near-Newtonian viscosity estimates for the PETG copolyester, the viscosity decreases with increasing temperature. The values of η_o are higher than the other polymers tested. The processing temperatures for the amorphous PETG copolyester are lower than those for the PET polymers.

Suitability For Extrusion Blow Moulding

PETG copolyester was developed primarily for the extrusion blow moulding process.[37] The high viscosity at low shear rates and low viscosity at high shear rates satisfy the criteria proposed by *Baron et al*[5], the tensile viscosity and elastic behaviour are reported in Chapter 3 and Section 2.6 respectively. The suitability of PETG for extrusion blow moulding is tested by processing trials in Chapter 6.

2.5.4 PCTG Copolyester

Pseudoplasticity

Figure 2.21 shows the pseudoplastic behaviour of the PCTG copolyester the viscosity decreasing with increasing shear rate. The shear viscosity decreases with increasing temperature and the pseudoplasticity decreases with increased temperature. The power law constants are shown in Table 2.12.

The PCTG copolymer has higher viscosity values, at lower temperatures, than the linear PET polymers. The higher viscosity of PCTG is due to the molecular chain being stiffer, the cyclic component in the comonomer being stiffer than the linear alkane component in the linear PET monomer. The copolymer is a glycol-modified poly(1,4-cyclohexylene dimethylene terephthalate) and is bulky enough to prevent crystallisation. It therefore has greater interchain distances and therefore decreased entanglement than linear PET. Also any residual glycol will act as a plasticiser. The reduced entanglements and ... plasticisation effects account for the level of pseudoplasticity of PCTG at low shear rates.

Suitability For Injection Moulding

The PCTG becomes less temperature sensitive at higher temperatures, this can be beneficial in the injection moulding process, for which this material has been developed[39], resulting in less variation in flow during filling; caused by temperature inhomogeneity through the polymer, shear heating and pressure effects on the temperature of the melt. If the flow behaviour remains steady then the shot-to-shot variation of the finished moulding will be reduced, resulting in better quality parts. The low temperature sensitivity could be a disadvantage at high temperatures in respect

to process economics, an increase in temperature will not result in any significant reduction in viscosity, hence energy could be wasted if the temperature increased without any gain in a reduced resistance to flow.

A useful adjustment, for optimising conditions has been effectively removed, therefore tool design needs to be carried out more carefully, taking material flow properties into account at the drawing board stage.

The application of this rheological data to injection moulding has been described in Chapter 5.

2.5.5 PCCE Copolyester

Pseudoplasticity

Figure 2.22 shows the PCCE copolyester behaves as a pseudoplastic, the shear viscosity decreasing with increasing shear rate and increasing temperature. The pseudoplasticity increases with shear rate and decreases with temperature. The power law constants are shown in Table 2.12. The values of viscosity for PCCE are similar to those of the linear PET polymers, albeit at lower processing temperatures. This indicates the comonomer would reduce the viscosity at a given temperature, possibly acting by the copolymer chain being bulkier, hence increasing the interchain distances and decreasing the entanglement and chain association effects, also the dipole interaction between the chains will have been diluted by the reduced number of active polar groups per unit volume. Alternatively, the rubbery segments of the copolymer, which have been introduced to produce this new thermoplastic elastomer, may act like a plasticiser spacing out the molecules, increasing the interchain distances and therefore physically reducing the amount of entanglement and chain association that can occur.

Suitability For Extrusion Blow Moulding

Eastman Plastics developed PCCE copolyester for blown film and flexible extrusion blow moulded products.[38] Comparing the viscosity curves in Figure 2.22 with the extrusion blow moulding polymers reported by *Baron et al*[5] in Figure 2.9, it can be seen that using the criteria proposed by *Baron et al* this polymer would appear to be

unsuitable for extrusion blow moulding, at the temperatures shown in Figure 2.22. However, this situation highlights the need for additional information, such as the elastic behaviour of the melt and the tensile rheological properties, these are discussed in Section 2.6 and Chapter 3 respectively.

2.6 Recoverable Shear Strain

2.6.1 Introduction

As polymer melts are viscoelastic, the melt elasticity is an important characteristic as well as the melt viscosity. When a polymer is sheared some of the molecular chain entanglements restrain the molecules preventing them slipping past each other as in viscous flow, resulting in restrained chain uncoiling. On release of shearing stresses, the molecules tend to recoil and are pulled back by the restraining forces, this is the elastic response, caused by the increased molecular bond angle and increased bond length, of the viscoelastic material. The elastic phenomena are superimposed on the viscous flow and are manifested during processing as die swell, melt fracture, 'sharkskin', frozen-in orientation and draw-down.[13]

In Section 2.1.2 the elastic shear modulus, G, is shown as the constant of proportionality in equation (2.5), it is an important rheological property used in the equations governing the analogue models used to describe flow behaviour, (see equations (2.9) and (2.10)). The shear modulus is given by equation (2.27).

$$G = \tau_w \div \gamma_R \qquad (2.27)$$

The apparent modulus is dependent on factors such as temperature, pressure, stress, geometry of deformation and time.[6] In the practical response of polymer processing it is often the interactions between viscosity, elasticity and rupture phenomena which determine the success of the operation.[6]

2.6.2 Test Procedure

Cogswell[6] described the method of inference of elastic response

from capillary flow, based on interpreting die swell as evidence of recoverable strain. The relationship used is shown in Section 2.1.3.1 as equation (2.17) and Figure 2.4. By making comparative measurements the elastic modulus can be derived.

Samples of the extrudate from the capillary rheometer were cut. The diameter of the solidified extrudate, within 5mm of the leading edge, was measured. The swell ratio of extrudate diameter over the die diameter was recorded. The swell ratio from the L=20mm die, B_L, and the zero length die, B_O, approximate to the minimum and maximum values of swell ratio.[6] The post-extrusion swelling from the zero length die was interpreted as the recoverable extension and is reported in Chapter 3. The post-extrusion swelling from the L=20mm die was interpreted as the recoverable shear strain, γ_R, using equation (2.17) and Figure 2.4. The shear modulus, G, was calculated using equation (2.27).

2.6.3 Shear Modulus Data

Several difficulties were encountered obtaining the capillary rheometer extrudate for the linear PET polymers: significant draw-down of the extrudate occurred, the extrudate sagged under its own weight and became tapered (especially with the hydrolysed grades); the extrudate deformed during the cutting and solidification period; the extrudate was very tacky and stuck to the knife, used to cut the sample, and consequently became misshapen. Thus, die swell data was not obtained for most of the linear PET polymers. However, Figure 2.23 shows the elastic modulus as a function of shear stress for B90S linear PET at 280°C.

Figures 2.24 and 2.25 show the effects of molecular weight and molecular weight distribution on the elasticity of the branched PET polymers at 270°C and 280°C respectively.

Figures 2.26, 2.27 and 2.28 show the effect of temperature on the elasticity of the three copolyesters: PETG, PCTG and PCCE respectively.

Table 2.14 summarises the effects of temperature, molecular weight and molecular weight distribution on the shear modulus G and the apparent Maxwell relaxation time η/G at a shear stress of 0.1MPa.

TABLE 2.14: SHEAR MODULUS AND RELAXATION TIME

POLYMER	$\bar{M}_w$	$\bar{M}_w/\bar{M}_n$	Temperature (°C)	G (MPa)	η/G (s)
B90S	64650	1.6	280	0.006*	0.034*
BRAN-1	92600	2.35	270	0.021	0.024
			280	0.024	0.017
BRAN-2	87000	2.2	270	0.055	0.008
			280	0.038	0.011
BRAN-3	122000	2.8	270	0.022	0.036
			280	0.023	0.029
BRAN-4	130000	2.6	270	0.020	0.150
			280	0.018	0.078
BRAN-5	88200	2.4	270	0.018	0.142
			280	0.017	0.067
PETG	67900	1.75	170	0.132†	0.002†
			200	0.083	0.057
			220	0.058	0.040
			240	0.101	0.013
			260	0.074	0.009
PCTG	67300	1.95	240	0.094	0.027
			250	0.090	0.009
			260	0.101	0.006
PCCE			230	0.032	0.011
			245	0.038	0.005
			260	0.045	0.002

* Data for τ = 0.0255MPa.
† Data for τ = 0.225MPa.

FIGURE 2.23: SHEAR MODULUS OF B90S
LINEAR PET AT 280C

FIGURE 2.24: SHEAR MODULUS OF BRANCHED
PET POLYMERS AT 270C
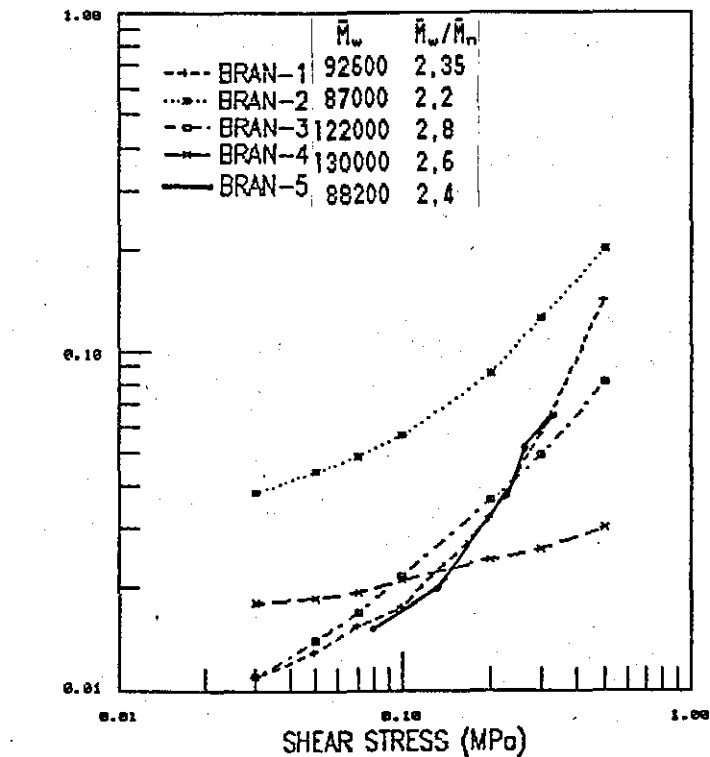
FIGURE 2.25: SHEAR MODULUS OF BRANCHED
PET POLYMERS AT 280C

SHEAR MODULUS (MPa)

	$\bar{M}_w$	$\bar{M}_w/\bar{M}_n$
BRAN-1	92600	2,35
BRAN-2	87000	2,2
BRAN-3	122000	2,8
BRAN-4	130000	2,6
BRAN-5	88200	2,4

SHEAR STRESS (MPa)
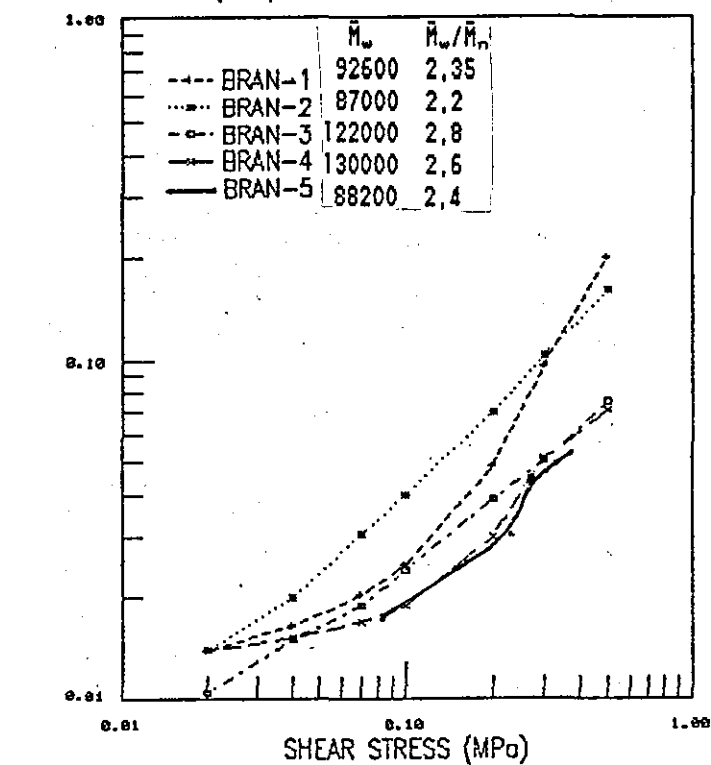
FIGURE 2.26: EFFECT OF TEMPERATURE ON
THE SHEAR MODULUS OF PETG COPOLYESTER

SHEAR MODULUS (MPa)

170C
200C
220C
240C
260C

SHEAR STRESS (MPa)
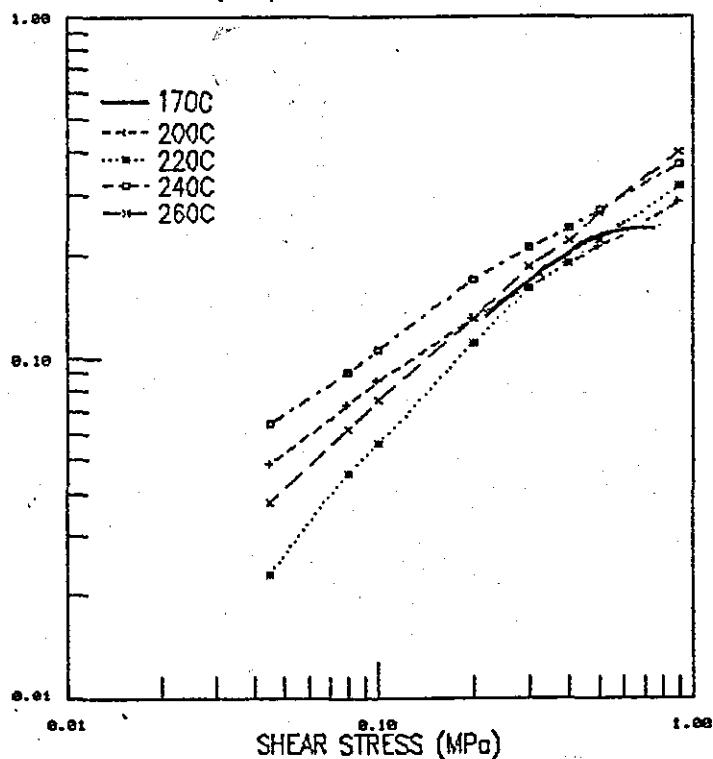
FIGURE 2.27: EFFECT OF TEMPERATURE ON
THE SHEAR MODULUS OF PCTG COPOLYESTER

SHEAR MODULUS (MPa)

SHEAR STRESS (MPa)
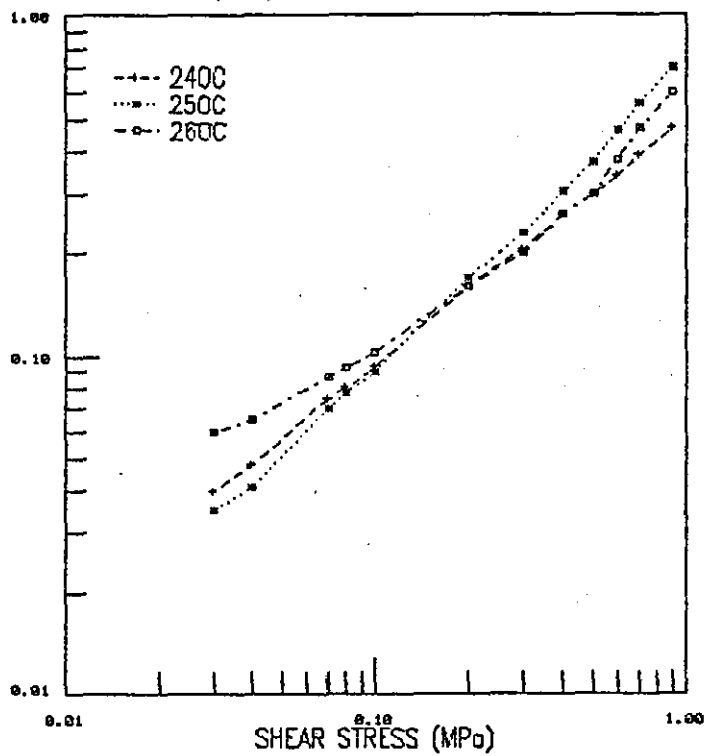
FIGURE 2.28: EFFECT OF TEMPERATURE ON
THE SHEAR MODULUS OF PCCE COPOLYESTER

SHEAR MODULUS (MPa)
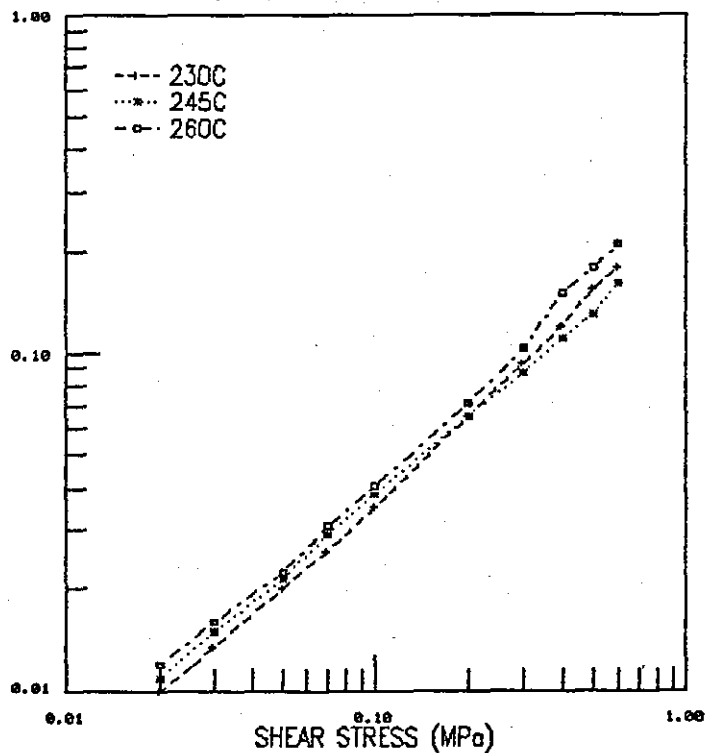
SHEAR STRESS (MPa)

2.6.4 Discussion Of Experimental Recoverable Shear Results

2.6.4.1 Linear PET Polymers

Figure 2.23 shows that B90S has a shear modulus that increases rapidly with increasing shear stress. Figure 2.23 and Table 2.14 show that B90S has very low shear modulus values (compared to the branched polymers) at 280°C and over the shear rate range used. The low shear modulus values are affected by the low viscosity values (see Figure 2.12) over the shear rate range used. Also linear polymers have less chain entanglements than branched polymers. The elasticity data supports the criteria proposed by *Baron et al*[5] and discussed in Section 2.5.6. These results explain why B90S PET cannot be extrusion blow moulded.

2.6.4.2 Branched PET Polymers

Table 2.14 shows that the shear modulus values for the branched PET polymers are greater than the value for B90S linear PET. Figures 2.24 and 2.25 show that the shear modulus for branched PET polymers increases with increasing shear stress. Table 2.14 shows that generally temperature has little effect on the shear modulus, BRAN-2 is an exception to this trend its modulus decreasing significantly with a 10°C temperature rise. Comparing Figures 2.24 and 2.25 with Figure 2.19, it can be seen that the shear modulus for branched PET polymers is less temperature sensitive than the shear viscosity. This result agrees with *Cogswell's*[6] generalised statement that the elastic modulus of a polymer is usually very much less sensitive to temperature than viscosity.

The effect of weight-average molecular weight on the shear modulus is shown in Figure 2.25 and Table 2.14, generally the shear modulus decreases with increasing molecular weight, this is due to an increased recoverable strain with higher molecular weight polymers, these being more entangled. BRAN-2 does not follow this trend the shear modulus values being higher than the other branched PET polymers.

Figures 2.24 and 2.25 and Table 2.14 also show a general trend of lower shear modulus with broader molecular weight distribution.

This results in a large but slow recovery. If the broadening of the distribution is caused by the polymers having a higher degree of branching then more molecular entanglement will occur and hence a greater elasticity.

The combination of high elasticity and viscosity make polymers suitable for extrusion blow moulding, The relaxation times shown in Table 2.14 can indicate the suitability of the polymer to certain processes. A low relaxation time indicates that the polymer is suitable for processes that involve dominantly viscous flow, higher relaxation times indicate that the polymer may be suitable for processes which require a higher elasticity, such as the low modulus requirement for a stable parison in extrusion blow moulding.

From Table 2.14 it can be seen that BRAN-4 and BRAN-5 have the greatest relaxation times, these two polymers were found to be suitable for extrusion blow moulding in respect to their viscous behaviour, see Section 2.5.2.

Table 2.14 shows that the relaxation times generally decreased with increasing temperature, decreasing molecular weight and narrower molecular weight distributions.

2.6.4.3 PETG Copolyester

Figure 2.26 shows the shear modulus of PETG copolyester increases with increasing shear stress, at the higher stresses the modulus values are not greatly effected by temperature, the values in Table 2.14 are at the low end of the stress range measured. Comparing Figure 2.26 with Figure 2.20 shows that the shear modulus of PETG is less temperature sensitive than the shear viscosity. Table 2.14 shows that the shear modulus values are greater than those of the linear and branched PET polymers, The relaxation times for PETG decrease with increasing temperature (the 170°C result is an exception to this trend due to the value being calculated from higher stress data). The relaxation times indicate the suitability of PETG to different processes depends on the processing temperature used. At 220°-240°C PETG should be extrusion blow mouldable, whilst at higher temperatures it should be injection mouldable.

2.6.4.4 PCTG Copolyester

Figure 2.27 shows the shear modulus of PCTG copolyester increases with increasing shear stress and is relatively unaffected by temperature. Table 2.14 confirms that the shear modulus is insensitive to temperature change, whilst the relaxation time decreases with increasing temperature. The relaxation times indicate that PCTG is not suitable for extrusion blow moulding but is suitable for injection moulding.

2.6.4.5 PCCE Copolyester

Figure 2.28 shows that the shear modulus of PCCE copolyester increases with increasing shear stress. Table 2.14 shows the shear modulus increases with increasing temperature. Comparing Figure 2.28 with Figure 2.22 shows that the shear modulus of PCCE copolyester is less temperature sensitive than the shear viscosity. Table 2.14 shows the relaxation times decrease with increasing temperature, the low values suggest this polymer is not suitable for extrusion blow moulding in the temperature range quoted.

2.7 Temperature Dependence Of Viscosity

2.7.1 Introduction

The effect of temperature on the shear viscosity of polymers has been discussed in Section 2.1.3.4. Following that discussion, two techniques have been used to study the temperature dependence of the viscosity of the PET polymers discussed in this chapter. The first technique used the relationship shown by equation (2.19), the second technique used a superposition method reported by *Mendelson*.[25] The two techniques have been considered separately below.

2.7.2 Zero Shear Rate Viscosity Temperature Dependence

As previously discussed in Section 2.1.3.4 the temperature dependence of Newtonian liquids can be described by an Arrhenius-type equation:

$$\mu = A.\exp(E/R.T) \qquad (2.19)$$

This method was used by *Boudreaux and Cuculo*[3] in their

comparison of PET, HDPE and PBT; and by *Mishri and Deopura*[32] in their study of PET/PBT blends.

At low shear rates the shear viscosity of polymer melts approaches Newtonian behaviour, and so, equation (2.19) can be applied to polymer melts, using low shear rate viscosity values (η_o).

Taking a natural logarithm form of equation (2.19) results in equation (2.39).

$$\ln(\eta) = \ln(A) + E/RT \qquad (2.39)$$

Equation (2.39) can be considered as equation (2.25),

$$\ln(\eta) = a_o + a_1 (1000/T) \qquad (2.25)$$

where $a_o = \ln(A)$, and $a_1 = E/1000R$.

The slope of a least squares plot of $\ln(\eta)$ versus $(1000/T)$ provides a_1 from which the activation energy, E, can be calculated using equation (2.26).

$$E = (1000) R. a_1 \qquad (2.26)$$

2.7.3 Results

The viscosity values used to determine the activation energies, the shear rate and power law index (n) are listed in Appendix 4. Table 2.15 shows the activation energy, E, and the constant, A, from equation (2.19).

TABLE 2.15: ACTIVATION ENERGIES FROM EQUATION (2.19)

Polymer	Activation Energy (E) (KJ/mole)	(Kcal/mole)	Constant (A)
B90S	134.68	32.19	7.76×10^{-11}
EX167	173.16	41.38	2.67×10^{-14}
LIN-A	76.28	18.23	8.78×10^{-6}
LIN-B	274.46	65.60	2.42×10^{-25}
LIN-C	74.96	17.92	8.34×10^{-6}
LIN-D	173.16	41.38	1.27×10^{-15}
BRAN-1	27.79	6.64	1.61
BRAN-2	10.20	2.44	52.18
BRAN-3	23.82	5.69	5.63
BRAN-4	146.85	35.10	3.40×10^{-11}
BRAN-5	202.60	48.42	1.48×10^{-16}
PETG	69.74	16.67	1.05×10^{-4}
PCTG	121.68	29.08	1.04×10^{-9}
PCCE	120.09	28.70	2.63×10^{-10}

2.7.4 Discussion Of Results

It was expected that the activation energy would increase with increasing molecular weight, as more energy would be needed to disentangle the longer chains. The exceptions to this trend shown in Table 2.15 correspond to either a low power law index value (n) or a relatively high shear rate for the zero shear rate viscosity, η_o, where the estimate was made, see Appendix 4.

The activation energies for the branched polymers can be classified into two sets: the first set, containing BRAN-4 and BRAN-5, in which the zero shear rate viscosity estimate was made from a viscosity curve which had an n value of approximately 0.6, which had activation energy values higher than the linear PET polymers; the second set, containing BRAN-1, BRAN-2 and BRAN-3, had near-Newtonian viscosity curves at the point where estimation of η_o was made, and had lower activation energy values than the linear PET polymers. The higher activation energies are due to more effective interchain entanglement; due to either a larger number of branches, or longer branches.

The copolymers had activation energy values that were similar to the linear PET polymers, indicating a similar temperature sensitivity, albeit for processing in different temperature ranges.

Comparing the activation energy results for B90S (0.733 I.V.) and LIN-A (0.71 I.V.) shown in Table 2.15 with those of *Boudreaux and Cuculo*[3], shown in Table 2.1, for a 0.72 I.V. linear PET. The B90S was found to have an activation energy at 10s^{-1} which was double that reported in Table 2.1 at 64s^{-1}, whilst LIN-A at 25s^{-1} had an activation energy which agreed within 15% with the result in Table 2.1 at 64s^{-1}.

Mishri and Deopura[32] reported an activation energy value for a 0.63 I.V. linear PET which was approximately one third of the value for LIN-B (0.665 I.V.) shown in Table 2.15. However, the value obtained for LIN-B is significantly different to the values for the other linear PET polymers shown in Table 2.15. The activation energy values for LIN-A (0.71 I.V.) and LIN-C (0.598 I.V.) agree to within 10% of the value quoted by *Mishri and Deopura*.[32]

2.7.5 Temperature Superposition

The temperature superposition technique reported by *Mendelson*[25] and described in Section 2.1.3.4 was applied to the polymers in this study to obtain master curves for the different polymers. The ability to construct a master curve for temperature for a given polymer, allows the subsequent use of the master curve for the determination of a flow curve for any temperature within the polymers processing range. A similar technique has also been used by *Gregory and Watson*[1] in their study of linear PET polymers.

The flow curves of a given polymer at various temperatures were plotted, e.g. Figure 2.11, from the curves the average shift factors a_T were calculated using equation (2.21). The shift factors are shown in Table 2.16, the activation energy values calculated using equation (2.22) are shown in Table 2.17.

From these results the master curves, (see Figures 2.29, 2.31, 2.33, 2.35, 2.37 and 2.39), were constructed by plotting $\log(\tau)$ versus $\log(a_T.\dot{\gamma})$. Along with the master curves plots of $\log(a_T)$ versus $1/T$ were plotted, (see Figures 2.30, 2.32, 2.34, 2.36, 2.38 and 2.40). The applicability of the shift factors can be judged by the degree of fit of the data, at the various temperatures, on the constructed master curves. The applicability of equation (2.22) can be judged by the linearity of a plot of $\log(a_T)$ versus $1/T$.

2.7.6 Results

Table 2.16 shows the shift factors determined for the different polymers using equation (2.21). Table 2.17 shows the activation energy values calculated using equation (2.22).

The master curves for the different polymers at a reference temperature and the corresponding shift factor-temperature plots are shown as Figures 2.29-2.40, listed below.

POLYMER	MASTER CURVE	SHIFT FACTOR-TEMPERATURE PLOT
B90S	Figure 2.29	Figure 2.30
Linear PET	Figure 2.31	Figure 2.32
Branched PET	Figure 2.33	Figure 2.34
PETG	Figure 2.35	Figure 2.36
PCTG	Figure 2.37	Figure 2.38
PCCE	Figure 2.39	Figure 2.40

2.7.7 Discussion Of Results

As discussed in Section 2.7.4, the activation energy values were expected to increase with increasing molecular weight. From Table 2.17 it can be seen that for linear PET polymers the activation energy increased with increasing intrinsic viscosity, due to a greater degree of chain entanglement. For the branched PET polymers the activation energy values can be put into two sets: the first set, containing BRAN-4 and BRAN-5, has activation energies higher than those reported for the linear PET polymers; the second set, containing BRAN-1, BRAN-2 and BRAN-3, has activation energies lower than the linear polymers. The higher activation energies are due to more effective interchain entanglement; due to either a larger number of branches, or longer branches.

The PETG copolyester has an activation energy lower than the values reported for the linear PET polymers and between the two sets of branched PET values. The PCTG and PCCE copolyesters had activation energies that were higher than that of PETG and of the same order as the linear PET polymers.

Gregory and Watson[1] reported that the activation energy was independent of molecular weight over an intrinsic viscosity range of 0.31-0.78, the value being 13.6Kcal/mole (56.89KJ/mole), this value is approximately a third of the values reported for linear PET in Table 2.17, also the activation energy has been found to be molecular weight dependent.

The excellent fit of the data at various temperatures to the constructed master curves: Figures 2.29; 2.31; 2.33; 2.35; 2.37 and 2.39 confirms the applicability of the appropriate shift factors. The linearity of the data in Figures 2.30 and 2.36 confirm the applicability of equation (2.22) for linear PET and PETG copolyester. Insufficient data-points inhibit commenting of the other shift factor-temperature curves, but as the technique works for two types of PET polymers it has been assumed to work for the other polymer structure types tested. The different slopes of the shift factor-temperature curves in Figures 2.32 and 2.34 confirms the result that the activation is molecular weight dependent, this suggests that a

third master-parameter, for molecular weight, should be built into the model, see Section 2.8.

Figure 2.29 shows that the choice of reference temperature is arbitrary, the degree of fit remaining unaffected. The lowest test temperature was taken as the reference temperature for each polymer.

The master curve for LIN-B shown in Figure 2.31, has a different shape to the other grades tested, this was probably due to some unknown experimental problem affecting the molecular weight distribution, e.g. degradation producing low molecular weight species which would broaden the distribution.

FIGURE 2.29: B90S LINEAR PET TEMPERATURE SUPERPOSITION MASTER CURVE
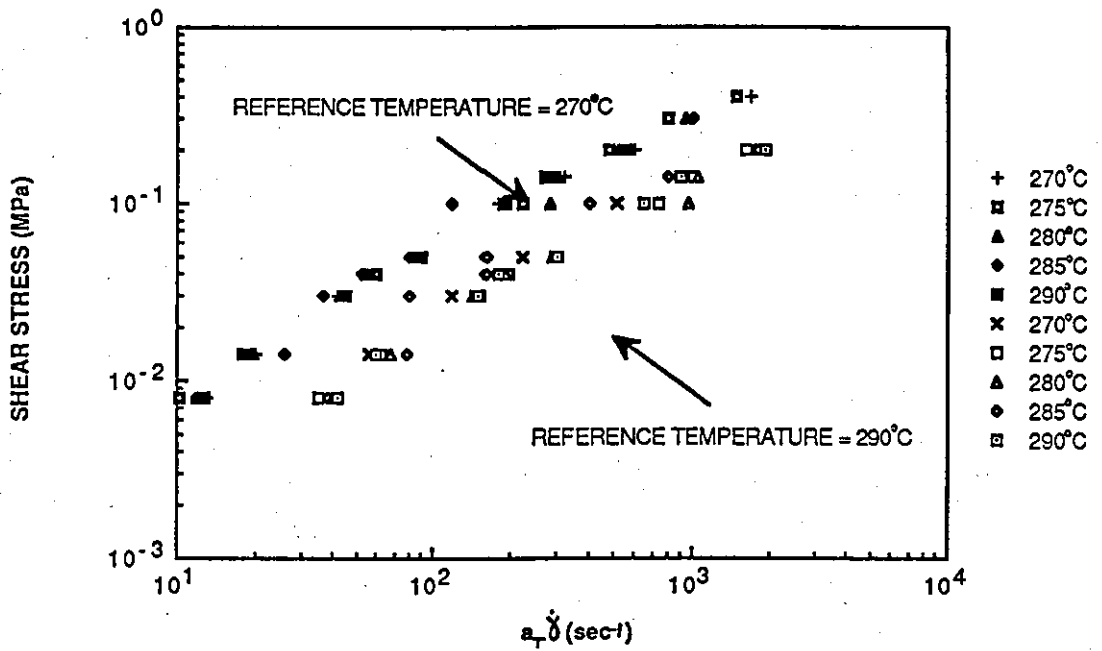
FIGURE 2.30: SHIFT FACTOR-TEMPERATURE RELATIONSHIP FOR B90S LINEAR PET
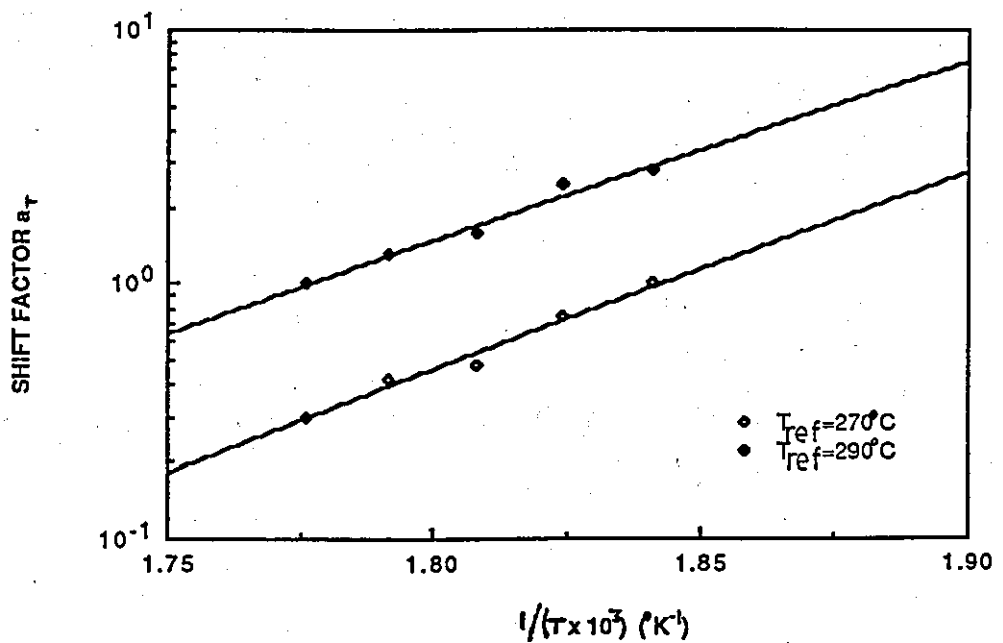
FIGURE 2.31: LINEAR PET TEMPERATURE SUPERPOSITION MASTER CURVES
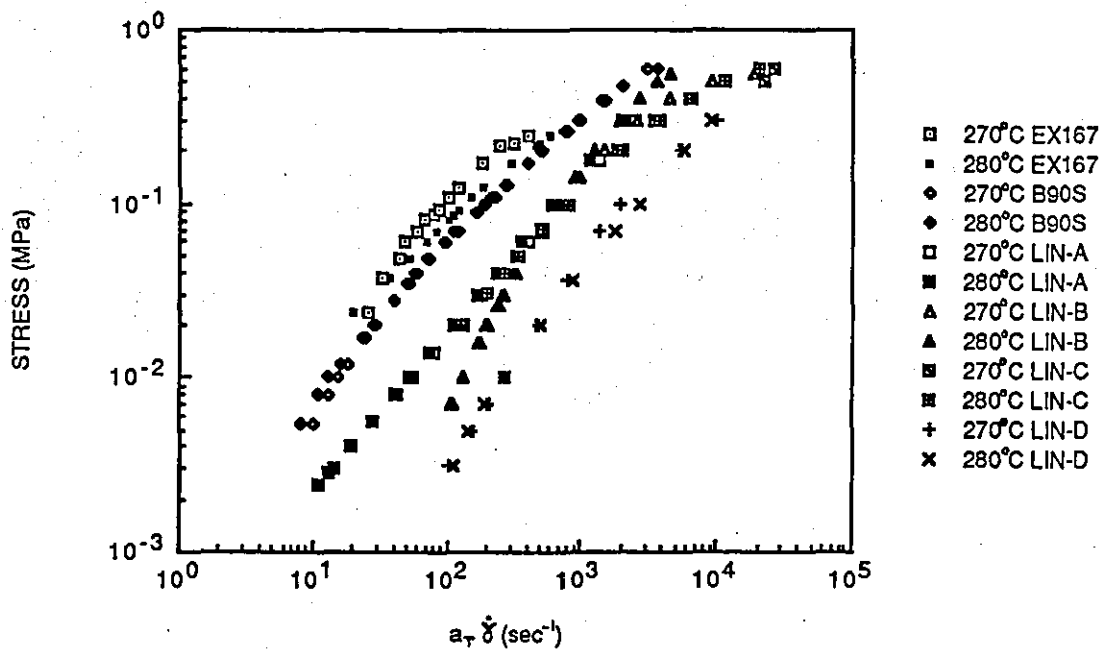
FIGURE 2.32: SHIFT FACTOR-TEMPERATURE RELATIONSHIPS FOR LINEAR PET POLYMERS
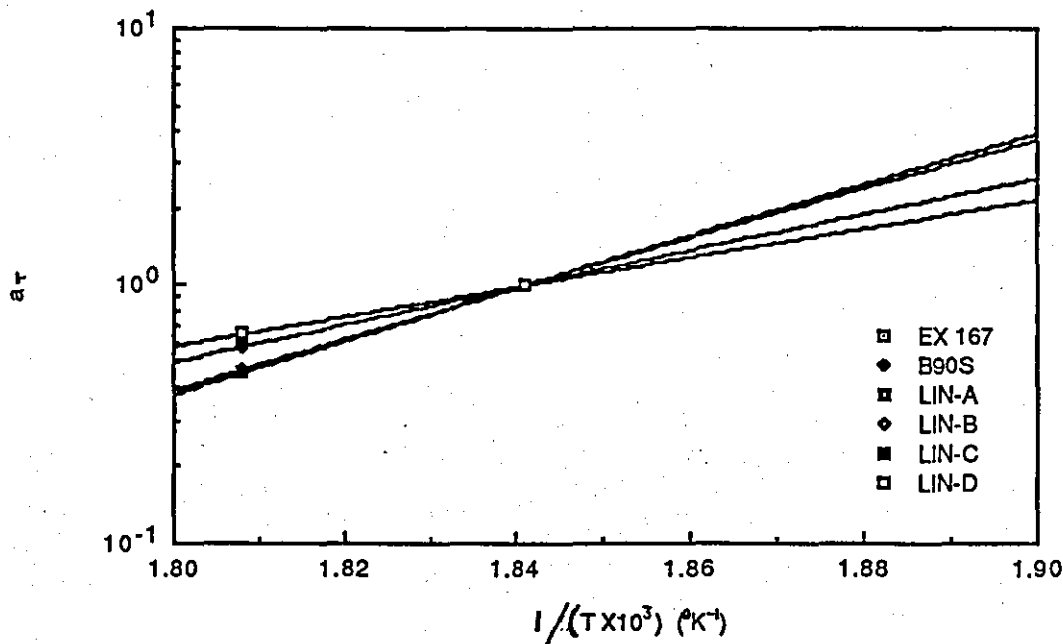
FIGURE 2.33 BRANCHED PET POLYMERS TEMPERATURE SUPERPOSITION MASTER CURVES
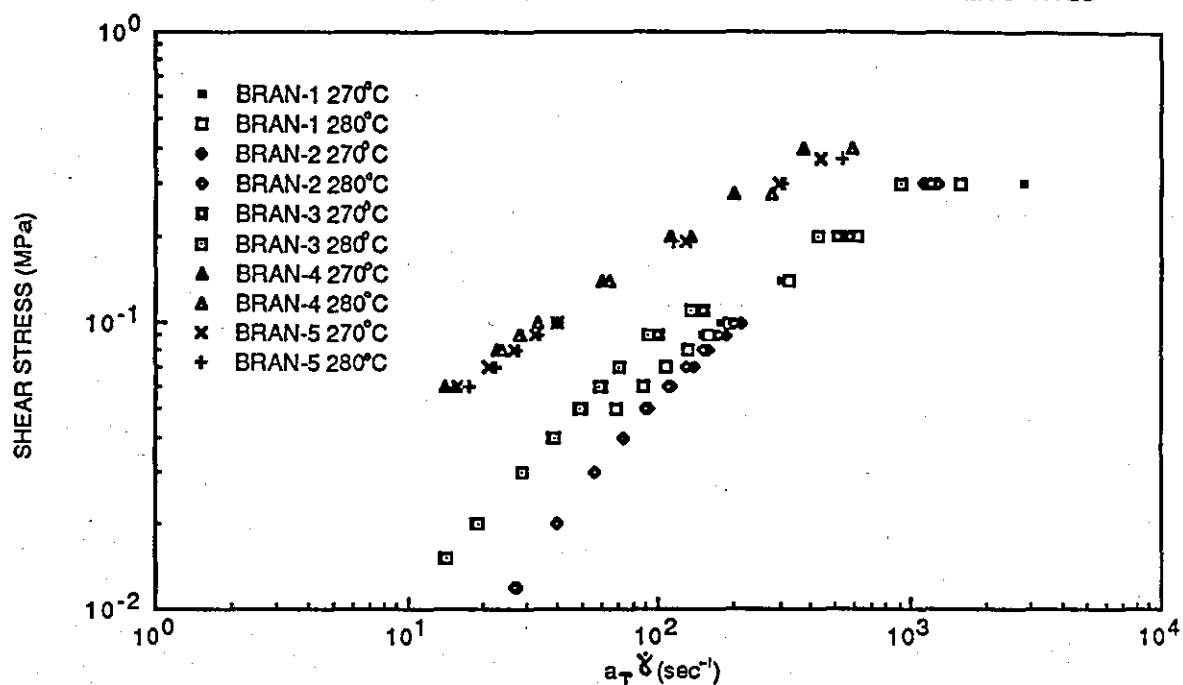
FIGURE 2.34: SHIFT FACTOR-TEMPERATURE RELATIONSHIPS FOR BRANCHED PET POLYMERS
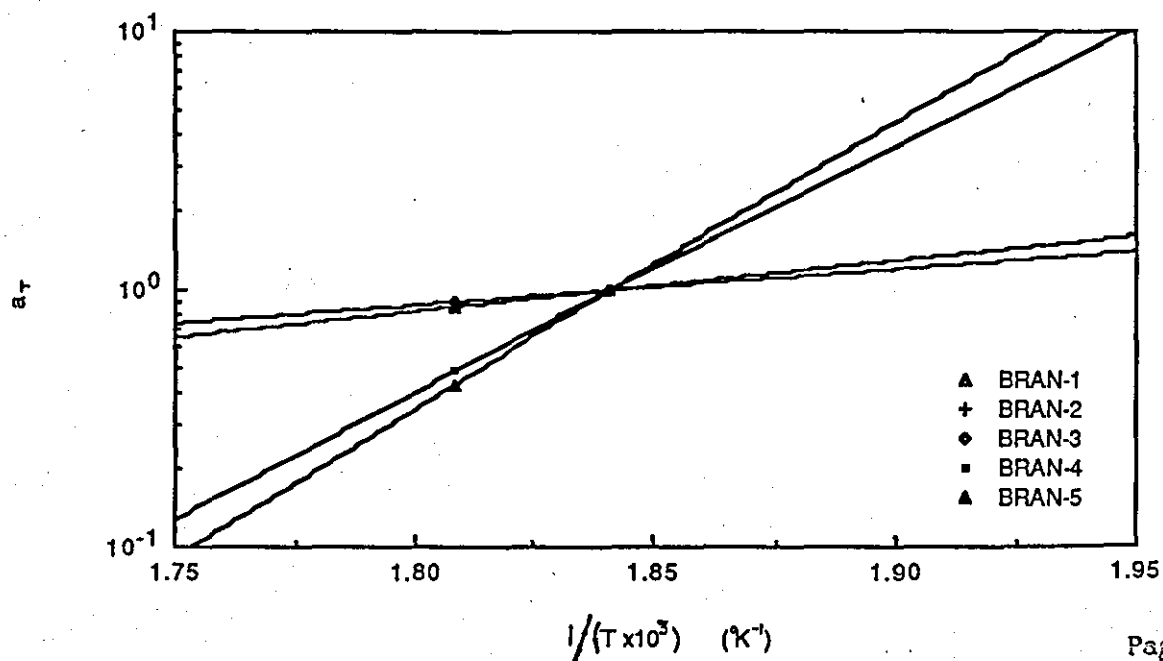
FIGURE 2.35: PETG 6763 COPOLYESTER TEMPERATURE SUPERPOSITION MASTER CURVE
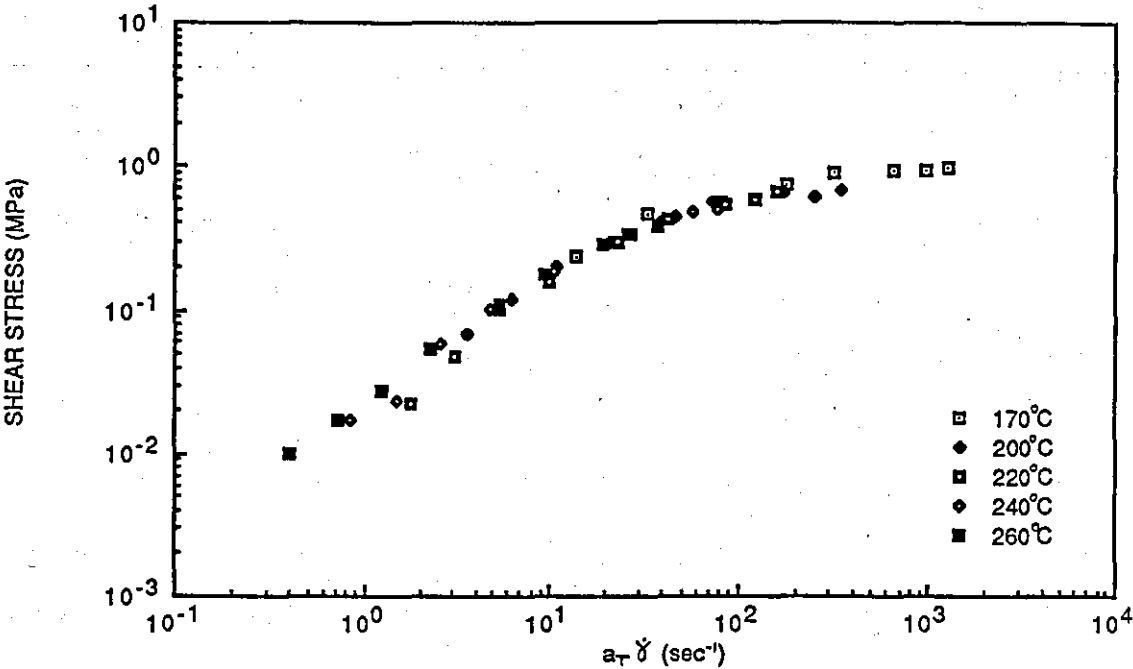
FIGURE 2.36: SHIFT FACTOR-TEMPERATURE RELATIONSHIP FOR PETG 6763 COPOLYESTER

$a_T = B. \exp (E/RT)$

$B = 9.38 \times 10^{-19}$

$E = 76.57$ KJ/mole (18.30 Kcal/mole)
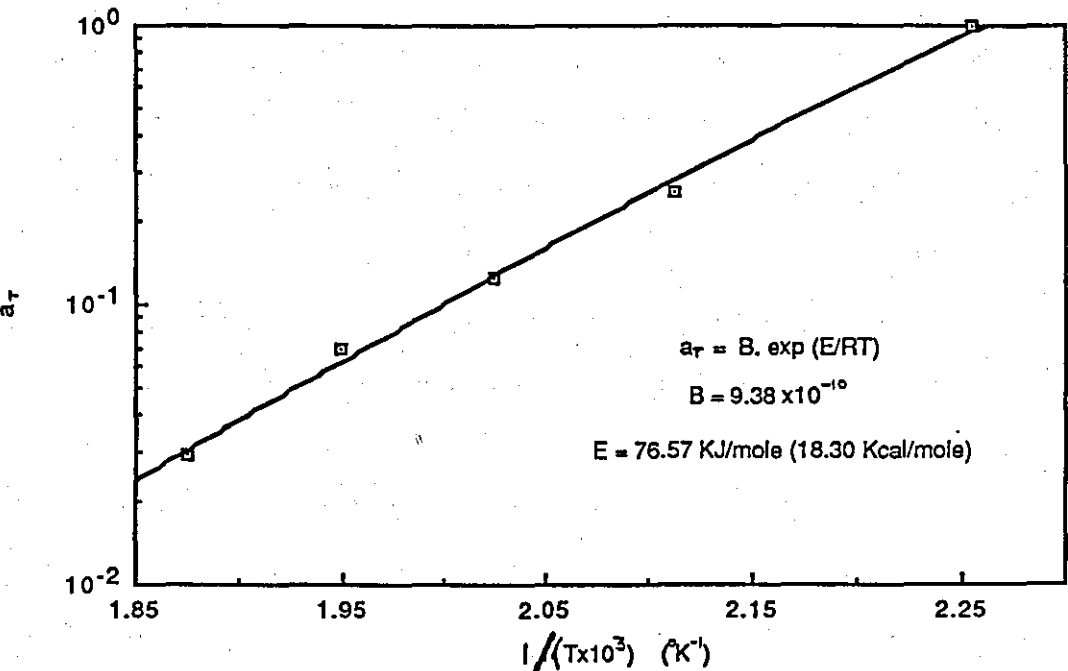
FIGURE 2.37: TEMPERATURE SUPER POSITION
MASTER CURVE FOR PCTG 5445 COPOLYESTER

SHEAR STRESS (MPa)

+ 240C reference
× 250C
□ 260C

$a_T \dot{\delta}$ (sec-1)
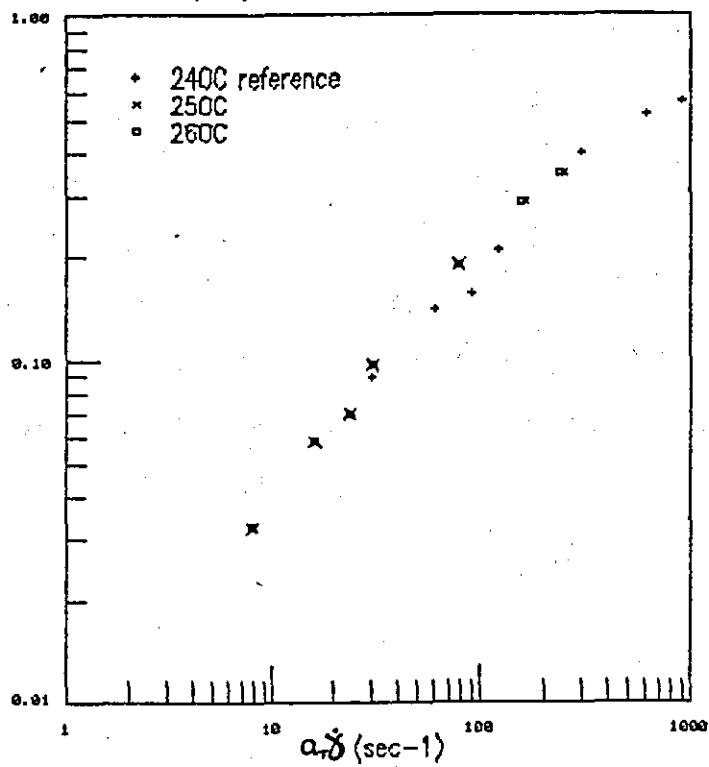
FIGURE 2.38: SHIFT FACTOR-TEMPERATURE
RELATIONSHIP FOR PCTG 5445 COPOLYESTER

SHIFT FACTOR

a_T

$(1/Tx10^3)$, $(°K^{-1})$
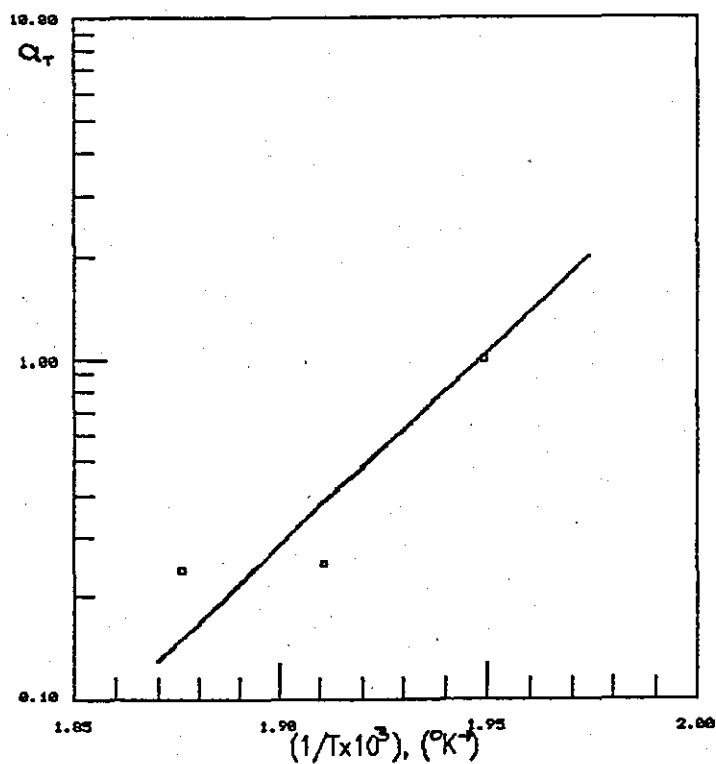
FIGURE 2.39: TEMPERATURE SUPER POSITION
MASTER CURVE FOR PCCE 9967 COPOLYESTER

SHEAR STRESS (MPa)

230C reference
245C
260C

$a_T \dot{\gamma}$ (sec-1)
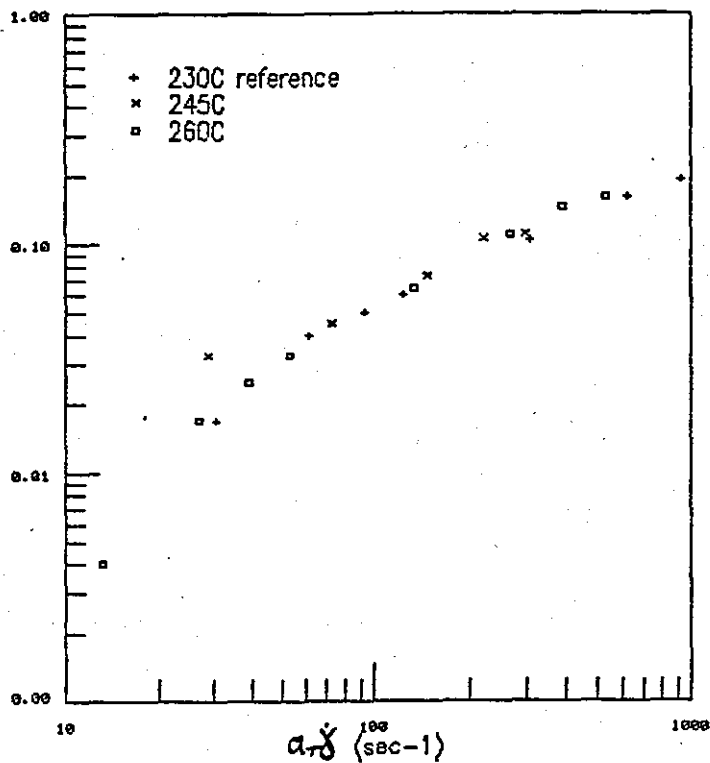
FIGURE 2.40: SHIFT FACTOR–TEMPERATURE
RELATIONSHIP FOR PCCE 9967 COPOLYESTER

SHIFT FACTOR

a_T

$(1/T \times 10^3)$, $(°K^{-1})$
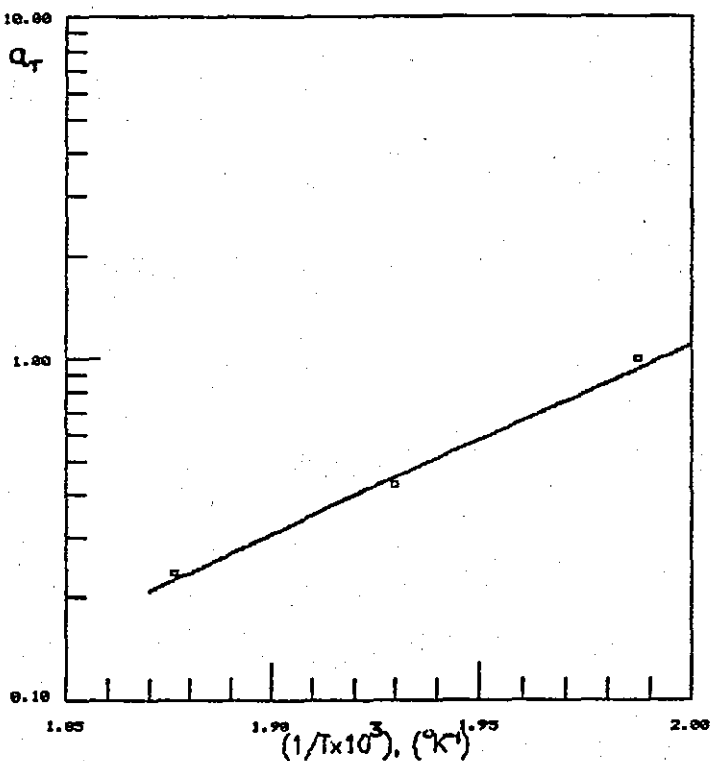
TABLE 2.16: SHEAR RATE-TEMPERATURE SUPERPOSITION SHIFT FACTORS

Polymer	T_{ref} (°C)	Temperature (°C)	Shift Factor(a_T)
B90S	270	270	1
		275	0.737
		280	0.472
		285	0.419
		290	0.300
B90S	290	270	2.807
		275	2.480
		280	1.609
		285	1:283
		290	1
LIN-A	270	270	1
		280	0.645
LIN-B	270	270	1
		280	0.577
LIN-C	270	270	1
		280	0.603
LIN-D	270	270	1
		280	0.658
EX167	270	270	1
		280	0.457
BRAN-1	270	270	1
		280	0.86
BRAN-2	270	270	1
		280	0.86
BRAN-3	270	270	1
		280	0.8985
BRAN-4	270	270	1
		280	0.48
BRAN-5	270	270	1
		280	0.425
PETG	170	170	1
		200	0.255
		220	0.125
		240	0.06
		260	0.029
PCTG	240	240	1
		250	0.25
		260	0.24
PCCE	230	230	1
		245	0.429
		260	0.237

TABLE 2.17: ACTIVATION ENERGIES FROM EQUATION (2.22)

Polymer	T_{ref} (°C)	Activation Energy (E) (KJ/mole)	(Kcal/mole)	Constant (B)
B90S	270	151.4	36.19	2.67×10^{-15}
B90S	290	138.4	33.08	1.45×10^{-13}
LIN-A	270	109.5	26.18	2.92×10^{-11}
LIN-B	270	137.4	32.83	6.15×10^{-14}
LIN-C	270	126.4	30.20	7.04×10^{-13}
LIN-D	270	104.6	24.99	8.80×10^{-11}
EX167	270	195.6	46.75	1.54×10^{-19}
BRAN-1	270	37.68	9.01	2.38×10^{-4}
BRAN-2	270	37.68	9.01	2.38×10^{-4}
BRAN-3	270	26.74	6.39	2.68×10^{-3}
BRAN-4	270	183.36	43.79	2.33×10^{-18}
BRAN-5	270	213.76	51.06	2.77×10^{-21}
PETG	170	76.57	18.29	9.38×10^{-10}
PCTG	240	163.23	38.99	1.95×10^{-17}
PCCE	230	107.19	25.60	7.19×10^{-12}

2.8 Molecular Weight Superposition

2.8.1 Superposition Technique

Gregory and Watson[1] plotted the temperature master curves for various molecular weight PET polymers and found the curves to be parallel; they successfully applied a superposition for molecular weight, see Section 2.1.4. A master curve was constructed allowing subsequent flow curve determination for any molecular weight. They plotted the log weight-average molecular weight $\bar{M}_w$ against the log of the b shift factor, this had a slope of about 3.5 which agreed with the exponent of the Bueche equation.

Following the work of *Gregory and Watson*[1], a molecular weight superposition has been attempted on Figures 2.31 and 2.33 for the linear and branched PET polymers. The shift factor, b, was plotted against three different molecular weight parameters I.V., $\bar{M}_w$ and $\bar{M}_n$, (taken from Tables 2.5 and 2.8) and the degree of mathematical fit was calculated.

2.8.2 Results

The results of the molecular weight superposition are shown below.

Table 2.18 shows the shift factors determined. Table 2.19 shows the mathematical fit of the log shift factor-log molecular weight parameter data to a linear transformation of the form,

$$\log(y) = \log(a) - b.\log(x) \qquad (2.40)$$

this gives a relationship of the form of,

$$y = a.x^{-b} \qquad (2.41)$$

Figure 2.41 shows the master curves constructed for the linear PET polymers. Figure 2.43 shows the master curves constructed for the branched PET polymers. The plots of the shift factor against the best fitting molecular weight parameters are shown as Figure 2.42 for the linear polymers and Figure 2.44 for the branched polymers.

TABLE 2.18: MOLECULAR WEIGHT SHIFT FACTORS

Polymer	T_{ref} (°C)	I.V.$_{ref}$	Temperature (°C)	Shift Factor (b)
EX167	270	0.545	270	25.212
B90S	270	0.545	270	15.587
LIN-A	270	0.545	270	4.654
LIN-B	270	0.545	270	2.099
LIN-C	270	0.545	270	3.297
LIN-D	270	0.545	270	1
BRAN-1	270	1.24	270	0.168
BRAN-2	270	1.24	270	0.1325
BRAN-3	270	1.24	270	0.2445
BRAN-4	270	1.24	270	1
BRAN-5	270	1.24	270	0.837

TABLE 2.19: MATHEMATICAL FITTING OF SHIFT FACTOR CURVES

Parameter	Reference	a	b	r	S.D.
Linear PET					
I.V.	0.96	3.706	5.717	0.899	5.26
$\bar{M}_w$	40500	-54.61	5.127	0.880	4.816
$\bar{M}_n$	25300	-57.11	5.621	0.95	2.218
Branched PET					
I.V.	1.24	-1.120	5.529	0.849	0.242
$\bar{M}_w$	130000	-23.882	1.977	0.406	0.458
$\bar{M}_n$	50700	-28.974	2.621	0.344	0.451

2.8.3 Discussion Of Results

2.8.3.1 Linear PET Polymers

Figure 2.41 shows that double superposition of all data for all temperatures and all molecular weights was achieved for the linear PET polymers. The data points for all molecular weights and temperatures generally form a smooth curve. This confirms the hypothesis of *Gregory and Watson*[1], that the PET molecular weight distribution is independent of molecular weight since it is possible to construct a master curve. They explained their hypothesis as being due to the rapid ester interchange that occurs with PET at temperatures above the melting point.

The LIN-B data deviated from these master curves. Figure 2.31 shows that the flow curve for LIN-B has a different shape than the other linear grades. This may have resulted during extrusion as a result of hydrolytic degradation, the short chain degradation products acting as a plasticiser and affecting the flow behaviour.

Gregory and Watson[1] used the weight-average molecular weight as the molecular weight parameter to relate to the shift factor. Table 2.19 shows that a reasonable correlation was achieved using $\bar{M}_w$, but better parameters to use were number-average molecular weight or intrinsic viscosity. The best correlation was achieved using $\bar{M}_n$.

The linear relationship shown in Figure 2.42, is of the form of equation (2.41) which is similar to equation (2.23) which relates zero shear rate viscosity to the weight-averaged molecular weight. The constant b in Table 2.19 corresponds to the exponent in equations (2.41) and (2.23). The values obtained are much higher than those reported by *Gregory and Watson*[1] who achieved a value of 3.5 which agreed with the exponent in the Bueche equation. The higher value obtained in this study indicates that the linear PET polymers tested here have a higher sensitivity to molecular weight than those previously reported.[1]

2.8.3.2 Branched PET Polymers

Figure 2.43 shows that all the data for all temperatures and molecular weights generally forms a smooth curve. There is greater scatter of the data points on the branched PET master curve than

for the linear PET master curve, though the branched data still correlates quite well, therefore the double superposition technique is still applicable. This suggests that *Gregory and Watson's*[1] hypothesis of PET having a molecular weight distribution independent of molecular weight has limited application to branched PET polymers, and that *Pezzin's* observations contested by the aforementioned hypothesis may apply; that is, the shape of the flow curve is dependent on the molecular weight distribution.

Table 2.19 shows that for the branched polymers the intrinsic viscosity gives the only reasonable fit of the shift factor data to equation (2.41). Figure 2.44 shows the relationship of the b shift factor to the intrinsic viscosity.

The b constant values in Table 2.19 do not agree with the "universal" value of 3.4-3.5 reported by *Brydson*.[13] The b values using the intrinsic viscosity as the molecular weight parameter agree with those for the linear PET polymers.

FIGURE 2.41: LINEAR PET POLYMERS $\bar{M}_n$ SUPERPOSITION MASTER CURVE AT 270°C

FIGURE 2.42: LINEAR PET POLYMERS $\bar{M}_n$
SUPER POSITION MASTER CURVE AT 270C
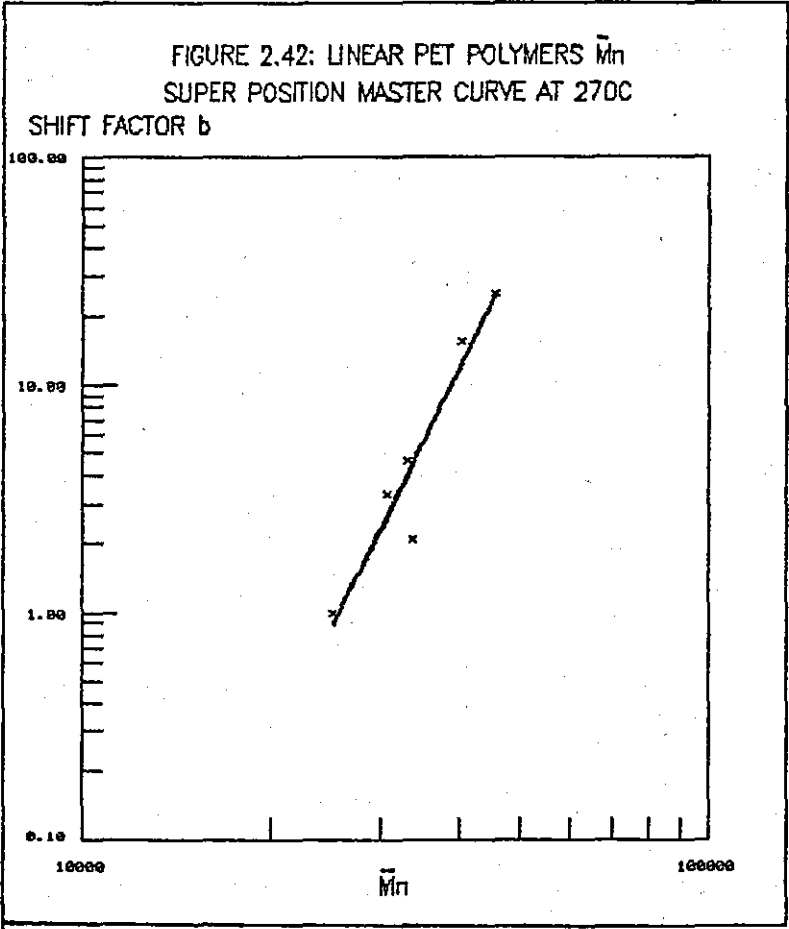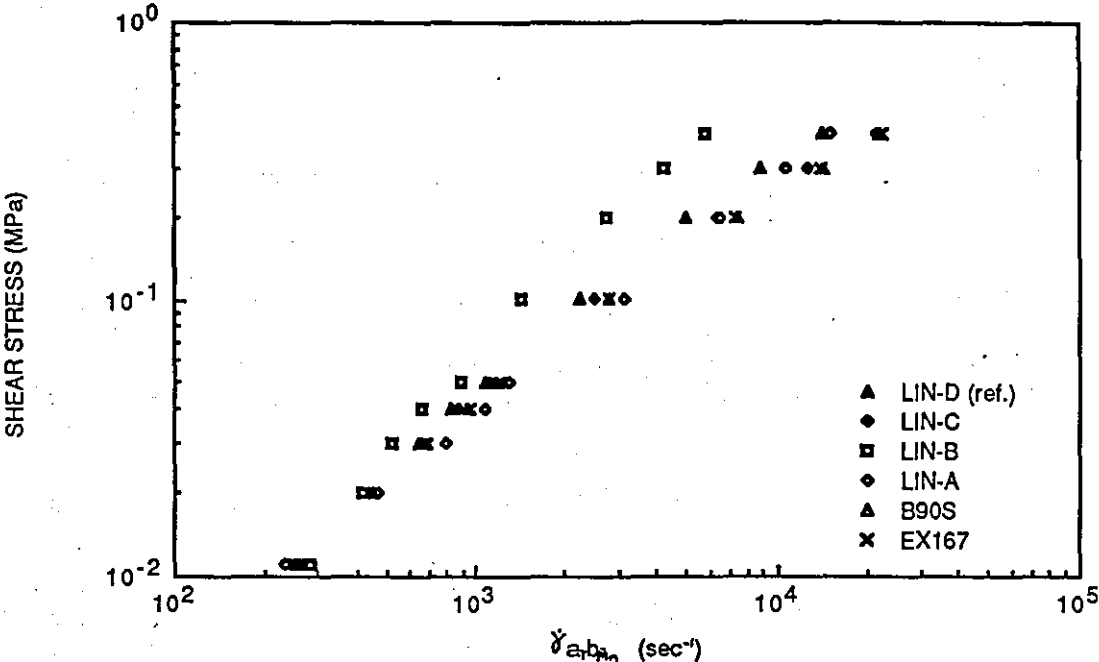
FIGURE 2.43: BRANCHED PET POLYMERS I.V. SUPERPOSITION MASTER CURVE AT 270°C

FIGURE 2.44: BRANCHED PET POLYMERS I.V.
SUPER POSITION MASTER CURVE AT 270C
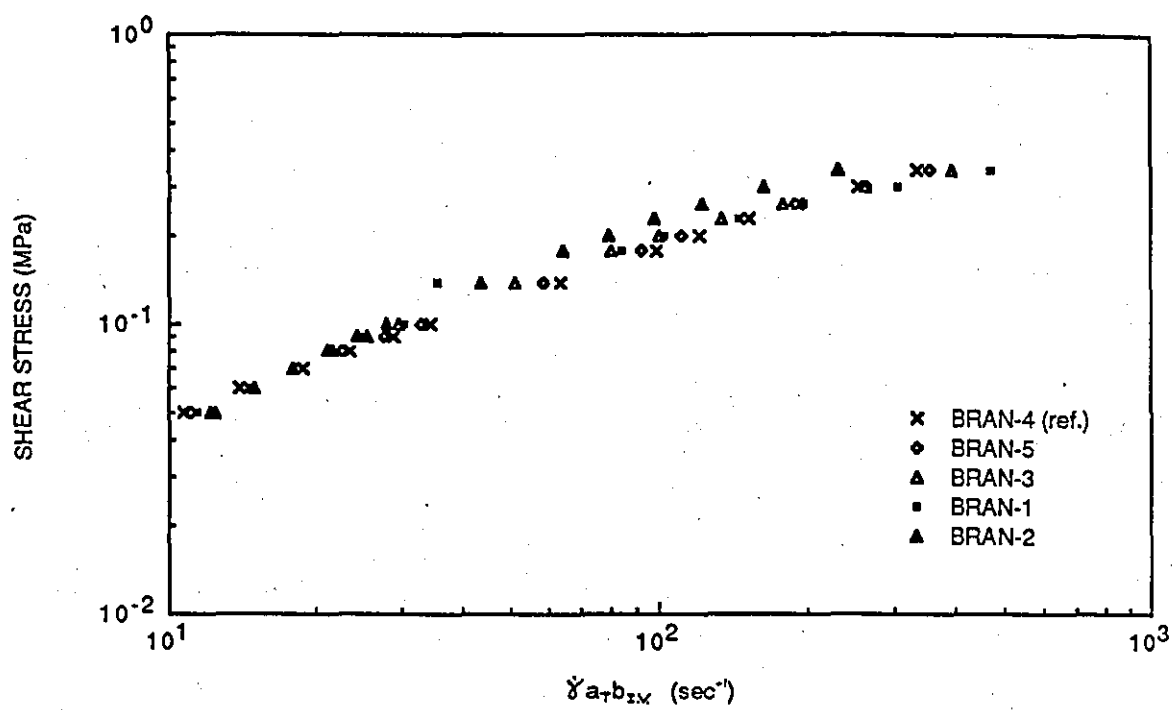
2.9 Conclusions

2.9.1 Summary Of Chapter 2

The aims set out at the beginning of this chapter have been achieved.

The results in this chapter include comprehensive shear flow characterisation for the linear polymers including melt viscosity, elasticity, temperature and molecular weight master curves, which have relevance to various processes for thermoplastic polyesters; some of the results have been applied to injection moulding in Chapter 5.

The results for the branched PET polymers represents what is believed to be the first comprehensive study to characterise these polymers by GPC and to provide full flow characterisation including melt viscosity, elasticity and temperature and molecular weight master curves. These development polymers were developed for the extrusion blow moulding process and these results will help the processor design and develop the process to comply with the flow properties of these novel polymers.

The three copolymers are all new developments and have not been widely studied. The PETG copolyester was developed for extrusion blow moulding and the results here are believed to be the first independent study to characterise the polymer and its flow properties including the melt viscosity and elasticity and the development of a master curve with respect to temperature. These results are relevant to the extrusion blow moulding process and have been applied directly to that process in Chapter 6.

The PCCE copolyester is a new development grade and its properties have not been independently studied before. The viscous flow and elasticity results reported in this chapter will permit processors to assess this novel polymer as to its suitability to various processes including extrusion blow moulding.

The PCTG copolyester was to be fully commercialised in April 1987, and as such is a state of the art polymer, developed to compete with polycarbonate as an injection moulding material. The characterisation of the polymer and flow properties has produced data

relevant to injection moulding processors for the development of the process to handle this novel polymer. The results have been directly applied to the injection moulding process in Chapter 5.

2.9.2 Conclusions From Chapter 2

The PLgel column fitted to the GPC equipment is not suitable for running using a (0.5:99.5) nitrobenzene-tetrachloroethane solvent system. Instead, m-cresol is recommended, as long as checks are made for signs of degradation.

The shear flow behaviour of the polymers has been fully characterised, allowing assessment of the suitability of the different polymers to various processes to be made.

All the polymer melts acted in a pseudoplastic manner, the power law index values ranged from 0.14 to 1.0.

A study of the effect of temperature on the shear rheology of all the polymers tested was carried out. It showed that the shear viscosity decreased with increasing temperature for all the polymers tested.

The activation energy values for all the polymers were determined by two techniques. These are dependent on molecular weight; they increased with increasing molecular weight.

A study of the effect of molecular weight on the shear rheology of the linear and branched PET polymers has been carried out. The shear viscosity increased with increasing molecular weight for all the polymers studied.

The relationship for linear PET polymers at 270°C is

$$\eta_{\dot{\gamma}=200s}{}^{-1} = K(\bar{M}_w)^{4.41}$$

The relationship for linear PET polymers at 280°C is

$$\eta_{\dot{\gamma}=200s}{}^{-1} = K(\bar{M}_w)^{4.12}$$

The relationship for branched PET polymers at 270°C is

$$\eta_{\dot{\gamma}=20s}{}^{-1} = K(\bar{M}_w)^{4.86}$$

The relationship for branched PEt polymers at 280°C is

$$\eta_{\dot{\gamma}=20s}{}^{-1} = K(\bar{M}_w)^{3.57}$$

The branched PET polymers appear to be more pseudoplastic than the linear PET polymers and the onset of shear thinning occurs at a lower shear rate with the branched PET polymers.

Two sets of flow behaviour were observed for the branched PET polymers, BRAN-4 and BRAN-5 were pseudoplastic over the entire shear rate range studied and had high apparent shear viscosities and were more temperature sensitive, whilst the second set of branched PET polymers behaved as near-Newtonian fluids at low shear rates and became more pseudoplastic with increasing shear rate. The lower shear viscosity set of branched PET polymers had near-Newtonian viscosity values which were similar to those of the linear PET polymers.

The activation energies of the branched PET polymers are dependent on the branch chain length. The activation energy values of the branched polymers with short-chain branches are lower than those for the linear PET polymers whilst those with long-chain branches are higher than the values for the linear PET polymers.

It can be concluded that the BRAN-4 and BRAN-5 grades of branched PET have relatively long-chain branches, or more branches, compared with the other three branched PET polymers.

The shear modulus for branched PET polymers and the three copolyesters increases with increasing shear stress. The shear modulus decreases with increasing molecular weight and broader molecular weight distribution for branched PET polymers. The shear modulus for branched PET polymers and the copolyesters are less temperature sensitive than their shear viscosities. The shear modulus of the PETG and PCTG copolyesters were relatively unaffected by temperature. The shear modulus of the PCCE copolyester increased with increasing temperature.

The shear rheology and relaxation times of the linear PET polymers and the PCTG copolyester indicate their suitability for injection moulding, this conclusion has been tested by practical processing trials in Chapter 5.

The branched PET polymers and the PETG copolyester have suitable melt viscosity properties and relaxation times for extrusion blow moulding. This conclusion is tested by practical processing trials in Chapter 6.

The PCCE copolyester does not appear to have melt viscosity properties suitable for extrusion blow moulding. However, it can be

extrusion blow moulded, therefore, it can be concluded that additional information is needed to positively determine the suitability of a polymer for processing by extrusion blow moulding (i.e. the viscosity in tension, see Chapter 3).

Master curves were constructed for all the polymers by a temperature superposition technique. Master curves were also constructed for the linear and branched PET polymers using a double superposition technique which shifted the temperature master curves with respect to molecular weight.

The number-average molecular weight was found to be the best molecular weight parameter to relate to the shift factor b for the linear PET polymers. The resultant relationship being

$$b = -57.11(\bar{M}_n)^{5.6}$$

The intrinsic viscosity was found to be the best molecular weight parameter to relate to the shift factor b for the branched PET polymers. The relationship being

$$b = -1.12(I.V.)^{5.6}$$

2.9.3 Suggestions For Further Work

Further work to extend the applicability of the results in this chapter includes the extension of the temperature range over which the flow properties have been studied and the study of molecular weight effects on the three copolyesters. The branch length and density should be determined for the branched PET polymers. The copolymers should be analysed to determine the second phase content. The flow properties determined should be verified by processing experiments.

3. The Rheology Of PET Melts In Converging Flow

3.1 Aims Of Chapter

This chapter introduces the subject of elongational flows and describes the experimental programme carried out with the objective of characterising the elongational flow behaviour of different thermoplastic polyesters (linear, branched, copolyesters) in converging flow. The aims of the chapter were:

- to produce tensile flow data for the polymers, which can be applied to process design and control;
- to suggest molecular structure explanations for any differences in elongational behaviour observed;
- to assess the suitability of the different polymers to various processes using the data from this chapter and Chapter 2.

3.2 Introduction To Elongational Flow[6,13,55,56]

An elongational flow is an irreversible extension of a body on the application of a tensile stress. *Trouton*[57] studied the elongational rheology of pitch and waxes in 1906. He observed that the coefficient of viscous traction λ, defined in equation (3.1), was three times the value of the shear coefficient of viscosity η; the relationship is shown as equation (3.2).

$$\lambda = \sigma/\dot{\varepsilon} \qquad (3.1)$$

where σ is the tensile stress and $\dot{\varepsilon}$ is the elongation rate.

$$\lambda = 3\eta \qquad (3.2)$$

The coefficient of viscous traction λ is referred to as the tensile viscosity.

Figure 2.1 illustrates the basic geometry of simple shear flow. The diagram of simple extension, shown in Figure 3.1, illustrates the basic geometry of elongational flow.

FIGURE 3.1: SIMPLE EXTENSION[6]
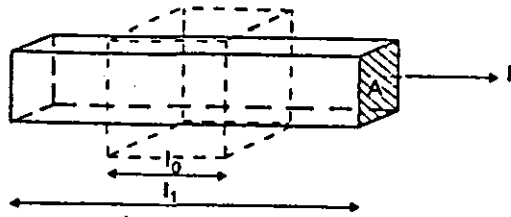
The cross-sectional area A and sample length l both vary during deformation. The stress is applied normal to the surface of the material. The definitions of stress, true strain, Hencky strain and rate of strain are shown in equations (3.3)-(3.6).

Stress, $\qquad \sigma = F/A$ $\qquad$ (Pa) $\qquad$ (3.3)

where σ is the stress and F is the applied force.

strain, $\qquad \varepsilon_T = (l_1 - l_o)/l_o$ $\qquad$ (3.4)

where ε_T is the true strain, l_o is the sample length before deformation and l_1 is the sample length after the deformation.

Hencky strain, $\qquad \varepsilon_H = \int_{l_o}^{l_1} dl/l = \ln(l_1/l_o)$ $\qquad$ (3.5)

where ε_H is the Hencky strain.

Rate of strain, $\qquad \dot{\varepsilon} = v/l$ $\qquad$ (sec^{-1}) $\qquad$ (3.6)
(Elongation rate)

where $\dot{\varepsilon}$ is the elongation rate and v is the velocity, $v = dl/dt$.

The Hencky strain is used in place of the true strain in order to keep the numbers manageable and because equation (3.5) differentiated becomes equation (3.6)

An elongational flow occurs where a material is stretched from one cross-sectional area to another. Polymer melts respond differently to shear stress and elongational stress. A polymer melt subjected to a shear field can disentangle the molecules because of

the rotational flow, see Figure 3.2. However, if the polymer melts are subjected to an elongational stress, being an irrotational flow, see Figure 3.2, the molecules do not necessarily disentangle. Thus, in shearing flows polymer melts are usually pseudoplastic (shear thinning) i.e. the greater the stress, the lower the viscosity. In elongational flows stress may not thin the material to the same extent and can sometimes cause it to stiffen. Polymer melts have been found to show three types of elongational flow behaviour; these are:

(i) Troutonian, where the elongational viscosity is
      independent of elongation rate and equal to three times
      the zero shear rate apparent shear viscosity.

(ii) Tension stiffening, where the elongational viscosity
      increases with tensile stress.

(iii) Tension thinning, where the elongational viscosity
      decreases with increase in tensile stress.

FIGURE 3.2: SIMPLE SHEAR AND EXTENSION[6]

(a) Shear   (b) Extension
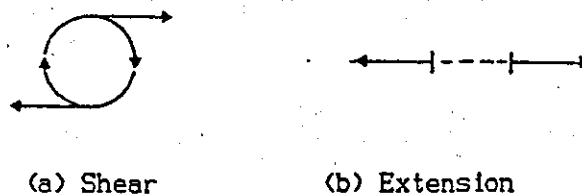
The response of a polymer in an elongational flow field is also dependent on the type of flow involved, (i.e. whether it is a free surface flow or a constrained flow) and also the type of deformation that occurs, i.e. uniaxial extension, uniform biaxial extension or pure shear extension, see Figure 3.3. Before applying any elongational rheological results to processes, the type of flow and deformation occurring in the process needs to be established and data used that has been obtained using a method that involves the same classification of elongational flow. A knowledge of the type of elongational viscosity related to a given process and how the viscosity depends on strain rate is important for equipment design and in defining process operating conditions.[56]

FIGURE 3.3: TYPES OF STEADY ELONGATIONAL DEFORMATION[56]

$$L \neq L'$$
$$R \neq R'$$

Uniaxial extension of a circular rod.
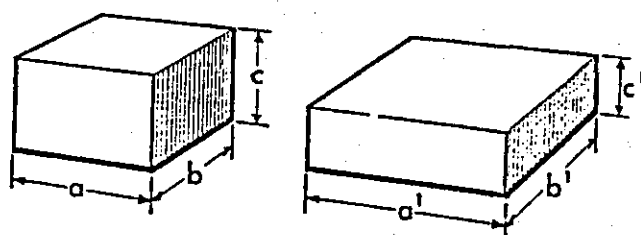
$$\frac{a'}{a} = \frac{b'}{b}$$

Biaxial extension of a rectangular slab. Stretch ratio in a direction ($= a'/a$) is equal to stretch ratio in b direction ($= b'/b$).
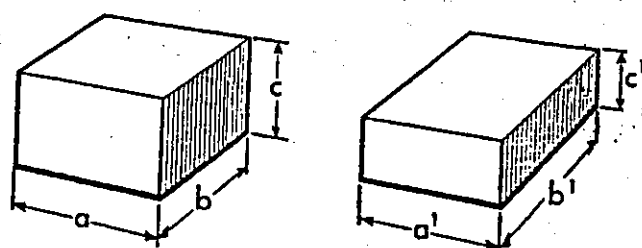
$$\frac{b'}{b} = \frac{c}{c'}$$

Pure shear extension of rectangular slab. Stretch ratio in a direction ($= a'/a$) is unity.

Elongational flows occur in several polymer processes and several reviews have considered different processes.[6,13,55,56] The common processes that involve free surface elongational flows are fibre spinning, film blowing, extrusion blow moulding and thermoforming. Other processes such as extrusion, injection moulding and calendering involve constrained elongational flows.

PET processing often involves an orientation process which

involves an elongational deformation; therefore there is a growing need to study the elongational rheology of PET. PET processes such as fibre spinning and monofilament extrusion involve uniaxial extension; other PET processes such as oriented film extrusion, thermoforming and injection stretch blow moulding involve biaxial extension; extrusion and injection moulding can involve converging flows depending on the die and mould design.

Converging flows involve both shear and elongational components as shown in Figure 3.4. In converging flows the elongational component is due to a radial squeezing which has the same effect as a stretching flow.[9]

FIGURE 3.4: CONVERGING FLOW[58]

Simple Shear Component
$$P_s = \frac{A\eta}{\tan\theta}$$

Extensional Component
$$P_E = B\lambda \tan\theta$$

$$P = P_S + P_E$$

$$\frac{dP}{d(\tan\theta)} = 0$$
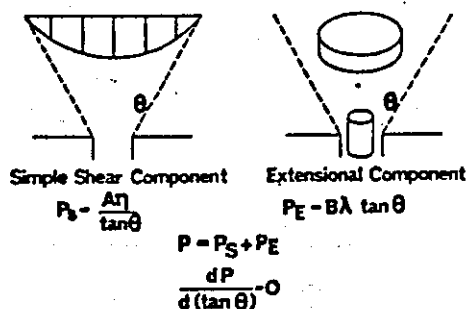
The many different types of elongational flow have led to the development of many different types of experimental methods to measure the elongational behaviour. These have been reviewed by Smoker[9], Cogswell[59], Dealy[60] and Meissner[61].

The different methods can be classified as being either direct or indirect. Direct methods include a range of purpose built instruments that have been used operating under various control mechanisms including: specimen end separation instruments using constant stress, constant strain rate, constant speed or constant load control; constant gauge length instruments using constant stress or constant strain rate control. Other methods that have been used include fibre spinning, bubble inflation, flow visualisation of converging flow, and die-entry pressure drop measurements from capillary rheometry.

Meissner[61] reviewed the use of rotary clamps to study multiaxial elongations of different classes by variations in the positions and rotational speeds of the clamps, though this method is currently restricted to room temperature measurements.

The elongational behaviour of PET has been studied by various methods, mainly to analyse the molecular orientation characteristics. *Ziabicki and Kedzierska*[62] studied the melt-spinning of PET fibres. Several authors have studied the thermoelastic tensile drawing of PET films.[63-66] The uniaxial and biaxial orientation of PET films and sheets were studied using a stress optical method by *De Vries, Bonnebat and Beautemps*.[67] The isothermal elongational rheology of PET monofilaments were studied by *Hill and Cuculo*[68] using an isothermal chamber fitted beneath the spinnerette die. *Crater and Cuculo*[69] studied the molecular ordering of PET in convergent dies by using a flow birefringence technique.

This Chapter describes a study of the elongational flow component in converging flows using a capillary rheometry method proposed by *Cogswell*.[6] Chapter 4 describes a study using a purpose built elongational rheometer, a specimen end-separation instrument which operates under constant strain rate conditions. The elongational flow data from these two chapters has been applied to PET processes in the subsequent chapters: injection moulding in Chapter 5; extrusion blow moulding in Chapter 6; and injection stretch blow moulding in Chapter 7.

3.3 Introduction To Converging Flow

Petrie[70] described converging flows as being either free convergent flow that occurs into an orifice, or upstream of an abrupt contraction from a reservoir; or constrained convergent flow that occurs at a tapered transition between a large diameter and a small diameter tube.

Forsythe[71] reviewed the different approaches that have been applied to the interpretation of converging flows. These approaches include the interpretation of the entrance pressure loss and exit pressure resulting from the first normal stress difference, or from differences in elasticity. Another approach, proposed by *Cogswell*[72] separates the pressure drop into three components, steady shear, acceleration due to convergence and entry effects. By adding the separately determined components the total pressure drop is obtained. Also, by separating the components of the pressure drop the stretching flow properties can be determined. Converging flow has also been used to study melt distortion, such as die swell and melt fracture.

Cogswell[73] reviewed the literature that interprets converging flow as involving a stretching flow. He proposed that a stretching flow occurs when streamlines cease to be parallel. With free convergence the accelerating column of melt approaches the die between rotating vortices. The converging stream is not sheared, the vortex velocity is assumed to be the same as the peripheral velocity of the vortex. The velocity profiles of viscoelastic liquids have been studied by flow visualisation methods, converging viscoelastic flow is usually accompanied by recirculating eddies, with all the flow taking place in a wine glass stem (WGS) region, see Figure 3.5.[74] Exceptions are linear polymers, e.g. HDPE which act like inelastic liquids flowing over the entire solid angle of possible entry in a convergent die. The WGS entry is usually accompanied by a pressure drop across the contraction. The size of the recirculating zones will be larger the greater the difference between the resistance to shear and elongation.[55] However, a direct knowledge of the velocity profile is

not needed as it can be assumed that the flow will adopt streamlines
leading to a minimum pressure drop.

FIGURE 3.5: WINE GLASS STEM FLOW AFTER *DENN*[4]
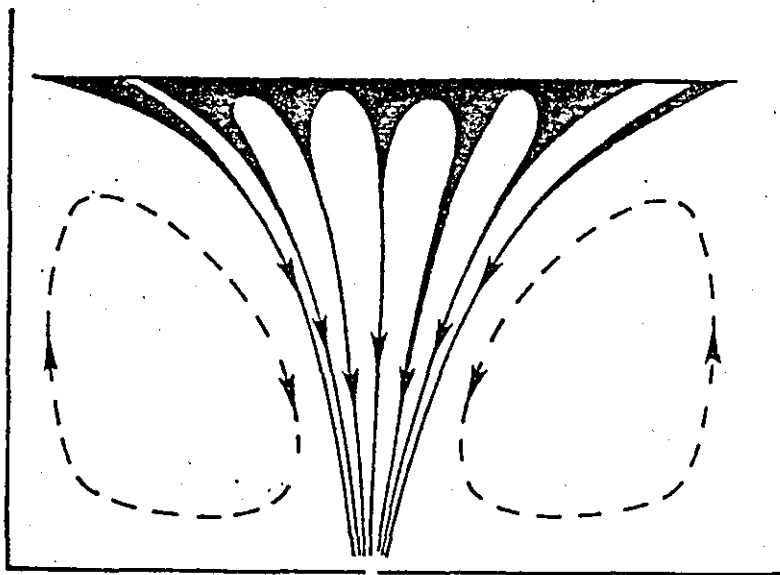
Stretching flows can be highly elastic. The elastic deformation
becomes saturated at low stress levels. In converging flow the total
deformation is large and the stress levels are high. The elasticity
effects are usually ignored as being assumed saturated compared to
the stresses and deformations causing the major dissipation during
the flow. The elastic deformation can be observed as die swell, and
the recoverable extension can be determined by observing the die
swell through an orifice die.[73]

In constrained convergence the angle of convergence is defined by
the walls of the die. The velocity profile includes telescopic shear
and elongation, as the velocity is assumed zero at the wall.
Cogswell[73] reported that when the velocity gradient is maximum for
shear, it is zero for elongation, and vice versa. The velocity profiles
blend together allowing the assumption that any interaction between
the shear and elongational components are of secondary importance.

Brydson[13] listed the attractions of interpreting elongational
flow from converging flow as including:

- the use of standard capillary rheometry with no
  additional experimentation;
- the ability to study high elongation rates;
- rapid and reproducible results;
- wide temperature range available;
- other geometries of die allow pure shear response as
  well as simple elongation to be studied.

To take advantage of these attractions *Cogswell*[6] proposed a method using a conventional capillary rheometer with a long die and an orifice die. The two die method allows for corrected shear data to be determined as well as elongational data.

The Cogswell method[6] assumes that:

- bulk deformations are sufficiently small to be neglected;
- the shear flow obeys Power Law behaviour;
- the viscosity under simple tension is independent of stress;
- that a stretching flow occurs when streamlines cease to be
  parallel;
- accelerative shear flows can be neglected, since in a non-
  linear Maxwell body their significance is minimal;
- the elastic deformation is finite, so at large deformations
  the flow is predominantly viscous;
- it can be assumed that the flow will adopt streamlines
  leading to a minimum pressure drop; (usually WGS flow with
  recirculating 'dead zones')
- the converging stream is not sheared, the recirculating 'dead
  zone' velocity is assumed to be the same as the peripheral
  velocity of the vortex;
- any interaction between the shear and elongational
  components are of secondary importance;
- the total entrance pressure drop is equal to the sum of that
  due to shear flow and that due to elongational flow;
- the elongational viscosity is an apparent value since a
  steady state is not achieved.

The apparent elongational flow properties are determined using the equations shown below. The values for stress and elongation rate are

average values since the assumed zero vortices velocity is not zero in practice. * see page 121.

elongational

viscosity,
$$\lambda = (9/32).[(n+1)^2/\eta].(P_o/\dot{\gamma})^2 \qquad (3.7)$$

where n is the power law index (see equation (2.11)), η is the shear viscosity at fully developed flow at the shear rate $\dot{\gamma}$ and P_o is the orifice die pressure drop at a flow rate Q which would give a shear rate at the die wall in fully developed flow of $\dot{\gamma} = 4Q/\pi r^3$, (equation (2.16)).

elongational stress,
$$\sigma = (3/8).(n+1).P_o \qquad (3.8)$$
elongation rate,
$$\dot{\varepsilon} = \sigma/\lambda \qquad (3.9)$$

The recoverable extension (strain), ε_R, is determined from the post-extrusion swelling from an orifice die by equation (3.10).
$$\varepsilon_R = \ln((B_o)^2) \qquad (3.10)$$
where B_o is the ratio of extrudate/die diameter from an orifice die corresponding to an elongational stress σ (see equation (3.8)). The elongational modulus, E, is determined by equation (3.11).
$$E = \sigma/\varepsilon_R \qquad (3.11)$$
Using the method developed by *Cogswell*[5] good correlation has been reported[73] for the elongational rheology of several polymers measured using this method and other more direct methods; (Table 3.1 summarises these studies).

. *Gibson and Williamson*[7] proved the validity of the treatment of converging flow proposed by *Cogswell*[72], they also modified the model by applying a power law relationship to the elongational flow behaviour of bulk moulding compound, in place of the original[72] assumption that the elongational viscosity is independent of stress.

The main objections to the method are that it lacks rigorous analysis compared to a continuum mechanics approach. This is countered by the ease of experimentation of the method. The assumption that any interaction of the shear and elongational flows in a converging flow can be neglected has been offered as a major error in the analysis.[70] *Cogswell*[58] reports that the argument of separability and simple additivity is open to dispute but the good

correlations obtained with direct measurements are more significant.

The problems of shear heating and non-isothermal flow, that occur at high shear rates, have been ignored as it is assumed that if these problems occur in an experiment then they will occur in a process that the experiment simulates. *Gibson and Williamson*[7,8] discussed two methods to correct for non-isothermal flow, whilst *Barrie*[76] claims that the effects of shear heating are counterbalanced by pressure effects during compression of the polymer.

TABLE 3.1:COMPARISONS WITH COGSWELL CONVERGING FLOW METHOD[73]

POLYMER	OTHER METHOD	AGREEMENT	REFERENCE
LDPE	constant $\dot{\epsilon}$	quantitative	Hurlimann and Knappe[76]
HDPE	isothermal		
LDPE	melt spinning	quantitative	Shroff, Cancio
PP	and flow		and Shida[77]
PS	visualisation		
PS			
LDPE			
HDPE			
PP	constant σ	qualitative	Cogswell[59]
ABS			
PMMA			
Polysulphone			
PVC			

In addition to the studies listed in Table 3.1, other studies have been made, using the Cogswell converging flow method, for a wide range of polymers including polycarbonate, nylon 6.6, PET, PBT and polyethersulphone reported by *Cogswell*[5] and glass-fibre reinforced thermosetting bulk moulding compound reported by *Gibson and Williamson.*[7]

Before the method proposed by *Cogswell*[5] is used, the theoretical principles used to derive equations (3.7)-(3.11) should be considered. The derivations of the equations have been reported previously.[9,58,72,77]

Considering the shear and elongational components of converging flow separately, as illustrated in Figure 3.4, if θ is the half-angle

of convergence, simple trigonometry yields the pressure drop due to simple shear flow as being:

$$P_s = A\eta/\tan\theta \qquad (3.12)$$

where η is the viscosity under simple shear at the shear rate at the wall of convergence and A is a proportionality factor. By a similar argument the pressure drop due to elongational flow is:

$$P_\epsilon = B\lambda\tan\theta \qquad (3.13)$$

where λ is the viscosity under tension and B is a proportionality factor. Cogswell[58] argues that the total pressure drop, P, is equal to the sum of the components shown in equations (3.12) and (3.13) to give equation (3.14).

$$P = P_s + P_\epsilon \qquad (3.14)$$

The flow is assumed to adopt such a streamline that will involve the minimum energy dissipation, this results in the least pressure drop, such that:

$$dP/d\tan\theta = 0 \qquad (3.15)$$

Solving these equations for an infinite set of very short tapers, as shown by Cogswell[72], yields equations (3.7)-(3.11). An alternative set of relationships for the flow into an orifice is:

$$\lambda/\eta = 2/\tan^2\theta \qquad (3.16)$$

$$\dot\epsilon/\dot\gamma = \tan\theta/2 \qquad (3.17)$$

$$\sigma/\tau = 1/\tan\theta \qquad (3.18)$$

where σ and $\dot\epsilon$ are the average elongational stress and rate, and τ and $\dot\gamma$ are the shear stress and rate at the die wall. These equations (3.16)-(3.18) allow the calculation of elongational rheology from a knowledge of die entry flow patterns and the shear rheology.

The analysis proposed by Cogswell[5] has been used in this study to determine the elongational flow properties of the different PET polymers whose shear rheological behaviour was reported in Chapter 2.

3.4 Converging Flow Experimental Method

The Davenport Extrusion Rheometer was used to obtain rheological data on several PET polymers. Cogswell's converging flow method[6], see Section 3.3, was used to obtain elongational rheological results. The experimental method was described in Section 2.3.2; data from a zero length die was analysed to obtain the elongational results. Pressure drop data was used in equations (3.7) and (3.8) to calculate the apparent elongational viscosity and the average elongational stress. Die swell data from the zero length die was used in equation (3.10) to determine the recoverable strain. The elongation rate and tensile modulus were then calculated using equations (3.9) and (3.11) respectively.

3.5 Converging Flow Data

The converging flow data is presented as plots of apparent elongational viscosity as a function of elongation rate, the table below lists the figures for the different polymers. As the rheometer used was a rate-imposed machine; flow rate and therefore elongation rate are set and the pressure and therefore the stress is measured, it seems inappropriate to plot apparent elongational viscosity versus elongational stress curves, as both are measured quantities. They have only been plotted for the purpose of comparison with previous work in Figure 3.16, as the previous work is reported in this format.

POLYMER	VISCOSITY-RATE
B90S	Figure 3.6
Linear PET 270°C	Figure 3.7
Linear PET 280°C	Figure 3.8
Branched PET 270°C	Figure 3.9
Branched PET 280°C	Figure 3.10
PETG Copolyester	Figure 3.11
PCTG Copolyester	Figure 3.12
PCCE Copolyester	Figure 3.13

The recoverable extension data, derived from die swell data, for the three copolyesters are represented as plots of tensile modulus against elongational stress in Figure 3.14. No data was obtained for the linear and branched PET polymers as the extrudate was too tacky to be cut without excessive distortion at low output rates and the extrudate sagged excessively at high output rates.

Table 3.2 summarises the apparent elongational viscosity values for the different polymers under various conditions.

TABLE 3.2: APPARENT ELONGATIONAL VISCOSITY VALUES

POLYMER	TEMPERATURE (°C)	$\lambda_{\dot\varepsilon=1}$ (Pa.s)	$\lambda_{\dot\varepsilon=10}$ (Pa.s)	$\lambda_{\dot\varepsilon=100}$ (Pa.s)	$\lambda_{\dot\varepsilon=1000}$ (Pa.s)
B90S	270	270000	30000	5200	1500
	275	270000	30000	4700	1200
	280	240000	25000	3800	600
	285	300000	28000	4200	750
	290	460000	48000	5600	750
EX167	270	350000	44000	9000	2700
	280	240000	37000	7000	–
LIN-A	270	–	25000	3800	900
	280	290000	33000	4800	–
LIN-B	270	400000	42000	6000	1200
	280	–	27000	4000	900
LIN-C	270	–	26000	3300	650
	280	–	28000	4200	680
LIN-D	270	280000	26000	2600	370
	280	260000	25000	3000	500
BRAN-1	270	275000	36000	9800	–
	280	260000	33000	6700	–
BRAN-2	270	320000	39000	7000	–
	280	320000	24000	7800	–
BRAN-3	270	390000	87000	29000	–
	280	300000	43000	12200	–
BRAN-4	270	280000	110000	85000	–
	280	300000	75000	29000	–
BRAN-5	270	320000	107000	90000	–
	280	420000	58000	20000	–
PETG	170	–	110000	38000	–
	200	390000	59000	16000	4800
	220	320000	34000	6000	2500
	240	240000	30000	4500	900
	260	1600000	27000	4800	1100
	280	330000	38000	4500	520
PCTG	240	–	27000	6600	1600
	250	–	18000	2800	680
	260	–	26000	2800	630
PCCE	230	–	26000	4700	1000
	245	–	40000	3600	800
	260	–	13000	2200	510

FIGURE 3.6: EFFECT OF TEMPERATURE ON THE
TENSILE VISCOSITY OF B90S LINEAR PET
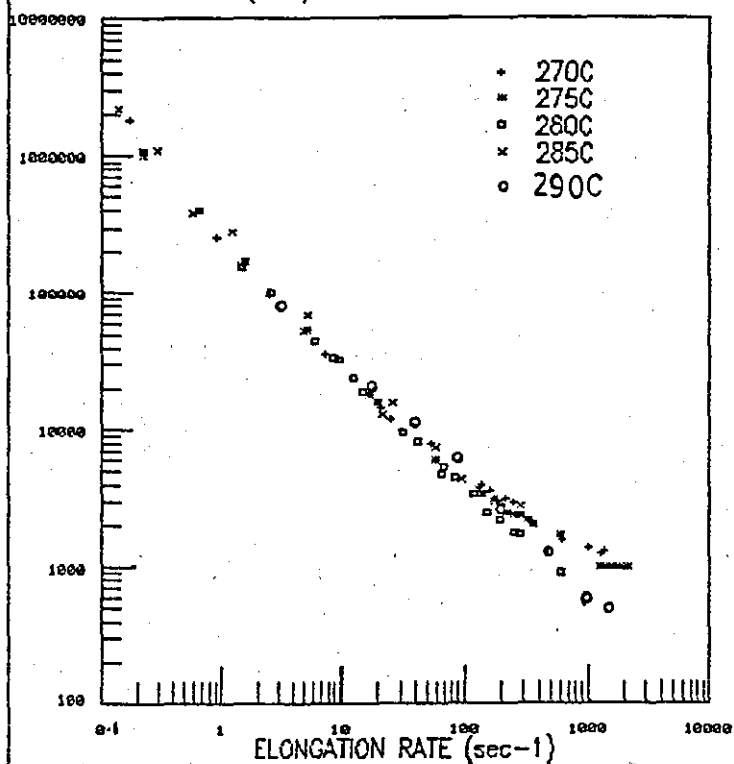
FIGURE 3.7: EFFECT OF MOLECULAR WEIGHT
ON THE TENSILE VISCOSITY OF LINEAR PET

FIGURE 3.8: EFFECT OF MOLECULAR WEIGHT
ON THE TENSILE VISCOSITY OF LINEAR PET

TENSILE VISCOSITY (Pa.s)   260°C
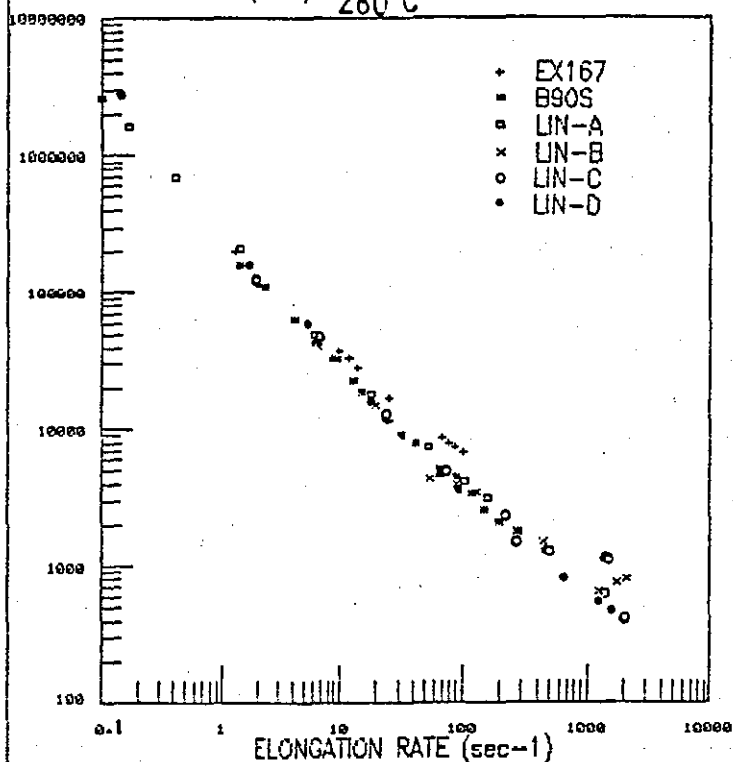
FIGURE 3.8: EFFECT OF MOLECULAR WEIGHT ON THE TENSILE VISCOSITY OF LINEAR PET

FIGURE 3.9: EFFECT OF MOLECULAR WEIGHT
ON THE TENSILE VISCOSITY OF BRANCHED PET

TENSILE VISCOSITY (Pa.s)   270C

FIGURE 3.9: EFFECT OF MOLECULAR WEIGHT ON THE TENSILE VISCOSITY OF BRANCHED PET
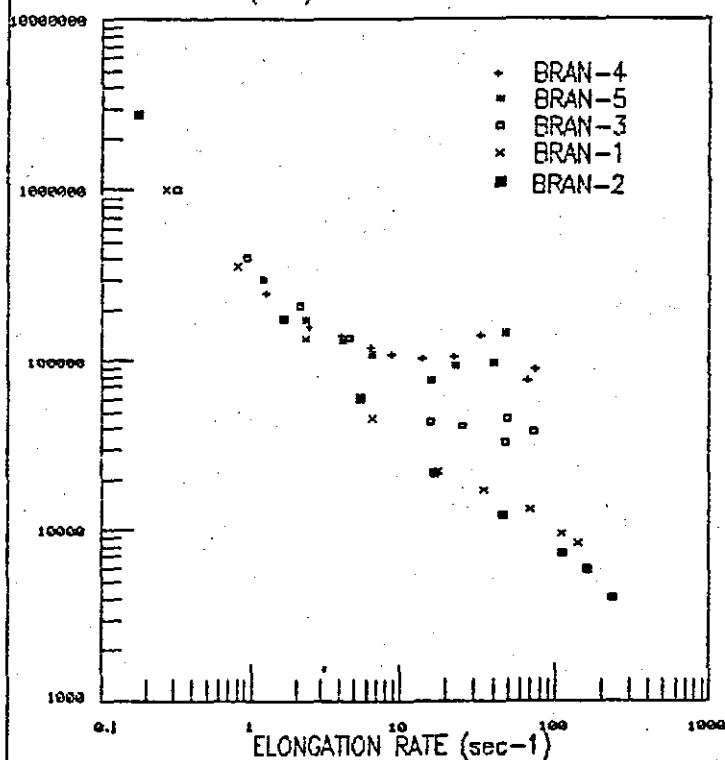
FIGURE 3.10: EFFECT OF MOLECULAR WEIGHT
ON THE TENSILE VISCOSITY OF BRANCHED PET

TENSILE VISCOSITY (Pa.s)   280C

BRAN-4
BRAN-5
BRAN-3
BRAN-1
BRAN-2

ELONGATION RATE (sec-1)
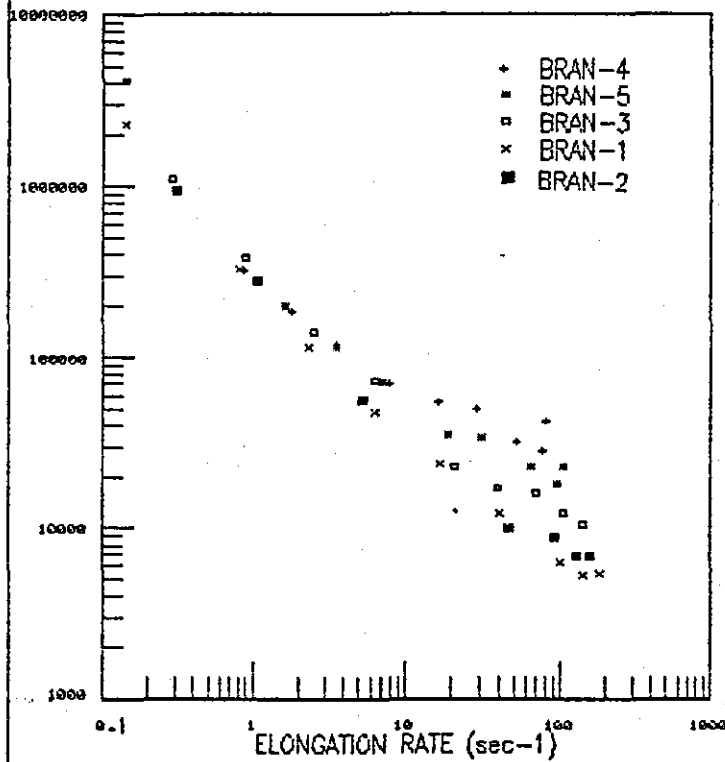
FIGURE 3.11: EFFECT OF TEMPERATURE ON
PETG 6763 COPOLYESTER TENSILE VISCOSITY

TENSILE VISCOSITY (Pa.s)

170C
200C
220C
240C
260C

ELONGATION RATE (sec-1)
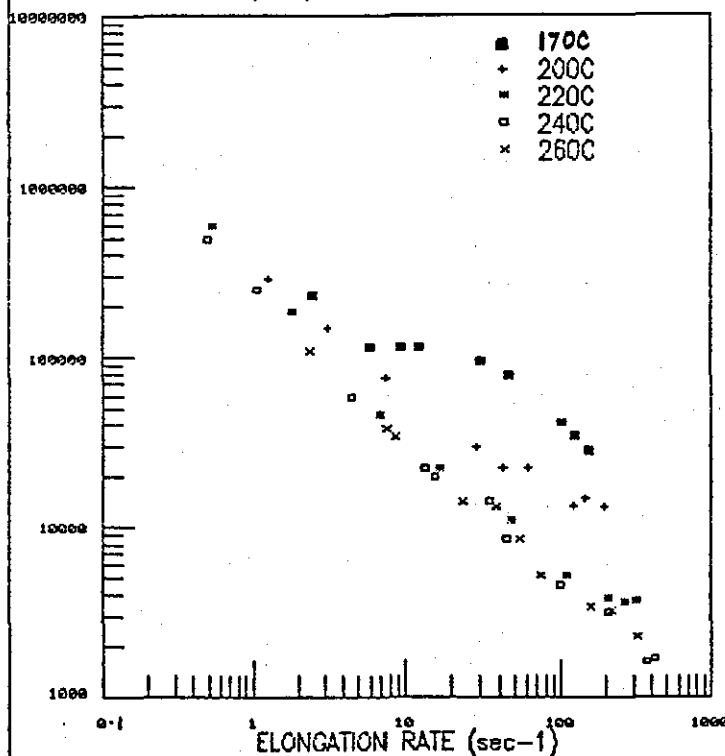
FIGURE 3.12: EFFECT OF TEMPERATURE ON
PCTG 5445 COPOLYESTER TENSILE VISCOSITY
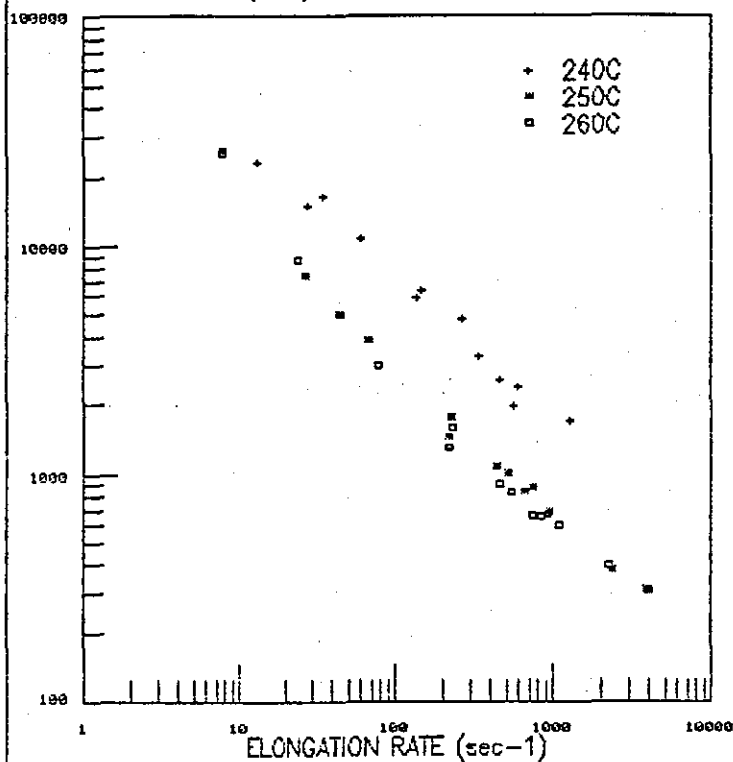
FIGURE 3.13: EFFECT OF TEMPERATURE ON
PCCE 9967 COPOLYESTER TENSILE VISCOSITY

FIGURE 3.14: COPOLYESTER TENSILE MODULUS

FIGURE 3.15: B90S AT 270C
COMPARISON WITH COGSWELL'S DATA

VISCOSITY (Pa.s)

+ TENSILE DATA
-- COGSWELL TENSILE DATA
□ SHEAR DATA
— COGSWELL SHEAR DATA

$\dot{\varepsilon}, \dot{\gamma}$ STRAIN RATE (sec-1)

FIGURE 3.16: B90S AT 270C
COMPARISON WITH COGSWELL'S DATA

VISCOSITY (Pa.s)

σ, τ STRESS (Pa)

+ TENSILE DATA
-- COGSWELL TENSILE DATA
□ SHEAR DATA
— COGSWELL SHEAR DATA

3.6 Discussion Of Elongational Rheology Results

3.6.1 Linear PET Polymers

Figure 3.6 shows that the apparent elongational viscosity decreases with increasing elongation rate, over the elongation rate range 0.1-10000s^{-1}. The apparent elongational viscosity is relatively independent of temperature over the temperature range 270°C-290°C, see Table 3.2. The observed deviation at high elongation rates of the lower temperature curves indicates the onset of stress-induced crystallisation of the PET, Figure 3.17 shows schematically what happens. *Boudreaux and Cuculo*[3] reported the occurrence of stress-induced crystallisation at high flow rates as causing an increase in the apparent shear viscosity.

FIGURE 3.17: MOLECULAR BEHAVIOUR WITH INCREASING ELONGATION RATE

$\dot{\varepsilon} = 0$ $\dot{\varepsilon} > 0$

λ high   decreasing λ

crystallisation

(a) random molecular arrangement   (b) molecular orientation   (c) stress-induced crystallisation
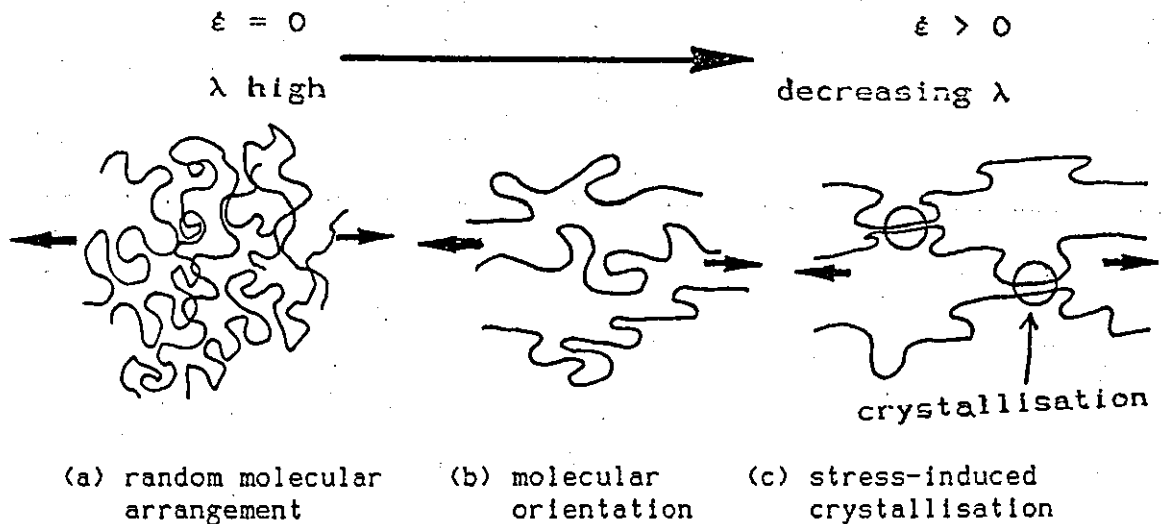
Figures 3.7 and 3.8 show the apparent elongational viscosity decreases with increasing elongation rate for all the linear PET polymers tested at 270°C and 280°C respectively. The observed deviations at high elongation rates indicate the onset of stress-induced crystallisation of the PET; which is accelerated for higher I.V. polymers.

Figures 3.6-3.8 all show that the linear PET polymers studied all have tension thinning behaviour in this mode, the linear polymer molecules become more ordered and flow past each other more easily

hence the resistance to flow decreases, Figure 3.17 models the molecular thinning that occurs with increasing elongation rate.

Effect Of Molecular Weight

Figure 3.7 shows the apparent elongational viscosity increases with increasing molecular weight for the linear polymers, the linear polymer molecules assume a greater degree of reorder, as the molecular weight increases. The molecular weight dependence increases with elongation rate.

Figure 3.8 shows the same trends as those observed in Figure 3.7 but the molecular weight dependence is not as significant as that at the lower temperature. PET molecules are fairly "short and stubby" in comparison to polyethylene, polypropylene, etc. therefore PET is less molecular weight dependent, the molecular motion being restrained by the intermolecular forces and the stiffer molecules having a high cohesive energy density (i.e. PET = 114cal/cm^3, PE = 62cal/cm^3)[79]. An increase in molecular weight will not produce as great an increase in molecular length or resistance to flow as with polyethylene.

Suitability For Injection Moulding

In injection moulding elongational flows occur in converging runners and gates, in divergence into the cavity after the gate, in converging and diverging areas of the cavity, around the circumference of a growing melt front, and in the fountain flow effect which occurs in the flowing polymer. The low tensile viscosity of the linear PET polymers results in easier processing of the polymers as there will be no significant effect on the pressure drop by increased flow rates, since the viscosity decreases with increased elongation rate. Also, the pressure drops will not increase excessively over areas of convergence and the quality of the mouldings will not suffer by problems of warpage due to high tensile stresses relaxing after the moulding has been ejected.

Comparison With Previous Work

Cogswell[58] developed this technique of inferring the elongational response of polymers from converging flows; he reported the apparent elongational viscosity of PET to be elongational stress independent. Figures 3.15 and 3.16 compare the data for B90S linear PET at 270°C

tested in this study with his data.[79] It can be seen that the shear data shows excellent agreement, whilst the elongational data differs.

Figures 3.15 and 3.16 show that to interpret Cogswell's[79] data as being Troutonian (stress-independent) a large scatter of data would have to be accepted.

Cogswell[80] used a dead-load method (pressure-imposed), rather than an extrusion rheometer as used in this study (rate-imposed), the dead-load method suffers from large errors due to friction, polymer compressibility, and head effects. Also, no mention of degradation prevention was described in his method[80], at low elongation rates the residence time of the polymer in the rheometer is great and degradation will occur unless preventative measures are taken. These errors could help to explain the data in Figures 3.15 and 3.16, the measured rate being much higher than the expected rate, at a given stress, for un-degraded polymer. The larger differences in Figures 3.15 and 3.16 occur at low elongation rates where the dead load method will show the greatest frictional losses, the true stress being lower than the applied stress, hence the rate measured by *Cogswell*[79] was higher, at a given stress, than that measured by an extrusion rheometer which measures the actual pressure above the die.

It is believed that rate-imposed measurements are more relevant for relating to practical polymer processing as these usually involve pushing polymer through a certain geometry at a constant rate, not at a constant stress, e.g. injection moulding is a rate-imposed process (the injection speed is set).

3.6.2 Branched PET Polymers

Figures 3.9 and 3.10 show the apparent elongational viscosity of the branched PET polymers decreases with increasing elongation rate. The behaviour for the branched PET polymers is different to the linear PET polymers above an apparently critical elongation rate of approximately $1sec^{-1}$; at lower rates the behaviours are similar regardless of molecular weight. There is a trend in the behaviour of the branched polymers, at rates greater than $1sec^{-1}$: BRAN-1 and BRAN-2 act in a similar manner as the linear PET polymers, i.e. they are tension thinning polymers, with values for the apparent elongational

viscosity which are similar to those for the linear PET polymers;
BRAN-3 has a higher apparent elongational viscosity than the linear
polymers and shows a smaller viscosity-drop for a given change in
rate, it approaches rate-independent behaviour above $10s^{-1}$; BRAN-4
and BRAN-5 have even higher elongational viscosities, than BRAN-3,
and at 270°C approach elongation rate independence above $10sec^{-1}$, at
280°C the apparent elongational viscosity continues to decrease with
increasing elongation rate, though maintaining higher viscosity values
than the other branched PET polymers.

FIGURE 3.18: ELONGATIONAL FLOW OF BRANCHED PET

$\dot{\varepsilon} = 0$ $\dot{\varepsilon} > 0$ $\dot{\varepsilon} >> 0$
λ high λ decreasing λ steady

hooking

(a) random molecular   (b) molecular   (c) "hooking" of branches
    arrangement   orientation   gives effective
                                  entanglements
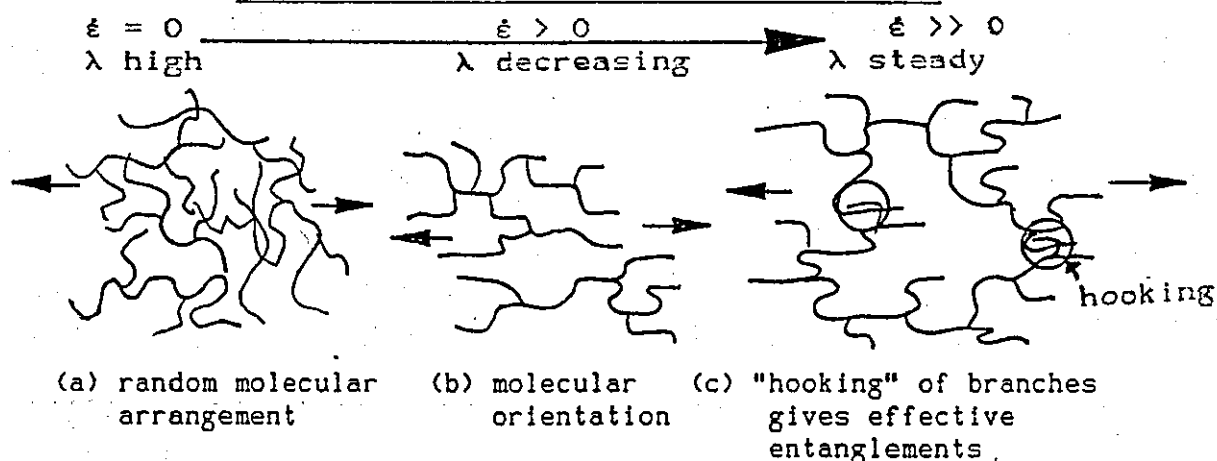
As branched polymers become ordered in a stretching flow the
branches act as "hooks" causing entanglements between adjacent
polymers, and resisting further deformation, see Figure 3.18, this
effect is illustrated by the deviation from tension thinning
behaviour towards elongational stress independent behaviour of the
branched PET polymers. The three sets of behaviour may be due to the
relative number and/or length of the branches of the different
branched polymers, similar to the observations of the shear behaviour
in Chapter 2, the more and/or longer the branches the sooner and
more effective they will act as "hooks" in a stretching flow; i.e.
BRAN-4 and BRAN-5 have branches that act as "hooks" and resist the
elongational deformation thereby the response becomes less tension
thinning, BRAN-3 shows similar behaviour to a lesser degree,
indicating fewer or shorter branches; and BRAN-1 and BRAN-2 are only
beginning to deviate at the maximum levels of elongation rate and

elongational stress measured, indicating even fewer or shorter branches. If higher levels of elongation rate were obtainable it is probable that BRAN-1 and BRAN-2 would show similar trends, as the other branched PET polymers, towards elongational stress independent behaviour.

The points of deviation in Figures 3.9 and 3.10 indicate the point where the branches of adjacent molecules become effective in entangling with each other and increasing the resistance to flow.

The increases in viscosity shown at high elongation rates and elongational stresses correspond to conditions where melt distortion ("sharkskin" and melt fracture) were observed. Crystallisation may be accelerated in branched polymers, which would contribute to the higher viscosity at high elongation rates, however, this point was not investigated further.

Effect Of Branching

The difference in behaviour in converging flow between linear and branched PET polymers can be explained by considering the theory behind *Cogswell's*[68] interpretation of converging flows. A converging flow contains a shear flow component and an elongational flow component. If there were no elongational component the flow would be as shown in Figure 2.1, if there were no shear component the flow would be as shown in Figure 3.1, in converging flow there is a contribution from both components and a combination of the two figures would illustrate the deformation which is sheared and stretched simultaneously.

For linear PET polymers both components can be considered as having equal contribution, but for the branched PET polymers the observed behaviour suggests the contribution of the shear and elongational components should be considered as being a function of shear rate. At low shear rates the flow is dominated by the shear component and the molecular disentanglement is more significant than the elongational deformation. Also the tensile forces are absorbed by taking up the slack in the randomly arranged molecules therefore the elongational stress will be independent of the elongation rate. Above a critical strain rate the converging flow is dominated by the

elongational component, the elongational deformation is too fast for the branches to disentangle and they snag and act as temporary crosslinks. This allows the elongational component to become more effective, the tensile forces being transmitted through the temporary crosslinks and dominating the flow, therefore the elongational stress will increase with the shear rate and elongation rate.

Effect Of Molecular Weight

Figures 3.9 and 3.10 show that, for a given elongation rate, the apparent elongational viscosity increases with increasing intrinsic viscosity (i.e. molecular weight). The different behaviour of the polymers is analogous to that observed for the shear rheological data in Chapter 2, where it was concluded that the "effectiveness" of interchain entanglements produced the variations in response. The entanglement "effectiveness" being dependent on, and increasing with either (or both) a greater number of chain branches or longer chain branches.

The rate sensitivity decreases with increasing molecular weight, see Table 3.2.

Effect Of Temperature

Table 3.2 shows that the apparent elongational viscosity, at a given elongation rate decreases with increased temperature. Also the temperature sensitivity increases with increasing elongation rate and increasing molecular weight, though the overall effect of temperature is slight. These trends can be observed by comparing the curves in Figures 3.9 and 3.10.

Suitability For Extrusion Blow Moulding

Elongational flows occur in extrusion blow moulding as parison sagging and during inflation of the parison into a moulded article. Considering the parison sagging, the elongational stress is proportional to the parison length and the sag velocity is proportional to the elongation rate; to minimise the degree of sagging for increasing parison length a higher elongational viscosity is necessary. However, sagging is a low-strain rate phenomenon; the data derived in this mode suggest that the polymers studied are equally able to satisfy the parison sagging low strain rate requirement in extrusion blow moulding.

Considering the inflation stage of extrusion blow moulding, of the tension thinning branched PET polymers, the resultant product would have an uneven wall thickness as the areas of higher stretch ratio will become thinner, however, the elasticity of these polymers compensates by making the polymers more tension stiffening and hence the high stretch ratio   areas will be stabilised, giving an even wall thickness.

The apparent elongational rate independent behaviour together with the shear viscosity and elasticity data, from Chapter 2, show that the branched PET polymers have more suitable rheological behaviour for extrusion blow moulding than the linear PET polymers.

3.6.3 PETG Copolyester

Figure 3.11 shows the decrease in the apparent elongational viscosity with increasing elongation rate, i.e. PETG Copolyester is also a tension thinning polymer. The values for the apparent elongational viscosity of PETG Copolyester are similar to those for the linear PET polymers. The tendency to rate-independence may be due to either the two phase nature of the copolymer or to the steric hindrance of adjacent copolymer segments.

Copolymers can contain more than one phase, the phases consisting of segments of different compositions of the two monomers. The flow behaviour can be dominated by different phases under various conditions.

The steric hindrance of adjacent copolymer segments may occur as the comonomer CHDM contains a bulky cyclohexane group lying in a plane normal to the aromatic ring in the chain. After the molecules have become oriented during elongational flows, further elongation will tend to draw molecular segments closer until the bulky cyclic groups can interfere with those in adjacent molecular segments; this interference will lead to a temporary 'mechanical locking' effect which increases the resistance to flow. Despite the molecules locking they are not able to become close enough for crystallisation to occur, i.e. the physical effect dominates. This behaviour is illustrated schematically in Figure 3.19. The 170°C data corresponds to unstable flow (melt fracture) above an elongation rate value of

6sec^{-1} (elongational stress = 0.67MPa).

FIGURE 3.19: STERIC HINDRANCE OF PETG SEGMENTS

Table 3.2 shows that at a given elongation rate the apparent elongational viscosity decreases with increasing temperature.

Figure 3.14 shows the tensile modulus of PETG Copolyester increases with increasing elongational stress, this effect will compensate for the corresponding viscosity-drop and stabilise any deformation occurring in an elongational flow. The tensile modulus is relatively independent of temperature.

Suitability For Extrusion Blow Moulding

The elongational elasticity will cause the polymer to act in a pseudo-tension stiffening manner, this will stabilise the parison, reducing the amount of sagging and giving inflated products that will have an even wall thickness distribution. Together with the shear viscosity and elasticity data shown in Chapter 2, the PETG Copolyester rheology is suitable for extrusion blow moulding. This result has been tested by practical extrusion blow moulding processing trials in Chapter 6.

3.6.4 PCTG Copolyester

Figure 3.12 shows the tension thinning behaviour of PCTG Copolyester as a function of elongation rate. The values for the apparent elongational viscosity of PCTG Copolyester are similar to those for the linear PET polymers.

Table 3.2 shows that at a given value of elongation rate the apparent elongational viscosity decreases with increasing temperature. The apparent elongational viscosity at 240°C was higher than at the other two temperatures which were approximately the same.

Figure 3.14 shows the tensile modulus of PCTG passed through a

minimum then increased with increasing elongational stress. The tensile modulus is relatively independent of temperature.

Suitability For Injection Moulding

The tension thinning behaviour makes the the PCTG suitable for injection moulding as the pressure drop across a convergent runner or gate will not be too excessive when the shear rate or elongation rate is high. Also any circumferential tensile stresses will be small enough to relax during cooling, therefore significant warping will not occur after ejection.

3.6.5 PCCE Copolyester

Figure 3.13 shows the tension thinning behaviour of the PCCE Copolyester as a function of elongation rate. The values for the apparent elongational viscosity of PCCE Copolyester are similar to those for the linear PET polymers.
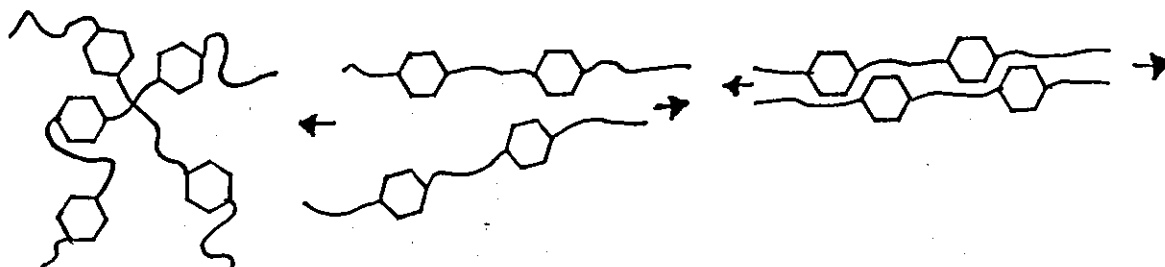
Table 3.2 shows at a given value of elongation rate the apparent elongational viscosity decreased with increasing temperature.

Figure 3.14 shows the tensile modulus of PCCE increased with increasing elongational stress. The tensile modulus is relatively independent of temperature.

Suitability For Extrusion Blow Moulding

The polymer suppliers of PCCE Copolyester claim the polymer to be an extrusion blow moulding polymer, but the evidence found here and in Chapter 2, show that the rheological properties are less suitable for this process, over the temperature range studied (230°C-260°C). The polymer has low shear and elongational viscosities and a short relaxation time, all of which are unsuitable properties for extrusion blow moulding. The elongational elasticity increases with increased elongational stress but not sufficient enough to overcome the aforementioned disadvantages, with respect to blow moulding.

3.7 Summary Of Chapter 3

3.7.1 Aims And Novelty

The aims set out at the beginning of this chapter have been achieved.

The results in this chapter include elongational flow characterisation for linear, branched and copolymer PET polymers, including apparent elongational viscosity and elongational elasticity, this data is relevant to various processes for thermoplastic polyesters; some of the results have been applied to injection moulding in Chapter 5 and extrusion blow moulding in Chapter 6.

The results for the branched PET polymers and the Copolyesters is believed to be the first study of the elongational flow behaviour of these novel polymers. Differences in their responses have been explained by the differences in their molecular structures.

3.7.2 Conclusions From Chapter 3

1.   The linear PET polymers showed a tension thinning response in converging flow, the apparent elongational viscosity decreased with increasing elongation rate. Compared with the apparent shear viscosity, the apparent elongational viscosity was relatively independent of temperature. The apparent elongational viscosity increased with increasing molecular weight. Stress-induced crystallisation occurred at high elongation rates with the linear PET polymers, especially at lower temperatures.

2.   The branched PET polymers showed a tension thinning response in converging flow below a critical rate; at the critical rate the elongational deformation exceeds the shear disentanglement and the chain branches snag. Above the critical rate the branched PET polymers deviate from the tension thinning response approaching Troutonian behaviour. The response was dependent on the degree of branching, with a greater number of branches or longer branches the onset of interchain branch "hooking" occurred at lower elongation rates. The branched PET polymers showed increasing apparent elongational viscosity with increasing molecular weight. The apparent elongational viscosity of the branched PET polymers decreased with increasing

temperature and the temperature sensitivity increased with increasing elongation rate and molecular weight. The role played by crystallisation was not established, though it may contribute to the higher viscosity values observed at high elongation rates.

3.   The PETG Copolyester is a tension thinning polymer in converging flow. At high elongation rates there is a deviation towards Troutonian behaviour, due to either (i) the different phases present in copolymer systems, or (ii) the flow induced molecular orientation causing steric hindrance of the bulky cyclic molecular groups and therefore increasing the resistance to elongational flow. The apparent elongational viscosity decreased with increasing temperature. The tensile modulus increased with increasing elongational stress and was relatively independent of temperature.

4.   The PCTG Copolyester is a tension thinning polymer, having similar apparent elongational values to the linear PET polymers in converging flow. The apparent elongational viscosity decreased with increasing temperature. The tensile modulus passed through a minimum with increasing elongational stress and was relatively independent of temperature.

5.   The PCCE Copolyester was a tension thinning polymer, having similar apparent elongational values to the linear PET polymers in converging flow. The apparent elongational viscosity decreased with increasing temperature. The tensile modulus increased with increasing elongational stress and was relatively independent of temperature.

6.   The elongational rheology of the linear PET polymers and the PCTG Copolyester indicate their suitability for injection moulding.

The branched PET polymers and the PETG Copolyester have suitable elongational rheological properties for extrusion blow moulding.

The PCCE Copolyester does not appear to have elongational flow properties suitable for extrusion blow moulding, over the temperature range tested.

3.7.3 Suggestion For Further Work

All the suggestions to extend the applicability of the shear data in Chapter 2 can also be applied to the elongational data in this chapter. Also, the elongational flow properties should be determined using a method that simulates free surface flows rather than constrained flows; this generates data more applicable for aspects of extrusion blow moulding. A comparison of the elongational data obtained using the two methods could then be compared. The elongational flow properties determined should be verified by processing experiments.

An investigation into the behaviour of the branched PET polymers should be carried out to determine whether it is the length or concentration of branches that causes the differences in the observed behaviour or earlier crystallisation. I feel the concentration of branches is more important; however, these branches must be long enough to be effective as "hooks" but not long enough to fold back on the main chain and act as linear polymers. An investigation into the effective length of branches and the effective concentration of branches should be carried out.

A possible extension to the molecular modifications to obtain an extrusion blow mouldable PET polymer might involve branched PET copolymers.

Recent work has shown that Cogswell's assumption of a free converging flow adopting the geometry of minimum pressure drop can only be satisfied when $P_E = P_s$, as shown in the adjoining figure. It is claimed that this condition restricts the validity of Cogswell's theory to a half-angle of convergence equal to 10°. [Private communication, A.G.Gibson.]
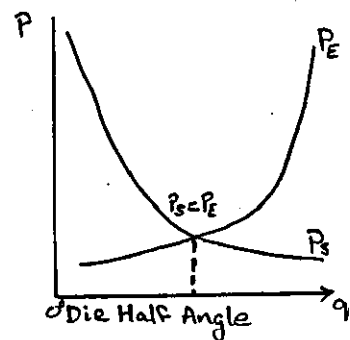
4.The Rutherford Elongational Rheometer

4.1 Aims Of Chapter

This chapter introduces the Rutherford Elongational Rheometer and describes the modifications made to permit high temperature testing to be carried out. Also, the experimental programme is described to meet the objective of directly measuring the elongational flow behaviour of PET in the melt and thermoelastic phases. The aims of the chapter were:

- to modify the Rutherford Elongational Rheometer to enable the testing of high temperature engineering polymers in the melt phase.
- to produce tensile flow data for PET melts, which can be compared to the converging flow data reported in Chapter 3 and which can be applied to process design and control.
- to produce tensile flow data for PETG Copolyester melts which can be compared to the converging flow data reported in Chapter 3 and which can be applied to extrusion blow moulding process design and control.
- to produce tensile flow data for PET in the thermoelastic phase which can be applied to the inflation of reheated preforms in the injection stretch blow moulding process.

4.2 Introduction

Elongational flow was introduced in Section 3.2 where the basic concepts were described and previous work on the elongational flow of PET was reviewed. Chapter 3 describes an experimental programme involving an indirect method (converging flow) of determining elongational flow characteristics of polymers; this chapter describes an experimental programme involving a direct method of determining the elongational flow properties.

In controlled elongational flow experiments either the stress or strain rate is kept constant whilst the other is determined, as it

varies with time. Several reviews of controlled experiments have been published.[60,81,82]

Many different machines have been developed for studying uniaxial extension, working in either the constant stress or constant strain rate mode.

Uniaxial extension can be considered as a flow which is time-dependent but spatially homogeneous, in the sense that the rate of strain tensor, $\dot{\varepsilon}_{ij}$, is independent of position x_{ij}.

$$\dot{\varepsilon}_{ij}(t) = \begin{bmatrix} \dot{\varepsilon}(t) & 0 & 0 \\ 0 & -\tfrac{1}{2}\dot{\varepsilon}(t) & 0 \\ 0 & 0 & -\tfrac{1}{2}\dot{\varepsilon}(t) \end{bmatrix}$$

and the stress field is: $\sigma_{11} - \sigma_{22} = \sigma_{11} - \sigma_{33} = \dot{\varepsilon}\lambda(\dot{\varepsilon})$ (4.1)

and $\qquad\qquad \sigma_{ij} = 0$ for $i \neq j$. (4.2)

The deformation illustrated in Figure 3.1 and the equations for stress and strain shown in equations (3.3)-(3.6) describe the basis on which the Rutherford Elongational Rheometer is designed.

When considering materials with fading memory, i.e. viscoelastic materials, the initial length, $L(0)$, has decreasing relevance with continuing extension. Therefore the current length, $L(t)$, is taken as the reference length that has the same importance from one instant to another, i.e. the instantaneous strain rate, $\dot{\varepsilon}$, is defined by equation (4.3):

$$\dot{\varepsilon}(t) = 1/L(t).dL/dt \qquad (4.3)$$

The derivative dL/dt is the velocity, v, of the specimen ends separation, therefore:

$$\dot{\varepsilon} = v/L \qquad (3.6)$$

This provides a convenient means of calculating the instantaneous strain rate from easily measured test parameters.

By maintaining a constant strain rate, i.e. by increasing the velocity proportionally with the length, a *"motion with constant stretch history"* [17] or 'steady uniaxial extension' is developed.

By analogy with equation (2.4) for shear viscosity,

$$\eta = \tau/\dot{\gamma} \qquad (2.4)$$

we can define an apparent elongational viscosity:

$$\lambda = \sigma/\dot{\varepsilon} \qquad\qquad (3.1)$$

There are relative advantages for both the constant stress and constant strain rate modes of testing. The constant stress mode has the advantage that the elastic response of the material reaches equilibrium immediately, producing a linear relationship between deformation and time. These tests reach equilibrium very quickly. The constant strain rate mode has been used in several very different designs of rheometer[83-87] utilising the ease of controlling the strain rate, by keeping the velocity increasing in proportion to the specimen deformation. However, since the velocity has to increase in line with the specimen end separation the constant strain rate can often take longer, than the constant stress machines, to reach a state of dynamic equilibrium, and often equilibrium is not achieved.[70] However, this mode of testing has been used to gain transitional behaviour data.[70,81,85,86] If steady state conditions are not attained, the ratio defined in equation (3.1) is known as the stress growth function.[60]

4.3 The Rutherford Elongational Rheometer

The Rutherford Elongational Rheometer was built to study relatively high elongational viscosity materials, primarily polymer melts to high strains. The Rutherford Elongational Rheometer produces approximately pure, simple, elongational flow; the flow field is Lagranean; this means that the experimentation has to be carried out repetitively on individual specimens.

The Rutherford Elongational Rheometer design drew largely on the principles embodied in the instrument developed by *Munstedt*,[88,89] the main difference being a horizontal layout which results in easier operation.

The Rutherford Elongational Rheometer (see Figures 4.1 and 4.2) has a specimen end separation format with a closed loop system controlling the constant strain rate.

Meissner[87] first suggested using a servo-control mechanism to control the deformation rate of an elongational rheometer. *Dealy*[90] was the first to use a feedback loop to produce a constant strain rate.

The principles of servo-control of separation velocity to produce a constant strain rate are that specimen length and separation velocity signals are combined according to equation (4.4):

$$\dot{\varepsilon}_{instantaneous} = U(t)/L(t) \qquad (4.4)$$

The instantaneous strain rate signal is then combined with a signal representing the desired strain rate so as to produce an error signal which is used to control the motor speed.

The advantages of a feedback system over a programmed separation rate increase are very strong in experimental terms. Any strain rate can be "dialled-in" and does not require changing of the cam or tape 'programmer'; the error signal reflects the true state of the deformation instantaneously, i.e. no assumptions are made about time zero or the deformation up to that point in time.

The stress circuit in the Rutherford Elongational Rheometer contains circuits incorporating elements which convert the **force** and **length** signals to a stress readout.

If constant volume (irrespective of volume) is assumed, the cross-sectional area, A_i, at a given strain can be calculated from equation (4.5):

$$A_i = [(\pi d_o^2)/4] . (l_o/l_i) \qquad (4.5)$$

where d_o is the initial specimen diameter, l_o is the initial specimen length and l_i is the length at a given strain.

Since $\qquad$ stress = force ÷ area

$$\sigma_i = (4F_i l_i) \div (\pi d_o^2 l_o) \qquad (4.6)$$

where σ_i is the stress at a given strain and F_i is the force at a given strain.

The force and length signals are monitored whilst the experiment is running, the other values are "dialled-in" prior to the experiment.

FIGURE 4.1: RUTHERFORD ELONGATIONAL RHEOMETER - FRONT VIEW
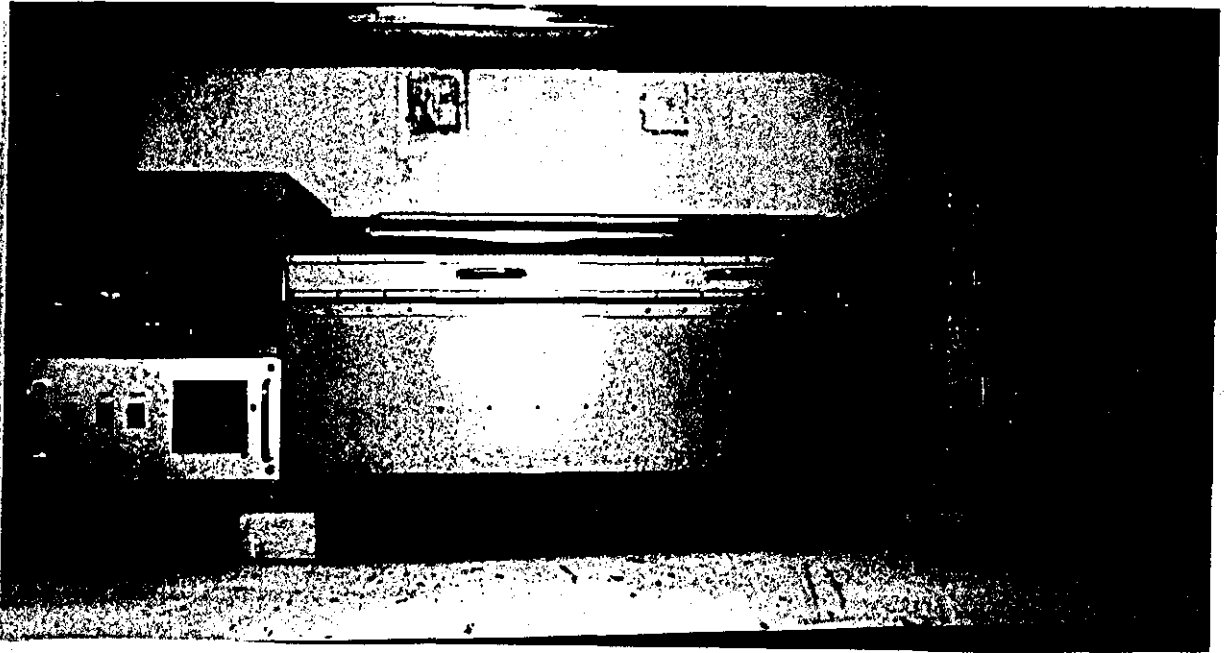
FIGURE 4.2: RUTHERFORD ELONGATIONAL RHEOMETER - PLAN VIEW (OPEN)
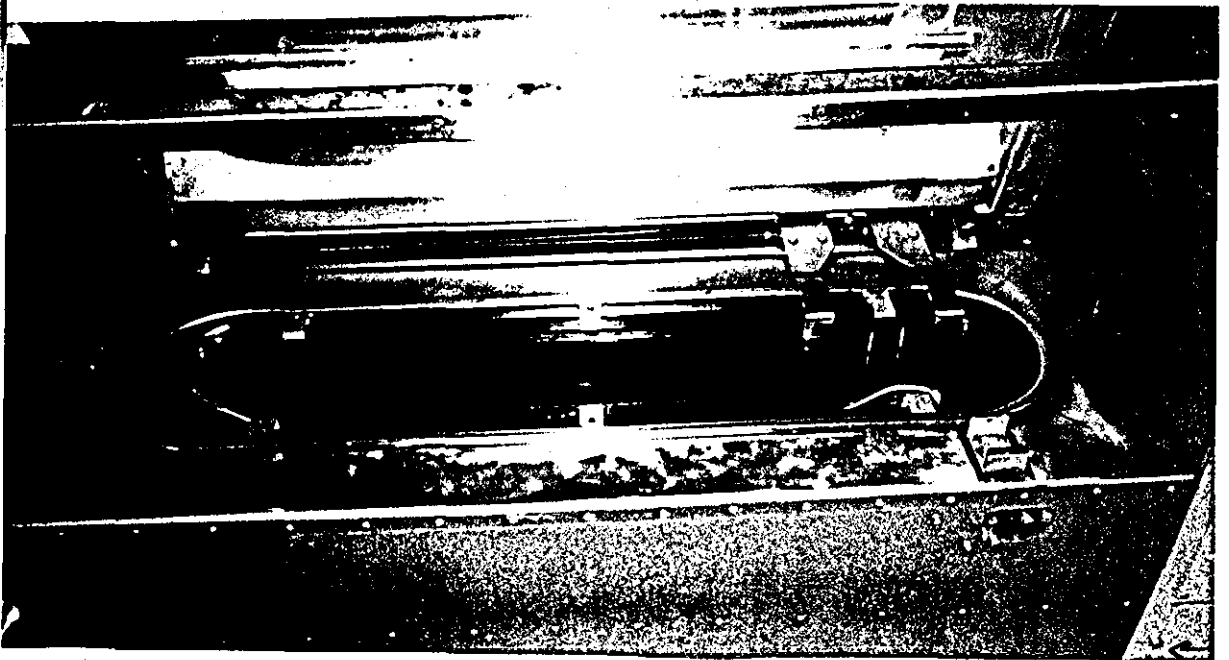
It has been claimed that the constant volume assumption is valid in the melt phase.[82] Thus the stress displayed on the rheometer is the true stress. The constant volume assumption is a good approximation at large strains even when the polymer is in the solid state.

A brief description of the Rutherford Elongational Rheometer is given below. *Smoker*[9] comprehensively described the specification of the Rutherford Elongational Rheometer, the operating procedure and the data analysis.

The Rutherford Elongational Rheometer is a constant volume elongational rheometer, having one end of the specimen held 'static' while the other is driven to produce the required extension by a variable speed servo-motor. The motor acts through a gearbox to drive a pulley, which is connected to the moving end of the specimen.

The specimen itself is mounted on specimen holders which are attached to arms of the carriages. The two carriages run on guide rails which are parallel to the axis of extension and ensure that the elongational deformation is maintained along that axis.

The 'static' carriage is attached via a pivoted beam to a linear variable displacement transformer (LVDT) based transducer. The transducer measures the force transmitted through the pivoted beam. The pivot position is adjustable, giving five force ranges from 1N to 100N.

The velocity range of the drive to the moving carriage is adjustable over six continuous decades, 10^{-5} to 10^0 m/s. A tachometer measures the rotational speed of the motor and a potentiometer, on the final drive shaft, monitors the position of the moving carriage.

Signals of force, velocity and displacement are fed into the control system. After comparison with the desired conditions a servo signal is sent to correct the motor speed, thus completing the closed loop system.

The specimen and specimen holders are immersed in a temperature controlled oil bath of silicone fluid. The silicone fluid acts as an efficient heat transfer medium and also supports the specimens preventing gravitational sagging.

4.4 Previous Work Using The Rutherford Elongational Rheometer

Since it was commissioned by *Smoker*[9] there have been two major studies carried out using the Rutherford Elongational Rheometer the first studied film blowing grades of low density polyethylenes[9] and the second studied rigid and plasticised grades of polyvinyl chloride[10]. Other polymers have been studied using this instrument these include PVC[91], SBS[92], propylene/ethylene copolymer[93,94] and polypropylene.[95,96]

Smoker[9] obtained data using the Rutherford Elongational Rheometer that confirmed *Meissner's*[97] assertion that transient data is the main use of constant strain rate experiments; a steady state is not reached. *Smoker*[9] reproduced *Meissner's*[97] time dependent stress growth function versus time curves for low density polyethylenes between 120°C and 150°C. The low density polyethylenes were tension thinning polymers: their apparent elongational viscosity (stress growth function) decreasing with increasing elongation rate and temperature. The form of the viscosity-time curves being a common curve with a deviation at extensions greater than a Hencky strain of 1.2. *Smoker*[9] also noted a further inflection at lower strains (0.47-0.90) which he correlated with the reciprocal of the minimum film thickness in the film blowing process. The two deviations in the curve were explained by molecular models; the lower strain inflection being due to discrete molecules 'snapping' into a temporary network structure and the inflection at a Hencky strain of 1.2 being the point where the structure 'locks-up'. The subsequent stress build-up above this strain being due to the extension strain increasing faster than the network relaxes; the 'old' entanglements causing a constantly increasing stress.

Arif[10] studied rigid and plasticised polyvinyl chloride polymers between 160°C and 190°C. He produced master curves for temperature and for plasticiser content (0 to 60pphr). Different types of plasticiser were also investigated but no simple relationship was found between the elongational flow behaviour and plasticiser molecular weight.

PVC was found to be a tension thinning polymer, both rigid and

plasticised compounds.[10] The experimental results were successfully modelled using the Chang and Lodge rubber-like model equations, but the applicability was restricted to low elongation rates and low strains, the model also failed to explain the stress build-up phenomenon.

The instrument was limited by the maximum operating temperature (200°C, the maximum working temperature of the silicone fluid), preventing many commercial polymers from being tested.

4.5 Modification Of The Rutherford Elongational Rheometer

Before the elongational flow properties of PET melts could be determined, the Rutherford Elongational Rheometer required some modifications for use at higher temperatures. The instrument previously had a maximum working temperature of 200°C. The data collection and analysis system constitutes a major time-consumer of this method; computer datalogging was seen to offer a significant improvement.

4.5.1 The Heating System

The heating system of the Rutherford Elongational Rheometer consists of heating elements, a temperature controller, a temperature monitoring device and a heat transfer medium. The modifications to increase the maximum working temperature of the instrument included replacement or adjustment to all of these items.

The Heating Elements

The existing set of three heating elements in series were replaced by a single more powerful heating element. A *Pyrotenax* electrical trace heating grid, consisting of a 1600Watt, 240Volt, stainless steel sheathed, mineral insulated, heating unit mounted onto a welded mesh grid, diagrams of the two heating element systems are shown in Appendix 5.

Temperature Control

The fitted *CRL 405* temperature controller had a maximum setting of 200°C which could not be modified; it was replaced by a *Eurotherm*

810 digital PID temperature controller, with a 0°C to 399.9°C range; a ±0.2°C accuracy and a ±0.25°C stability.

Temperature Monitoring

The temperature monitoring device is a Platinum resistance thermister, this has been modified and is now mounted vertically in a clamp (with the seal above the oil level), shown schematically in Appendix 6, rather than just lying on the bottom of the oil bath (where it was potentially prone to be damaged by the hot oil leaking through the crimped seal).

Heat Transfer Media

The heat transfer medium was a silicone fluid (ICI F190) which had a maximum working temperature of 200°C. Two high temperature fluids were tested for their suitability. Tests of weight loss, gelling behaviour and interaction with PET were carried out, details of the tests and the results are shown in Appendix 7. The two fluids tested were a dimethyl polysiloxane fluid (Dow Corning 210H fluid) and a phenyl methyl polysiloxane fluid (Dow Corning 710 fluid).

A series of experiments were carried out to investigate any possible attack on PET by the fluids. The experiments involved were: oil absorbance tests; retention of tensile strength; plasticisation effects; attack on the molecular structure; and any surface attack. The tests were carried out on injection moulded dumbbell specimens of a 0.9 I.V. PET material.

From the results above the DC 210H silicone fluid was selected. This fluid had the best high temperature lifetime and did not significantly attack the PET samples. However due to the fluid fuming at high temperatures, the Rutherford Elongational Rheometer was placed under forced-air extraction.

4.5.2 The Drive Wire

The radio cord drive wire described by *Smoker*[9] had been replaced by high tensile brass tyre cord wire by *Canevarolo*[92]. This was considered too easily kinked and was replaced by a braided wire (as used for leader wires in angling) which proved to be more durable, less springy and not easily kinked.

4.5.3 The Specimen Holders

The PTFE horseshoe specimen-holders described by *Smoker*[9] prevented quick placement of the rigid PET specimens in the rheometer. The holders were modified, see Figure 4.3, to allow the hoop specimens to be immersed in the hot oil in the correct position in the rheometer as quickly as possible.

4.5.4 Datalogging By Computer

The chart recorder was replaced by an Apple IIe microcomputer and CIL interface unit. Software developed by *Wilkinson*[98] was modified; this enabled stress and length data to be collected, calculations to be carried out, then tables to be printed of the results. The computer program is listed in Appendix 8.

FIGURE 4.3: MODIFIED SPECIMEN HOLDERS
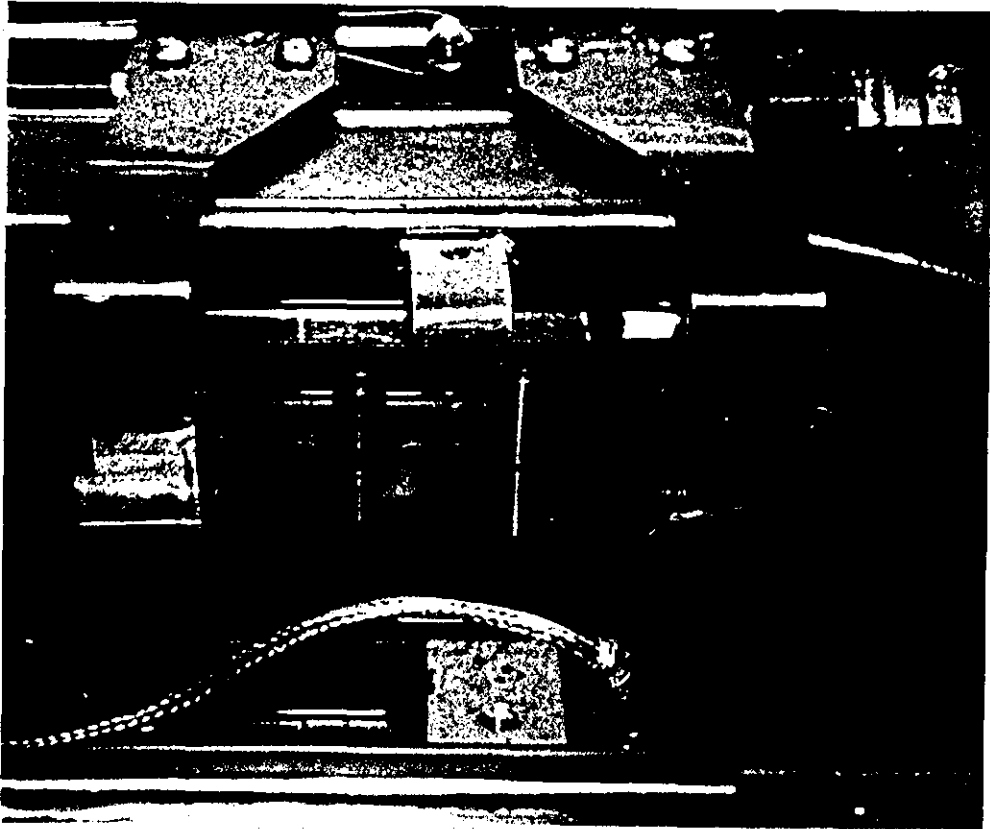
4.5.5 Testing Of Modifications

To test the effectiveness of the modifications that were made to the Rutherford Elongational Rheometer the elongational behaviour of polycarbonate sheet (Lexan) was determined using die cut specimens. Polycarbonate was used as it is a high temperature polymer, available in sheet and it is used in processes involving elongational flows, i.e. blow moulding and thermoforming. Figure 4.4 shows the results obtained for polycarbonate tested at 260°C and 280°C. The elongational stress growth function is seen to increase with time and a deviation to strain-hardening behaviour can be observed (at a Hencky strain of 2.25) for the 0.75s⁻¹ Hencky strain rate curve at 280°C. The results show that the Rutherford Elongational Rheometer can be used to study polymer melts at high temperatures (>200°C).

FIGURE 4.4: ELONGATIONAL BEHAVIOUR OF POLYCARBONATE

FIGURE 4.4: ELONGATIONAL BEHAVIOUR OF POLYCARBONATE

STRESS GROWTH FUNCTION (Pa.s)

+ 280C, HSR = 0.75s-1
* 280C, HSR = 0.95s-1
□ 260C, HSR = 0.50s-1
× 260C, HSR = 0.75s-1

TIME (seconds)
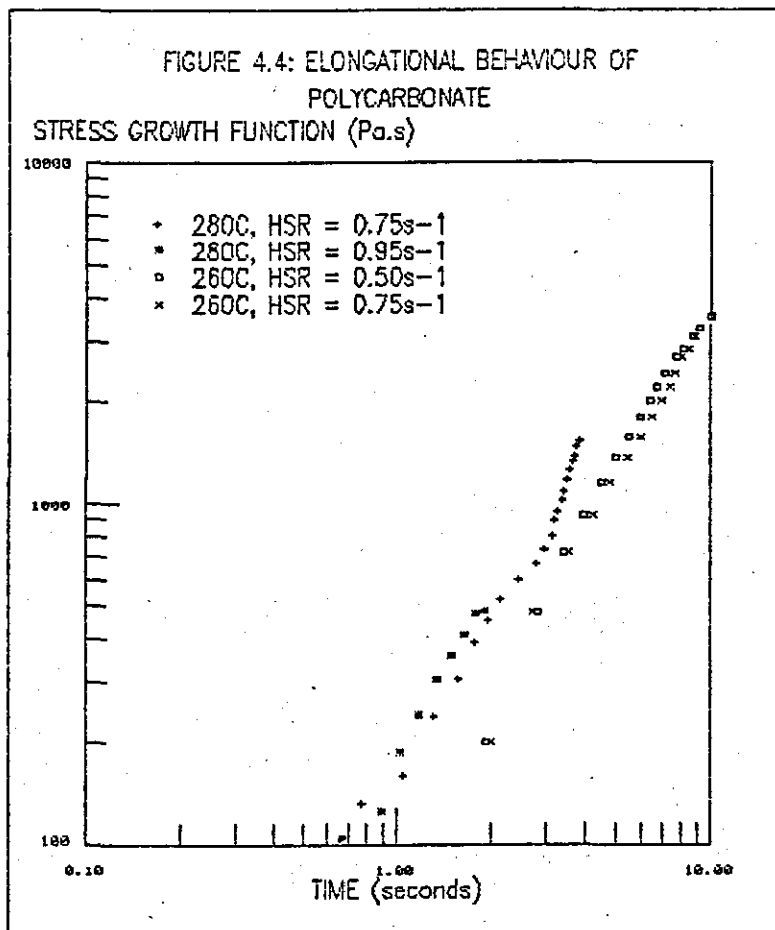
4.5.6 Modification To Specimen Preparation Method

The injection moulded specimens used by *Smoker*[9] proved unsatisfactory due to the occurrence of weld-lines resulting in premature failure at the weld during testing, see Figure 4.5a, also non-round cross-sectioned specimens, see Figure 4.5b, and with crystalline PET specimen separation from the runner system without damaging the specimen proved difficult. All of these problems were caused by poor mould design.

FIGURE 4.5: SPECIMEN DEFECTS
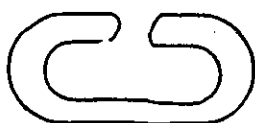
(a) Weld-line failure   (b) Non-circular section

An alternative method to injection moulding was die cutting from sheet; this method proved acceptable for amorphous unoriented PET but not for crystalline PET. However, obtaining samples of polymer in sheet form presents a supply problem; therefore, it was decided to modify the injection moulding tool.

Whilst modifying the mould to produce specimens free of weld-lines and easy to separate from the runner system, the opportunity was taken to change the specimen shape.

The specimen shape was changed to a dumbbell type, having a thickness of 1.5mm and a width of 3mm in the test region (see Figure 4.6). The specimen cross-section was changed from circular to rectangular but the potential disadvantage of possible edge effects was outweighed by the advantages of producing consistent specimens which deform within a known test region. [This change required a change in the operating procedure: the equivalent diameter was used to set up the instrument, before a run, calculated from the total cross-sectional area of the specimen.] The gate position was moved to prevent weld-lines occurring in the tapered test region of the

specimen. To utilise the same mould-block the number of cavities was reduced from six to four, and new insertable cavities were machined.

FIGURE 4.6: RUTHERFORD INJECTION MOULDED SPECIMENS

| (a) Original Injection | (b) Modified Injection |
| Moulded Specimens | Moulded Specimens |
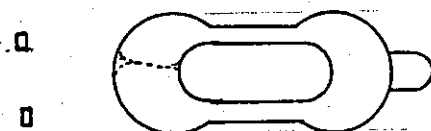
Gate Dimensions

The design principles used were those published by *Pye*[99]; a tab gate was chosen (see Figure 4.6) the dimensions of which were calculated using the following algorithms:

Tab

Tab depth = 0.9 X (cavity thickness)   (4.7)

Tab length = 1.5 X (runner diameter)   (4.8)

Tab width = runner diameter   (4.9)

Rectangular gate

Land length = 0.5mm minimum   (4.10)

Depth = n X (wall section thickness)   (4.11)

Width = [n X (surface area of cavity)$^{0.5}$] ÷ 30 (4.12)

(where n is a material constant, taken as 0.8 for PET).[99]

Maximum Shear Rate (Through Gate)

With these dimensions for the tab gate the shear rate during injection was calculated.

$$\dot{\gamma} = 6q \div WH^2 \qquad (4.13)$$

$$\dot{\gamma} = (6 \times 1422) \div ((1.2)^2 \times 0.93) = 637 \text{sec}^{-1}$$

(where q = volumetric flow rate for an approximate volume of 711mm^3 and an injection time of 0.5 sec.)

This shear rate was considered acceptable for moulding PET (see Chapter 2).

4.6 PET Melt Elongational Flow

Several attempts to determine the elongational flow properties of linear PET melts using the Rutherford Elongational Rheometer were made. Injection moulded and die cut specimens (amorphous and crystallised specimens) were studied. All attempts failed, as the specimens sagged excessively, before the instrument could be set up and a run started. The sagging was due to the melt density of the polymer ($\rho \simeq 1.2$ @ 270°C)[100] being significantly greater than the specific gravity of the hot silicone fluid (S.G.$\simeq 0.75$ @ 270°C, determined from volume expansion experiments). If the densities could have been matched more closely, the fluid may have supported the low viscosity molten specimen. However, none of the commercially available heat transfer media that meet the other test requirements (high temperature stability, inertness to PET, low weight loss at high temperatures, slow gelling rate, non-toxic, high boiling point, high flash point, low dependence of viscosity on temperature), had an appropriate specific density.

4.7 PETG Copolyester Melt Elongational Flow

4.7.1 Experimental Procedure

Dried PETG was injected moulded into Rutherford Elongational Rheometer specimens. The constant Hencky strain rate mode of operating procedure, described by *Smoker*[9], was followed. The specimens (double and triple specimens were used) were placed on the specimen holders and the instrument was zeroed, after a pre-heat time of 6 minutes, to allow for the specimen temperature to reach equilibrium, the run was started and the stress and displacement signals were recorded. Several runs were made at each elongation rate and average results are reported here. Several elongation rates were used at two temperatures 110°C and 170°C (PETG has a T_g of 81°C and is wholly amorphous).

4.7.2 Results

The results are shown in Figures 4.7 and 4.8, as stress growth function-time curves, *Meissner*[97] first reported elongational data using this format as the data is transient, no steady state condition being attained. Using a time axis is the clearest method of presentation as plots, at constant elongation rate, of stress growth function against strain would become cluttered. The data becomes spread out along the time axis as the lower elongation rates involve longer time scales. Figures 4.9 and 4.11 are true stress-true strain curves, showing the effect of elongation rate, and Figure 4.10 is an example of a true stress-Hencky strain rate plot. Figures 4.7, 4.9 and 4.10 show the results at 110 °C and Figures 4.8 and 4.11 show the results at 170 °C.

FIGURE 4.7: PETG RUTHERFORD RESULTS AT 110°C
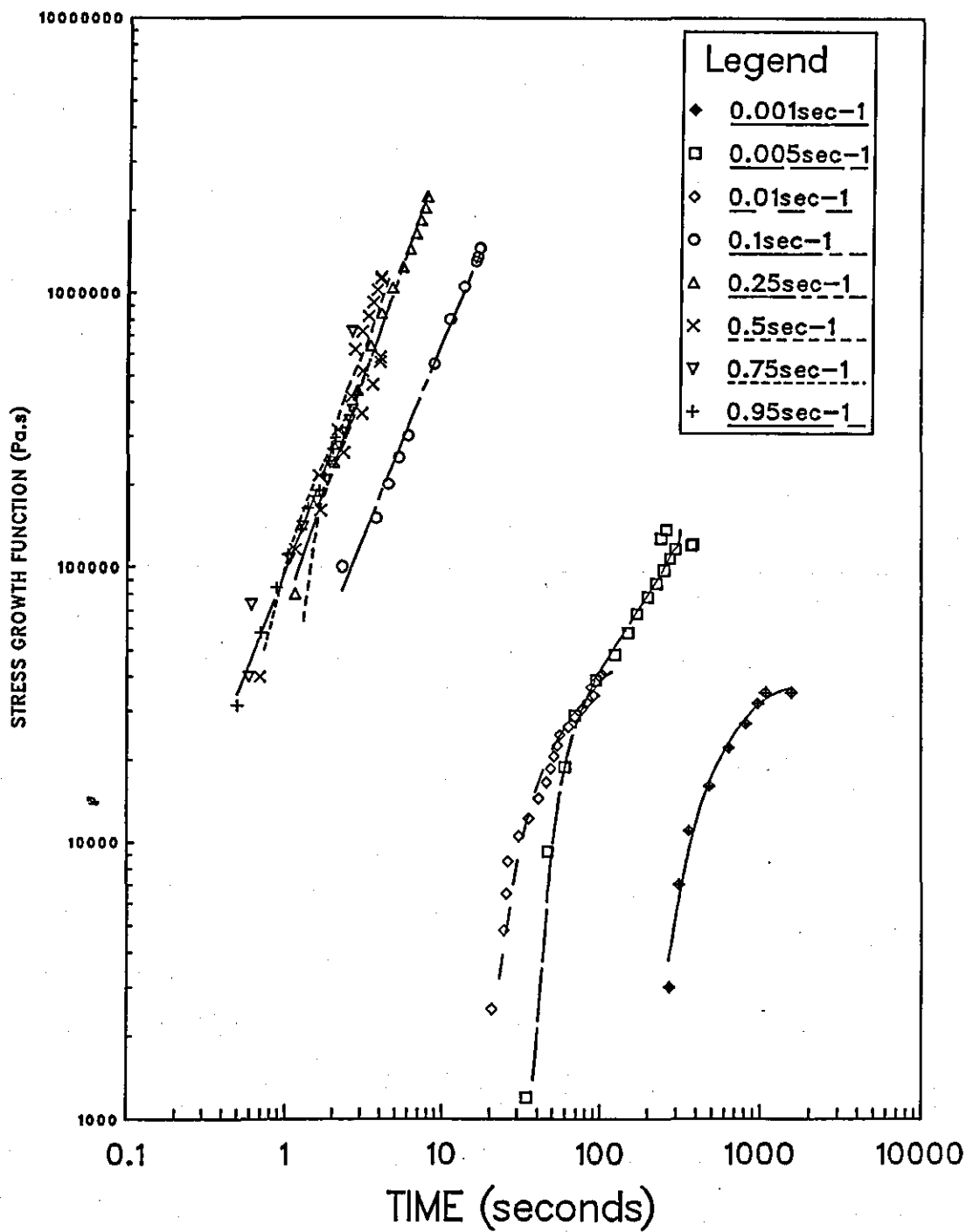
FIGURE 4.8: PETG RUTHERFORD RESULTS AT 170°C
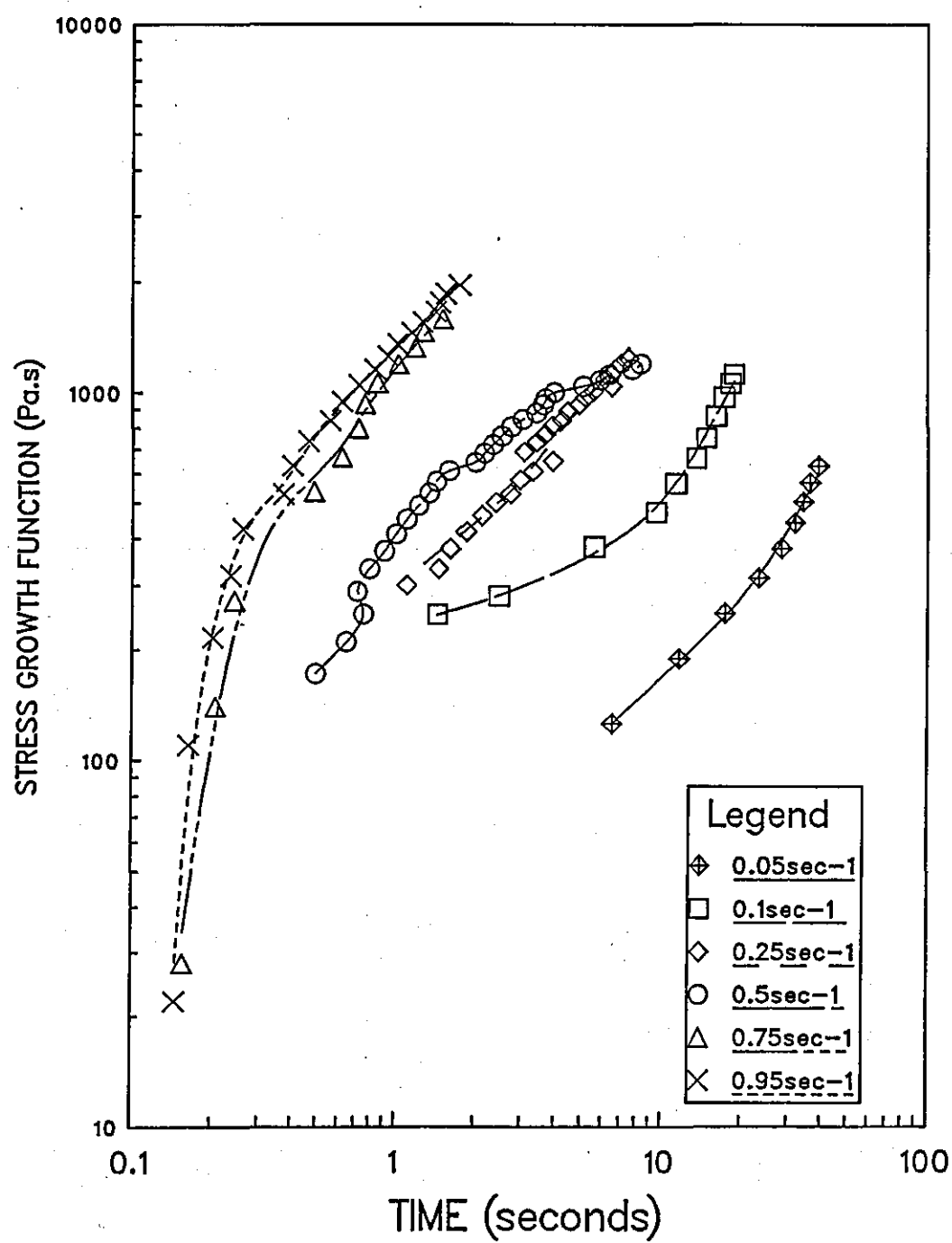
FIGURE 4.9: PETG AT 110C

TRUE STRESS (MN/m2)

Legend:
- HSR = 0.1s-1
- HSR = 0.25s-1
- HSR = 0.5s-1
- HSR = 0.75s-1
- HSR = 0.95s-1

TRUE STRAIN
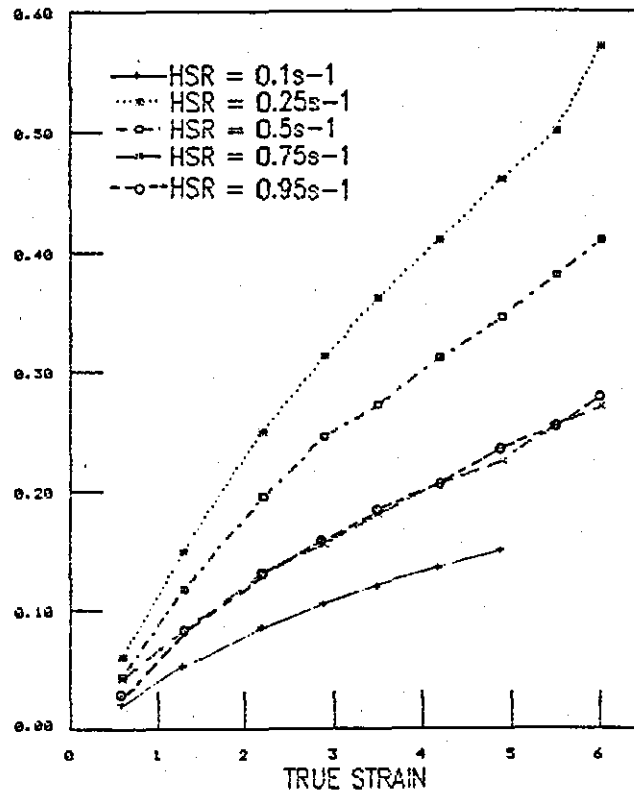
FIGURE 4.10: PETG AT 110C

TRUE STRESS (MN/m2)

Legend:
- TRUE STRAIN = 1
- TRUE STRAIN = 2
- TRUE STRAIN = 3
- TRUE STRAIN = 4
- TRUE STRAIN = 5
- TRUE STRAIN = 6

HENCKY STRAIN RATE (sec-1)

FIGURE 4.11: PETG AT 170C
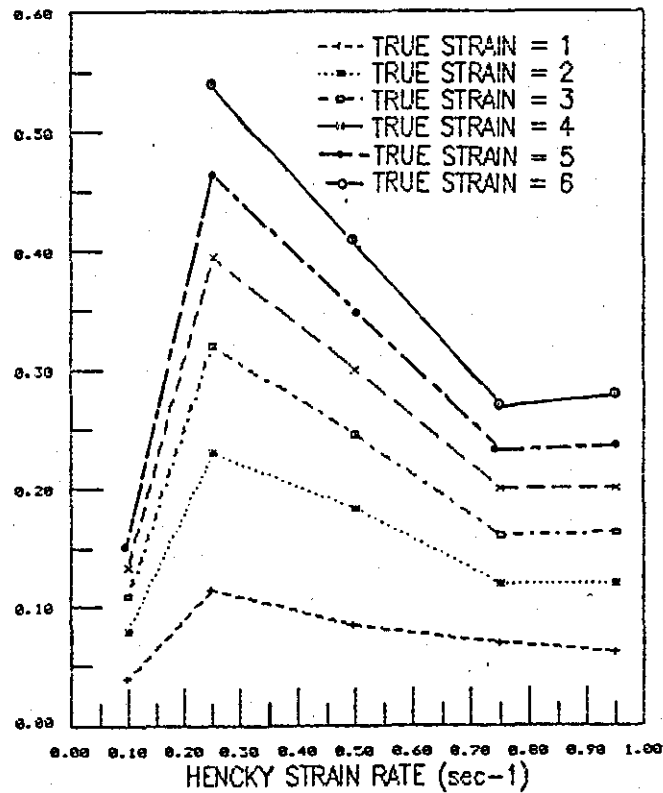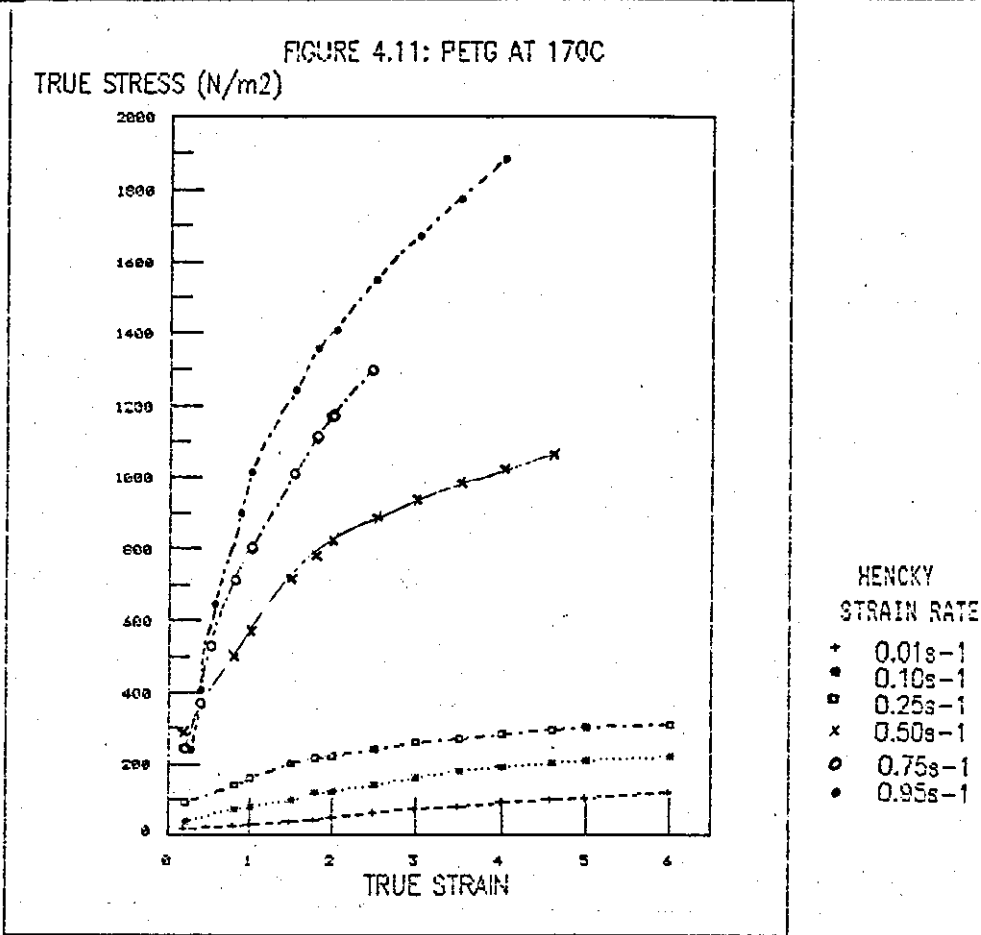
FIGURE 4.12: MOLECULAR BEHAVIOUR OF PETG IN AN ELONGATIONAL FLOW
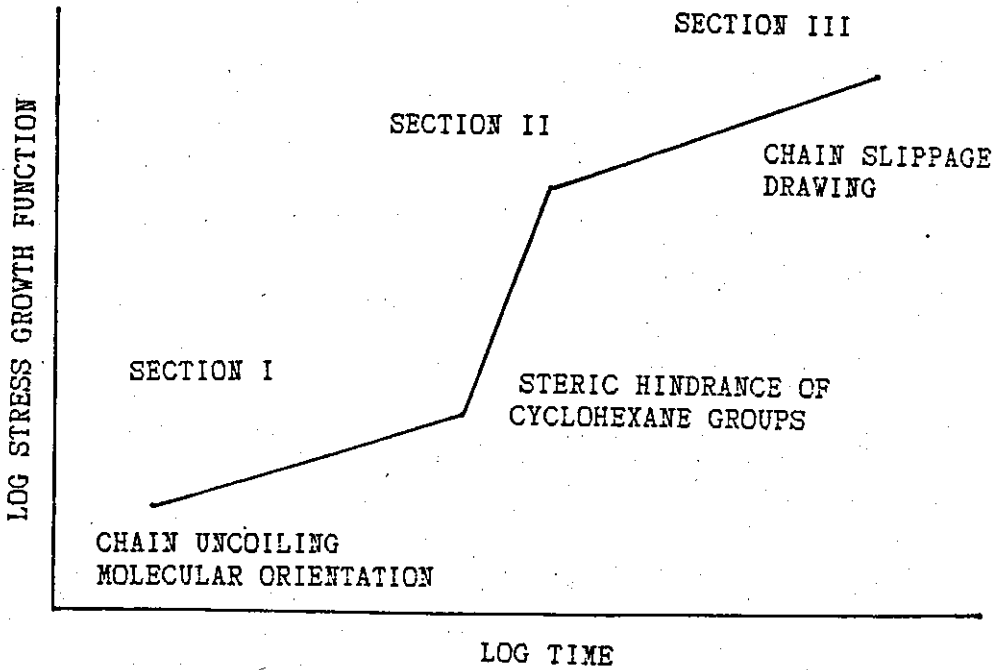
4.7.3 Discussion

The PETG experiments did not suffer the same specimen sagging problems as the linear PET experiments, therefore the melt density of the PETG Copolyester (ρ = 0.98 @ 250°C)[37] is closer to that of the silicone fluid (S.G. $\approx$ 0.75 @ 270°C) at the temperatures used. Also the PETG was studied at lower temperatures than the PET melt, the melt viscosity was higher making the specimens more self-supporting.

Figure 4.7 shows that at 110°C the resistance to extension increased rapidly with deformation time and was also greater with increasing elongation rate. At 110°C the deformation will be predominantly elastic and the response is due to chain uncoiling. The values of stress growth function are very much greater than those in Figure 4.8 for the 170°C data where viscous flow of the melt is predominant over the elastic response.

The curves shown in Figure 4.8 indicates that three types of elongational behaviour occurred with PETG Copolyester during the Rutherford Elongational Rheometer experiments at 170°C. The curves can be divided into three sections, which relate to the three different behaviours, see Figure 4.12.

Section I shows an increasing elongational stress growth function with increasing time, this is due to the molecular orientation that is occurring as the molecular chains are pulled from their random configuration into an ordered arrangement.

Section II is shown by an increase in the rate of elongational stress growth function rise, this increase in resistance to flow is caused by the large cyclohexane groups interfering with each-other in adjacent oriented molecular chains. The steric hindrance produces a "mechanical locking" of the chains.

Section III is shown by a decrease in the rate of elongational stress growth function rise, this decrease in resistance to flow is caused by the onset of chain slippage, the polymer is drawn down until failure occurs.

Figure 4.7 shows the PETG behaviour at 110°C elongational stress growth function increasing with time, the response above an elongation rate of 0.01s^{-1} is linear and relatively independent of

rate, the stress build-up can be explained by the rubber-like network theory; at a critical point in time molecular chain segments of adjacent molecules interfere sufficiently for a temporary network to be established, this network behaves in a rubber-like manner to deformation. In the high elongation rate curves in Figure 4.7, the stress build-up occurs when the extension strain increases faster than the rubber-like network can relax, the stress cumulating with time . At the low rates of testing, $\dot{\varepsilon}$ = 0.001s^{-1} to 0.01s^{-1} the curves are seen to deviate from a linear response, these curves show Section II and Section III of the viscous flow behaviour, the elastic component having had time to fully recover. Section I behaviour was not detected, possibly due to the low stresses involved being below the minimum detectable limit for the instrument. The elongational stress growth function values are much smaller at the lower elongation rates as only the viscous response is detected. At the higher testing rates the response contains both the elastic and viscous components of the deformation, as the response is recorded before the elastic component has fully recovered.

Figure 4.8 shows the elongational stress growth function increasing with deformation time. At a given time, the elongational stress growth function is greater with increasing elongation rate. The low elongation rate curves show melt flow Section I and Section II type behaviour consecutively, failure occurred before the specimens were drawn down. The higher elongation rate curves show Section II and Section III type behaviour consecutively, the Section I type behaviour is hidden by the elastic component of the response, which is detected before it has fully recovered at the faster testing rates.

Figure 4.9 shows the true stress against the true strain as a function of the elongation rate at 110°C; the true stress increases universally with increasing true strain. The $\dot{\varepsilon}$ = 0.1s^{-1} curve was anomalous to the curves at the other rates, this curve having lower stress values than the other curves, the true stress values above elongation rates of $\dot{\varepsilon}$ = 0.25s^{-1} decreased with increasing rate. The low stress values observed for the 0.1s^{-1} elongation rate illustrates

the time-dependent behaviour of the deformation, the rate of deformation being slow enough for the elastic response to fully recover before the stress is measured. At higher elongation rates the time-dependent recovery is incomplete during testing and as the response at 110°C is predominantly elastic the stress values are higher than those reported for the $0.1s^{-1}$ strain rate.

Figure 4.9 shows that at a given true strain the stress decreases with increasing rate. Also, the rate of stress increase with extension decreases with increasing elongation rate, this is shown more clearly in Figure 4.10. The decreasing stress with increased rate occurs above a critical elongation rate, when the elongation rate is high enough the molecules become 'unlocked' from the temporary rubber-like network and during chain uncoiling the molecules pass each other more freely, they also have less time to attain an ordered arrangement where steric hindrance could increase the resistance to flow. The behaviour above a Hencky strain rate of $0.75s^{-1}$ can be explained as once the critical stress, at which chain slippage occurs, has been reached the increase in elongation rate is countered by the thinning out of the molecules and so the response appears independent of stress. (Below an elongation rate of $0.1s^{-1}$ the stress levels recorded were extremely low and have therefore not been included in Figure 4.9.)

Figure 4.11 shows the true stress against the true strain as a function of the elongation rate at 170°C, the true stress increased with increasing true strain. At a given true strain the true stress increased with increasing elongation rate. This trend is the opposite to that observed at 110°C in Figures 4.9 and 4.10, this is due to the effect of temperature on the viscoelasticity of PETG. At the higher temperature the response is predominantly viscous. At a given true strain the stress increases with elongation rate as the deformation will have progressed along the route illustrated in Figure 4.12, at low rates the molecular chains are becoming oriented; whilst at higher rates the chains are already oriented and the cyclohexane groups in adjacent chains are preventing chain slippage and increasing the stress required to deform the specimen.

4.7.4 Suitability For Extrusion Blow Moulding

The Rutherford Elongational Rheometer data can be applied directly to the problem of parison sagging in extrusion blow moulding. The tension stiffening response of PETG melt illustrated in Figure 4.11 shows behaviour that is desirable for an extrusion blow mouldable material, since any sagging would result in an increasing elongational stress growth function and therefore a greater resistance to further flow, i.e. a stabilisation of the parison preventing excessive sagging. The tension thinning response reported in Chapter 3 cannot be applied to the parison sagging problem as the geometries of the flows are different. Such data can only be applied to the extrusion of the parison through a converging die.

4.8 Comparison Of Rutherford Data And Converging Flow Data

When comparing elongational flow data from different experiments their respective flow geometries, types of flow and deformation occurring, and the boundary conditions need to be considered, see Table 4.1.

TABLE 4.1: COMPARISON OF METHODS

	Rutherford	Converging Flow
Flow	Free surface, pure simple elongational flow, no shear.	Constrained, combination of shear and elongational components.
Method	Direct, specimen end separation, unsteady state, uniaxial extension.	Indirect, capillary rheometry, converging flow.
Control	Controllable, constant elongational Hencky strain rate. Measured true stress.	Non-controllable, constant output rate. Measured die entry pressure drop, orifice die.
Results	Apparent data.	Apparent data.

FIGURE 4.13: COMPARISON OF TENSILE DATA
OF PETG 6763 COPOLYESTER AT 170C
TRUE STRESS/ELONGATION RATE (Pa.s)
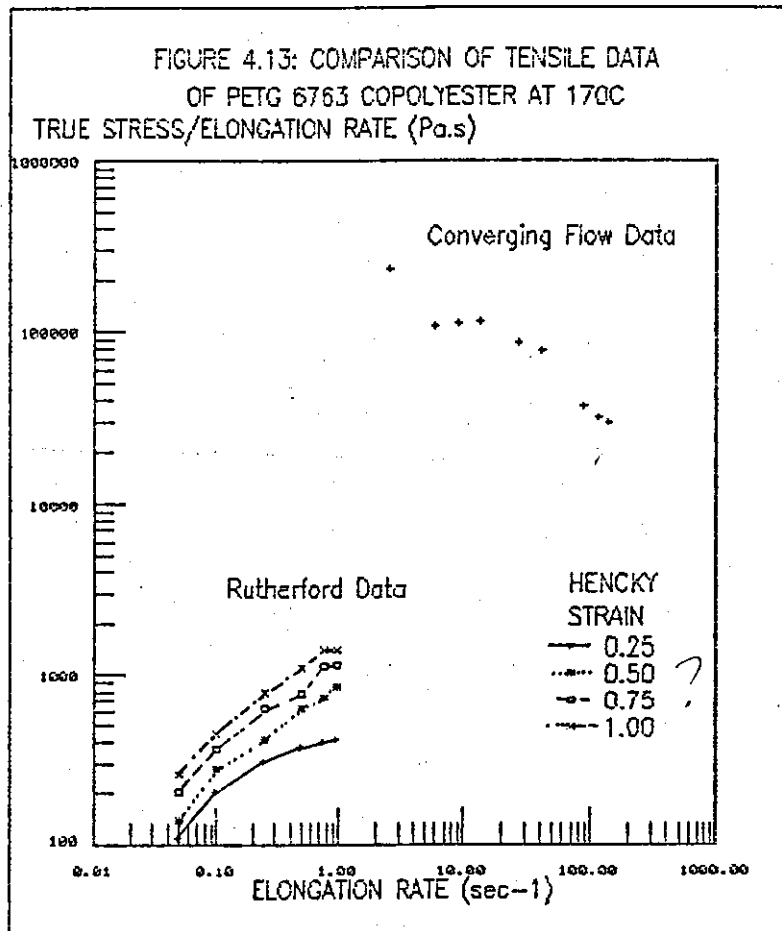
The differences in the elongational data compared in Figure 4.13 emphasise the need for caution in attempting to make direct correlations between elongational data and practice. The differences must be due to the differences in the methods shown in Table 4.1. It can be seen that the two sets of data are not quantitatively equivalent and in fact appear to display opposite trends with respect to elongation rate. This illustrates the need to restrict direct comparisons of elongational flow data to like-to-like comparisons.

In shear flows the cyclohexane groups of the copolymer will not interfere, as they do in elongational flows, as the rotational flow occurring in shear will prevent any steric hindrance. In converging flows both shear and elongational flows occur simultaneously, whilst in the Rutherford experiments no shear flow occurs, this difference will result in a different response for PETG tested using the two methods.

In converging flow the deviations in response explained by cyclohexane groups interfering does not occur at the same elongation rates as that observed with the Rutherford data. However, above a critical elongation rate the rotational shear deformation will become less effective than the elongational deformation and the cyclohexane interference can occur. Therefore, the deviations in resistance to flow behaviour, of PETG in elongational flows, as discussed in Sections 3.6.3 and 4.7.3, though occurring at different elongation rates, are explained by the same molecular deformation behaviour, i.e. molecular orientation, followed by the cyclohexane groups of adjacent molecules interfering and increasing the resistance to flow, followed by chain slippage at higher stress levels.

The two methods provide data that is applicable to different processes. Elongational flow data should only be applied to processes where an equivalent type of flow occurs as that in the flow measurement method used, i.e. like-to-like applications. The converging flow method provides data applicable to injection moulding and extrusion through dies. The Rutherford data provides · data applicable to parison sagging in extrusion blow moulding, drawing of fibres, monofilaments, films and sheet. Attempts will also be made in

Chapters 6 to apply the data to the inflation stage of extrusion blow moulding.

4.9 Comparison With Previous Rutherford Data

Figure 4.14 shows a comparison of PETG data at 170°C with several of the polymers tested previously using the Rutherford Elongational Rheometer. It can be seen from Figure 4.14 that the PETG data differs in three significant ways. Firstly the $0.95s^{-1}$ curve bends in the opposite direction than the other polymers tested at similar rates. Secondly, the PETG has higher stress growth function values for the higher elongation rate data, i.e. apparent "tension stiffening" behaviour, this can be seen to be the opposite trend than those reported for the other polymers: LDPE, PVC and the PP/PE copolymer are all tension thinning polymers. Thirdly, the PETG curves do not tend to form a common baseline curve with deviations above a critical strain, this is a consequence of the PETG copolyester being tension stiffening and the data being presented using a time axis. The first two differences suggest the PETG has a different elongational flow mechanism at 170°C than the other polymers tested. This has been described in Section 4.7.3 as due to the cyclohexane groups present in the molecular chain.

Figure 4.15 confirms the differences in elongational flow behaviour between PETG and LDPE by showing the stress growth function against elongation rate for constant Hencky Strain values. This figure illustrates the tension stiffening behaviour of the PETG, being studied, and the tension thinning response of the film blowing grade of LDPE (Escorene LD183) reported by Smoker.[9] The differences in response are evidence for the various polymers suitability for different polymer processes. PETG was developed for extrusion blow moulding and its suitability has been discussed in Section 4.7.4. The PP/PE random copolymer was a film blowing grade polymer (ATO 3050FG3) and the PVC was an extrusion blow moulding or injection

FIGURE 4.14: A COMPARISON OF RUTHERFORD DATA FOR DIFFERENT POLYMERS

FIGURE 4.15: A COMPARISON OF RUTHERFORD RESULTS FOR PETG AND LDPE
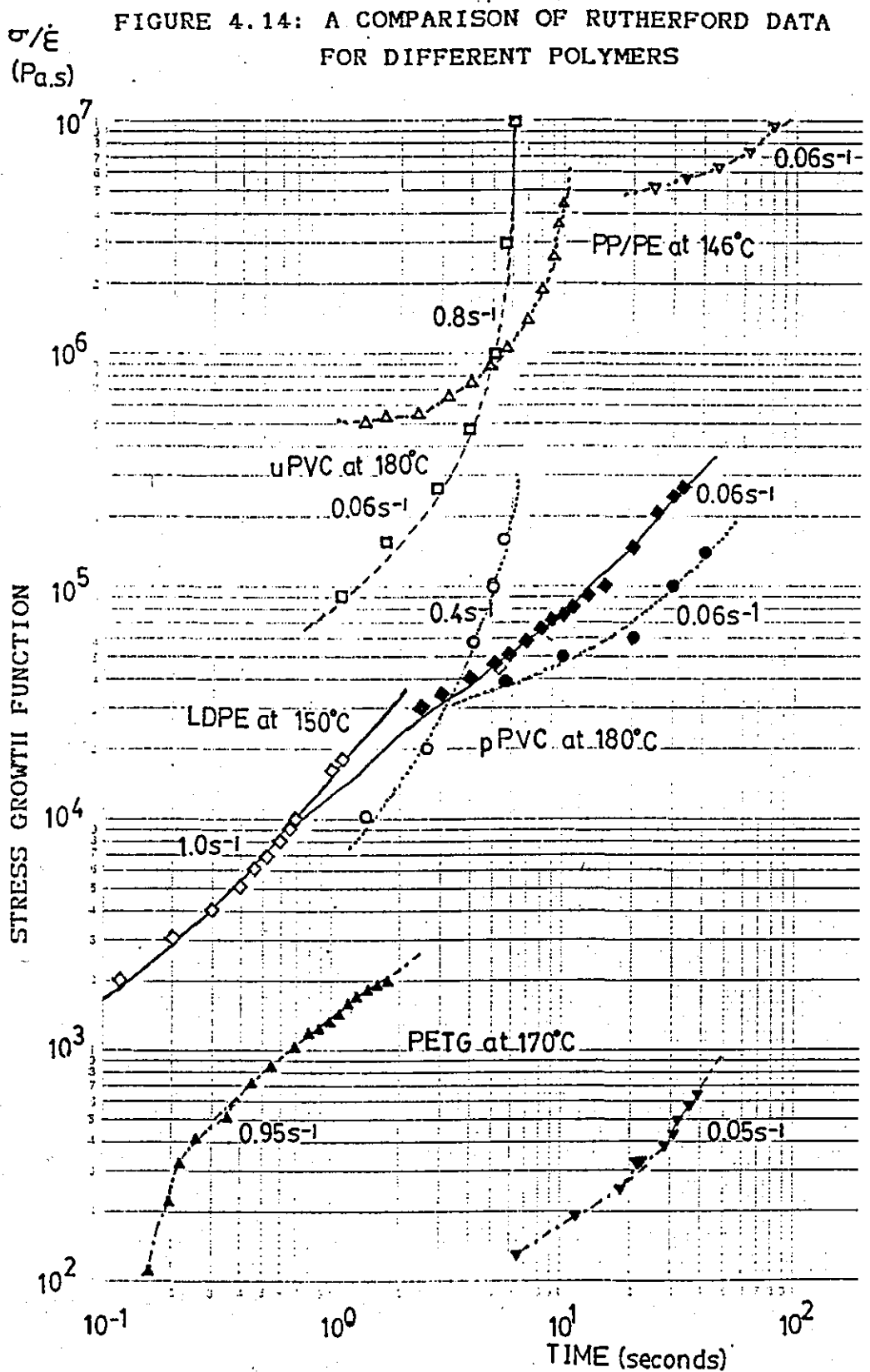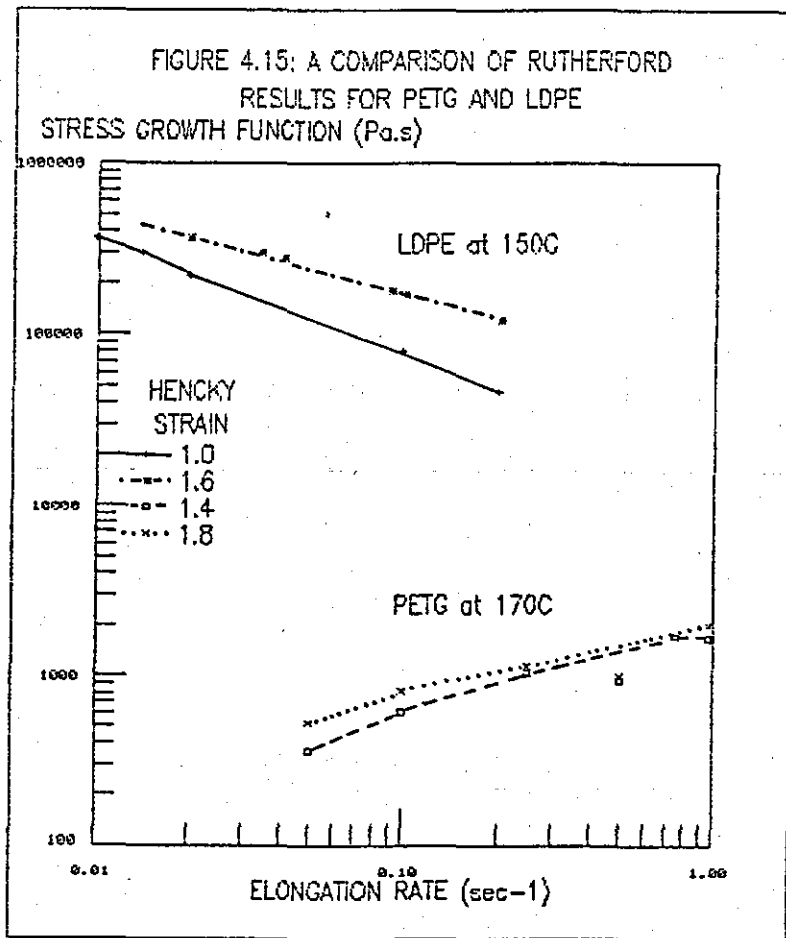
moulding grade (Corvic S57/116). The tension thinning response of these other polymers would seem a disadvantage for their applications and would determine the limiting conditions of processing, such as minimum film thickness and maximum parison length. Rutherford Elongational data is based on flows which are not representative of elongational flows in injection moulding and should not be applied to that process.

4.10 PET Thermoelastic Elongational Behaviour

4.10.1 Experimental Procedure

Rutherford Elongational Rheometer specimens were die-cut from 1mm PET thermoforming sheet. The constant Hencky strain rate mode of operating procedure, described by *Smoker*[9], was followed. The specimens were placed on the specimen holders and the instrument was zeroed. After a pre-heat time of 15 minutes, the run was started and the stress and displacement signals were recorded. Several runs were made at each elongation rate and the average results are reported here. Several elongation rates were used at four temperatures 80°C, 90°C, 100°C and 110°C; at these temperatures $(T > T_g)$ PET is in the thermoelastic phase: At higher temperatures the PET crystallises rapidly and the (spherulitic-type) crystalline polymer requires much higher forces to induce deformation. As well as the standard elongational flow measurements, the Rutherford Elongational Rheometer was used to generate data in the stress relaxation and strain recovery modes. Stress-induced crystallisation occurs with PET at large strains: to evaluate this occurrence, the specimens were retained after the tests and their density values were determined.

Stress Relaxation

The specimens were stretched at constant strain rate to a pre-set strain then the specimens were held at that given elongation and the decay of the stress was recorded. The stress relaxation experiments were carried out at the Rutherford Elongational Rheometer's maximum strain rate $(1.0s^{-1})$ to minimise any simultaneous

relaxations which could occur during elongation of the specimens.

Strain Recovery

At different strain rates, the specimens were stretched at constant Hencky strain rate to a pre-set strain. The test was stopped and the motor reversed to release the fully-extended specimens from the restraint of the specimen holders. The specimens underwent partial elastic recovery and the specimen length 15 seconds after the maximum strain was reached was recorded, this was taken as a spot-value measure of the elastic strain recovery of the specimen as calculated from equation (4.14):

$$\varepsilon_R = [\ (L_{MAX}-L_{15s})/(L_{MAX}-L_O)]\ X\ 100 \quad (\%) \quad (4.14)$$

Stress-Induced Crystallisation

Though the amorphous specimens are isotropic and the deformed specimens show optical anisotropy, the birefringence will be due to both the orientation and the crystallisation. Also, compensation of the birefringence could not be obtained and so simple optical methods proved unsuitable for determining the occurrence of stress-induced crystallisation.

As the density of amorphous and crystalline PET is different (non-oriented amorphous density = 1335kg/m³; oriented heat set density = 1390kg/m³; and calculated crystal density = 1455kg/m³)[100] the occurrence of stress-induced crystallisation will increase the density of a given specimen. A density column was prepared (as described in ASTM D1505-68)[101] and the density of the specimens was determined after elongation. The effects of residence time in the oil bath at the temperatures involved were determined by measuring the density of unstretched specimens after various time intervals in excess of those experienced in the stretching experiments; residence time effects were found to be negligible.

4.10.2 Results

Data is presented in various forms, from collation of force, time and distance data. For example, Figures 4.16-4.19 show elongational stress growth function-time curves, illustrating the effect of elongation rate at constant temperature, the temperature being 80°C, 90°C, 100°C and 110°C respectively. Also, Figures 4.20-4.23 show the

effect of temperature at constant elongation rate, the elongation rates being $0.001s^{-1}$, $0.01s^{-1}$, $0.1s^{-1}$ and $0.95s^{-1}$ respectively.

True stress-true strain curves are shown as Figures 4.24-4.27 as a function of temperature at constant elongation rates, $0.25s^{-1}$, $0.5s^{-1}$, $0.75s^{-1}$ and $0.95s^{-1}$ respectively. Figures 4.28-4.31 show the true stress-true strain curves as a function of elongation rate at constant temperatures 80°C, 90°C, 100°C and 110°C respectively.

Figures 4.32-4.35 show the stress relaxation curves as a function of strain at constant temperatures; 80°C, 90°C, 100°C and 110°C respectively.

Figure 4.36 shows the relative elongation rate independence of the percentage strain recovery. Figure 4.37 illustrates the effect of temperature on the percentage strain recovery as a function of the true strain.

Figure 4.38 shows the density of elongated specimens as a function of true strain and temperature.

Figures 4.39 and 4.40 compare the PET data with that of PETG reported in Section 4.7 and LDPE reported by *Smoker.*[9]

FIGURE 4.16: PET RUTHERFORD DATA AT 80°C
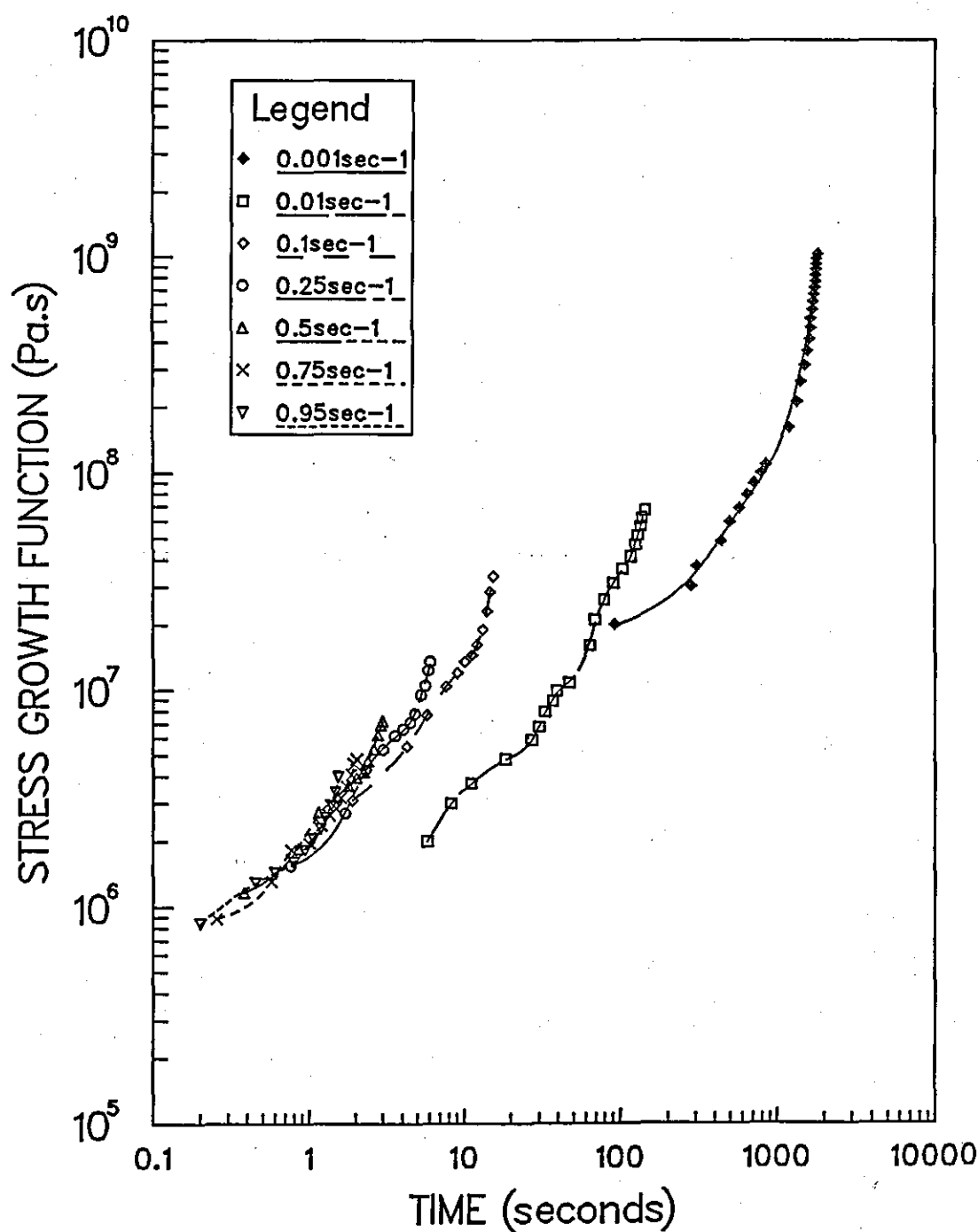
FIGURE 4.17: PET RUTHERFORD DATA AT 90°C
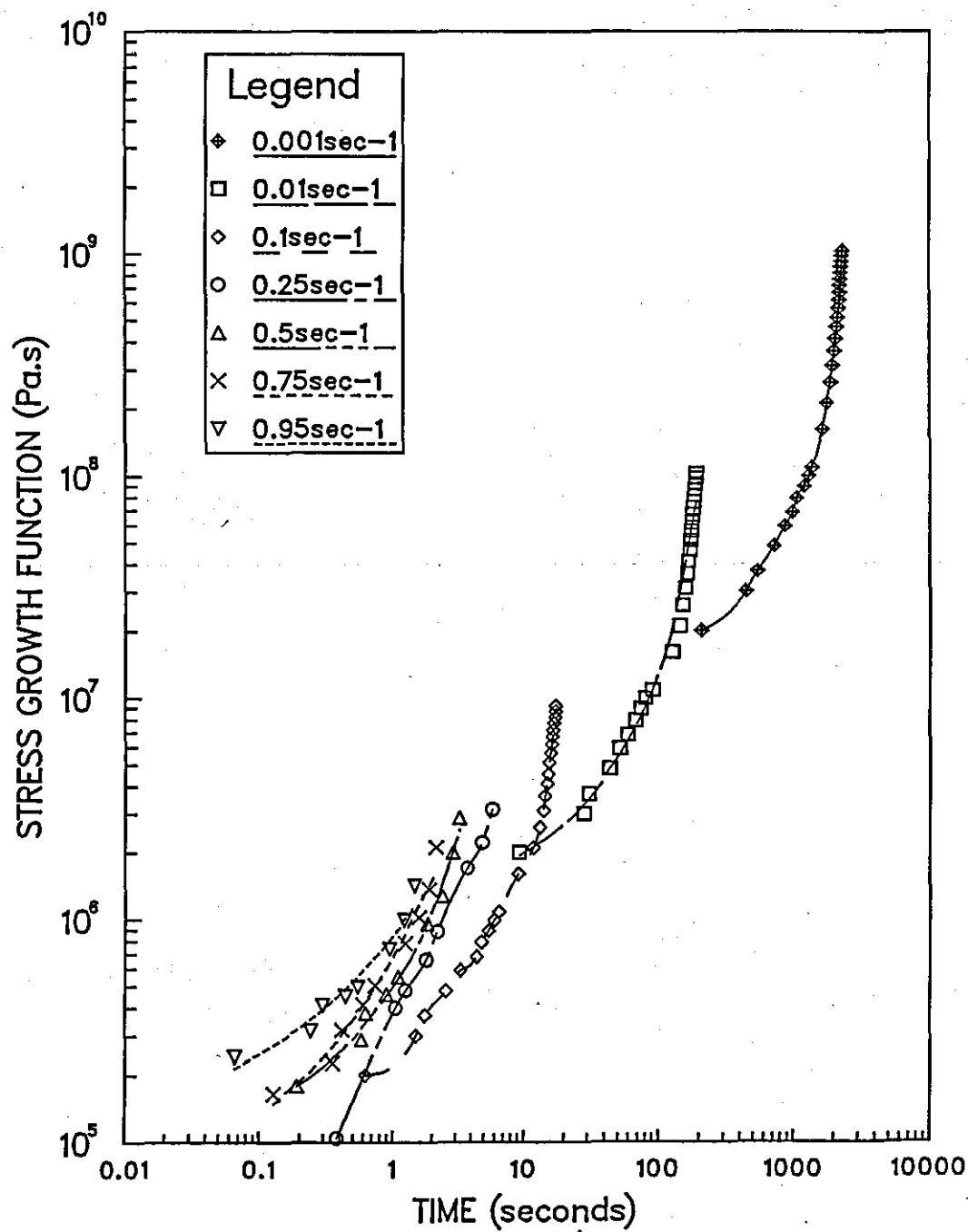
FIGURE 4.18: PET RUTHERFORD DATA AT 100°C
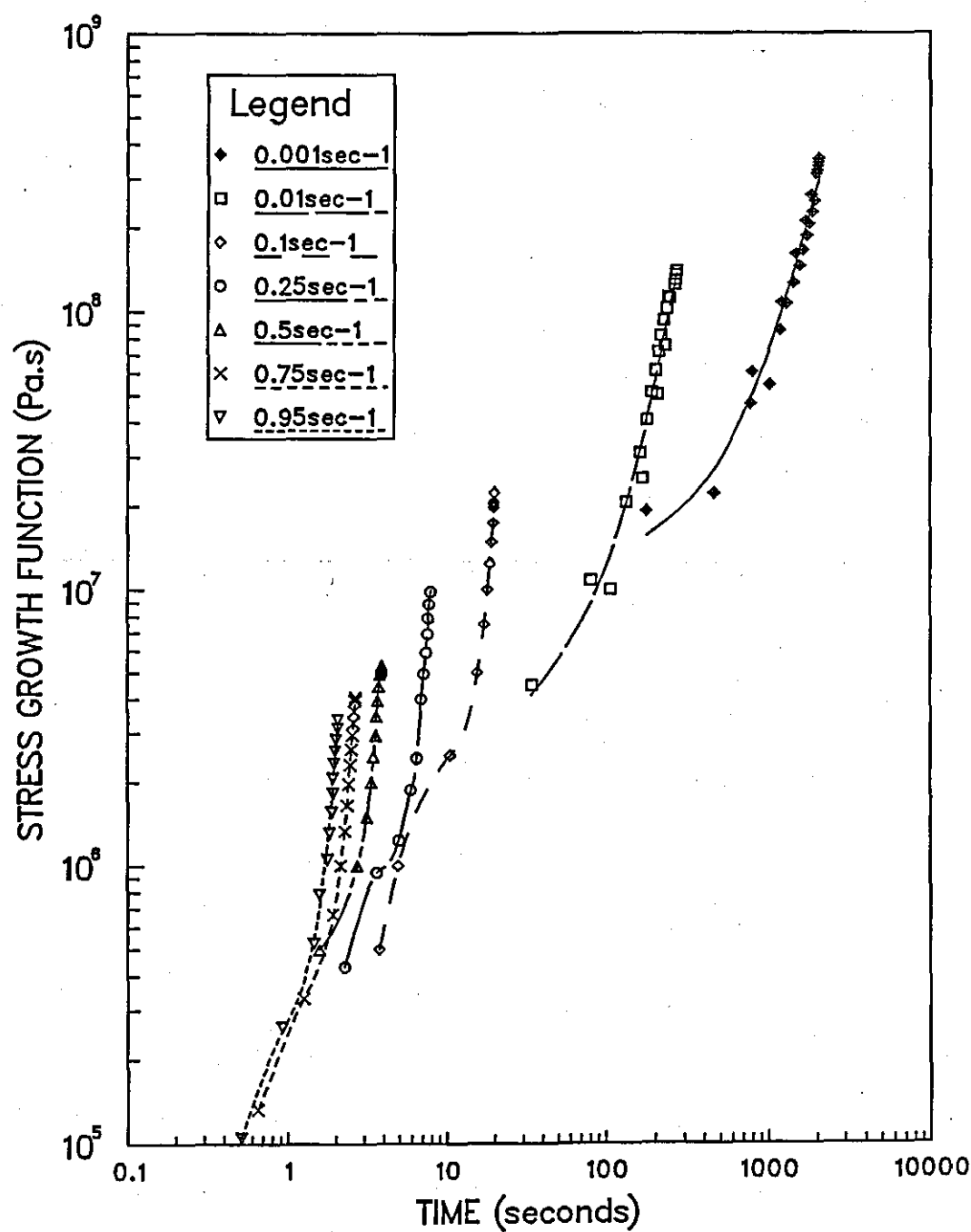
FIGURE 4.19: PET RUTHERFORD DATA AT 110°C
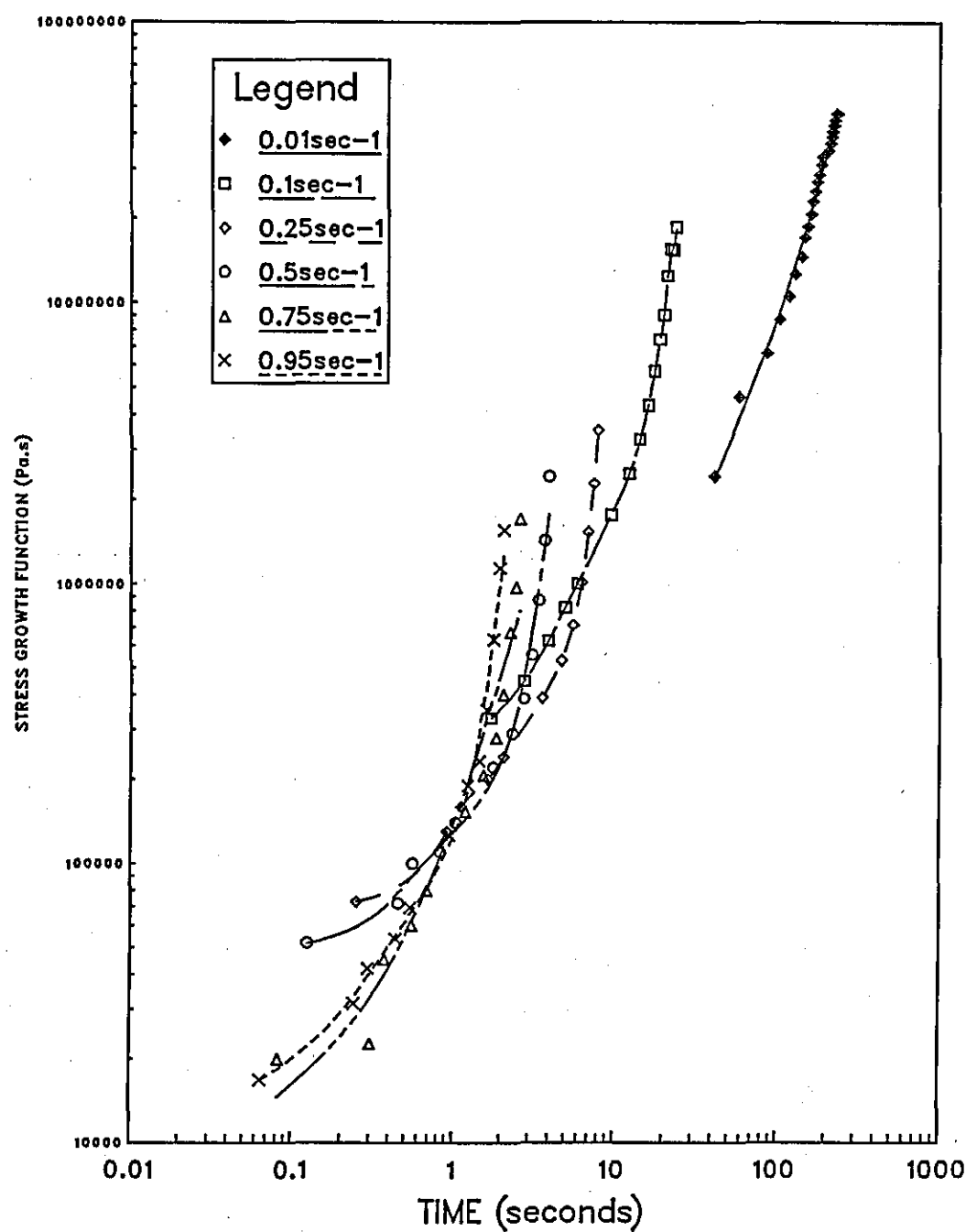
FIGURE 4.20: PET RUTHERFORD DATA AT 0.001s^{-1}
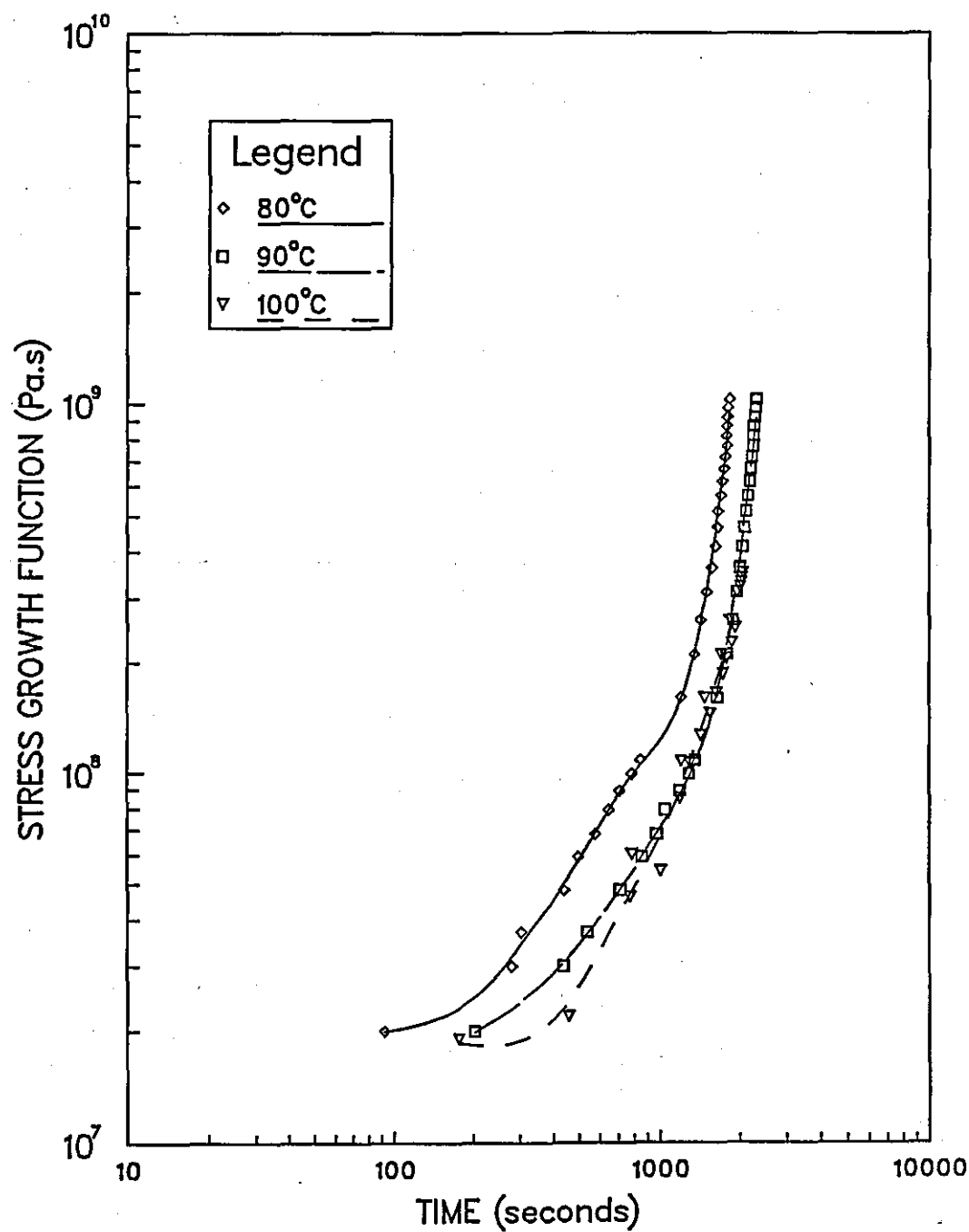
FIGURE 4.21: PET RUTHERFORD DATA AT $0.01s^{-1}$
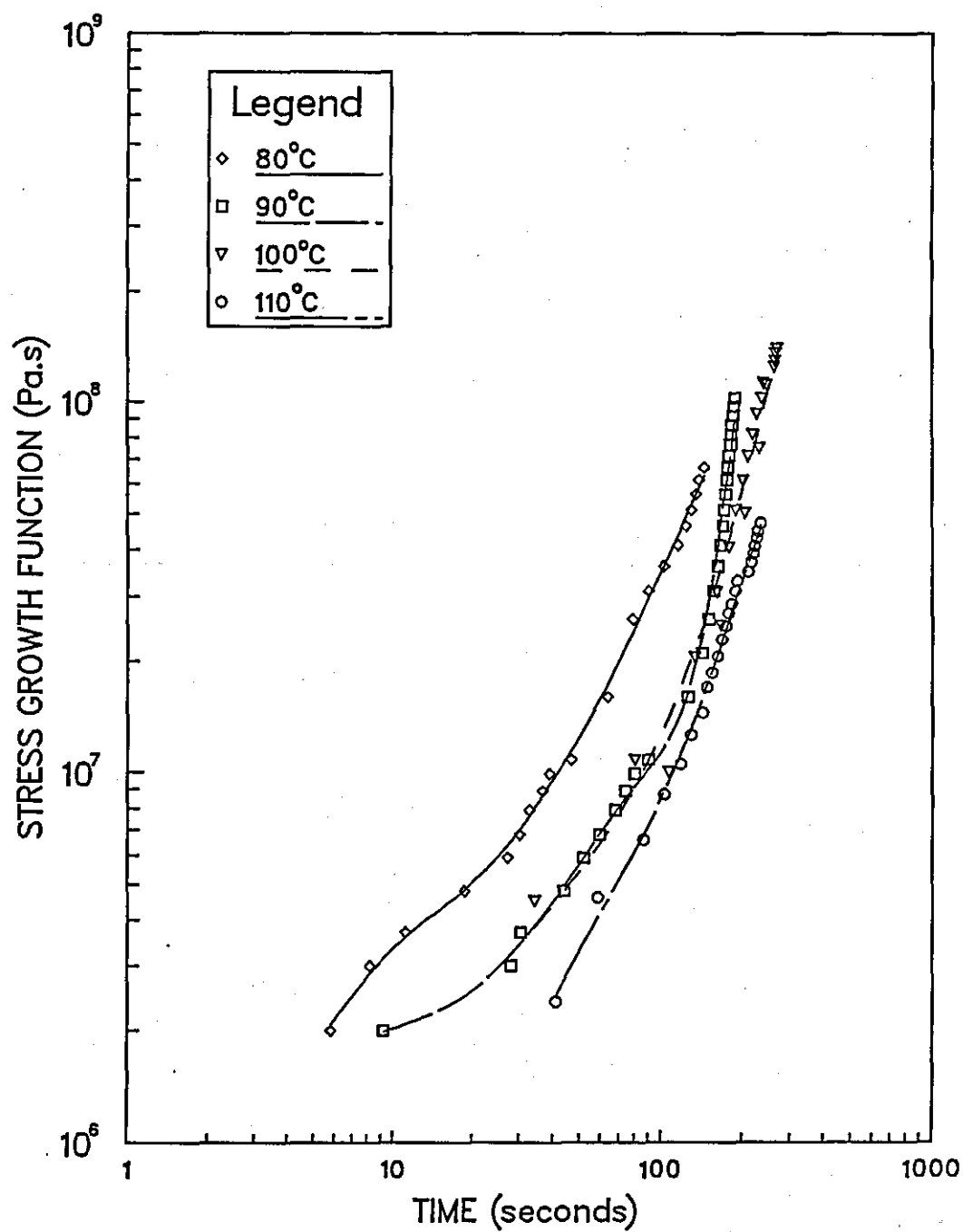
FIGURE 4.22: PET RUTHERFORD DATA AT 0.1s⁻¹
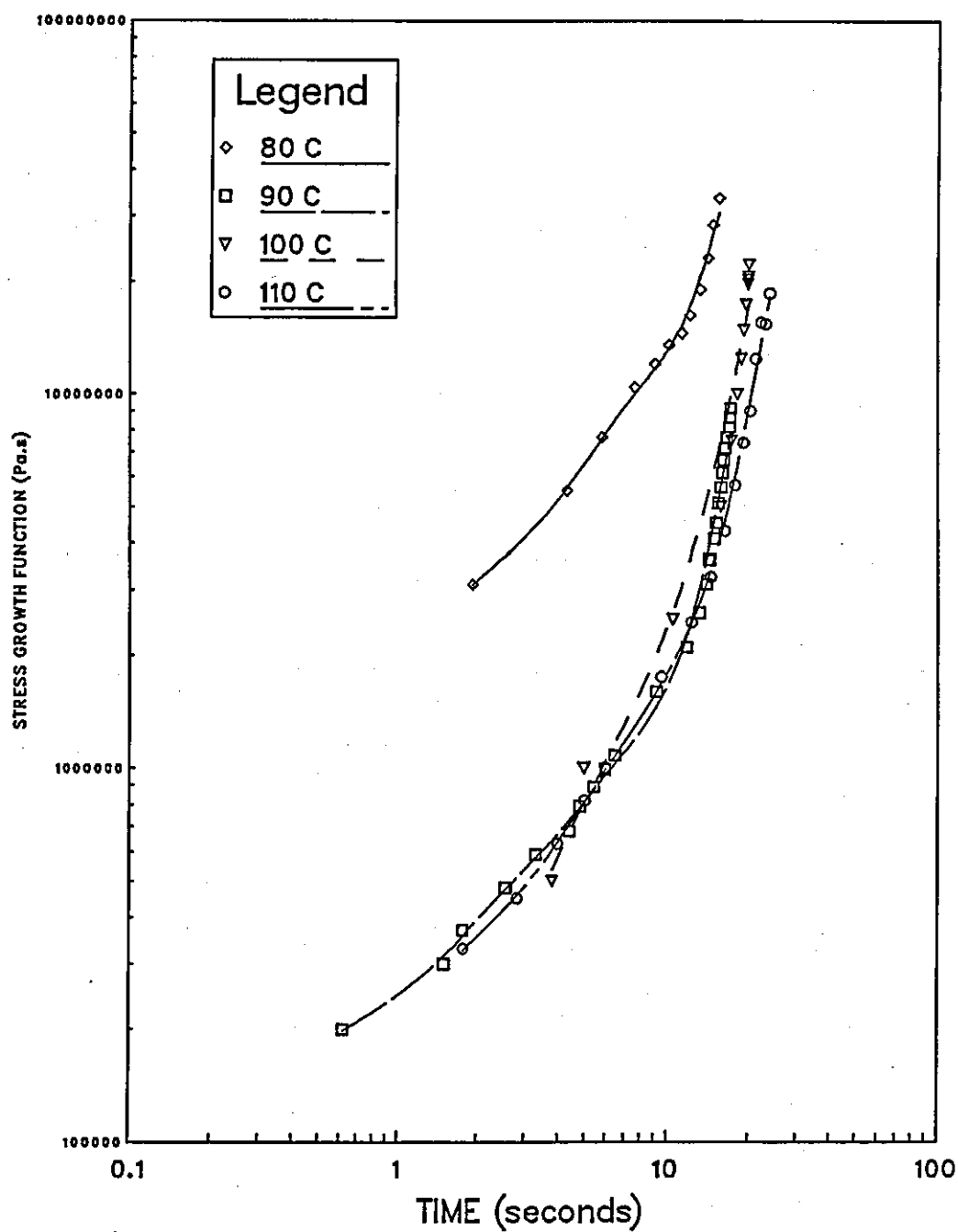
FIGURE 4.23: PET RUTHERFORD DATA AT 0.95s⁻¹
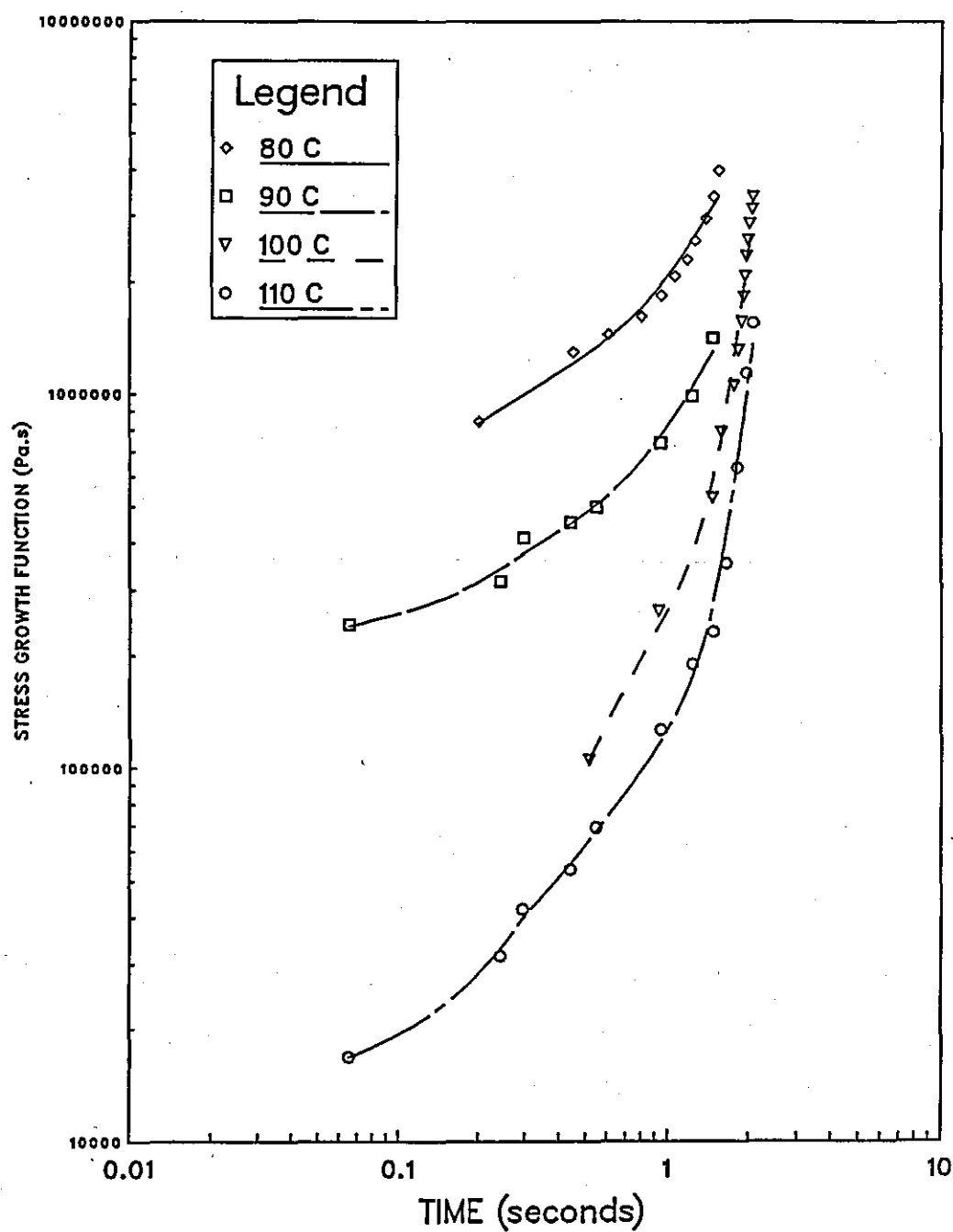
FIGURE 4.24: EFFECT OF TEMPERATURE ON
PET RUTHERFORD DATA, STRAIN RATE=0.25s−1
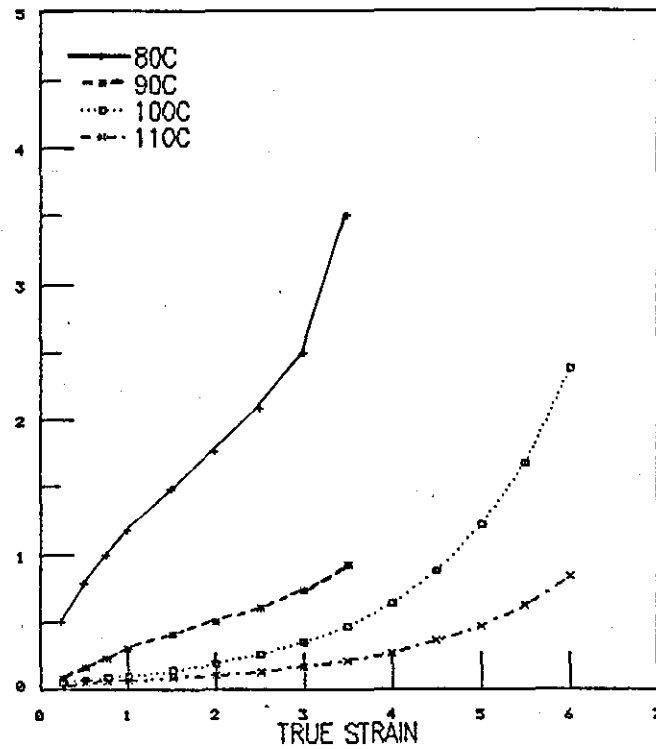
FIGURE 4.25: EFFECT OF TEMPERATURE ON
PET RUTHERFORD DATA, STRAIN RATE=0.5s−1
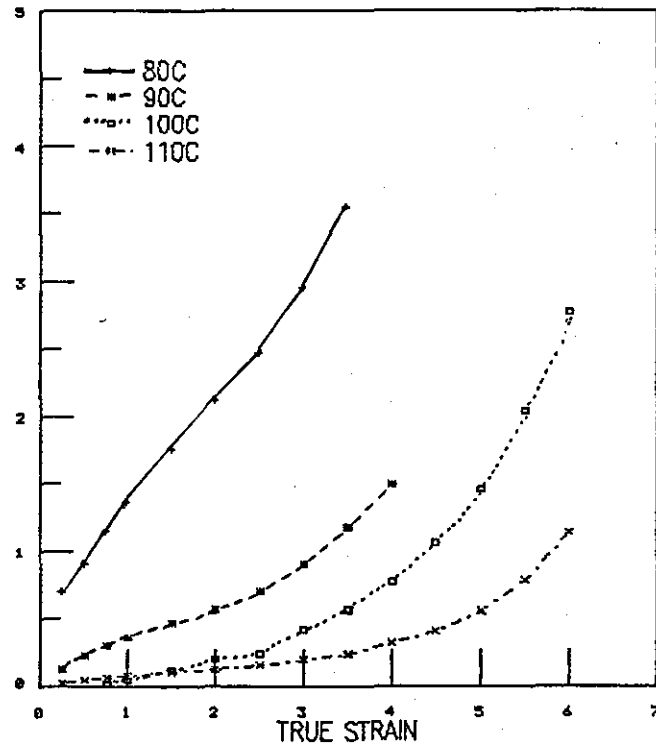
FIGURE 4.26: EFFECT OF TEMPERATURE ON
PET RUTHERFORD DATA, STRAIN RATE=0.75s-1
TRUE STRESS (MN/m2)

- 80C
- 90C
- 100C
- 110C
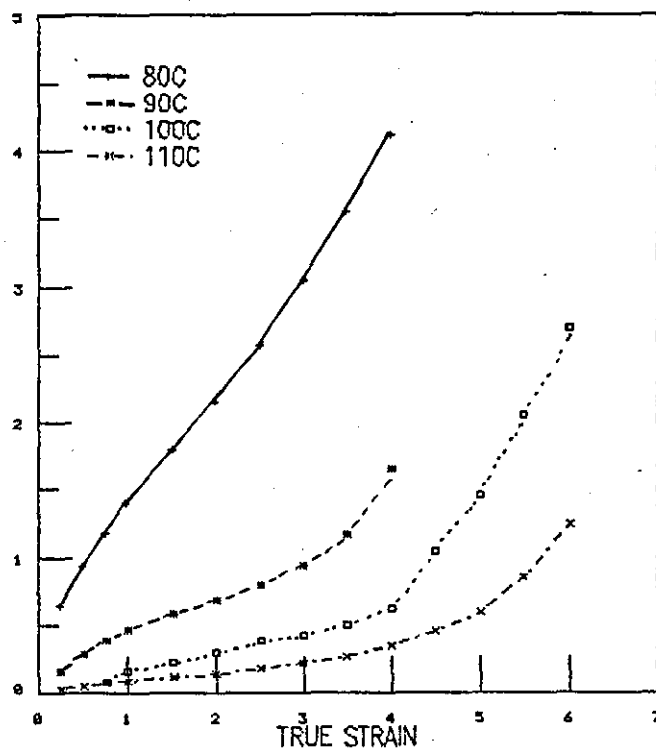
TRUE STRAIN

FIGURE 4.27: EFFECT OF TEMPERATURE ON
PET RUTHERFORD DATA, STRAIN RATE=0.95s-1
TRUE STRESS (MN/m2)

- 80C
- 90C
- 100C
- 110C
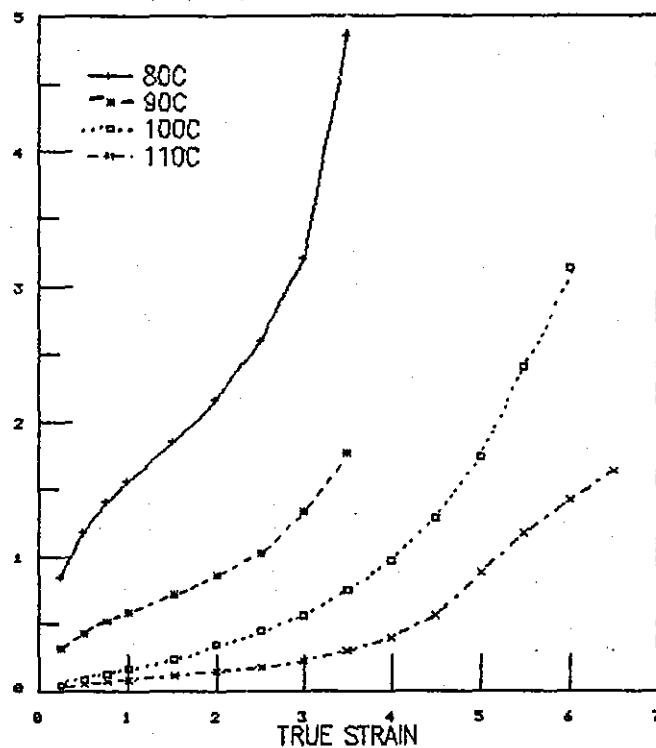
TRUE STRAIN

FIGURE 4.28: EFFECT OF HENCKY STRAIN
RATE ON PET RUTHERFORD DATA AT 80C

TRUE STRESS (MN/m2)

---·--- HSR = 0.25s-1
·····■··· HSR = 0.50s-1
---o-· HSR = 0.75s-1
--×-- HSR = 0.95s-1
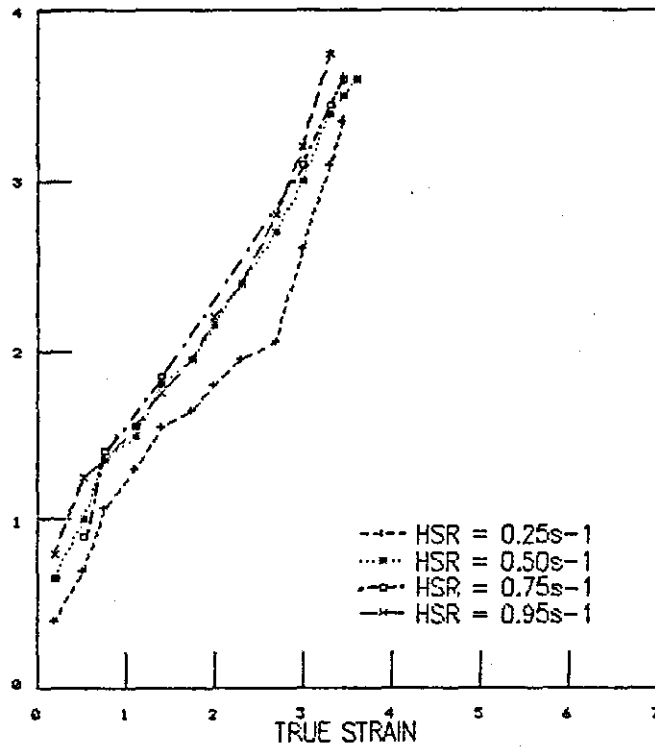
TRUE STRAIN

FIGURE 4.29: EFFECT OF HENCKY STRAIN
RATE ON PET RUTHERFORD DATA AT 90C

TRUE STRESS (MN/m2)

--+--HSR = 0.25s-1
·····■·· HSR = 0.50s-1
--o-· HSR = 0.75s-1
--×--HSR = 0.95s-1
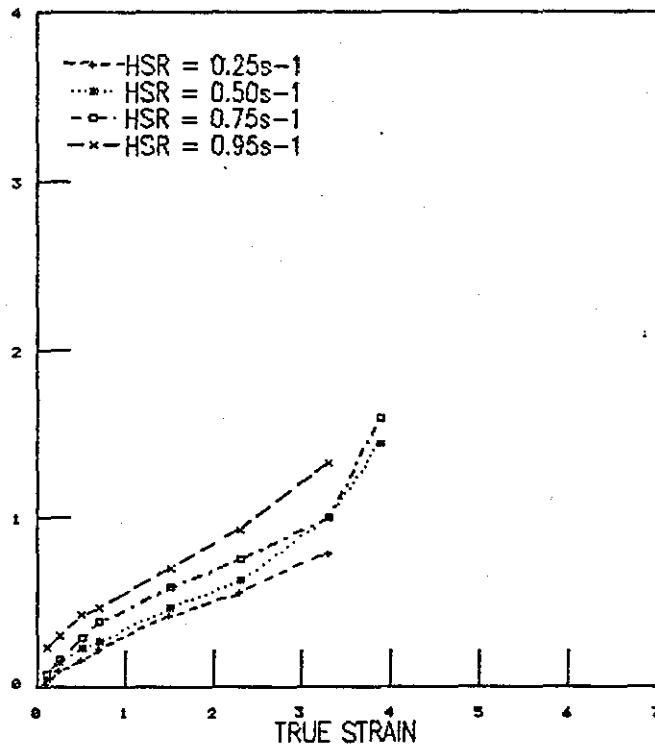
TRUE STRAIN

FIGURE 4.30: EFFECT OF HENCKY STRAIN
RATE ON PET RUTHERFORD DATA AT 100C
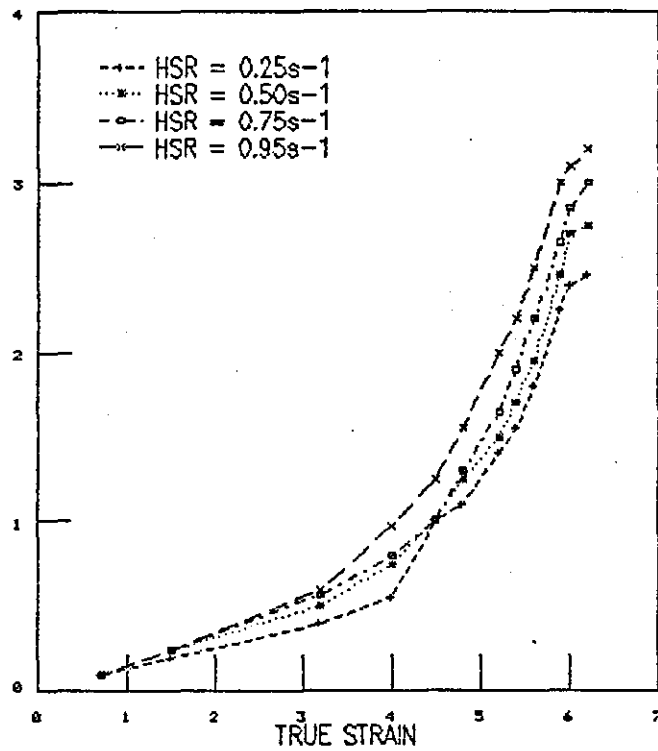
FIGURE 4.31: EFFECT OF HENCKY STRAIN
RATE ON PET RUTHERFORD DATA AT 110C

FIGURE 4.32: STRESS RELAXATION AT 80C

FIGURE 4.33: STRESS RELAXATION AT 90C
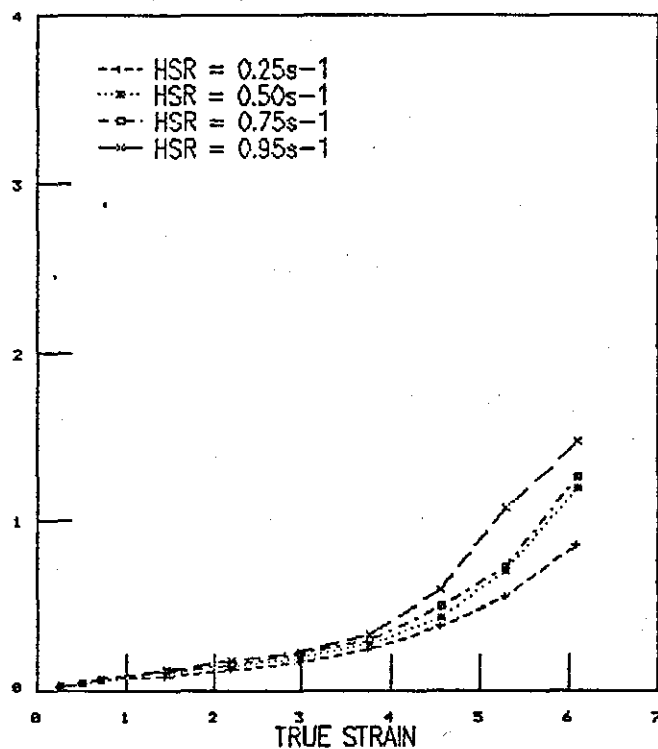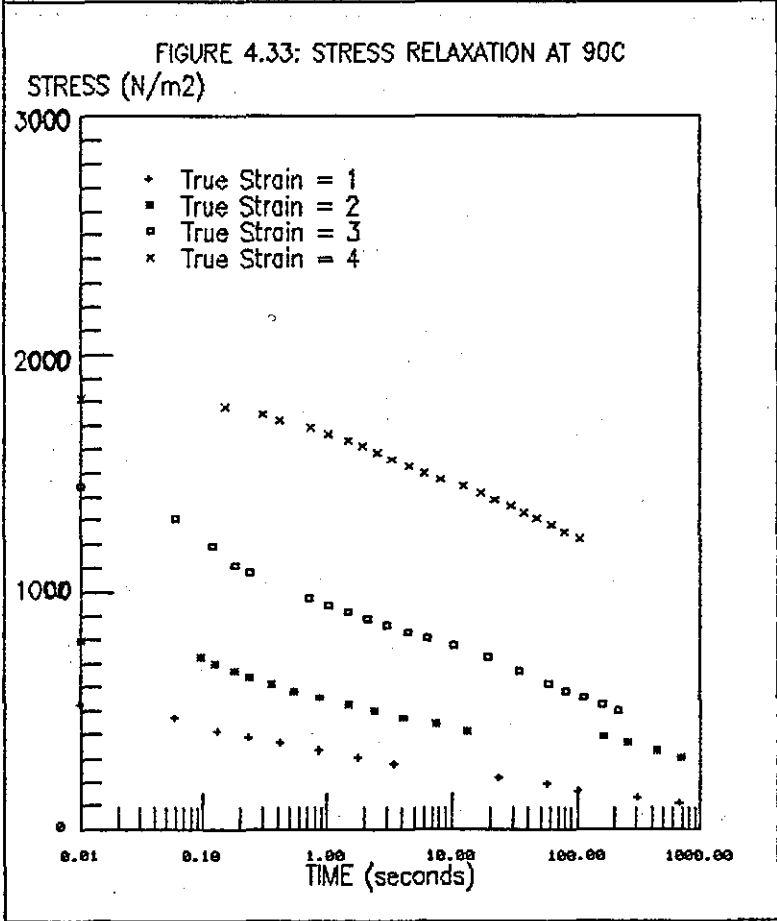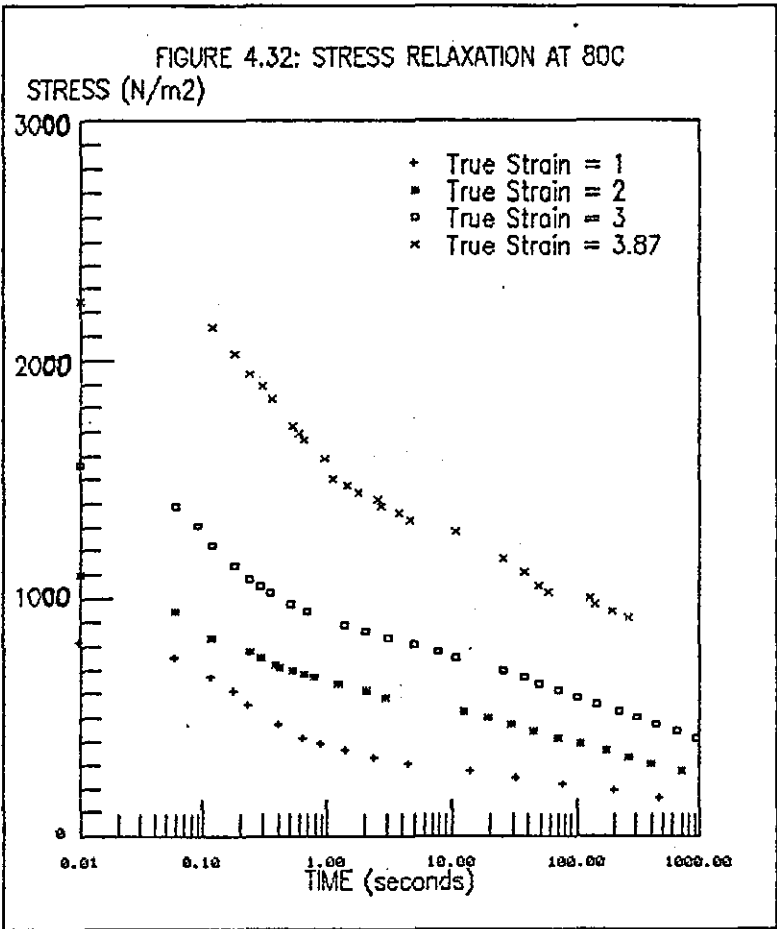
FIGURE 4.34: STRESS RELAXATION AT 100C
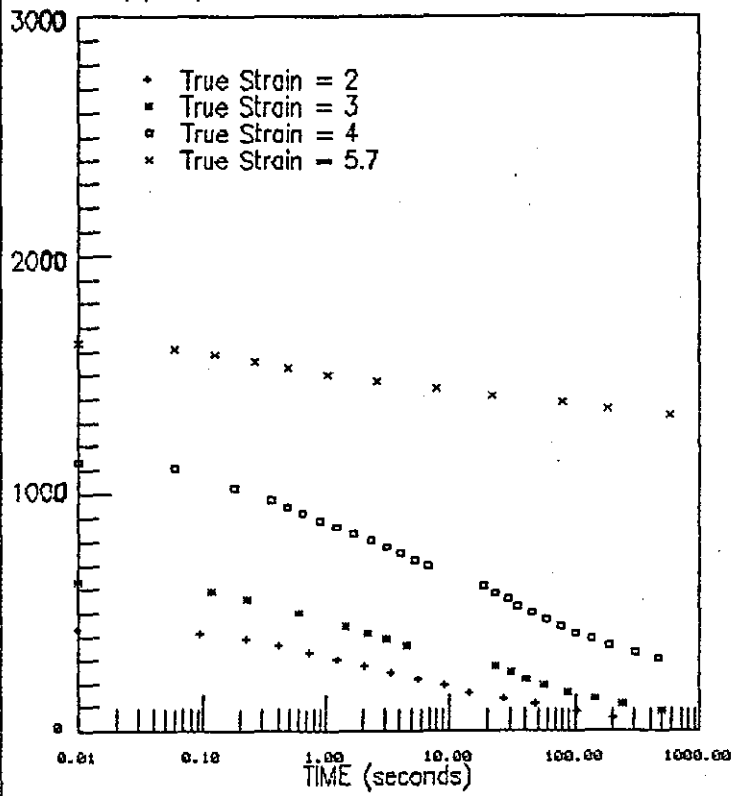
FIGURE 4.35: STRESS RELAXATION AT 110C
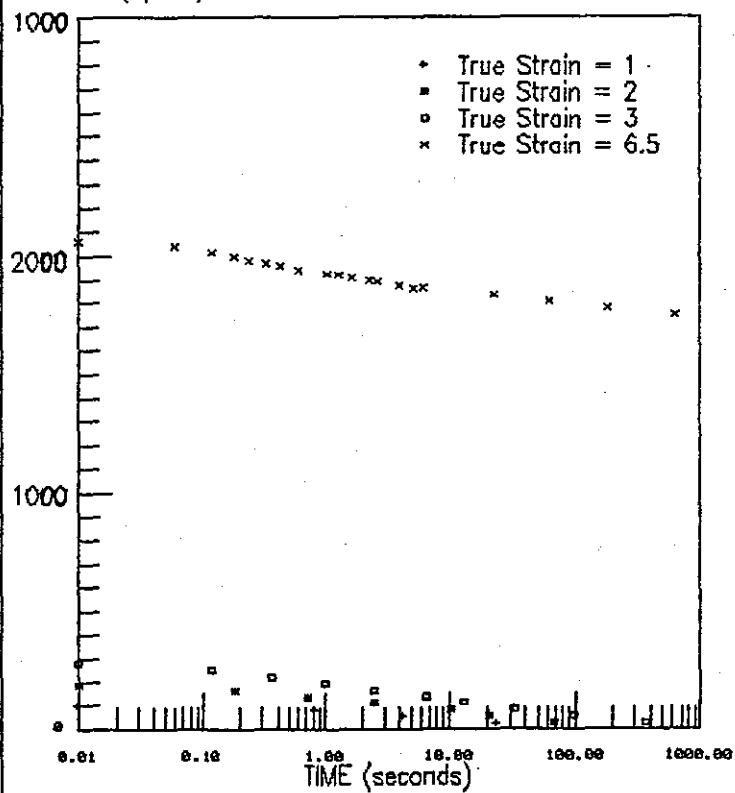
FIGURE 4.36: PET STRAIN RECOVERY
TEMPERATURE = 100C

% STRAIN RECOVERED

HENCKY STRAIN RATE (sec-1)
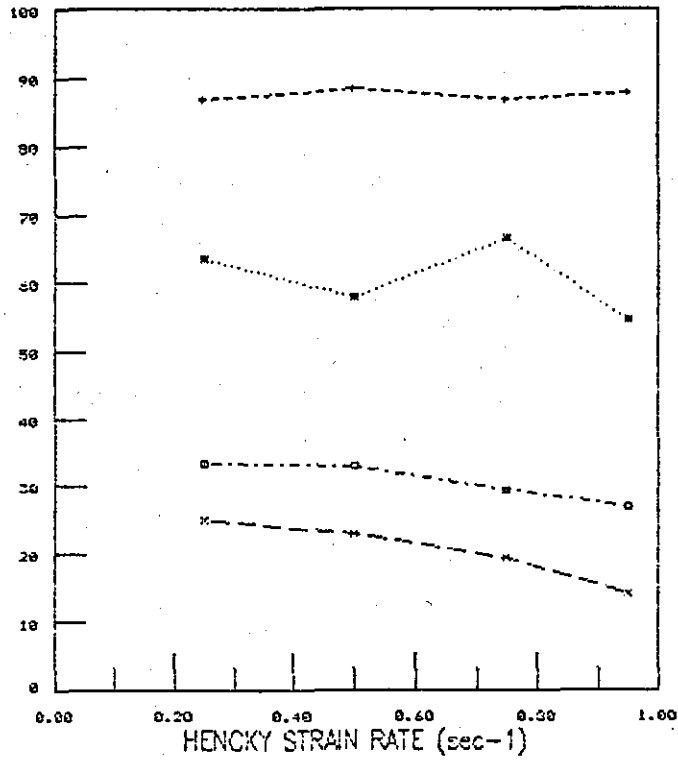
--·-- True Strain = 1
····*··· True Strain = 2
-·o-- True Strain = 3
-·x- True Strain = 4

FIGURE 4.37: PET STRAIN RECOVERY
HENCKY STRAIN RATE = 0.25s-1

% STRAIN RECOVERED

INITIAL TRUE STRAIN

80C
90C
100C
110C
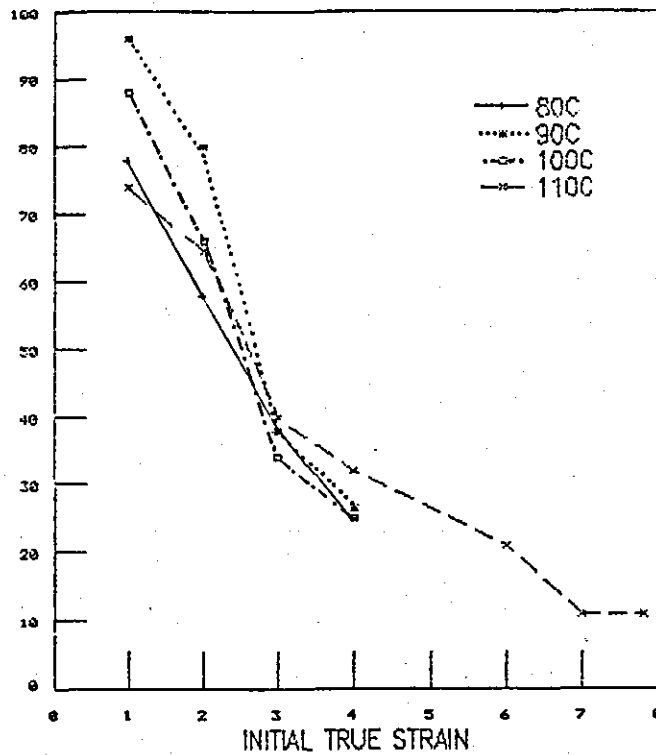
FIGURE 4.38: DENSITY VS TRUE STRAIN

DENSITY (g/cm3)

Calculated Crystal Density

SOC
90C
100C
110C

Oriented Heat Set Density

Unoriented Amorphous Density

TRUE STRAIN
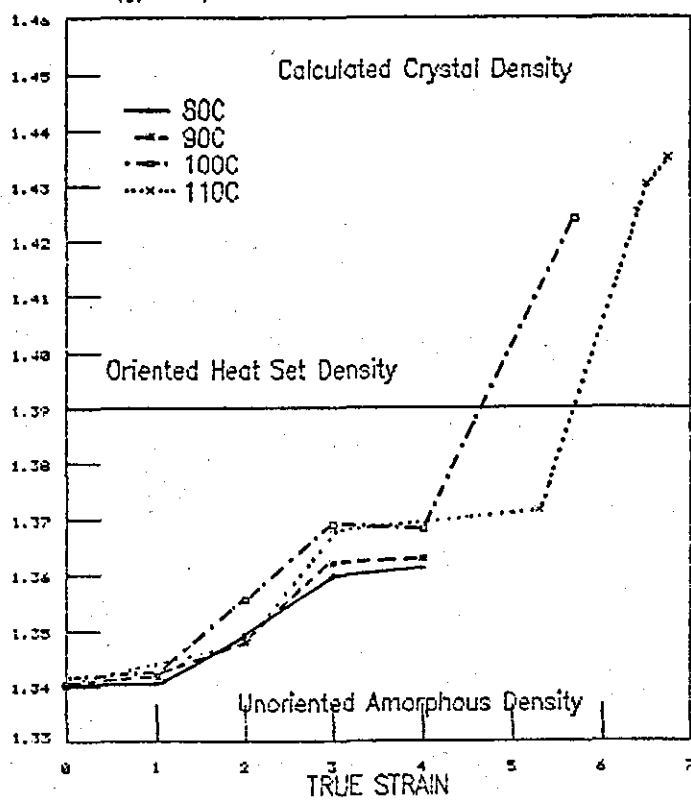
FIGURE 4.39: RUTHERFORD DATA COMPARISON

STRESS GROWTH FUNCTION (Pa.s)

○ ● PET at 110C
▲ ▼ PETG at 110C
■ □ LDPE at 120C

ε_H

1.5

1.0

1.5

1.0

1.6

1.0

HENCKY STRAIN RATE (sec−1)

FIGURE 4.40: RUTHERFORD DATA COMPARISON
STRESS GROWTH FUNCTION (Pa.s)
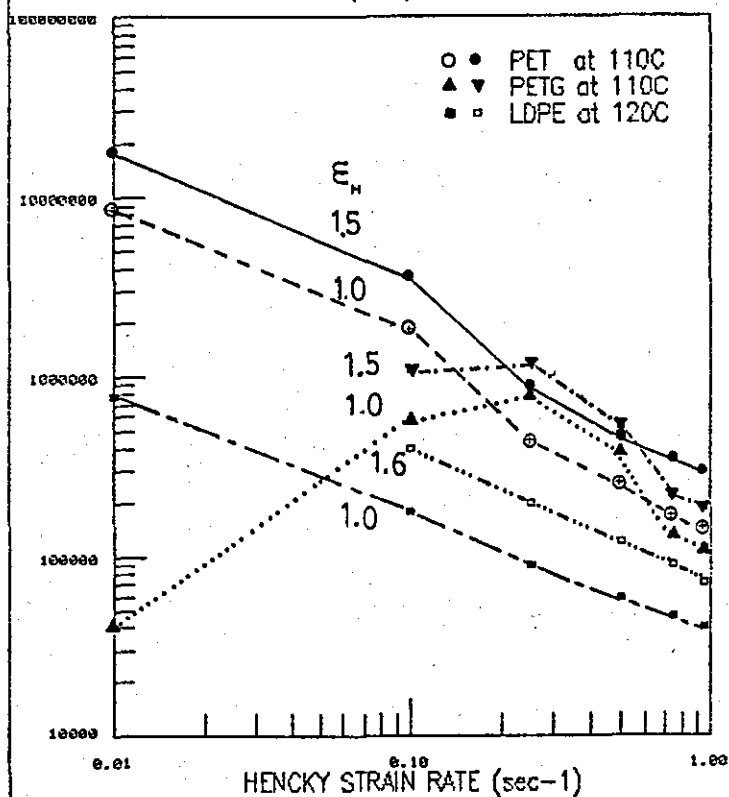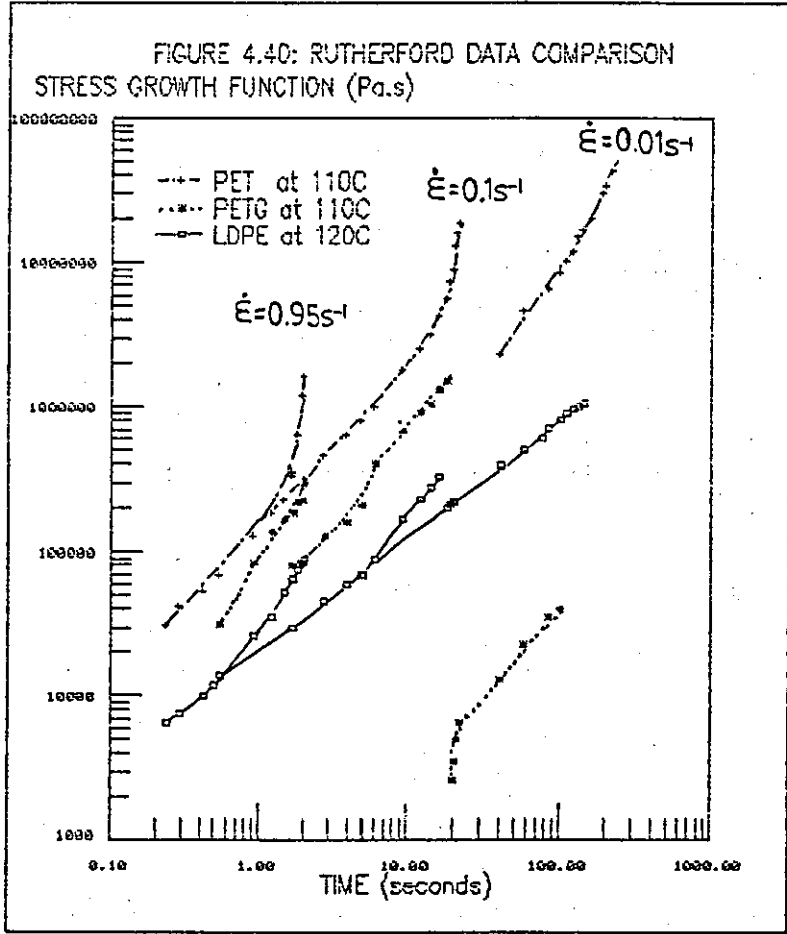
4.10.3 Discussion

4.10.3.1 Time Dependent Behaviour

The PET polymer does not behave as a polymer melt in the thermoelastic phase as shown in these experiments. The polymer tends towards elastic behaviour as illustrated by the strain recovery data shown in Figures 4.36 and 4.37.

Effect Of Elongation Rate

Figures 4.16-4.19 show the elongational stress growth function increasing as a function of time at a given temperature. This increase in resistance to deformation with time would be beneficial in certain processing situations, such as stretch blow moulding and thermoforming where the increased resistance to further deformation would promote more even thickness distributions in the final product.

When the elongational stress growth function is plotted against elongation rate as in Figure 4.39 the PET behaves in an apparent "tension thinning" manner, the resistance to deformation decreasing with increasing elongation rate, similar behaviour was reported for LDPE by *Smoker*[9] and PETG at 110°C reported in Section 4.7.

The high strain rate data shows a shift away from the common baseline that spans the data for different elongation rates. As the scatter occurs at times less than one second it may be due to the instrument establishing a constant Hencky strain rate via the closed loop control. The closed loop involves the actual elongation rate signal being compared, electronically, to the desired rate and any resultant error measured is then corrected for by a servo-signal being sent to adjust the motor speed.

In Figures 4.16-4.19 the curves show a transition point, above which the data deviates away from the baseline, best illustrated by Figure 4.17, this represents a strain-hardening response which is opposite to the response that occurs in shear flow of melts. *Meissner*[87,97] proposed that the baseline represents linear viscoelastic behaviour, and the deviation at a Hencky strain of about 1.2 represents the limit of linear viscoelastic behaviour. *Smoker*[9] obtained results that disagreed with this hypothesis; he proposed the

deviations from the baseline occur as the deformation exceeds the limit of elastic tensile behaviour.

The transition point shifts proportionally along the time axis with elongation rate, see Table 4.2, suggesting the existence of a critical strain which is less dependent upon elongation rate. The time at which the transition occurs approximately corresponds to a Hencky strain of between 1.2 and 1.425 (True strain range 2.32-3.16).

TABLE 4.2: STRESS-INDUCED CRYSTALLISATION TRANSITION POINTS

Elongation Rate	Time Of Transition	True Strain	Hencky Strain
$0.001s^{-1}$	1200seconds	2.32	1.2
$0.01s^{-1}$	120seconds	2.32	1.2
$0.1s^{-1}$	14seconds	3.06	1.4
$0.95s^{-1}$	1.5seconds	3.16	1.425

Although this transition occurs at approximately the same strain as the deviations reported by *Meissner*[87,97] and *Smoker*[9], and the stress relaxation data reported in Section 4.10.3.3 supports *Meissners'* hypothesis[87,97], the change in response with PET is very severe, see Figures 4.17 and 4.18. Figure 4.40 shows that the rate of stress growth after the transition point is greater for the PET than that reported for LDPE.[9] The increased resistance to deformation is possibly due to stress-induced crystallisation occurring above the transition point. This hypothesis is supported by the density data shown in Figure 4.38 which shows an increase in density at strains that correspond to either side of the transition point, the specimen is amorphous below the transition point and partially crystalline above the transition point. This suggests the specimens would exhibit a change in morphology from an oriented amorphous structure to a system containing crystallites in a rubbery network, shown schematically in Figure 4.41. Further evidence suggesting the existence of stress-induced crystallisation is shown in Figures 4.34 and 4.35 and Tables 4.3 and 4.4 by the inhibited stress relaxation at high strains.

FIGURE 4.41: SPECIMEN MORPHOLOGY ABOVE THE TRANSITION POINT

crystallites (chain-extended)
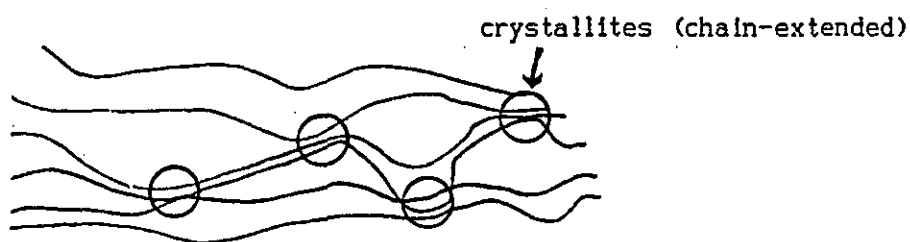
Effect Of Temperature

Figures 4.20-4.23 show the elongational stress growth function increasing as a function of time at a given Hencky strain rate. At a given time and elongation rate the resistance to deformation decreases with increasing temperature. After a short deformation time (i.e. low strain) the temperature dependence of the elongational stress growth function is greater than after higher deformation times. Below an elongation rate of $0.1s^{-1}$ the elongational stress growth function at the same elongation rate is relatively temperature independent (over the range tested: $80\,°C$ to $110\,°C$), only at $80\,°C$ are the stress growth function values slightly higher at a given time. Above an elongation rate of $0.1s^{-1}$ the elongational stress growth function decreases with increasing temperature, below a deformation time of 1 second.

The deviation from the baseline is shown in Figures 4.20-4.23 to occur at approximately the same time for all the temperatures at a given elongation rate, this suggests that the critical strain is independent of temperature as well as elongation rate.

4.10.3.2 Stress-Strain Curves

Effect Of Temperature

Figures 4.24-4.27 show the true stress increasing as a function of true strain at a given Hencky strain rate. At a given elongation rate and a given true strain the true stress decreases with increasing temperature. The transition that is observed at approximately a true strain of 3 (Hencky strain of 1.39) corresponds to the transition points observed in Figures 4.16-4.23.

Effect Of Elongation Rate

Figures 4.28-4.32 show that at a given true strain the true stress increased with increasing Hencky strain rate. The curves show the high strain transitions corresponding to the onset of stress-induced crystallisation, which appears to be independent of the Hencky strain rate.

To confirm that the the transition is due to stress-induced crystallisation, specimens were elongated to different strains and then their densities were determined using a density column. The results in Figure 4.38 show that the density increases with increasing true strain. The increase in density is greater than that expected from the molecular orientation and the more ordered packing of the molecules as drawing progresses, the larger density increase can be explained by the crystallisation that occurs due to the more ordered molecular arrangement, see Figure 4.41.

4.10.3.3 Stress Relaxation

Figures 4.32-4.35 show the stress decreasing with increasing time as a function of the strain at a given temperature. The gradients of the linear-log curves are similar, and near-linearity implies linear viscoelasticity (Maxwell) response. At 100°C and 110°C the curves for specimens extended to true strains greater than 5.7 have shallower gradients than the other curves, this is due to the specimens being stress-induced crystallised and the viscous component becoming suppressed as the crystallisation pins and restrains the molecules, preventing significant molecular relaxation and flow.

The Maxwell model of viscoelasticity described in Section 2.1.2 can be used as a model of the stress relaxation behaviour of polymers, see Figure 2.2. Equation (2.9) governs the Maxwell model:

$$\dot{\varepsilon} = (1/E).\dot{\sigma} + (1/\lambda).\sigma \qquad (2.9)$$

where $\dot{\varepsilon}$ is the elongation rate, E is the tensile modulus, $\dot{\sigma}$ is the elongational stress rate, λ is the tensile viscosity and σ is the elongational stress.

Applying this equation to the stress relaxation situation produces equations (4.15)-(4.19). At constant strain the strain rate, $\dot{\varepsilon}$, is zero, see equation (4.15), where t is time, ε_e and ε_v are the elastic

and viscous component strains respectively.

$$\dot{\varepsilon} = d\varepsilon/dt = d\varepsilon_e/dt + d\varepsilon_v/dt = 0 \qquad (4.15)$$

therefore,

$$(1/E)d\sigma/dt = \sigma/\lambda = 0 \qquad (4.16)$$

and

$$\int_{\sigma(0)}^{\sigma(t)} d\sigma/\sigma = (-E \div \lambda) \int_{0}^{t} dt \qquad (4.17)$$

integrating equation (4.17) gives,

$$\ln(\sigma_{(t)} \div \sigma_{(t=0)}) = (-E.t) \div \lambda \qquad (4.18)$$

and a time-dependent modulus $E_{(t)}$ can be defined by equation (4.19), where ε_o is the initial strain,

$$E_{(t)} = \sigma_{(t)} \div \varepsilon_o = E.\exp((E.t) \div \lambda) \qquad (4.19)$$

If the polymer was linearly viscoelastic the time-dependent modulus would be independent of the initial strain.[102] Table 4.3 shows the time-dependent modulus as a function of strain, time and temperature.

TABLE 4.3: TIME-DEPENDENT MODULUS

TRUE STRAIN	TEMPERATURE (°C)	t=0.1s (s)	t=1s (s)	t=10s (s)	t=100s (s)
1	80	675	375	300	220
2	80	425	325	265	200
3	80	430	300	250	197
3.87	80	555	408	330	258
1	90	430	320	240	175
2	90	360	275	210	200
3	90	400	317	263	190
4	90	445	418	483	303
2	100	203	153	98	42.5
3	100	200	153	100	53
4	100	265	222	163	102
5.7	100	278	263	249	240
1	110	90	70	40	
2	110	85	60	37.5	
3	110	83	65	42	20
6.5	110	310	295	286	275

From Table 4.3 it can be seen that the time-dependent modulus for PET is relatively independent of the initial strain, and therefore approximates linear viscoelastic behaviour, up to a true strain limit

---

of 3 (Hencky strain = 1.39) for all four temperatures. As shown in Table 4.2 the deviation from the common baseline on the time-dependent stress growth function curves (Figures 4.16-4.19) occur at approximately Hencky strains of 1.2-1.425. Therefore, the time-dependent modulus data together with the critical strain for deviation from the time-stress growth baseline, supports the hypothesis proposed by *Meissner*[87,97] that the deviation from the common baseline is the departure from linear viscoelastic behaviour.

The term λ/E, the "relaxation time", is a measure of the rate at which stress decays.[102] Table 4.4 shows the relaxation times for the PET as a function of time, temperature and strain.

TABLE 4.4: RELAXATION TIMES FOR PET

TRUE STRAIN	TEMPERATURE (°C)	t=0.1s (s)	t=1s (s)	t=10s (s)	t=100s (s)
1	80	0.615	1.30	10.2	77.5
2	80	0.388	1.90	13.7	99.0
3	80	0.505	1.82	13.7	103.1
3.87	80	2.189	2.72	17.9	124.1
1	90	0.526	2.06	12.3	89.3
2	90	0.840	2.67	19.0	144.9
3	90	0.584	2.45	16.9	108.7
4	90	8.952	13.35	46.3	256.4
2	100	1.669	3.39	13.1	64.1
3	100	3.048	3.36	15.1	77.5
4	100	1.818	4.15	18.4	98.3
5.7	100	5.376	12.05	72.5	602.4
1	110	0.952	3.48	10.9	
2	110	1.216	2.18	10.8	
3	110	0.735	2.91	13.3	65.7
6.5	110	5.102	14.20	93.0	711.7

From Table 4.4 it can be seen that the rate decreases with time as is clearly illustrated in Figure 4.32. Also, the relaxation times increase with strain. At the lower temperatures the effect of temperature is the reverse of what was expected; the relaxation was expected to be greater with increased temperature, as seen between 100°C and 110°C. The significant jump in the values of relaxation time at true strains greater than 3 suggest the Maxwell model is not

applicable at these high strains as the viscoelastic behaviour becomes non-linear due to crystallisation. The very high relaxation times at true strains greater than 5 support the proposed hypothesis that stress-induced crystallisation that occurs at these high strains could be restraining the molecular relaxation.

4.10.3.4 Strain Recovery

Effect Of True Strain

Figures 4.36 and 4.37 show the percentage strain recovered against the Hencky strain rate and true strain respectively. The strain recovery can be seen, in Figure 4.36, to be relatively independent of the elongation rate. *Meissner*[87] reported that the strain recovery for LDPE increased with increasing elongation rate, the difference in response between the PET data and the LDPE can be explained by the differences in molecular structure and relaxation kinetics. The long straggly branched LDPE molecule readily forms interchain entanglements which act as anchor-points restraining the molecular chain deformation during the bulk specimen extension, this reduces the degree of chain slippage, at extension rates that are high enough to prevent chain entanglement. On release of the tensile force greater recovery occurs with LDPE than with the relatively short, stubby, linear PET molecules.

Figure 4.37 shows that the percentage strain recovered decreases with increasing maximum true strain and is relatively independent of temperature. The viscoelastic deformation involves recoverable (elastic) and permanent (viscous) components. At low strains the deformation is predominantly elastic or delayed elastic (molecular bond opening and chain uncoiling) a proportion of the strain is recovered on release of the specimen. At higher values of strain both elastic and viscous deformations occur (chain uncoiling and chain slippage) and at the higher values of true strain in Figure 4.37 the viscous component of the deformation becomes dominant and the percentage strain recovered decreases. Also, at higher strains crystallisation occurs due to the more ordered molecular packing, the crystalline state is very stable, resulting in less of the original deformation being recovered.

4.10.4 Applicability To Processing

The elongational deformation data for PET in the thermoelastic phase can be applied to those processes where the PET is deformed in the relevant manner: e.g. thermoforming, the inflation stage of injection stretch blow moulding, fibre, monofilament and sheet drawing.

The increased stress growth with deformation time is beneficial for the stretch blow moulding and thermoforming processes where the increased resistance to further deformation will stabilise the process and give a more even thickness distribution in the final product. The tension thinning response with increasing extension rate prevents linear PET from being extrusion blow moulded, as attempts to form a parison would fail due to excessive sagging, the resistance to further sagging would decrease, leading to unstable run away draw-down. The tension thinning behaviour resulting in exploitation of any inherent weaknesses by preferential deformation at the weak points, also prevents linear PET being used in the film blowing process.

In the reheat blow stretch blow moulding process the problem of parison formation are overcome by injection moulding a preform which has a uniform thickness which when reheated can be stably inflated. The tension thinning response is beneficial to this process as it permits faster inflation rates to be used without unduly increasing the air pressure requirements. The onset of stress-induced crystallisation will limit the size of article to be produced by a given machine, as after crystallisation the air pressure requirements rise drastically. Also, the crystallisation could impart undesirable properties in the product, e.g. loss of clarity.

From the stress relaxation data reported in Section 4.10.3.3 it can be seen that relaxation occurs rapidly over short time scales, so within the first second after a given deformation significant relaxation will occur. In a stretch blow moulding process that has two stage orientation, the first by a vertical push-rod and the second by inflation, the control of the dwell time between the two stages could affect the final degree of orientation and so the final product properties, such as strength and gas barrier properties. Also,

this rapid relaxation will determine the maximum number of moulds a particular machine carousel could contain, as the different stretching stages are performed at different carousel locations. The number of moulds and size of product would determine the rotational speed of the carousel and this would determine the dwell time between the two stages.

The PET data reported in this chapter has been applied to a study of the inflation stage of the injection stretch blow moulding process in Chapter 7.

4.11 Summary Of Chapter 4
4.11.1 Aims and Novelty

All but one of the aims set out at the beginning of this chapter have been achieved. The aim to produce tensile flow data for PET melts failed because the silicone fluid did not support the molten specimen sufficiently, due to the differences between the melt density and the specific gravity of the fluid. However, the successful experiments with polycarbonate prove that the modifications made to the rheometer have extended its operating range to allow studies of high melting point polymers.

The results in this chapter represent an extension to the range of usage for the Rutherford Elongational Rheometer, itself a unique instrument. The high temperature results for polycarbonate are the first results from the instrument above 200°C, the thermoelastic phase measurements represent the first application of the instrument to this area of study, which offers data suitable for application to important commercial processes, the stress relaxation and strain recovery data have not been obtained using this instrument before and these are the believed to be the first observations of stress-induced crystallisation using an instrumented elongational rheometer. The thermoelastic data has been applied to preform inflation in Chapter 7.

The data obtained for the PETG copolyester is believed to be the

first study using a direct method of elongational flow measurement for this copolymer. This data has been applied to parison sagging in Chapter 6.

4.11.2 Conclusions From Chapter 4

1.   The Rutherford Elongational Rheometer has been successfully modified to enable operation above 200°C. Elongational flow properties have been measured up to 280°C for polycarbonate melts. These show the stress growth function to increase with deformation time when a specimen is extended at a constant Hencky strain rate. Also, a deviation to strain-hardening behaviour was observed at a Hencky strain of 2.25 for the polycarbonate tested at an elongation rate of $0.75s^{-1}$ and 280°C.

2.   The injection mould for the Rutherford Elongational Rheometer specimens has been redesigned to produce specimens less prone to premature weld line failure in the test region. The new design also ensures the deformation occurs primarily in the test regions of the specimens by adopting a dumb-bell shape. Injection moulded specimens of PETG copolyester were used without weld line problems.

3.   The Rutherford Elongational Rheometer cannot presently be used to study the elongational flow properties of PET melts as the melt density exceeds the specific gravity of commercially available silicone fluids at the relevant temperatures. The specimens sag excessively before the test can be started.

4.   The PETG Copolyester melt at 170°C showed a tension stiffening response when tested at constant Hencky strain rate and constant temperature using the Rutherford Elongational Rheometer. The response can be divided into three sections related to chain uncoiling and molecular orientation, followed by steric hindrance due to the cyclohexane groups, followed by gross chain slippage. The rate of elongational stress growth function rise increases as the molecular hindrance occurs and decreases as chain slippage occurs. The elongational stress growth function values decrease with increased temperature.

At 110°C the PETG Copolyester was predominantly elastic and

the stress build-up behaviour obeyed the rubber-like network theory. The elongational behaviour was highly time-dependent, the stress decreased above a critical elongation rate as the temporary rubber-like network breaks down. At a critical stress chain slippage occurs and the response becomes stress independent.

5.   The data from the Rutherford Elongational Rheometer is quantitatively different from converging flow data. The comparative data for PETG Copolyester showed qualitatively opposite trends with respect to elongation rate. Direct comparisons of elongational flow data from different sources should only be made after considering the respective test methods used. Elongational data should only be applied to processing situations involving similar flow environments.

6.   The PETG Copolyester displayed elongational flow properties on the Rutherford Elongational Rheometer that are desirable in a polymer used for extrusion blow moulding, the tension stiffening response stabilising the parison preventing excessive sagging.

.7.   The PET polymers showed a tension thinning response in the thermoelastic phase when tested at constant Hencky strain rate and constant temperature using the Rutherford Elongational Rheometer. The combination of stress growth-time data and stress relaxation data offer supporting evidence for the hypothesis that the deviations from the time-dependent stress growth baseline at a Hencky strain of about 1.3 represent the departure from linear viscoelastic behaviour. The response showed a very rapid increase in the elongational stress growth function after the onset of stress-induced crystallisation. The elongational stress growth function decreased with increasing temperature, the temperature dependence is greater at low strains.

8.   The onset of stress-induced crystallisation occurs at a critical Hencky strain of approximately 1.4 which is relatively insensitive to elongation rate and temperature.

9.   The time-dependent stress relaxation modulus $E_{(t)}$ was relatively independent of strain at all four temperatures (80°C-

110°C) below a true strain of 3, this represents the region of linear viscoelastic behaviour. The relaxation time λ/E increased with strain. The very large increases in time-dependent modulus and relaxation times at high strains is possibly due to restraint of molecular relaxation due to stress-induced crystallisation.

10.   The percentage strain recovered decreased with increasing maximum strain and is relatively independent of temperature and Hencky strain rate.

4.11.3 Suggestions For Further Work

Relevant processing trials should be undertaken and the results compared with predictions made using the data reported in this chapter. The branched PET polymers and the PCCE and PCTG copolyesters could be tested if further quantities of material were made available. Other polymers can now be tested using the Rutherford Elongational Rheometer such as polycarbonate and other engineering polymers, PET/PC and other polymer blends, and the new high-barrier thermoforming materials (e.g. PP/EVOH/PP). By using 'molecular engineering' to produce plastics and then testing them in this mode it would be possible to determine if the desired properties have been achieved.

5. Injection Moulding

5.1 Introduction[103-105]

This chapter describes and discusses an experimental programme of work using an injection moulding machine (55-tonnes Negri Bossi) and a computer simulation of the injection moulding process (the SIMPOL computer software package). This chapter aims to apply the rheological data reported in Chapters 2 and 3 to the injection moulding process. There were four main objectives for this experimental programme:

1. To measure the processability of three polymers under varied conditions and to compare the results with those of the rheology of the polymers, reported in Chapters 2 and 3.

2. To compare the computer simulation modelled rheological data for the three polymers with the experimental rheological data reported in Chapters 2 and 3.

3. To compare the computer simulated processability results for the three polymers under varied conditions with the experimentally measured processability results.

4. To assess the usefulness of, and suggest computer model refinements to enhance the accuracy of, the SIMPOL computer simulation, on the basis of injection moulding PET polymers.

The injection moulding of thermoplastics is a cyclic process which produces formed articles. The process involves plasticating the moulding material and injecting it under pressure into a cold mould, cooling under conditions of near constant mass and volume, where it solidifies in the shape of the cavity.

A U.S. patent for an injection moulding machine was issued in

1872. The first plunger-type machine was manufactured in 1926. The first injection moulding machine with a reciprocating screw was built in 1956.[103]

A better understanding of the rheological properties should be of practical use in injection moulding, leading to improved part and mould design, in choosing optimum moulding conditions, and also in formulating proper moulding compounds.[104] Also a better rheological understanding will lead to better machine control (e.g. on the basis of cavity pressure measurements) and therefore improve part consistency and eliminate flow-induced defects.

The flow problems involved with injection moulding can be described as "unsteady-state, nonisothermal flows of viscoelastic polymer melts in a complex flow channel".[104] The flow field depends on non-isothermal rheology and transient heat transfer and it is therefore very complex.

The principle stages of the injection moulding cycle are[105]:-

(i)   preplasticisation (and hence melting) of the polymer to be injected;

(ii)   injection of the molten polymer at a relatively high flow rate from the reservoir, through the nozzle, sprue, runners, gates and into the mould cavities;

(iii)   packing of the mainly molten polymer in the mould network at high pressure to ensure complete filling and to minimise the effects of thermal shrinkage (hold-on stage);

(iv)   cooling, and hence freezing and crystallising;

(v)   ejection and hence removal of the mainly solidified products from the mould cavities and waste from the rest of the mould network.

5.1.1 The Plasticisation Stage[106,107]

The melt quality is largely determined by the complex thermo-mechanical history that the polymer undergoes during the plasticisation stage. Kamal et al.[106] studied the melt quality as a function of processing variables in the plasticisation stage of injection moulding.

The plasticisation stage can be divided into two portions: The

first is the screw rotation portion which is a transient plasticating extrusion process and the second is the rest of the cycle which is basically a conduction heating process. The plasticating behaviour approaches steady-state extrusion behaviour, if the screw rotation time is a high percentage of the total cycle, but is significantly different if a small percentage. Better plasticisation is achieved by a low screw rotation speed and a long rotation time than by a high screw speed and a short rotation time.

The screw plasticisation stage has a small mixing effect on the polymer due to the shearing action, however this shearing of the polymer can lead to degradation of sensitive polymers such as PET.

5.1.2 The Injection Stage[16,108-110]

The flow through the nozzle, sprue, runners, gates and into the mould cavities is called the injection stage of the process. As the melt flows into the mould heat transfers to the mould then solidifies the fluid polymer. The restriction to flow increases due to the freezing of a 'skin' next to the mould surface. The frozen 'skin' thickness is the product of the skin's rate of growth and the time it has had to grow. The frozen 'skin' which constricts the flow is thin near the entrance to the mould network as, despite the greatest growth time, there is enough heat transfer from the injection unit to slow down the freezing rate. Further into the mould the frozen 'skin' gets thicker, and is then thinner near the polymer front where the 'skin' growth time is zero.

In mould filling, the flow is often nearly-viscometric for simple moulds. Figure 5.1 shows the position of the polymer front at different times during filling, the diagram shows the fully developed flow region and the 'fountain effect' in the front region. Fluid elements decelerate as they approach the slower moving front and spill over outwards toward the mould walls.

The filling of a mould is likely to take place over both the injection and hold-on phases due to the significant compressibility and thermal shrinkage of most polymers.

Mould filling control techniques include timed injection, ram position, cavity pressure, nozzle melt pressure, and hydraulic

pressure. *Malloy*[108] studied all five control methods and their consistency in controlling part weight, and process pressures.

FIGURE 5.1: INJECTION MOULD FILLING AFTER *TANNER*[6]
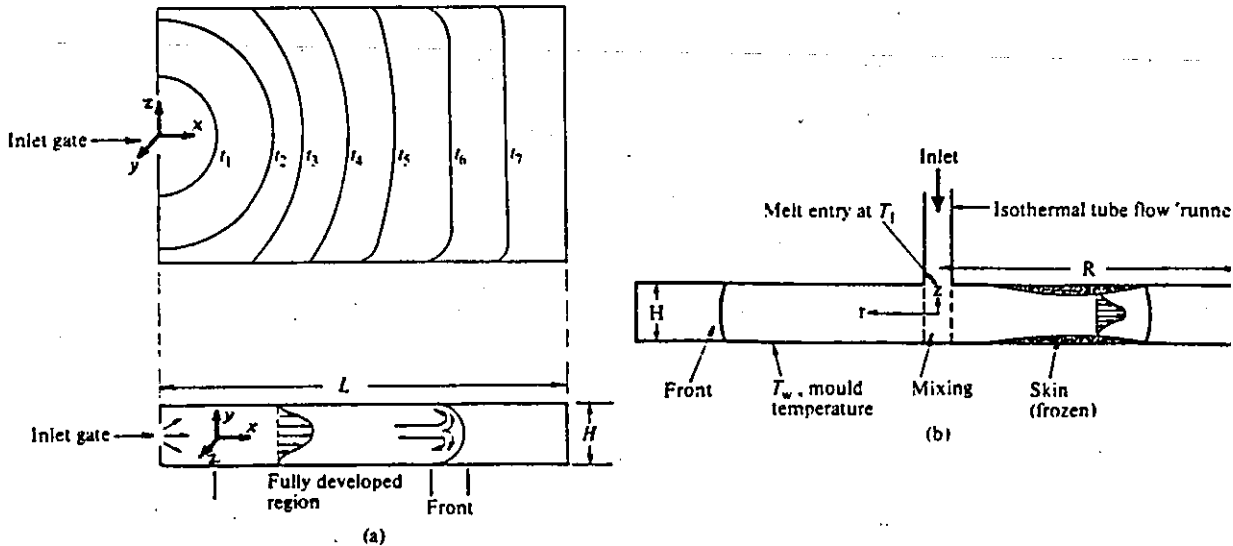
5.1.3 The Packing Stage[111-114]

The packing stage follows the injection stage, the carriage of the machine is kept forward, against the mould, applying the hold-on pressure, this pressure packs extra polymer into the cavity, to compensate for the shrinkage of the polymer due to cooling.

The pressure in the mould, especially at the end of the flow-front, is quite low at the moment the mould becomes full. With the (hold-on) pressure still applied the polymer continues to flow as long as the mould pressure is lower than the hold-on pressure. This flow raises the pressure in the mould rapidly. Opposed to this is the tendency of the mould pressure to drop because of the cooling of the polymer. Flow continues until the flow rate drops low enough to permit the gate to freeze. The flow rate during packing is very low, hence the pressure is near hydrostatic. During packing bulk compressibility of the melt is of great importance.

Darlington et al.[112] reviewed the work published on packing stage

studies, in their study they concluded that the cavity pressure is lower than the nozzle pressure during the packing stage.

The hold-on pressure causes packing in the moulding core. If excessive hold-on pressure is applied then high residual stresses occur in the moulded part. These can be frozen into the part, unless sufficient relaxation occurs before freezing. If the packing stage ends before the gate freezes then backflow from the cavity occurs causing molecular orientation in the moulded part. Insufficient packing also causes residual stresses, or voiding in the moulded part.

Greener[113] discussed the situation with bulky mouldings where the packing stage is the "limiting" phase. He proposed criteria for the packing phase that could be used in optimisation schemes.

Allan and Bevis[114] developed a technique for producing thick-section mouldings which were free of voids. The technique involves an oscillating packing pressure and continuation of flow due to shear heat energy. A cavity pressure transducer was positioned near the gate, a trace such as that shown in Figure 5.2 is used for setting up the process and for subsequent monitoring of the mouldings. The envelope shown in Figure 5.2 shows the cavity pressure variation which occurred during the packing time.

FIGURE 5.2: CAVITY PRESSURE TRACE SHOWING OSCILLATING PACKING PRESSURE AFTER *ALLAN AND BEVIS*[114]
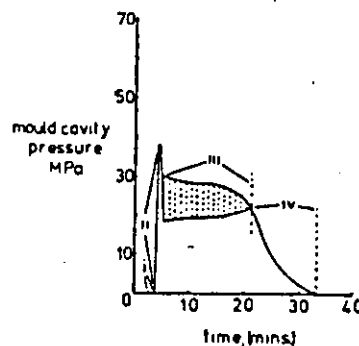
5.1.4 The Cooling Stage[115]

The cooling time is the total time the polymer is in the closed mould, however in this section the cooling stage refers to the period after the packing stage until the moulding can be ejected from the

mould without detrimental distortion.

In the cooling stage the changes in polymer temperature and pressure can be determined by solving the unsteady state heat conduction equation. The quality of a moulded object is determined by pressure and temperature and their rate of variation during the cooling stage. The solidification temperature is dependent on the temperature, pressure and rate of cooling.[115]

Residual stresses can be caused by different cooling rates in various layers of the the part. The rapidly cooling and solidifying surface layer forms a rigid shell, which restrains the still warm interior from contracting during the ensuing cooling process. This results in tensile stresses in the interior and compressive stresses in the external layer.[103]

5.1.5 The Ejection Stage[116]

The ejection stage involves the mould opening and the part being removed from the cavity, usually by ejectors (pins, stripper plates, core pullers). The mould may be opened when the pressure in the cavity is low enough so the moulding will release from the cavity as a result of contraction and the part has hardened enough to maintain its shape after removal from the mould. If the part contains residual strains then failure can occur during ejection. Higher injection pressures and mould temperatures usually necessitate higher ejection forces.

5.1.6 Residual Strains And Molecular Orientation[110,117,118]

The viscoelastic nature of the polymer results in shear and normal stresses and large elastic deformation developing during the injection and packing stages. This is followed by incomplete relaxation during the cooling stage. The resultant residual stresses are dependent upon the thermal, rheological and relaxation properties of the polymer as well as the processing conditions. The orientation in the final moulded part, together with the residual stresses, influences the mechanical properties and performance of the moulded part.

Residual strains in injection moulded parts can arise in three different ways: those accompanying quenching stresses; frozen-in

molecular orientation; and configurational volume strains. The origins and means of relieving or preventing residual strains were first reported by *Spencer and Gilmore*[117] in their pioneering studies.

The molecular orientation frozen-in a moulded part is induced by shearing forces during flow and relaxation when flow stops. *Ballman and Toor*[110] proposed that orientation decreased with increasing mould temperature, cavity thickness and barrel temperature; and that orientation increased with increasing gate size, injection pressure and hold-on time.

5.1.7 Rheological Modelling Of Injection Moulding[16,23,104,105,119]

Several reviews of the work done in this area have been published by *Han*[104], *Tanner*[16], *Casale et al.*[119], *Richardson*[105], *Bowers*.[23] The most recent of these by *Bowers*[23] is a comprehensive review of inelastic models for injection moulding and includes 119 references. These reviews cover the early work from the 1950s through to the more recent complex computer analyses. The modelling of each stage of the injection moulding process will be considered separately.

5.1.7.1 The Modelling Of The Plasticisation Stage[105,106,120,121]

A theoretical melting model for a reciprocating-screw injection moulding machine has been reported by *Donovan*.[120] He proposes a theoretical model for the melting process which predicts the transient melting profile along the screw during the moulding cycle. The model is based on a steady-state extrusion model modified for the transient behaviour during the rotation phase using a simple exponential function and using Neumann's solution for conduction melting for transient behaviour during the nonrotating phase. *Fenner* also deals with the plasticisation stage of injection moulding in his chapter in the book by *Pearson and Richardson*.[121]

A recent study by *Kamal et al.*[106] involved the modelling of the plasticisation stage using theoretical models and empirical models.

5.1.7.2 The Modelling Of The Injection Stage[23,109,116,119,122-136]

Casale et al.[119] and *Bowers*[23] reviews, cover the historical development of models for flow during the filling stage, including both the empirical and the purely theoretical approaches.

The theoretical studies of the mould cavity filling process are based on equations derived from the three fundamental equations of continuity, momentum and energy. The difficulties are related to the continuous variation of viscosity at each point of the mould in relation to the continuous and simultaneous variation of temperature and shear stress. The problem of deriving a numerical computation of the equations from the three fundamental ones has been attempted by several authors. They have different conclusions depending on the physical assumptions made.

Harry and Parrott[22] devised a model based on heat conduction and viscous heat generation along with the temperature dependence of the flow parameters to predict fill lengths and fill times of thin cavities. The assumptions made in this work were:

1.   The pressure gradient in the flow direction is constant at any given instant. (see Figure 5.3)

2.   The effect of cavity edges were neglected.

3.   Incompressible fluid.

4.   Constant conductivity, density and heat capacity.

5.   Constant mould surface temperature.

6.   One dimensional flow.

The simulation neglected the effects of the runners and gate.

The simulation accurately distinguishes between the short shot and fill conditions, but there was considerable error in the prediction of the length of short shots and the fill time for full shot conditions. A predicted fill time of 0.073s compares with an experimentally measured fill time of 0.10s. A predicted short shot length of less than 3.25" was experimentally found to have an average value of 4.84".

FIGURE 5.3: PRESSURE GRADIENT ASSUMPTION AFTER *HARRY AND PARROTT*[22]
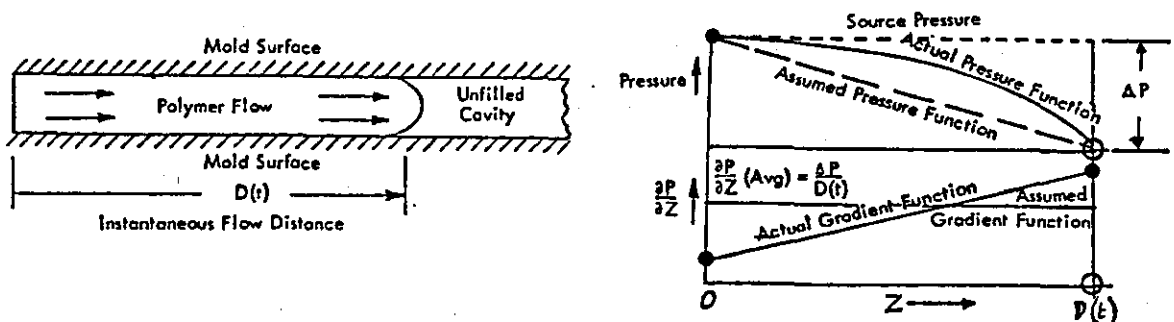
Berger and Gogos[123] presented a numerical simulation for the filling of a disc shaped cavity under constant pressure injection. They used a constant density power law fluid to model rigid PVC. The simulation predicts fill times and enables the formation of the frozen 'skin' to be followed via the velocity profiles. The simulation can also be used to study thermal degradation effects. They concluded that the gate and runners are the most important factors in mould design as they can affect the efficiency of the cycle by dissipating the applied pressure and the shear heating that occurs during flow through the runners and gate.

Kamal and Kenig[124,135] reported a theoretical model which simulates flow in the filling, packing and cooling stages of the injection moulding cycle. The simulation yields data on the progression of the melt front, the flow rate and the velocity profiles at different times and positions in the cavity. It also yields temperature and pressure profiles throughout the packing and cooling stages.

The same authors reported an experimental test of the model[136] which showed very good agreement on the melt front in the cavity. Good agreement between theory and practice was found for all three stages with polyethylene using a semi-circular cavity. Problems near the cavity entrance due to viscoelastic and end effects during the filling stage questioned the validity of some of the assumptions in the model. These problems were illustrated by the results reported: predicted filling times were 15-20% shorter than the experimental filling times. The predicted and observed pressure profiles reported are shown in Figure 5.4.

FIGURE 5.4: PRESSURE PROFILES AFTER *KAMAL AND KENIG*[124]
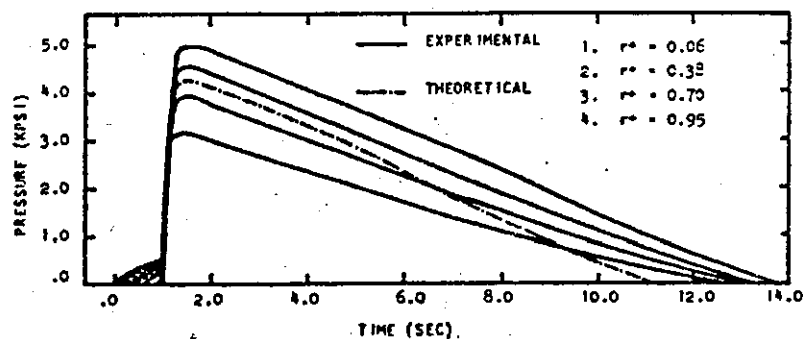
The 'fountain' flow effect has been modelled by *Mavridis et al.*[109,134] using a finite element program which solves the conservation equations. The predictions agree with experimental observations of 'fountain' flow followed by shear flow giving the deformation history.

A computer simulation of mould filling behaviour using a theoretical mathematical model has been reported by *Kamal et al.*[133] The simulation incorporates a viscoelastic rheological equation, the 'fountain' flow effect and non-isothermal crystallisation kinetics. The simulation assumed:

1.   the fluid was viscoelastic and incompressible;

2.   body forces were negligible;

3.   two-dimensional flow (negligible variation in the Y-direction gradients);

4.   the pressure term in the energy equation was neglected due to the numerical complications involved.

The simulation yields data on filling time and melt front position as well as velocity, temperature, pressure, and shear stress distributions within the mould cavity. The magnitude of the 'fountain' flow effect was shown by a transverse velocity component, also the temperature distribution in the melt front region is affected. The 'fountain' flow was shown to influence the stress distributions near the melt front. The predicted filling time of 1.13s compared to an experimentally measured value of 1.01s.

The empirical approach simplifies the differential equation system but still gets an analytical solution. *Grinblat*[125] assumed the melt flows within an immobile envelope of cooled polymer during mould filling (see Figure 5.5).

FIGURE 5.5: POLYMER FLOW IN A MOULD CHANNEL AFTER *GRINBLAT*[125]
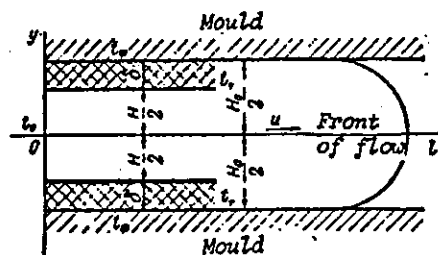
The envelope has the mould temperature at the mould interface, and the melt temperature at the melt interface. These temperatures remain constant in the analysis, which is reduced to isothermal flow in a section which decreases steadily until the polymer stops moving. Barrie[126-129] also assumes this simplification, he also assumes that the thickness of material frozen is proportional to the cube root of filling time, he reported good agreement between his model and experimental results.

An extensive study of the pressure transfer in mould filling is reported by Vostorgov and Kalinchev.[130] Filbert[116,131,132] correlated the mould filling time with the geometrical dimensions of the cavity, the material properties and the processing conditions.

A review of attempts to correlate technological tests such as the spiral flow test, or the mouldability area with mould cavity filling is found in Casale et al.[119] Properties such as degradation temperature, flow length, and optimum gate size to avoid jetting have been predicted from this type of approach.

5.1.7.3 The Modelling Of The Packing Stage[112,113,135,136]

The modelling of the packing stage has been reviewed by Darlington et al.[112]. The cavity pressure variation with both time and axial distance from the gate during the packing stage have been reported for several cavity geometries. Kamal and Kenig[135,136] modelled the filling, packing and cooling stages in one theoretical simulation.

Greener[113] reported criteria to be used for the packing stage in optimisation schemes.

5.1.7.4 The Modelling Of The Cooling Stage[113,115,135-137]

Kamal and Kenig[115,137] obtained quite good theoretical predictions of actual cooling behaviour. Their model predicts the progress of the freezing front through the moulding, the freeze front profiles showed a maximum position with semi-crystalline HDPE and a monotonously decreasing profile for polystyrene. The same authors later reported a simulation that modelled the filling, packing and cooling stages.[135,136]

5.1.7.5 The Modelling Of Residual Strain And Orientation[118,138]

Isayev and Hieber[118] used a Leonov viscoelastic model of the filling and cooling stages to get predictions of the residual stresses in moulded parts. They found the main factors affecting residual stresses and orientation were the flow rate and the melt temperature. They proposed these should both be kept as high as permissible to accelerate the relaxation of the orientation during cavity filling. A high melt temperature will lead to a quenching effect; this will increase the residual stress.

Tadmor[138] used a semi-quantitative model incorporating flow and heat transfer mechanisms coupled with molecular theories to explain the complex molecular orientation distribution observed in injection moulded parts. He suggested that the orientation in the surface skin is related to steady elongational flow in the advancing front ('fountain' flow), whereas the orientation in the core is related to the shear flow, behind the advancing front, and between the two solidifying layers (see Figure 5.6). He found orientation increased with increasing injection speed and decreased with increasing cavity thickness and temperature. The molecular relaxation process, coupled with the heat transfer, explains the drop in orientation with distance from the surface.

FIGURE 5.6: SCHEMATIC ORIENTATION DISTRIBUTION AFTER *TADMOR*[138]
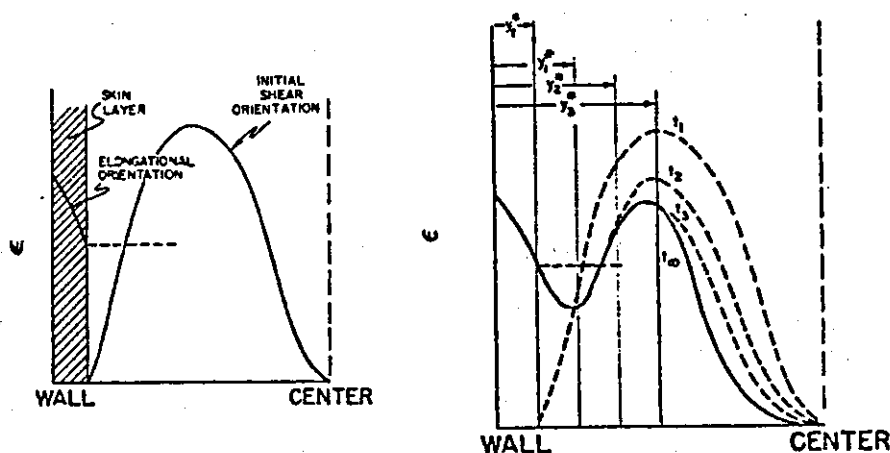
5.1.8 Assumptions And Approximations In Flow Models[23,105]

Simplification is necessary to overcome the mathematical complexity in modelling every aspect of the injection moulding process. Most modelling of the flow in the injection stage ignores the following:

- the shear viscosity dependence on pressure;
- normal stresses, extensional and elastic effects (important at gates, changes in direction or section, and in mould cavities which are not long and narrow);
- the 'fountain' flow effect behind the melt front (except in a few recent papers[109,133,134]);
- slippage at the walls;
- simultaneous heat transfer;
- density changes in the flow;
- conduction along the streamlines;
- solidification during the injection stage.

Models of the packing and holding stages ignore the following:

- flow in the packing stage (all ... assume ... a full cavity);
- the small flow due to thermal expansion and compressibility effects;
- the convection and dissipation terms in the conservation equation;
- solidification during the packing stage.

Models of the cooling stage ignore the following:

- crystallisation that occurs on freezing;
- the latent heat term in the energy conservation equation.

As well as ignoring the above list other approximations and assumptions are made to simplify the calculations. These are listed below:

- the sprue and runner system is assumed to be a series of circular pipes;
- complex moulds are treated as a series of simple geometries, e.g. disc, slab;
- simple shearing flow predominates;

- the apparent shear viscosity has a power law dependence on shear rate and an exponential dependence on temperature;
- there is fully developed flow in the velocity field;
- there is not fully developed flow in the temperature field;
- the 'lubrication approximation' can be applied;
- no jetting occurs;
- cooling occurs through the thickness only (i.e. two dimensionally, not three dimensionally);
- rules are assumed to predict the frozen layer growth during cooling;
- volumetric injection rate, maximum injection pressure, packing pressure, hold-on pressure are constant;
- instantaneous changes occur between each cycle stage;
- injection moulding conditions change slowly, so local temperature is that given by steady flow;
- heat transfer, during the packing and holding stages, is a transient conduction process, with an energy change associated with freezing.

Bowers[23] reported quantitative assessments of the effects of various degrees of simplification of the governing equations. Using pressure predictions as a basis for comparison he concluded that:
- Neglecting viscous dissipation causes pressure to be under-estimated by 10%.
- Neglecting the pressure dependence of viscosity causes pressure to be over-estimated by 10%.
- Neglecting axial convection of heat causes pressure to be under-estimated by 1 to 4%.
- Neglecting normal stresses due to shear flow causes pressure to be over-estimated by 6 to 12%.

Some of these assumptions and approximations are reviewed later in Section 5.3.3.

It is clear that there are many assumptions which influence the accuracy of the models and simulations. Any move to close the gap between theory and practice, especially for some of the newer engineering plastics, will be of benefit to the industry.

5.1.9 Computer Simulation[105]

The computer simulation of the injection moulding process is discussed by *Richardson*.[105] The mathematical model chosen for any process should reflect the needs of the worker concerned and be selected to provide the information required in its most convenient form and at acceptable cost computationally.[105]

An important factor from the practical viewpoint is that the data needed for the input of a computer simulation must be relatively inexpensive to obtain by using well established test methods so that is both reliable and consistent.

The simulation of the injection moulding process is actively pursued largely because the procedure of mould design, machine selection and choice of operating cycle represents a lengthy and expensive part of what is often a relatively small-scale operation. Also, a large "black-art" element still exists in the industry.

Mould design has been done by trial-and-error, the aim of the computer simulation is to eliminate the redesign stages, assuming that the use of a computer is much cheaper than mould or prototype manufacture.

The information required for computer simulation of the injection moulding cycle comprises:

(i) geometrical and topological information defining the mould network;

(ii) physical (rheological and thermal) properties of the polymer;

(iii) operating parameters defining the manner in which the moulding machine is run.

The information that a computer simulation must produce comprises:

(i) estimates of minimum injection, packing, and cooling times;

(ii) estimates of flow rate and the pressure drop within the mould network and hence the required hydraulic pressure, and of the forces that develop within the mould network (hence the clamping requirements);

(iii) estimates of the polymer temperature and hence the flow-

average temperature difference within the mould network and of the frozen layer thickness.

Since the mould geometry, physical properties of the polymer, maximum operating pressures, forces and injection rate of the machine and the minimum and maximum operating temperatures within the machine are fixed; the only variables usually available to the designer are the geometry and topology of the sprue, runners and gating system, and the thermal conditions on the walls of the mould network.

Figure 5.7 shows a flow chart of a injection moulding simulation process.

FIGURE 5.7: SIMULATION FLOWCHART[105]
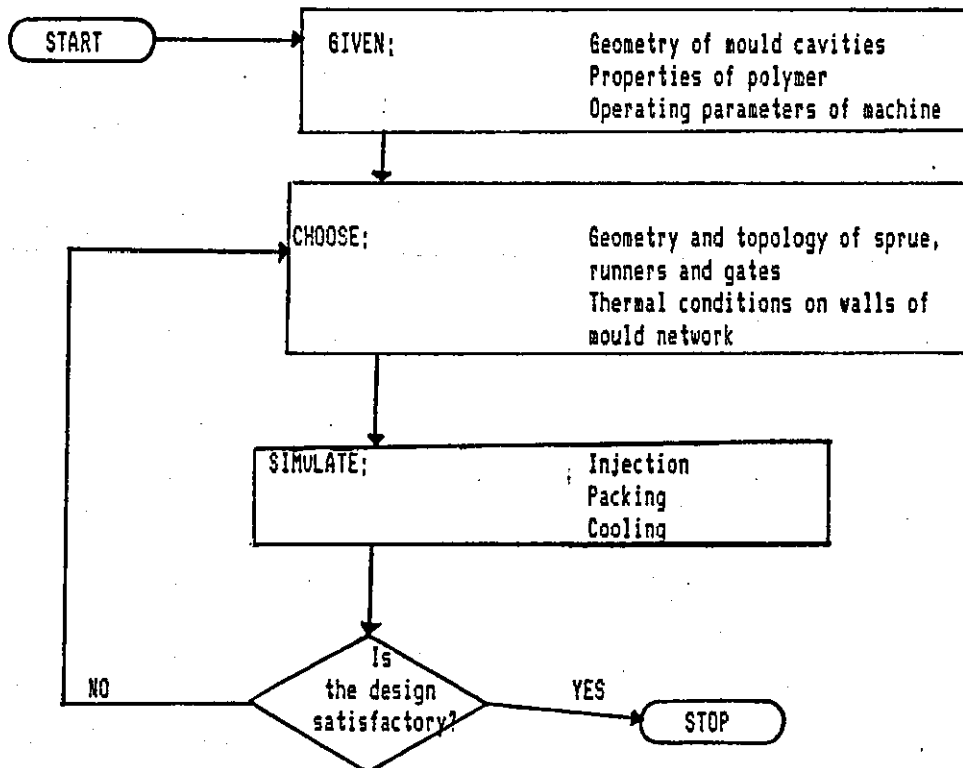
5.1.10 Current Trends In Simulation[139-141]

There are a few commercial software packages currently available which simulate part of the injection moulding process. MOLDFLOW,

MOLDCOOL[140,141], POLYFILL and POLYCOOL are packages which allow the computer aided design of moulds, permitting different placing and scaling of runners, sprues, cooling channels and weld lines.

MOLDFLOW enables a computer to simulate how a given plastic will flow around a part 'drawn' on the screen under whatever process conditions the operator has keyed in. A finite element analysis process is used. The program shows pressures and stresses created within the part by the fill under the conditions set, where weld lines fall, and if damaging elements such as overpack, air traps and hesitation are likely.

A commercial package which is aimed at the production engineer, rather than the designer is SIMPOL (SIMulated POLymer behaviour system) which permits optimisation of processing conditions, and specifies machine requirements and estimates the costs involved. (See Section 5.3 for more details).

5.1.11 Injection Moulding Technology For PET Processing

In the manufacture of PET bottles by the reheat blow process, the first stage is to injection mould preforms which are subsequently reheated and blown into bottles. The main objectives of the injection moulding stage are to retain the polymer molecular weight, to minimise acetaldehyde generation, and to obtain a clear amorphous preform.

The viscosity will drop if hydrolytic degradation occurs and so PET has to be dried properly before processing. Above the melting point any residual moisture will rapidly hydrolyse the polymer. Another source of viscosity reduction is thermal degradation in the melt.[44,142]

Acetaldehyde is generated during PET processing, it is dependent on the heat history of the polymer.[142] It has a distinctive fruity odour and can diffuse into foodstuffs tainting them, hence the acetaldehyde level has to be minimised when manufacturing food packaging products. The acetaldehyde level can be minimised by minimising the melt residence time, minimising the screw speed and back pressure, hence reducing the shear heating. *Branscome*[143,144] reported the results of moulding trials. He found the barrel

temperature to be the most significant factor in acetaldehyde generation. Other factors he found to affect acetaldehyde level were screw speed, back pressure, injection rate, mould manifold and gate temperatures.

Preform clarity can be associated with the degree of crystallisation,[44,142] PET being transparent when amorphous and opaque when crystallised. PET will crystallise between the glass transition temperature, 85°C, and 250°C, the rate is fastest between 140°C and 180°C, a visible degree of crystallinity being visible in less than one minute at 165°C.[44] Therefore to obtain a clear preform cooling through this temperature range must occur as quickly as possible. The low thermal conductivity of PET limits the thickness of injection moulded products to 4mm for clear mouldings.[44] Increasing melt temperature improves clarity. There is a conflict of interests in optimising moulding temperature, minimising acetaldehyde requires low temperatures whilst minimising haze requires high temperatures. There is a similar conflict with intrinsic viscosity level, the crystallisation rate decreases with increasing intrinsic viscosity, however a high intrinsic viscosity polymer requires higher temperatures, hence more acetaldehyde is generated. Other factors affecting clarity are: increasing gate temperature results in reduced haze; high injection pressures can induce flow crystallisation, a reduction of the flow rate reduces this effect; mould coolant efficiency should be high to minimise the crystalline associated haze.

Branscome[143,144] reported that haze level is dependent on barrel temperature, hold-on pressure, injection rate, and mold cooling temperature. Therefore a haze-free preform with an overall decrease in acetaldehyde can be obtained using an increased injection rate and a reduced barrel temperature.

For other injection moulding applications, PET found limited usage due to the slow crystallisation rate. Bier and Ong[145] reported on modified PET polymers which had faster crystallisation rates allowing injection moulding at mould temps of 80°C-110°C and at shorter cycle times than unmodified PET.

5.2 Experimental Work - Negri Bossi

5.2.1 Introduction[108]

A series of experiments were undertaken on a 55 tonne *Negri-Bossi* NB55 injection moulding machine, investigating the effects of injection rate, mould temperature and melt temperature on hydraulic and cavity pressures, fill time, and feasibility of moulding for three different polymers.

The polymers used were B90S 'Melinar' ICI's standard bottle grade linear PET, which has a nominal I.V. of 0.74; a high viscosity experimental grade EX167 from ICI, which is a linear PET having a nominal I.V. of 0.92; and a injection moulding grade copolyester PCTG 5445 from Eastman Plastics, which has a nominal I.V. of 0.65.

The specification for the injection moulding machine is shown below in Table 5.1.

TABLE 5.1: NEGRI BOSSI NB55

Maximum Clamp Force	55 tonnes
Screw Diameter	38 mm
Maximum Shot Volume	120 ml
Screw L/D Ratio	14.5
Maximum Heating Power	4.5 KW
Maximum Drive Power	10 hp
Dry Cycle Time	0.83 s
Maximum/Minimum 'Daylight'	350 mm x 150 mm
Platen Dimensions	535 mm x 490 mm
Distance between Tie Bars	310 mm x 310 mm

The hydraulic line pressure is measured by a strain gauge pressure transducer and is displayed on the control panel, an output for connection to a chart recorder has been fitted. The injection time is displayed on the control panel, it results from the axial movement of the screw which is measured by a distance transducer.

The mould used was designed to produce either two rectangular test bars or two dumbbell tensile bars. For this study the runner system was routed to produce two rectangular bars. The mould was instrumented with a cavity strain gauge transducer positioned flush

with the cavity surface close to the gate end of the cavity.

The mould used had a very long runner system and simple cavity geometry (see Figure 5.8). The flow path did not include any significant convergent or divergent sections, hence elongational flow via convergence was not significant in this system. This prevented a comparison of the theoretical die-entry factor for section changes with practical measurements being made. Time constraints prevented an alternative mould being prepared for use in this study.

FIGURE 5.8: INJECTION MOULDING

The injection moulding conditions that were kept constant are shown in Appendix 9. The other moulding conditions injection rate, barrel temperature, and mould temperature were varied. The machine was run using the hydraulic pressure closed loop control method. This control method produces the least variation in peak cavity pressure and good control of peak nozzle pressure, peak hydraulic pressure, and part weight variation.[105]

The mould temperatures used were 10°C and 50°C for each of the three polymers. A *Conair Churchill* Water Heater was used to maintain

a constant mould temperature of 50°C. A *Refrigeration, Heating and Recirculation Ltd.* Chiller Unit was used to maintain a constant mould temperature of 10°C.

The barrel temperatures were set in a rising profile from the hopper to the nozzle. For both of the linear PET polymers the two profiles used were: 270°C/275°C/275°C/280°C
280°C/285°C/285°C/290°C
For the PCTG copolyester the two profiles used were:
250°C/255°C/255°C/260°C
260°C/265°C/265°C/270°C

Several injection rates were used for each of the polymers at each of the mould and melt temperatures. The injection rate profile was kept flat (e.g. machine setting Vv: 400/400/400/400).

The raw materials were dried overnight in a *Conair Churchill* Dehumidifying Hopper at the polymer suppliers recommended temperature. The hopper was fitted directly onto the injection moulding machine.

A *Philips* two pen chart recorder was attached to the pressure outputs from the control panel of the injection moulding machine so that traces of the hydraulic pressure and the cavity pressure were recorded throughout the moulding cycle.

The conversion of the mV outputs to MPa are given below.

Hydraulic Pressure

(specific pressure on the screw) : 1 mV = 83.6 MPa   (5.1)

Cavity Pressure : 1mV = (190÷160) x 0.1774 MPa   (5.2)

(The (190÷160) factor is to compensate for the position of the transducer, the resultant pressure is for the whole length of the cavity.)

5.2.2 Results

The type of cavity pressure profile obtained can be described as being one of the types shown in Figure 5.9

The injection stage is shown by the initial linear part of the cavity pressure profile, the rapid increase in pressure shows the compression phase during the filling stage, the remaining part of the profile shows the holding pressure stage. The profile **Type I** indicates a correct switch-over and smooth transition from injection

to hold-on pressure. The **Type II** profile indicates a premature switch-over which results in the cavity being partially filled by the hold-on pressure. The **Type III** profile indicates incomplete filling of the cavity (short shot).

FIGURE 5.9: TYPES OF CAVITY PRESSURE PROFILE
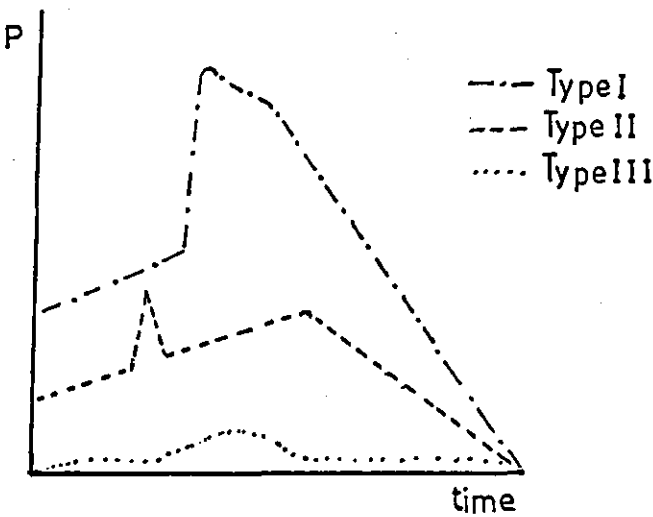
FIGURE 5.10: TYPICAL HYDRAULIC PRESSURE PROFILES
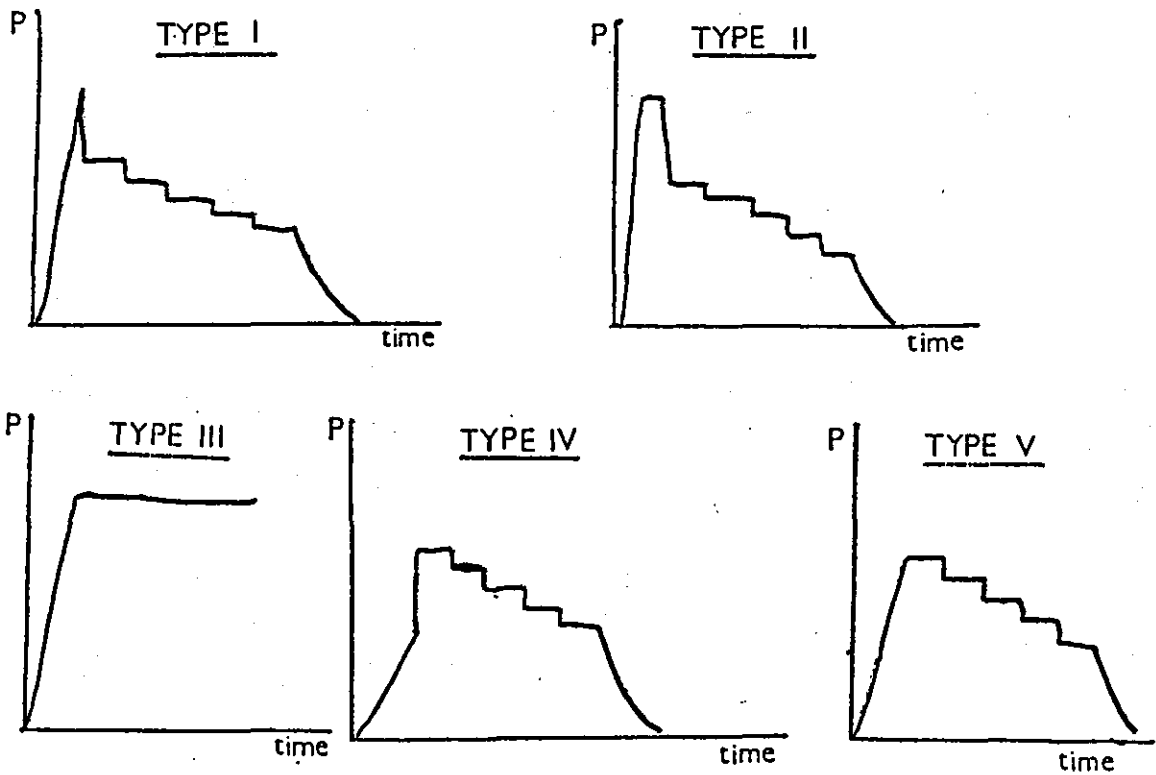
Typical hydraulic pressure profiles are shown in Figure 5.10, the injection stage is followed by the five decreasing steps in the hold-on pressure. There are five typical types of profile shown: **Type I** indicates correct switch-over from the injection to hold-on pressure the peak showing the maximum specific pressure on the screw; **Type II** indicates a situation where the limit of the machines injection pressure is reached before complete cavity filling occurs; **Type III** indicates a short shot; **Type IV** indicates the situation where the hold-on pressure is greater than the required injection pressure; **Type V** indicates the situation where the injection pressure is the same as the hold-on pressure.

The maximum hydraulic pressure is reported in the results section, together with the cavity pressure at the instant the cavity was filled and the type of pressure profiles obtained.

The results for the experimental work carried out using the Negri Bossi injection moulding machine are shown as Figures 5.11-5.16. The results for B90S grade PET are shown in Figures 5.11-5.12; the results for EX167 grade PET are shown in Figures 5.13-5.14; and the results for PCTG copolyester are shown in Figures 5.15-5.16. The pressure profile types listed in Tables 5.2-5.4 refer to Figures 5.9 and 5.10.

TABLE 5.2: B90S PRESSURE PROFILE TYPES

Injection Rate (ml/s)	Cavity Pressure				Hydraulic Pressure			
	280 10	280 50	290 10	290 50	280 10	280 50	290 10	290 50
1.5	III*	III*	III*	III*	III*	I*	I*	I*
2.15	I	I	II	II	V	I	I	I
2.8	II	I	II	II	I	V	I	I
3.4	I	I	I	I	I	IV	I	I
4.9	I	I	I	I	IV	IV	I	I
6.5	I	II	I	I	I	IV	I	I
8.2	I	II	I	IIt	I	IV	I	It
10.0	I	It	I	I	I	It	I	I
13.7	I	I	It	I	I	I	It	I
18.2	It	I	It	II	It	I	It	I
21.9	I	II	It	II	I	I	It	I
27.4	I	II	It	II	II	II	It	I
39.1	I	II	It	II	II	II	It	II

* indicates a short shot.
t indicates flashing.

TABLE 5.3: EX167 PRESSURE PROFILE TYPES

Injection Rate (ml/s)	Cavity Pressure				Hydraulic Pressure			
	280 10	280 50	290 10	290 50	280 10	280 50	290 10	290 50
2	–	–	–	III*	–	–	–	I*
2.6	–	–	–	II	–	–	–	I
3.5	–	–	–	I	–	–	–	IV
4.9	II	–	–	II	II	–	–	I
6.4	II	III*	II	It	II	II*	II	IVt
8.0	I	–	II	II	I	–	II	I
10.0	II	II	II	IIt	II	II	II	IVt
12.0	II	II	II	II	II	II	II	IV
15.0	II	II	II	–	II	II	II	–
18.2	–	II	II	–	–	II	II	–
19.9	–	–	I	–	–	–	II	–
21.9	–	II	I	II	–	II	II	I
39.1	–	II	–	I	–	II	–	I

* indicates a short shot.
t indicates flashing.

TABLE 5.4: PCTG PRESSURE PROFILE TYPES

Injection Rate (ml/s)	Cavity Pressure				Hydraulic Pressure			
	260 10	260 50	270 10	270 50	260 10	260 50	270 10	270 50
1.8	–	III*	III*	III*	–	III*	III*	I*
2.6	–	III*	III*	I	–	III*	III*	I
3.35	II*	III*	II	I	IV*	III*	II	I
6.4	II	II	II	I	II	II	I	I
10.0	II	II	II	I	II	II	I	I
13.7	IIt	II	II	It	IIt	II	I	It
16.8	II	II	–	I	II	II	–	I
19.0	II	II	I	It	II	II	I	It
21.9	II	I	It	I	II	II	IIt	I
24.3	II	I	I	I	II	II	II	II
27.4	II	I	I	I	II	II	II	II
39.1	–	–	I	I	–	–	II	II

* indicates a short shot.
t indicates flashing.

FIGURE 5.11: B90S NEGRI BOSSI RESULTS
FLOW RATE VERSUS CAVITY PRESSURE
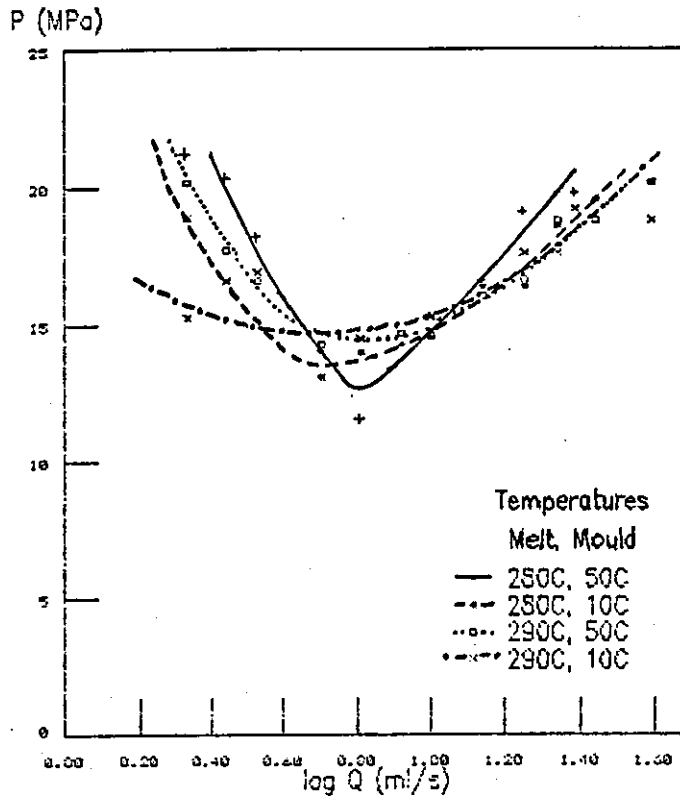
FIGURE 5.12: B90S NEGRI BOSSI RESULTS
FLOW RATE VERSUS HYDRAULIC PRESSURE
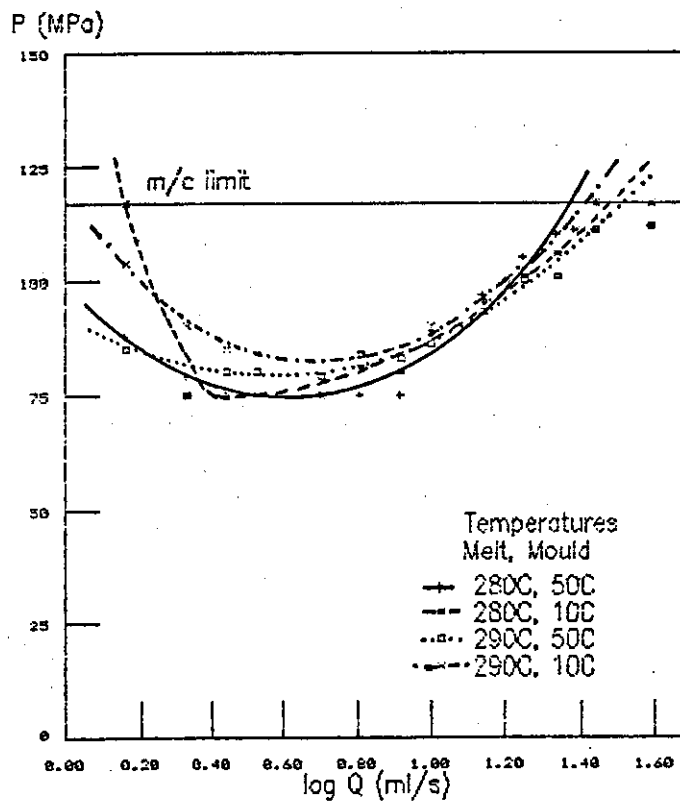
FIGURE 5.13: EX167 NEGRI BOSSI RESULTS
FLOW RATE VERSUS CAVITY PRESSURE
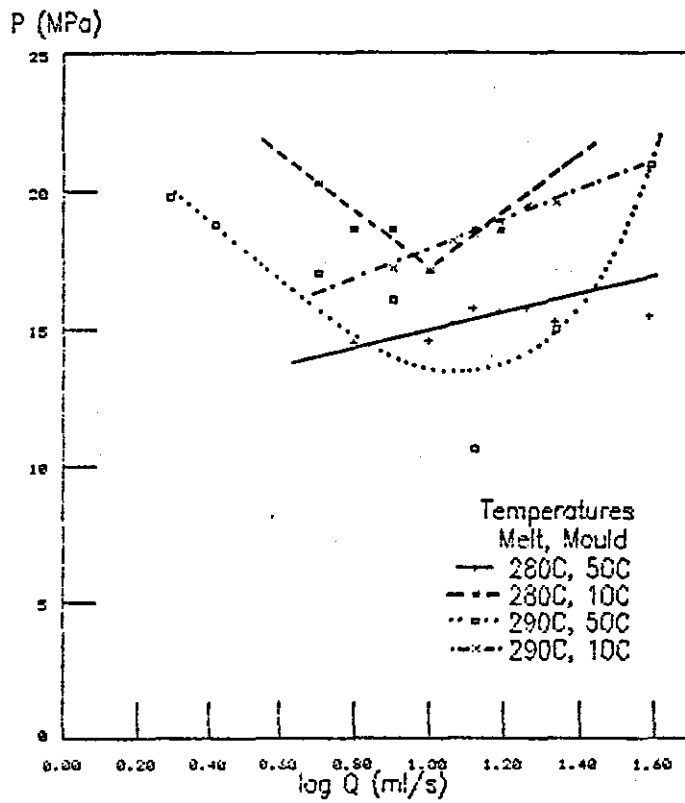
FIGURE 5.14: EX167 NEGRI BOSSI RESULTS
FLOW RATE VERSUS HYDRAULIC PRESSURE
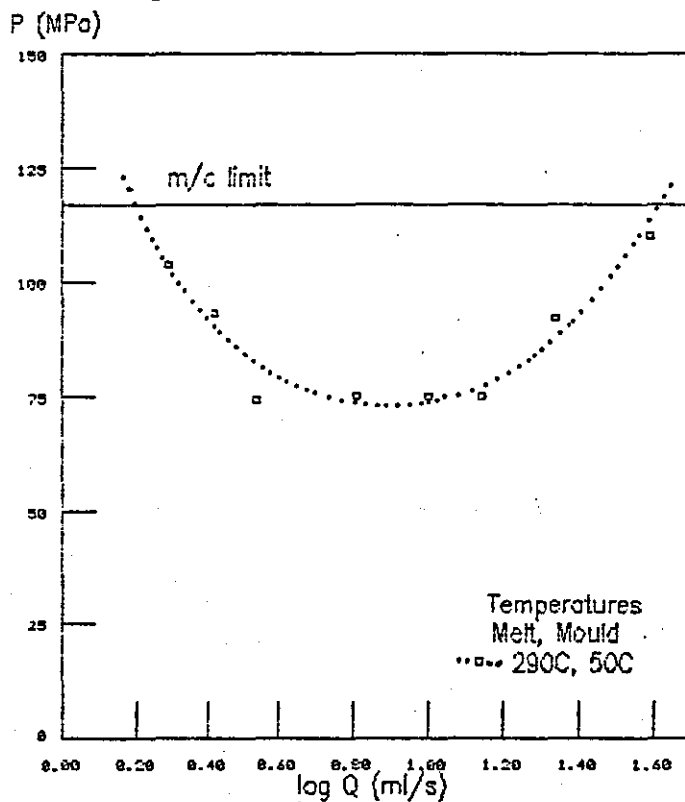
FIGURE 5.15: PCTG NEGRI BOSSI RESULTS
FLOW RATE VERSUS CAVITY PRESSURE
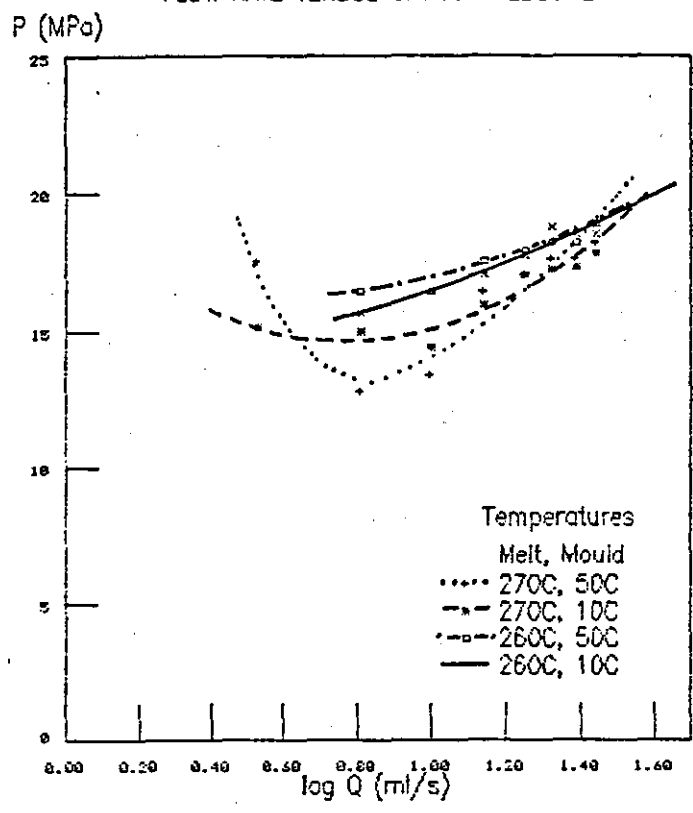
FIGURE 5.16: PCTG NEGRI BOSSI RESULTS
FLOW RATE VERSUS HYDRAULIC PRESSURE
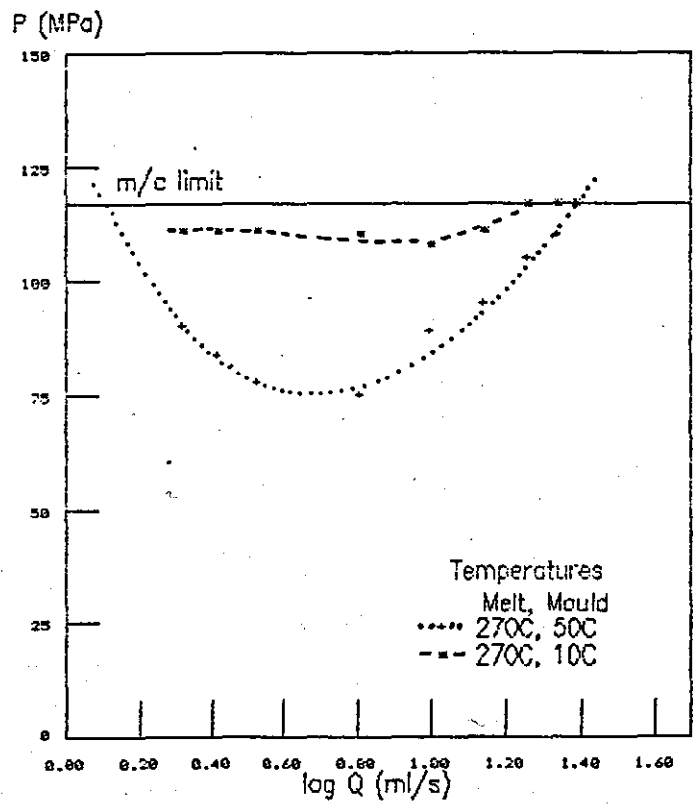
5.2.3 Discussion Of Experimental Results

The three polymers used all have relatively high viscosities. Together with the long runner system in the mould, this led to high filling pressures for all the conditions used.

5.2.3.1 Pressure Profiles[103,130,146]

From Tables 5.2-5.4 the short shot conditions are shown by hydraulic pressure profiles of Type III or cavity pressure profiles of Type IV. At very low flow rates the polymer solidifies before the mould is completely filled, resulting in a short shot. The lower mould and melt temperatures accelerate the solidification process and so the problem is encountered at higher flow rates only with the lower temperatures, as shown by the PCTG results.

Situations where the injection pressure required exceeded the machine limit also occurred, in these cases the mould is not filled during the injection stage, the 117MPa pressure maximum available being insufficient, in these cases the cavity is filled during the packing stage. Hydraulic pressure profile Type II (see Figure 5.10) illustrates this situation, the plateau on the trace showing where the machine pressure limit has been exceeded. These conditions were prevalent at the higher injection rates and lower melt temperatures, the minimum flow rate at which this situation was observed was lower with the lower mould temperature, shown clearly by EX167 at 290°C and by PCTG at 270°C. To achieve higher flow rates more energy has to be applied to the injection process, i.e. a higher injection pressure is required. This agrees with the relationship between flow rate and pressure drop quoted in Chapter 2. *Cox and Mentzer* reported[146] that with short fill times (i.e. high flow rates) the fill pressure is high and the flow is controlled by the viscous forces which resist the flow (see Figure 5.17). *Vostorgov and Kalinchev*[130] reported that the pressure required for filling of the mould is determined by the flow rate. High rates requiring high filling pressures.

Under the conditions where hydraulic pressure profile Types IV and V occurred, the hold-on pressure was greater than the injection pressure. This results in overpacking the polymer into the cavity and

the moulded parts contain residual strains. This occurred with B90S at 280°C for both mould temperatures and with EX167 at 290°C with a mould temperature of 50°C. The flow rates where this occurs are in the middle of the acceptable processing range: it could be that these are the optimum flow rates to use, requiring the minimum injection pressures and inducing the minimum of stress. However in a production environment the hold-on pressure would have to be reduced to a value lower than the injection pressure to benefit from the optimisation. The B90S results at 280°C show that these low injection pressures occur over a wider range of flow rate at the higher mould temperature. The EX167 results show that by increasing the mould and melt temperatures these low injection pressures can be obtained. The pressures decrease at higher temperatures due to a reduction of the polymer viscosity.

FIGURE 5.17: TYPICAL FILL PRESSURE FILL TIME RELATIONSHIP[146]
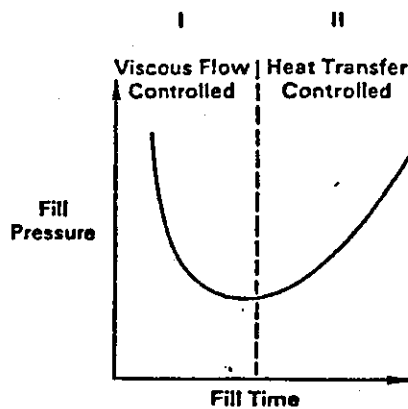
The pressure profiles of Type I show what is expected from correct injection and switchover to hold-on. These profiles are obtained within the boundaries of short shot and available machine pressure limits. The results for all three polymers show that the acceptable processing range of flow rates widens at the higher melt and mould temperatures. The Type I profiles were more prevalent with the easier flowing, lower viscosity PET (i.e. B90S), this highlights the importance of using a grade of polymer with a low enough

viscosity to allow a wide range of processing conditions to be used
and still result in acceptable mouldings.

The cavity pressure profiles of Type II, indicate a premature
switchover from injection to hold-on pressure, which will result in
the cavity filling under the packing pressure, which is too low for
proper filling and consequently with reduced injection speed.[103]

The pressure traces showing the switchover point supply
information that can be utilised for process control. A knowledge of
how the pressure profiles are affected; and what effects result in
the material, and the part, from a particular type of profile allow
the features of the traces to be used to set up the operating
conditions and monitor the production of mouldings. The profiles can
signal problems arising in the mouldings, by conditions drifting away
from the set values, and the traces can indicate the possible source
of the problem.

5.2.3.2 Pressure As A Function Of Flow Rate[103,127-130,146]

From Figures 5.11-5.16 the effects of mould and melt temperature
on the pressure-flow rate curves can be studied. The pressure-flow
rate curves for all three polymers used produced curves that pass
through a minimum pressure value. This type of result has been
reported by *Barrie*[127-129], *Vostorgov and Kalinchev*[130], and *Cox and
Metzner*[146]. At high flow rates the injection pressure is high and the
flow is controlled by the viscous forces which resist the flow. With
fast flow rates there is little time for heat transfer to occur,
hence the behaviour approaches the isothermal flow situation. At
lower flow rates the viscous resistance decreases, resulting in a
lower injection pressure. At some point the fill pressure passes
through a minimum and starts increasing with decreasing flow rate.
This region is heat transfer controlled as the hot melt slowly fills
the cold mould, and substantial heat transfer occurs. The melt
temperature drops which increases the viscosity and thus the
pressure. Simultaneously, frozen material on the walls increases,
narrowing the flow channel and increasing the resistance to flow.

Processing can usually be carried out within a range of flow
rates either side of the minimum pressure point. Within this

processing window variations in processing parameters which affect the flow rate have the least effect on the total pressure drop. The optimum flow rate is that which corresponds with the minimum pressure level, resulting in the minimum stress levels and the mould opening force. Though *Cox and Mentzer*[146] warn that this is economic from an energy conservation viewpoint there may be a trade-off with an increased cycle time.

The B90S curves (Figures 5.11 and 5.12) all lie close together, indicating little dependence of melt or mould temperatures, over the ranges of temperature and flow rate considered. Therefore the geometry is more important than melt and mould temperature, with respect to the design of the runner system and mould. *Barrie*[127-129] reported no significant difference in pressure with changes of 20°C in mould temperature for a stabilised propylene/ethylene copolymer. From Figures 5.11 and 5.12 it can be seen that the trends in the cavity pressure drop data are less clear than in the hydraulic pressure drop data, this indicates that the material is changing in the barrel, e.g. the melt viscosity is fluctuating. This could be an error arising from the experimental design in that the results for each condition are from a small number of machine cycles, not from steady-state continuous running.

The difference in minimum cavity pressures with decreasing mould temperature, at 280°C melt temperature, can be explained as the lower temperature resulting in faster solidification during filling, therefore a narrower molten core and less transmission of the hydraulic pressure to the cavity. *Johannaber*[103] reported better pressure propagation and higher cavity pressures at higher mould temperatures. The value of minimum hydraulic pressure decreased with increasing mould temperature, due to the lower temperature causing faster cooling of the melt during filling and higher viscosity, hence a higher pressure: these results therefore agree with those of *Johannaber*[103].

Considering the affects of melt temperature on the minimum cavity pressure the results agree with *Barrie*[127-129] and *Johannaber*[103] who reported decreasing cavity pressure with increasing

melt temperature, due to the decrease in viscosity. Generally as the temperatures increase the processing window spans a broader range of flow rates.

The EX167 curves (Figures 5.13 and 5.14) showed the same trends in behaviour as the B90S curves. The minimum cavity pressure is not shown for all the curves due to the flow rate range used not being wide enough to encompass the minimum region. In contrast to the B90S results the cavity pressures varied significantly with mould temperature for EX167. The pressure values were higher for the lower mould temperature. The dependence on mould temperature was different for the different melt temperatures, the greater effect of mould temperature was observed at 280°C. Johannaber[103] reported higher cavity pressures as a result of better pressure propagation at higher mould temperatures.

The effect of the melt temperature was not so marked for EX167 as it was for B90S. Only one hydraulic pressure curve is shown in Figure 5.14, that for 290°C melt temperature and 50°C mould temperature. The other conditions all gave peak hydraulic pressures greater than 117MPa, the machines limiting pressure. The other conditions were all cooler and hence the increase in the viscosity of the melt pushed the pressure above that available to the machine. This trend agrees with that reported by Barrie[127-129] and Johannaber.[103]

By comparing the B90S and EX167 results, in Figure 5.18, the effect of molecular weight can be observed, both being linear PET polymer with EX167 having the higher molecular weight. The results for a mould temperature of 10°C show higher pressures were measured with the higher molecular weight polymer, which is the expected result, as viscosity is known to increase with molecular weight. The results for the 50°C mould temperature are similar at the minimum pressure, but the optimum injection rate is lower, hence the pressure values of the lower molecular weight B90S are higher than those for EX167 at the same flow rate, above the optimum flow rate.

FIGURE 5.18: B90S VERSUS EX167 COMPARING FLOW RATE VERSUS CAVITY PRESSURE
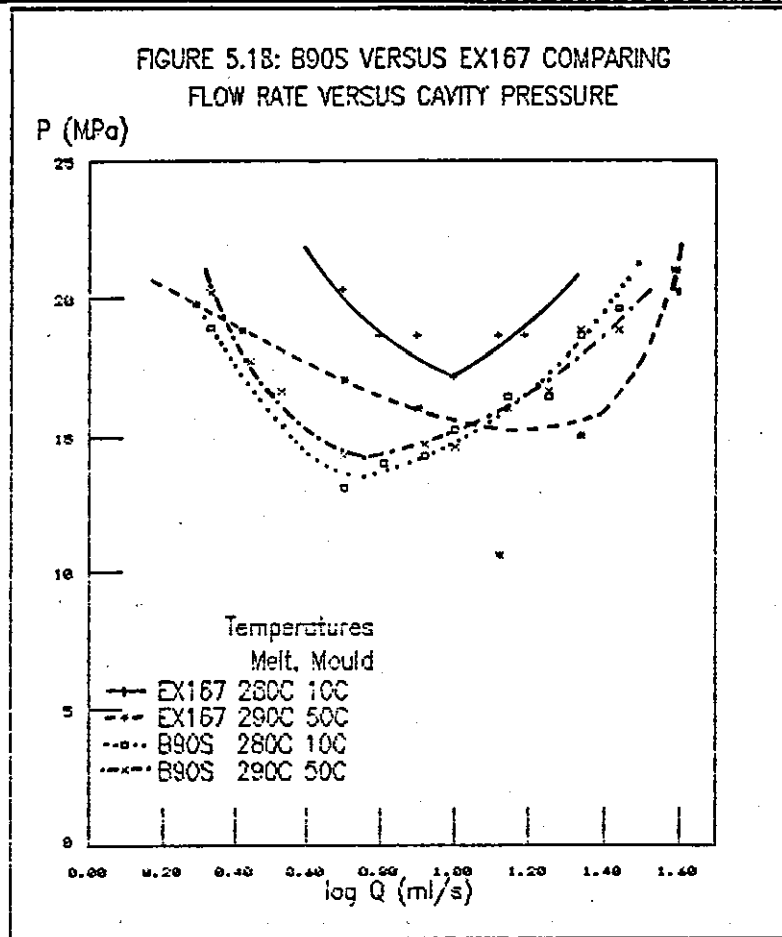
The PCTG curves (Figure 5.15 and 5.16) showed the existence of a minimum pressure for the melt temperature of 270°C, for the 260°C curves the hydraulic pressures didn't show an increase at low flow rates, short shots were obtained below the flow rates shown in Figure 5.15. Lowering the mould temperature resulted in lower values of cavity pressure due to reduced transmission of the hydraulic pressure to the cavity, the effective melt flow channel being smaller due to an increased thickness of frozen polymer at the walls, as reported by Johannaber[103]. Figure 5.16 only shows two curves as at the 260°C melt temperature the peak hydraulic pressures exceeded the 117MPa machine limit. Figure 5.16 clearly illustrates the effect of mould temperature on peak hydraulic pressure, the pressure decreasing with increasing temperature due to a lower reduction in melt viscosity, by cooling, during filling, as reported by Johannaber.[103]

The absence of the 260°C curves, from Figure 5.16, due to their exceeding the limiting value also illustrates the effect of melt

temperature on the peak hydraulic pressure, the pressure decreasing with increasing temperature, due to a reduction in the viscosity. The cavity pressure decreased with increasing melt temperature due to the resultant decrease in viscosity. Both these trends agree with the results published by *Barrie*[127-129] and *Johannaber*.[103]

Other reasons for the variation in pressures may be due to variations in the hydraulic fluid temperature, or the effects of shear heating in the long runner system of the mould used, or pressure effects on the polymer under the high pressures encountered in the mould used. Some of these points are considered later in Section 5.4.3. The pump efficiency and energy losses depend on the viscosity (and therefore the temperature) of the hydraulic fluid. An increase in the hydraulic oil temperature will give rise to higher hydraulic pressure being required, due to the lower viscosity of the oil. In the gate and runner sections of the mould, dimensions are smaller and viscous shear heating occurs which increases the melt temperature, reduces viscosity, and makes flow easier. The heat generated is proportional to the pressure drop. High pressures force molecules closer together, increasing viscosity. Higher pressure drops result. At high flow rates the shear stresses are high and may adversely affect shear sensitive materials, such as PET.

To summarise: the pressure is lower with lower viscosity, hence an increase in melt temperature, or a lower degree of melt cooling, will result in lower pressures. The mould temperature affects the rate of heat transfer during injection, the rate of cooling, the rate of viscosity increase during flow and the rate of frozen layer growth. The cooler the mould, the more rapid the rate of viscosity increase resulting in a higher pressure; simultaneously the rate of frozen layer growth gives a subsequent reduction in the amount of pressure transmission from the injection unit to the cavity, and hence lowers the measured cavity pressure, the dominant effect varies with other conditions as can be seen from the results. There is an optimum flow rate, for a given set of conditions, where the pressure required to fill the cavity is a minimum. Besides the effects of mould and melt temperature studied here, the results may be showing

effects whose contribution to the pressure value has not been quantified. Such effects include shear heating, pressure dependence of viscosity and hydraulic oil temperature at switchover from the injection to hold-on pressure.

5.2.3.3 Pressure Drop Predictions From Rheological Data

In Chapter 2 the shear rheological properties of the three polymers, used in this injection moulding exercise, were reported. Since the pressure drop through a channel is proportional to the shear stress, and the volumetric flow rate is proportional to the shear rate, the flow curve data (Figure 2.11) from Chapter 2 for B90S at 280°C has been converted into a pressure-flow rate curve in Figure 5.19 and combined with data from Figure 5.11. The objective was to see if rheological data from a capillary rheometer can offer direct prediction of the behaviour of the melt during injection moulding.

The rheometer curve does not have a minimum point and does not resemble the portion of the pressure-flow rate curve at flow rate values below the optimum point. This is due to the heat transfer dependence of that portion of the curve, the behaviour being dominated by cooling during slow injection. At the higher flow rates however the curves show the same trends, this portion of the pressure-flow rate curves being dominated by viscous flow and approaching the isothermal behaviour assumed in the capillary rheometry experiments.

Ignoring the differences below the optimum flow rate, the two sets of data were compared for their similarities, both show increases with increasing rate, increasing molecular weight and decreasing temperature.

Effect Of Rate

Considering the effect of rate, both sets of data have curves that are almost linear and increase with rate, shear stress increasing with shear rate, and pressure increasing with flow rate.

FIGURE 5.19:RHEOMETER VS PROCESSING DATA
B90S AT 280C
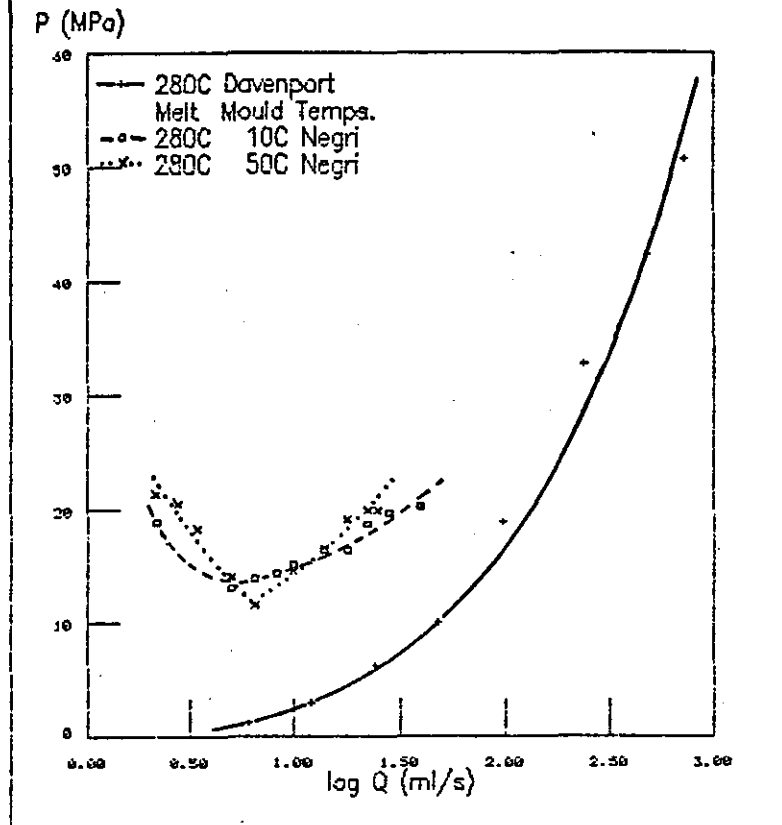
Effect Of Temperature[25,32]

Assuming isothermal flow during the injection stage temperature shift methods were applied to the pressure-flow rate data, using the methods reported in Chapter 2, developed by Mendelson[25] and Mishri[32]. The methods are applied using the pre-injection temperature, and taking 10ml/s as the reference flow rate, the polymers were ranked for their pressure dependence on temperature. The results are shown in Table 5.5.

In order of increasing activation energies the polymers ranking was B90S <EX167 <PCTG using the Mishri method, or B90S <PCTG <EX167 using the Mendelson method. Comparing these results to the results shown in Chapter 2, at low shear rates, the rankings were PCTG <B90S <EX167 for the Mishri method and PCTG <B90S <EX167 for the Mendelson method, and at a shear rate of 1000s^{-1} the rankings were PCTG <EX167 <B90S for the Mishri method and PCTG <B90S <EX167 for the Mendelson method. The rankings are inconsistent for the different cases and the confusion increased when the values of activation energy were considered, the relative values were not in proportion for the different cases considered.

TABLE 5.5: TEMPERATURE SHIFT COMPARISON

Method	Reference Point	Polymer	Activation Energy (kJ/mole)	Constant
Mishri(D)	low $\dot{\gamma}$	B90S	135	7.76×10^{-11}
Mishri(D)	low $\dot{\gamma}$	EX167	173	2.67×10^{-14}
Mishri(D)	low $\dot{\gamma}$	PCTG	44	4.39×10^{-2}
Mishri(D)	$1000s^{-1}$	B90S	290	4.79×10^{-26}
Mishri(D)	$1000s^{-1}$	EX167	167	3.46×10^{-14}
Mishri(D)	$1000s^{-1}$	PCTG	71	4.71×10^{-5}
Mishri(N)	10ml/s	B90S	6	24.28
Mishri(N)	10ml/s	EX167	30	2.12×10^{-2}
Mishri(N)	10ml/s	PCTG	49	2.80×10^{-4}
Mendelson(D)	low $\dot{\gamma}$	B90S	151	2.67×10^{-15}
Mendelson(D)	low $\dot{\gamma}$	EX167	196	1.54×10^{-19}
Mendelson(D)	low $\dot{\gamma}$	PCTG	102	2.20×10^{-10}
Mendelson(D)	$1000s^{-1}$	B90S	131	5.22×10^{-13}
Mendelson(D)	$1000s^{-1}$	EX167	341	6.83×10^{-33}
Mendelson(D)	$1000s-1$	PCTG	111	3.26×10^{-11}
Mendelson(N)	10ml/s	B90S	24	4.93×10^{-3}
Mendelson(N)	10ml/s	EX167	180	1.11×10^{-17}
Mendelson(N)	10ml/s	PCTG	76	3.76×10^{-8}

(D) indicates Davenport experiment; (N) indicates Negri Bossi experiment

The assumption of isothermal flow is known to be invalid and the pre-injection temperature is not necessarily proportional with the temperature of the melt when the pressure measurements were made. The actual temperature at the instant of pressure measurement was unknown, temperature changes occurred by the melt cooling during flow into the mould and by shear heating during flow. One relationship can be concluded, B90S shows a lower activation energy than EX167 for both the rheological data and the injection moulding data.

Effect Of Structure

The flow curves for the three polymers show that at a given shear rate ($1000s^{-1}$) the polymers can be ranked in order of increasing stress as B90S <EX167 <PCTG, the values at 280°C were 0.183, 0.216, and 0.368MPa respectively. (The PCTG data taken from Eastman Plastics[39]).

For a flow rate of 10ml/s the three polymers can be ranked in order of increasing cavity pressure drops as B90S=EX167 <PCTG, the values at 280°C melt temperature and 50°C mould temperature were

14.6, 14.6, and 16.4MPa respectively; the ranking for the hydraulic pressure drops were B90S <EX167=PCTG, the values were 88, >117, and >117MPa respectively. Combining the results for hydraulic and cavity pressure drops results in the ranking for increasing pressure drop as B90S <EX167 <PCTG, which agrees with the ranking for the shear stresses of the polymers.

5.3 Description Of SIMPOL

5.3.1 Introduction To SIMPOL[139]

SIMPOL (SIMulated POLymer behaviour system) is a commercial software package which permits the production engineer to optimise the process design (i.e. processing conditions, specify machine requirements and estimate the costs involved in the injection moulding process). Using a databank of materials and machinery data the software allows users to experiment with almost any variable in the moulding process - melt temperature, packing pressure, injection rate, mould temperature, screw back pressure, cavity thickness and hot and cold runner diameter - to assess the feasibility of a moulding job. SIMPOL can also be used for mould design, allowing the exploration of the process before any metal is cut.

It has been made as easy to use as possible. Three screens can display a mould 'trial', the equipment needed to achieve the chosen set of conditions, and an estimate of the costs. Simpol is more of a production optimisation tool than a design tool such as Moldflow.[139]

5.3.2 Theory Behind SIMPOL[126,127]

The injection moulding process is divided into three stages: melt preparation; melt injection; and melt cooling.

5.3.2.1 Melt Preparation Stage

The modelling of the melt preparation stage involves the concepts of the heat flux and the Fourier Number. Heat flows across a boundary when a material is placed in an environment of a higher temperature, the heat flux being proportional to the area of the boundary, A, and the temperature difference, ΔT.

$$\varphi = h.A.\Delta T \tag{5.3}$$

where the constant of proportionality, h, is the Surface Heat Transfer Coefficient. This indicates the maximum rate at which heat can flow. The Fourier Number, F_o, indicates the degree of thermal equilibrium

$$F_o = (a.t) \div x^2 \tag{5.4}$$

where a is the Thermal Diffusivity for the material; t is the time taken to reach equilibrium; and x is the polymer thickness in which the thermal gradient has been established. If $F_o > 1$ then thermal equilibrium exists; if $F_o < 0.05$ high thermal gradients exist.

The optimum melt temperature for processing, the degree of crystallinity and the specific heat of a polymer all affect the changes in enthalpy. From enthalpy curves for the polymer, the total heat required to raise its temperature a given amount can be obtained. Linking this to the heating rate possible from a cylinder of a given diameter, the plasticisation rate for melt preparation can be estimated. This estimate will give values lower than those found in practice as shear-heating effects have been ignored in this analysis, though the shear heating effect is not be as important as in extrusion since the screw only rotates for a small proportion of the cycle.

After the rate of heat input has been obtained the Fourier Number calculation gives the time and conditions required to attain thermal equilibrium throughout the melt. This is calculated for the passage of the melt through the screw.

5.3.2.2 Melt Injection Stage

The melt injection stage is considered as two flow paths: one isothermal, at the melt temperature, from the barrel through the nozzle, and through any hot-runner sections; and the second, through the sprue, cold-runners, gate, and cavity sections, is non-isothermal.

The calculation of pressure drops for flow through uniform-sectioned channels or simple radial flow includes consideration of elongational flow as well as shear flow when convergent or divergent flow occurs. Die-entry pressure loss data are used in calculations of pressure drops due to strongly convergent flow. Flow through the barrel and nozzle also include friction losses between the screw and

the barrel, and hydraulic losses in the oil circuit.

The model used for melt flow behaviour is to assume isothermal behaviour within a restricted channel. With increasing time, the frozen layer of material increases on the walls, but within the narrower path, conditions are assumed to remain isothermal, see Figure 5.20.

The main concern is the critical situation when the mould is just filled. At this moment the total pressure drops are at a maximum and feasibility of mould-filling for a given geometry with a given machine is fully tested.

FIGURE 5.20: FROZEN LAYER MODEL
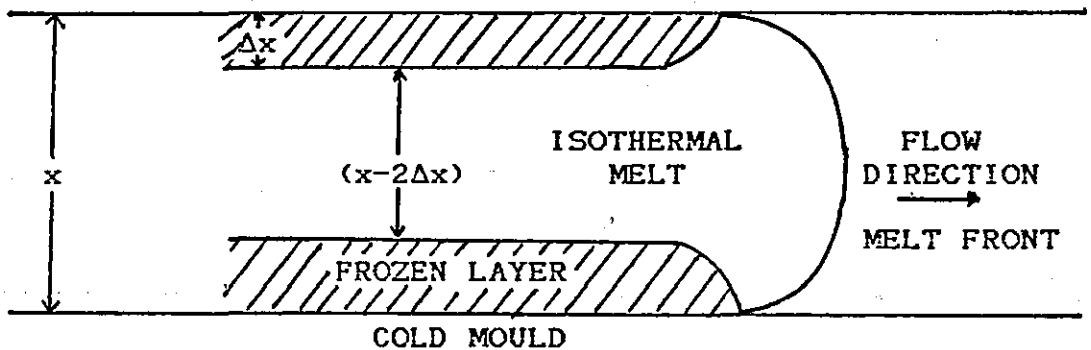
There is an optimum injection rate for minimising pressure and stress levels and the mould opening force arising from the distributed pressure over the projected moulding area. This optimum injection rate occurs at the minimum pressure drop. At high injection rates there is little freezing-off, so more pressure is transmitted into the cavity. At low injection rates the frozen material on the walls increases, causing more restriction and hence higher pressure drops. The flow path can get blocked before the cavity is full.

The frozen layer thickness build up, see Figure 5.20, is approximately modelled by a power law:-

$$\Delta x = C.t^s \qquad (5.5)$$

where: Δx is the frozen layer thickness; C is a coefficient of cooling; and s is empirically set at $^1/_3$. The coefficient C involves

the Thermal Diffusivity and the ratio:

$$\theta = (T_{freeze-off} - T_{mould}) \div (T_{melt} - T_{mould}) \qquad (5.6)$$

The non-isothermal flow equations are modified versions of the isothermal flow equations, replacing the thickness component with an effective thickness $(x-2\Delta x)$.[127]

Using this frozen layer model, the pressure drop in a mould cavity at the optimum injection rate, is obtained from an equation of the form:

$$P = \mu.G.N \qquad (5.7)$$

where μ is a term containing material properties of flow and freeze-off,

G is a term containing the cavity geometry and dimensions,

N is a numeric.

All three terms are a function of the power law index n.

An estimation of the clamping force required, to prevent the mould opening during injection or packing, is made assuming the melt pressure in the cavity to be hydrostatic.

$$F = P.A \qquad (5.8)$$

where F is the mould-opening force,

P is the pressure in the cavity,

A is the projected area of the moulding.

(There is a pressure distribution in the cavity, making F < P.A, in practice.)

From the above analysis three important machine parameters are estimated the maximum pressure demand, the optimum injection rate and the minimum clamp force.

5.3.2.3 Melt Cooling Stage

In the melt cooling stage there are major differences between the problems of extracting heat from the material and those examined when putting heat into it, during the melt preparation stage. The differences relate to the quantity of heat involved, the rate of its removal, and the thermal equilibrium desired.

It is assumed that the heat content of material in the mould at the instant of filling is only slightly less than after melt preparation and before injection. Heat lost to cold channel walls

during filling is assumed to be a little more than that added through shear heating.

On ejection from the mould the moulding has a surface temperature 20°C to 30°C higher than the raw material in the hopper, and the centre of the moulding can be 30°C to 50°C higher still. This results in the situation where only 65% of the quantity of heat, put into the material, has to be removed before ejection.

A moulding is assumed to be ready for ejection when the temperature of the centre-line of the thickest section is about 30°C below the freeze-off temperature.

To estimate the cooling times the general form of the equation for one-dimensional heat flow in simple geometries is used; i.e.

$$\theta = c . \exp(-b . a . t / d^2) \qquad (5.9)$$

where θ is the dimensionless temperature-gradient function,

   a is the Thermal Diffusivity,

   t is the lapsed time,

   d is the most remote distance from a cooled surface,

   c and b are constants characteristic of the geometry.

The 'uniform slab' model is used as an approximation for practical mouldings. In this case, $b = \pi^2/4$, $c = \pi^2/8$ and $d = x/2$. Substituting in equation (5.9) and re-arranging gives

$$t_{cooling} = [(x^2) \div (\pi^2 . a)] . \ln(8\theta/\pi^2) \qquad (5.10)$$

The value taken for θ is given by

$$\theta = [(T_{freeze-off} - 30) - T_{mould}] \div (T_{melt} - T_{mould}) \qquad (5.11)$$

Both the effects of shear heating and pressure on the viscosity of the melt are ignored. Though both effects are significant, it is assumed that when both occur they counteract each other. Also unless reliable material data is available for both effects, better practical estimates can be obtained by ignoring both of them.

5.3.3 Assumptions And Approximations Made In SIMPOL

To simplify the calculations, and therefore reduce computing time, and to minimise the amount of data required before using the simulation. The writers of SIMPOL have made several assumptions and approximations, based on their practical experience and with the restriction of still obtaining good estimates from the simulation. The

following discussion examines the assumptions and approximations made referring to other workers for justification or contradiction of the validity of the simplifications.

Shear heating is ignored during all three stages of the SIMPOL simulation. Shear heating causes a rise in temperature, reduces viscosity, and makes flow easier. The heat generated is proportional to the pressure drop. In the melt preparation stage shear heating would reduce the heat input needed from the heated barrel, i.e. the real plasticisation rate will be higher than that estimated.

During the injection stage shear heating effects reduce the pressure requirement to fill the mould, at a given flow rate and fill time. The frozen layer thickness is affected as the melt temperature is higher than it was in the barrel before injection, i.e. affecting the accuracy of coefficient C, also shear heating causes localised temperature build-up near the frozen walls resulting in a complex temperature profile in the moulding, rather than the uniform boundary assumed in SIMPOL. The clamping force required is greater than estimated since the faster injection rate results in less cooling during flow through the runner system and hence a greater transmittance of pressure from the piston to the cavity.

During the cooling stage shear heating increases the amount of heat to be removed, causing longer cooling times.

The effect of pressure on the viscosity of the melt is ignored by SIMPOL. High pressures force molecules closer together, increasing viscosity, hence resulting in higher pressure drops. SIMPOL assumes the pressure effect on viscosity to be counteracted by the shear heating effect on viscosity and therefore ignores both. *Bowers*[23] review agrees that quantitative estimates show a mutual cancelling effect. However the assumption of an incompressible polymer melt has been proved wrong[23] but the effect is difficult to measure, one approach would be to treat pressure change as a negative temperature effect, using an exponential function to describe the pressure dependence of viscosity.

SIMPOL uses an estimated constant freeze-off temperature. Whilst *Kenig and Kamal*[37] concluded that the solidification temperature

('freeze-off' or 'no-flow' temperature) for crystalline polymers and the glass-transition temperature for amorphous polymers are not constants in the mould under moulding conditions, but increase with increasing pressure or decreasing cooling rate.

The assumption of a uniform thickness of frozen layer has been deduced from experimental results with a spreading disc cavity *Barrie*[127] these results are in conflict with other published work for spreading disc flow[16,110] which state that the frozen layer thickness depends on the rate of freezing and the time the melt has had to freeze. This means that the 'skin' thickness must go through a maximum somewhere between the melt front and the channel entrance (see Section 5.1.2). *Brydson*[13] considering tubular or rectangular mouldings, describes the frozen 'skin' as tapering from the gate to the melt front, the degree of tapering being dependent on the injection rate, the temperature difference between the melt and the cavity wall and of the polymers thermal properties. However, *Grinblat*[125] made similar assumptions to those made in SIMPOL, he assumed the melt flows within an immobile envelope of cooled polymer during mould filling. He suggests three sections make up the flow in the mould; a thin layer of low mobility polymer at the channel surface; a thin layer of polymer subject to high shear deformations; and 'plug' flow in the remainder in which there is little velocity change. His model assumes constant pressure control of the injection process.

The simplified boundary conditions assumed in the mould for the various temperatures considered does not account for the solidification profiles reported by *Kamal and Kenig*.[118,137]

The frozen 'skin' thickness growth is assumed to have a cubic-root relationship in SIMPOL, this is based on an empirical model reported by *Barrie*[126,127], who reported a better estimate of experimental data than that offered by the 'slab model' which uses a square-root relationship. This model has inherent errors as it ignores shear heating, which will affect the growth rate of the frozen layer.

The assumption of isothermal flow between the frozen layers is

made in SIMPOL, *Dietz and White*[147] also assumed an isothermal flow between the frozen layers and found good agreement between measured and calculated pressure losses. *Berger and Gogos*[123] found little difference between isothermal and non-isothermal predictions for fill times, and claimed this justified the assumption of isothermal flow made by *Barrie*.[127]

SIMPOL uses the relationship proposed by *Cogswell and Lamb*[148] that the total flow behaviour of a polymer can be described by the sum of the tensile behaviour and the shear behaviour, this assumption has been discussed in Chapter 2, it has been criticised as it ignores any interaction of the two types of flow.

SIMPOL assumes a 'slab model' for the cooling time calculations; this model ignores convection and axial conduction[115,137] which will lead to an over-estimation of cooling time.

SIMPOL permits an estimate of the relative cooling efficiency to be made, but the basis on which to estimate this value is not provided. Hence a single value approximates for differences in tooling materials, cooling channel sizes, positions and numbers, coolant flow rates and coolant efficiency in removing heat, types of channel design.

SIMPOL ignores the 'fountain' flow effect which occurs at the melt front, this has been modelled by *Kamal et al.*[133] and *Mavridis et al.*[109,134]

In SIMPOL frictional losses are assumed to have a constant value, as in the earlier work by *Barrie*[126-129] however, *Huseby*[111] reported that frictional losses are a function of melt temperature and injection rate.

The idea that there is an optimum flow rate has also been proposed by *Vostorgov and Kalinchev*.[130] Though *Cox and Metzner*[146] warn that the "optimum" flow rate proposed as being that resulting in the minimum fill pressure can result in an increased cycle time.

5.3.4 How SIMPOL Works[11]

SIMPOL is a suite of computer programs called MAT-IN, MAC-IN, CAV-IN, SIMPOL, and MATDATA. These programs are related to each other as shown in the flow diagram Figure 5.21, all the programs are linked

to a central MENU program.

5.3.5 MAT-IN Modelling Of Rheological Data

The SIMPOL simulation uses modelled rheological data, raw data is entered into the MAT-IN program which then models the data and transfers it to the databank accessed by SIMPOL. The theory used in the model is described below.

One or two fine refinements of the models on which SIMPOL is based are not known exactly. However the principles used are known. The shear rheology of thermoplastic polymers is well documented and theorised. Thermoplastics are known to be shear thinning, their viscosity decreasing with increasing shear.

FIGURE 5.21: THE SIMPOL SYSTEM[1]
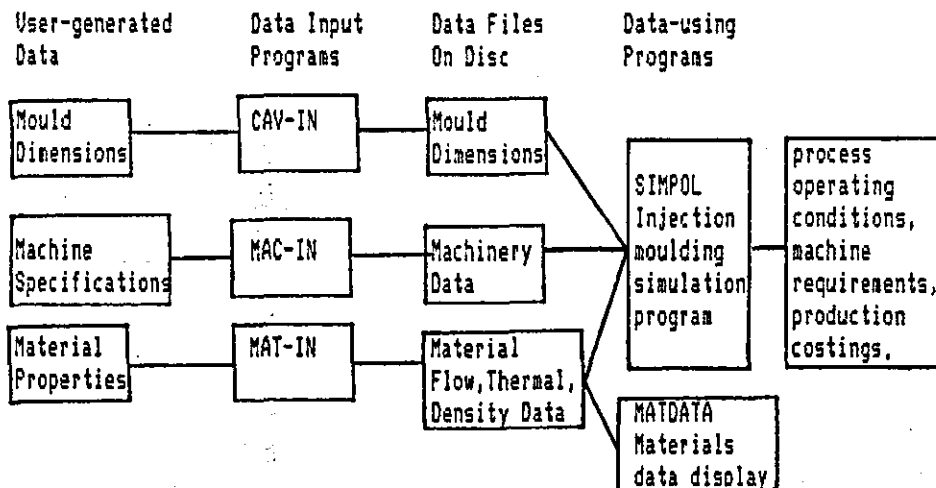
Shear thinning polymers are known to have a limiting upper viscosity for the low shear region. It is known that pseudoplastics also exhibit a limiting lower viscosity at extreme rates of shear. This phenomenon has been explained as being a consequence of slippage between the wall and adjacent polymer, or between adjacent layers of polymer. The slip is initiated at some critical value of shear stress required to cause melt fracture. Above this critical value the basic concepts used to predict the flow are invalid.

The effects of converging and diverging flow are dependent on the tensile viscosity of the polymer, this can be deduced from

converging flow, through zero length dies, using a capillary rheometer. *Cogswell and Lamb* reported[149] that the log die entry pressure versus log shear rate curves are almost linear up to the critical shear rate for the onset of melt fracture.

MAT-IN uses the above observations in its modelling, as shown by Figure 5.22, by assuming that at low shear rates the viscosity approaches Newtonian behaviour (i.e. n=1) and at high shear rates the viscosity approaches a 45° decreasing slope at the limiting stress i.e. (n approaches 0). The die entry pressure from a zero length die is modelled as approaching a straight line. Up to eight values of known shear rate, viscosity data pairs are entered, and optionally eight zero length die pressures for the corresponding shear rates. The raw data is statistically examined for consistency and coherence, then fitted to an unpublished model which assumes the boundary conditions for low and high shear rates mentioned above. The modelled viscosity values and percentage errors are displayed. The die-entry pressure drop data is similarly treated. If existing data for the same grade is found in the data files, the two sets can be statistically combined, or saved separately. The modelled data is transferred to a databank which is accessible to the SIMPOL program.

FIGURE 5.22: SIMPOL MODELLING PRINCIPLES
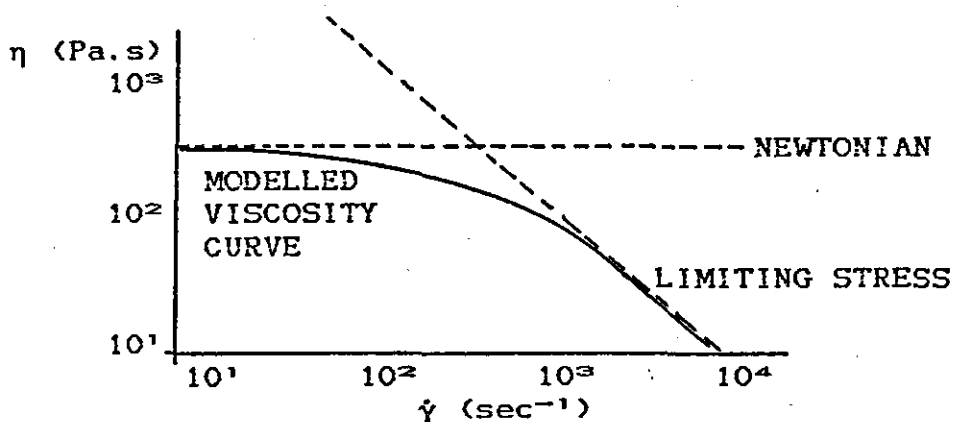
Rheological data at different temperatures for the three polymers used in the injection moulding exercise was entered and modelled by the MAT-IN program. Die-entry pressure drop data for EX167 were not used, SIMPOL models the generic data as a default.

5.3.6 Results From MAT-IN

The results of the rheological modelling done by the MAT-IN program are shown in Figures 5.23-5.27, the raw data is shown for comparison. From the shear data curves (Figures 5.23-5.25) it can be seen that the raw data shows excellent fit for B90S and EX167, and the PCTG raw data fits fairly well. The percentage errors being within the ranges shown below:

```
B90S  at   270°C   -3.9% to   +4.1%
B90S  at   275°C   -3.3% to   +1.1%
B90S  at   280°C   -6.9% to   +5.4%
B90S  at   285°C   -9.5% to   +9.8%
B90S  at   290°C   -0.1% to   +1.0%
EX167 at   270°C   -2.1% to   +2.2%
EX167 at   280°C   -1.8% to  +11.2%
PCTG  at   240°C  -13.2% to  +21.1%
PCTG  at   250°C   -8.5% to  +17.2%
PCTG  at   260°C   -4.6% to   +7.1%
```

The die-entry pressure drop data curves (Figures 5.26 - 5.27) show a reasonable fit of the raw data to the model. The percentage errors being within the ranges shown below:

```
B90S at 270°C -27.8% to +23.9%
B90S at 275°C -25.8% to +24.9%
B90S at 280°C -20.7% to +17.6%
B90S at 285°C -10.1% to +11.6%
B90S at 290°C  -9.4% to +26.6%
PCTG at 240°C -17.3% to +12.9%
PCTG at 250°C -20.1% to +15.1%
PCTG at 260°C -20.1% to +17.1%
```

The model appears satisfactory for the shear data, but an improved model could be developed for the die-entry pressure drop data, the data for B90S and PCTG shown here (and the data in Chapter 2) suggest a better curve fit than the log shear rate-log die-entry pressure drop should be achievable.

MAT-IN models the die-entry pressure drop, shear rate data using a linear transformation of the form:

$$y = a.x^{-b} \qquad (5.12)$$

i.e. $\log(y) = \log(a) - b.\log(x)$ \hfill (5.13)

The curves fitted to the data are shown in Figures 5.15 and 5.16. with the raw data shown as points. Table 5.6 shows that this form of linear transformation gives a reasonable correlation, the Pearsons Correlation Coefficient, r, being greater than 0.9, and the Index of Determination being better than 0.9, (see Appendix 10). However, the spread of data about the best fit line is shown by the standard deviation, this is high for the MAT-IN model.

By applying different forms of linear transformations[150] to the raw data, a form which gave a better fit for the die-entry pressure drop, shear rate data was found, the form of linear transformation:

$$y = a - b.x^{\frac{1}{2}} \qquad (5.14)$$

gave curves shown in Figures 5.28-5.35, Table 5.7 shows better correlation by higher values for Pearsons Correlation Coefficient and Index of Determination, and less spread of data about the line of best fit by lower standard deviation values than the MAT-IN fit, (see Table 5.6).

Polynomial regression analysis[150] was applied to the raw data and Table 5.8 shows that the quadratic equations gave even better correlation and lower standard deviations than the linear transformations tried (see Tables 5.6 and 5.7). The fitted curves are shown in Figures 5.28 and 5.35. However, caution is needed if polynomial regression models are extrapolated far beyond the original data.

TABLE 5.6: MAT-IN FIT: log(x), log(y)

log(y) = a - b.log(x)

	a	b	r	r²	S.D.
B90S					
270°C	11.06	0.444	0.984	0.967	258296
275°C	11.21	0.403	0.985	0.970	185509
280°C	11.37	0.345	0.978	0.957	119639
285°C	11.62	0.290	0.982	0.965	94402
290°C	9.41	0.607	0.999	0.999	8160
PCT6					
240°C	11.64	0.455	0.984	0.967	208379
250°C	10.92	0.427	0.972	0.945	67001
260°C	11.07	0.390	0.976	0.952	60505

TABLE 5.7: LINEAR TRANSFORMATION FIT: $x^{1/2}$, y

$$y = a - b.x^{1/2}$$

	a	b	r	r^2	S.D.
B90S					
270°C	-26519	42389	0,996	0,992	137498
275°C	104827	31918	0,997	0,994	93602
280°C	191656	22001	0,993	0,987	73804
285°C	277225	15595	0,994	0,987	53485
290°C	-314395	35045	0,999	0,999	44926
PCTG					
240°C	232336	71883	0,964	0,929	204239
250°C	29837	35093	0,992	0,984	45885
260°C	77261	29103	0,994	0,988	37792

TABLE 5.8: QUADRATIC REGRESSION FIT

$$y = a + b.x + c.x^2$$

	a	b	c	r	r^2	S.D.
B90S						
270°C	391387	672	-0,030	0,998	0,997	88481
275°C	394287	551	-0,027	0,998	0,995	87926
280°C	380603	486	-0,037	0,997	0,995	46891
285°C	442856	284	-0,017	0,993	0,985	57893
290°C	392063	429	-0,015	0,999	0,999	1,5
PCTG						
240°C	416562	5359	-3,804	0,994	0,988	84555
250°C	237148	1278	-0,336	0,999	0,998	16667
260°C	255551	1012	-0,252	0,999	0,997	19279

FIGURE 5.23: MAT-IN MODELLING OF B90S SHEAR DATA

FIGURE 5.23: MAT-IN MODELLING OF B90S
SHEAR RHEOLOGY DATA
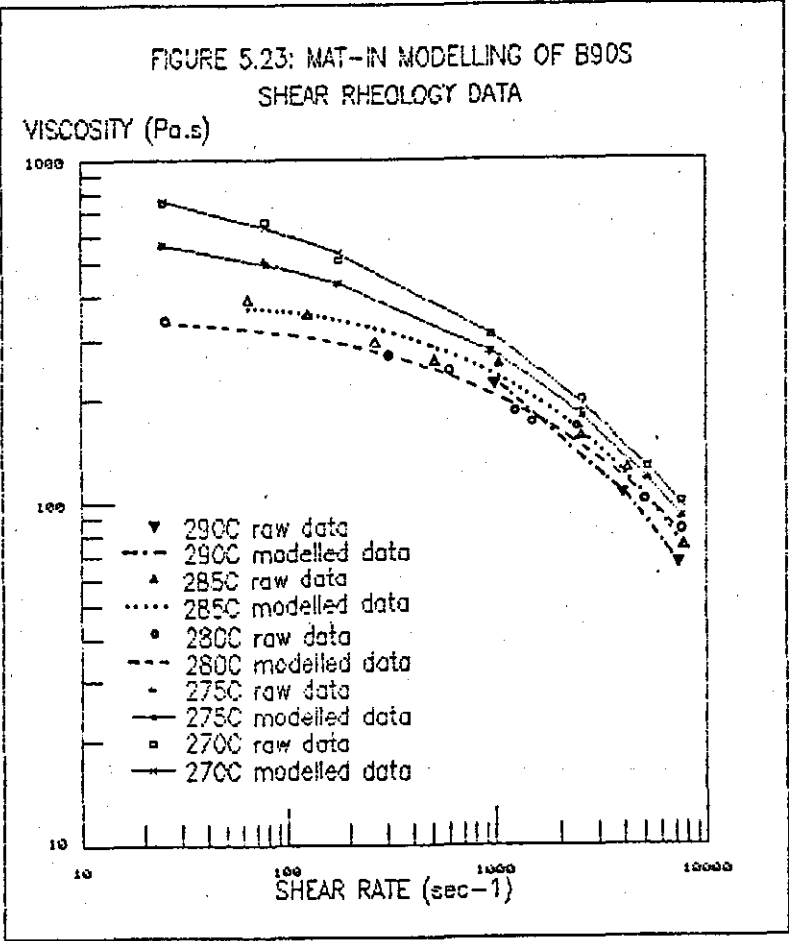
FIGURE 5.24: MAT-IN MODELLING OF EX167
SHEAR RHEOLOGY DATA

VISCOSITY (Pa.s)

+ 270C raw data
—— 270C modelled data
○ 280C raw data
····· 280C modelled data
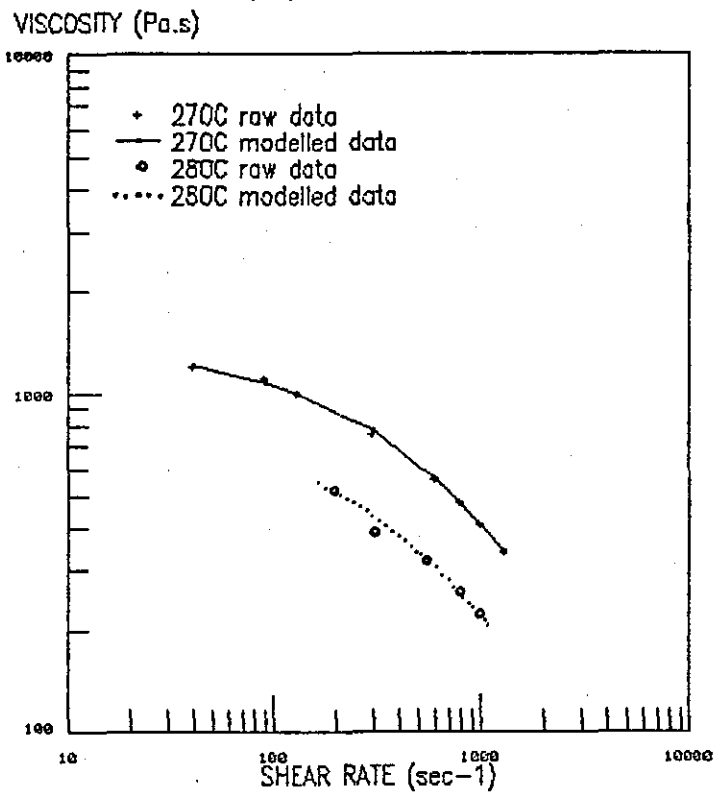
SHEAR RATE (sec-1)

FIGURE 5.25: MAT-IN MODELLING OF PCTG
SHEAR RHEOLOGY DATA

VISCOSITY (Pa.s)

+ 240C raw data
—+— 240C modelled data
□ 250C raw data
---- 250C modelled data
▼ 260C raw data
····· 260C modelled data
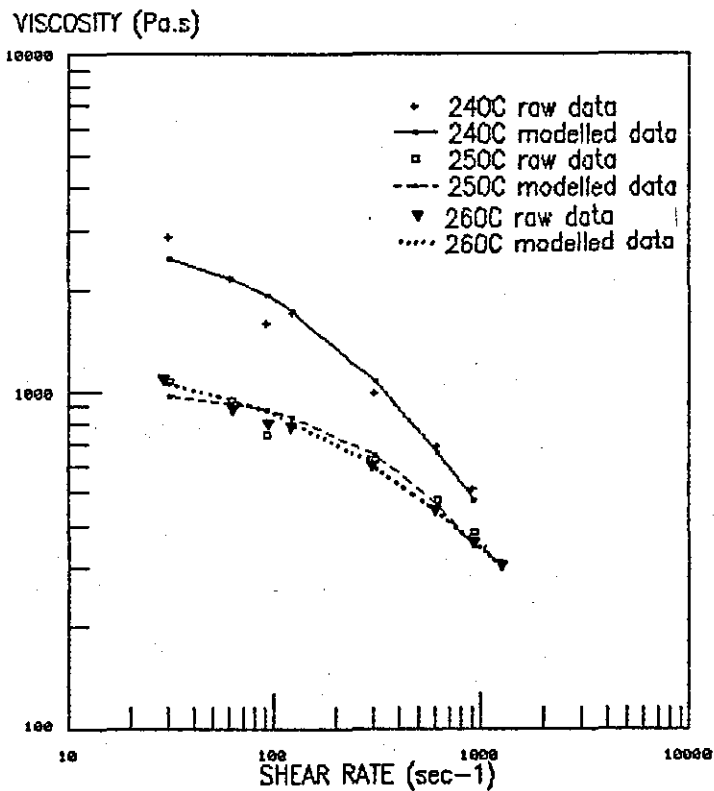
SHEAR RATE (sec-1)

FIGURE 5.26: B90S MAT-IN MODELLED
DIE-ENTRY PRESSURE DROP DATA

Pa (MPa)

+   270C raw data
─   270C modelled data
▫   275C raw data
─·── 275C modelled data
▼   280C raw data
····· 280C modelled data
·─✕·· 285C raw data
     285C modelled data
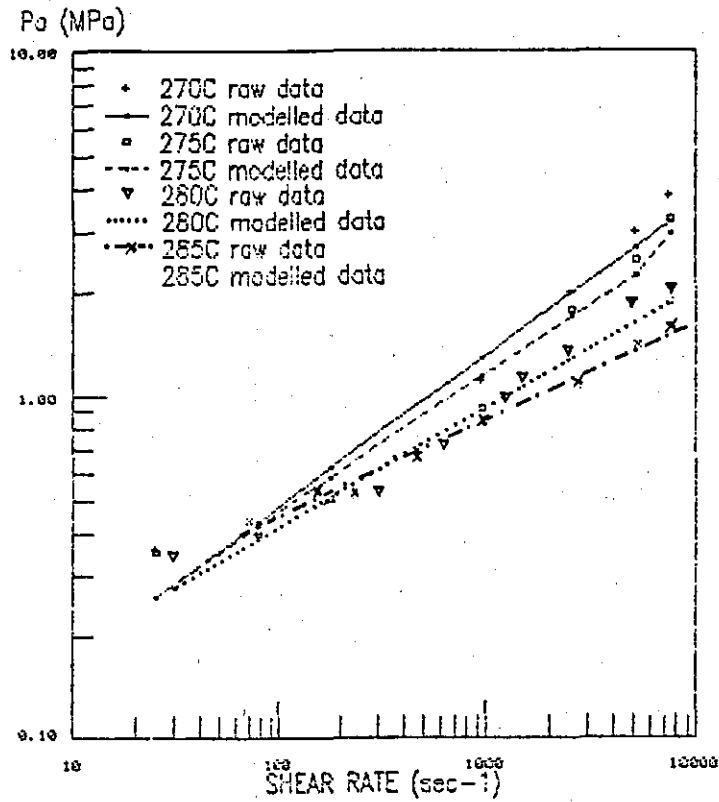
SHEAR RATE (sec-1)

FIGURE 5.27: PCTG MAT-IN MODELLED
DIE-ENTRY PRESSURE DROP DATA

Pa (MPa)

+   240C raw data
─   240C modelled data
▫   250C raw data
─·── 250C modelled data
✕   260C raw data
····· 260C modelled data
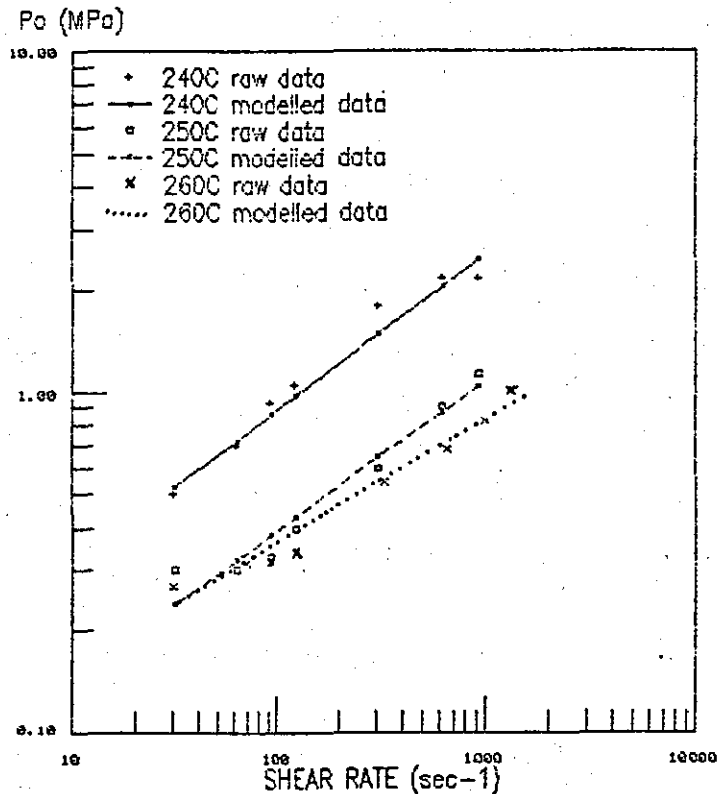
SHEAR RATE (sec-1)

FIGURE 5.28: B90S CURVE FITTING OF
DIE−ENTRY PRESSURE VS SHEAR RATE DATA

Po (MPa)

- 270C raw data
— 270C MAT−IN fit
-·-· 270C linear fit
······ 270C quadratic fit
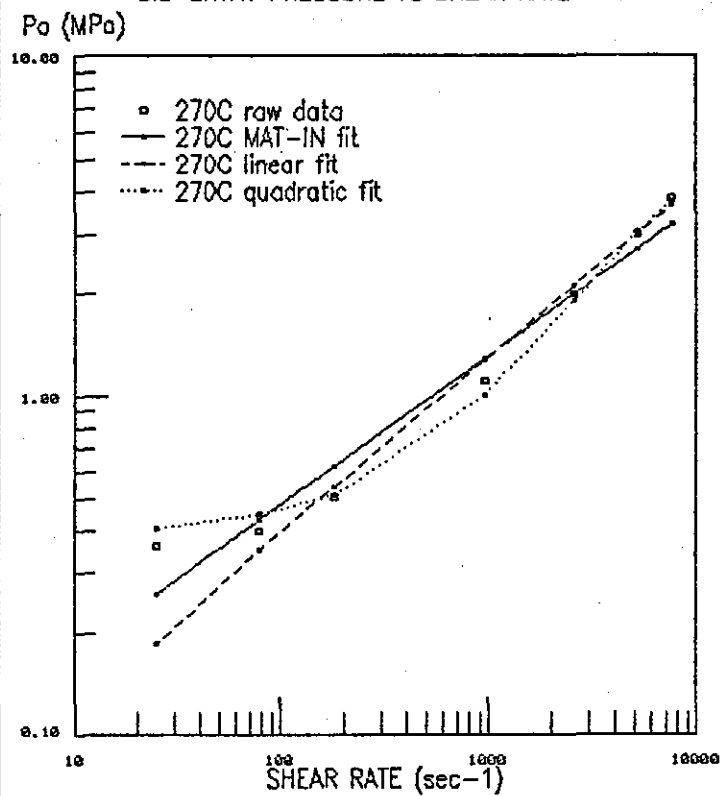
SHEAR RATE (sec−1)

FIGURE 5.29: B90S CURVE FITTING OF
DIE−ENTRY PRESSURE VS SHEAR RATE DATA

Po (MPa)

- 275C raw data
— 275C MAT−IN fit
-·-· 275C linear fit
······ 275C quadratic fit
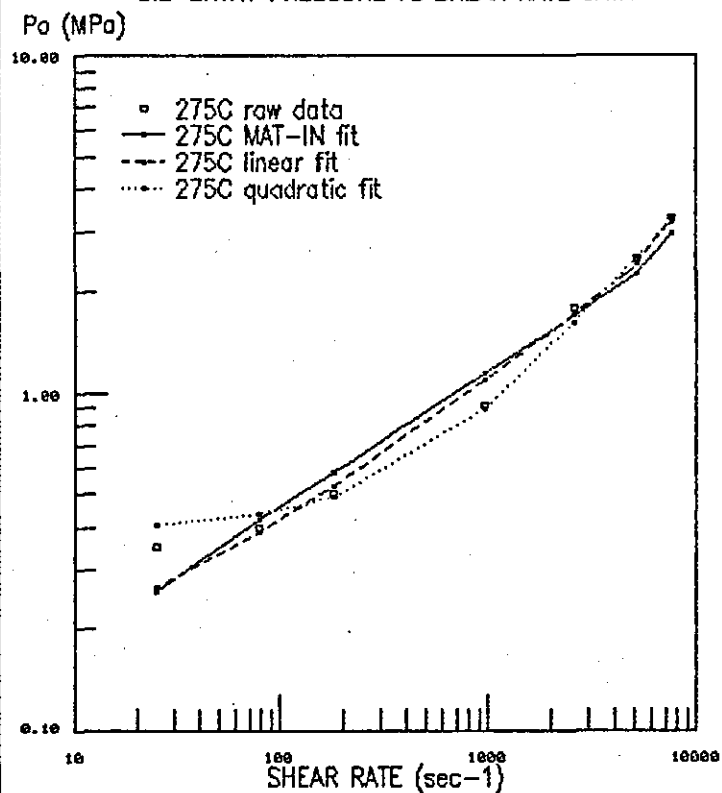
SHEAR RATE (sec−1)

FIGURE 5.30: B90S CURVE FITTING OF
DIE-ENTRY PRESSURE VS SHEAR RATE DATA

Po (MPa)

280C raw data
280C MAT-IN fit
280C linear fit
280C quadratic fit
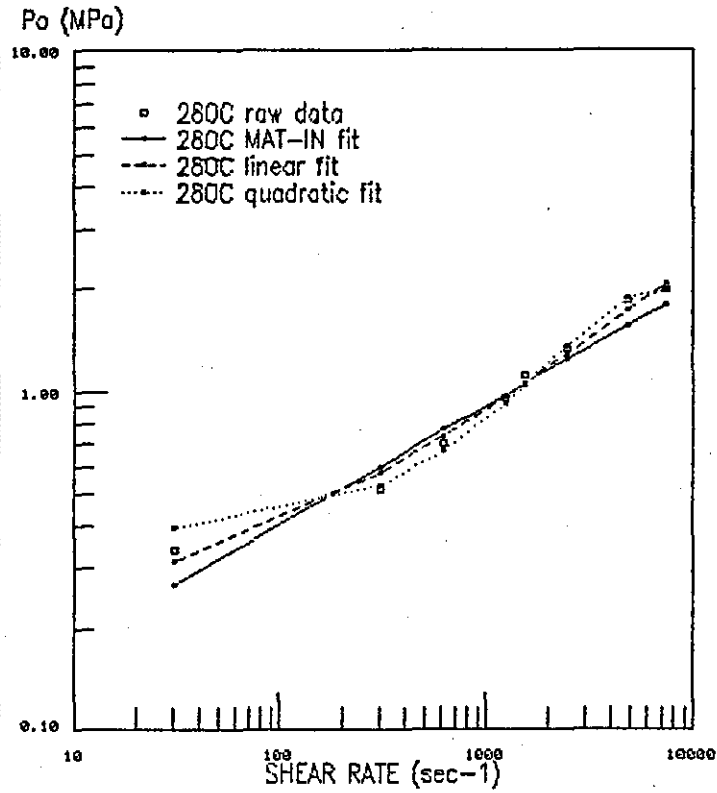
SHEAR RATE (sec-1)

FIGURE 5.31: B90S CURVE FITTING OF
DIE-ENTRY PRESSURE VS SHEAR RATE DATA

Po (MPa)

285C raw data
285C MAT-IN fit
285C linear fit
285C quadratic fit
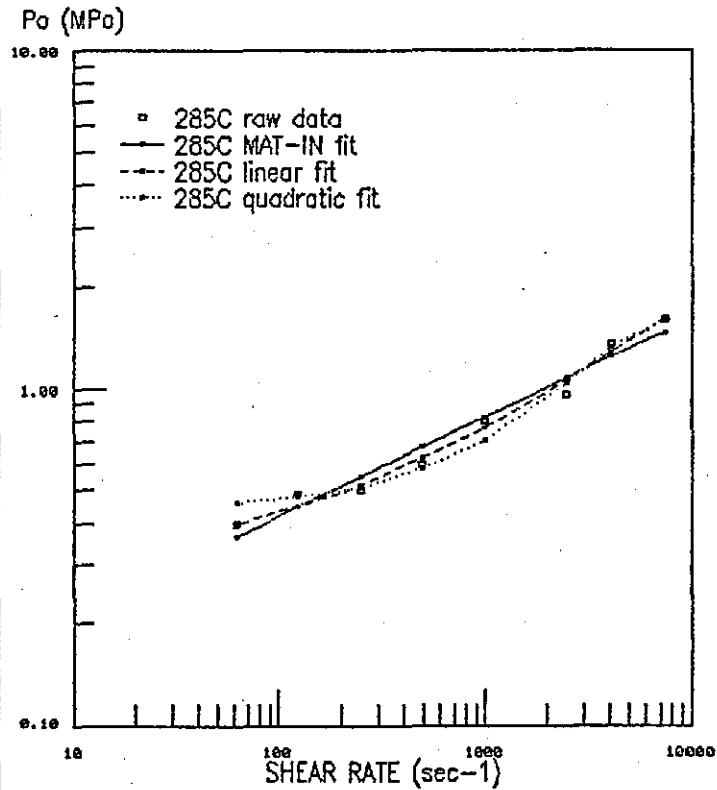
SHEAR RATE (sec-1)

FIGURE 5.32: B90S CURVE FITTING OF
DIE–ENTRY PRESSURE VS SHEAR RATE DATA
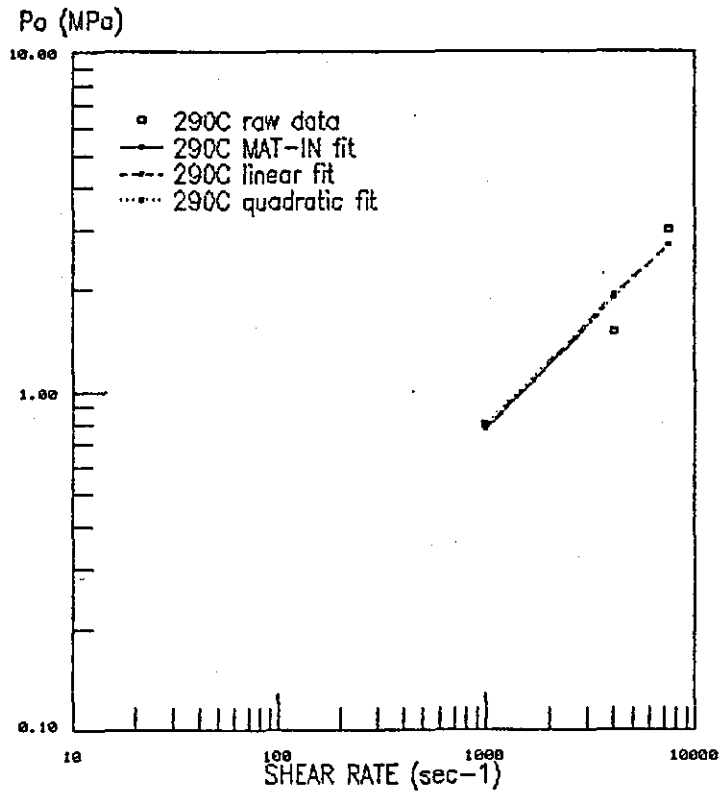
FIGURE 5.33: PCTG CURVE FITTING OF
DIE–ENTRY PRESSURE VS SHEAR RATE DATA
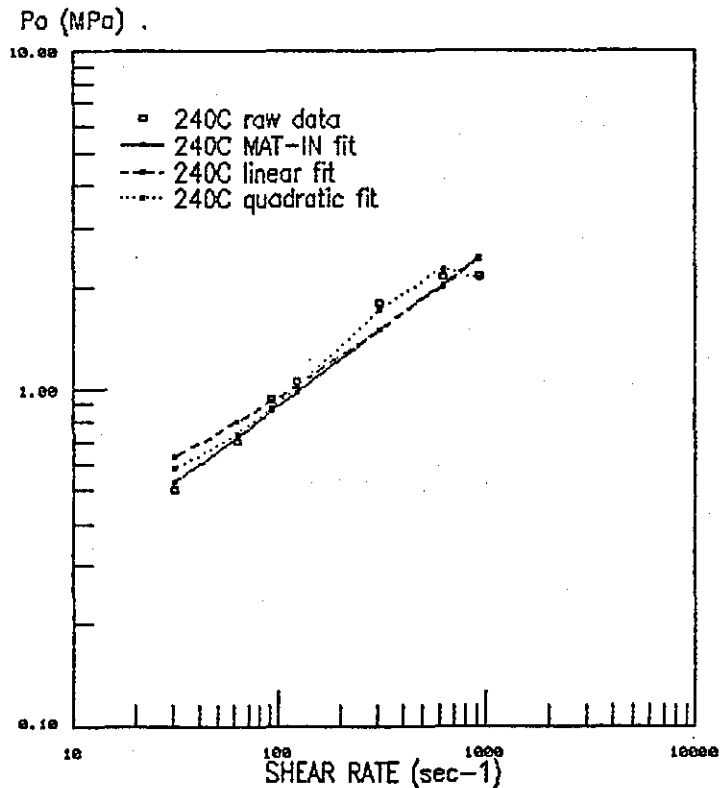
FIGURE 5.34: PCTG CURVE FITTING OF
DIE-ENTRY PRESSURE VS SHEAR RATE DATA

Po (MPa)

□   250C raw data
—— 250C MAT-IN fit
-·—·- 250C linear fit
····-··· 250C quadratic fit
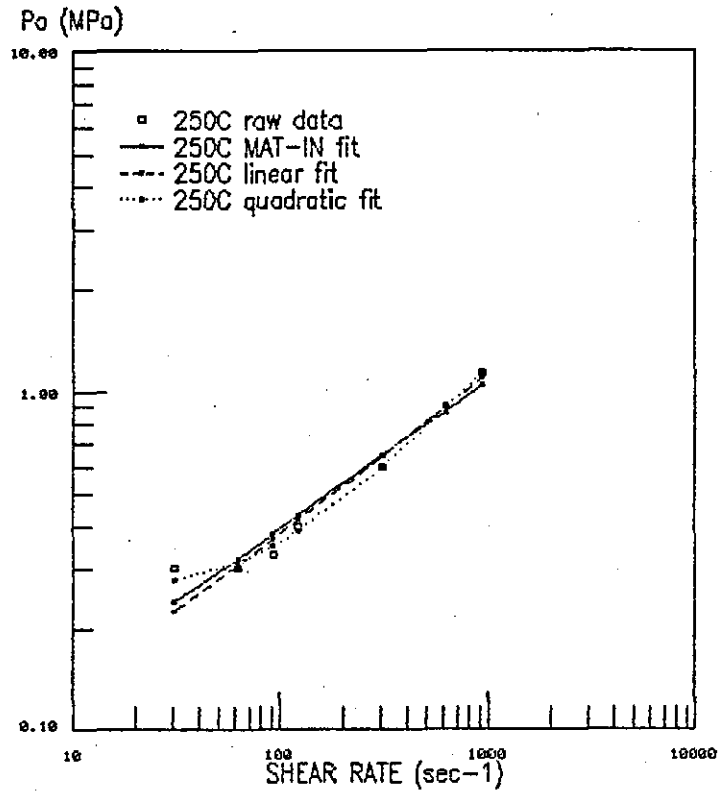
SHEAR RATE (sec-1)

FIGURE 5.35: PCTG CURVE FITTING OF
DIE-ENTRY PRESSURE VS SHEAR RATE DATA

Po (MPa)

□   260C raw data
—— 260C MAT-IN fit
-·—·- 260C linear fit
····-··· 260C quadratic fit

SHEAR RATE (sec-1)
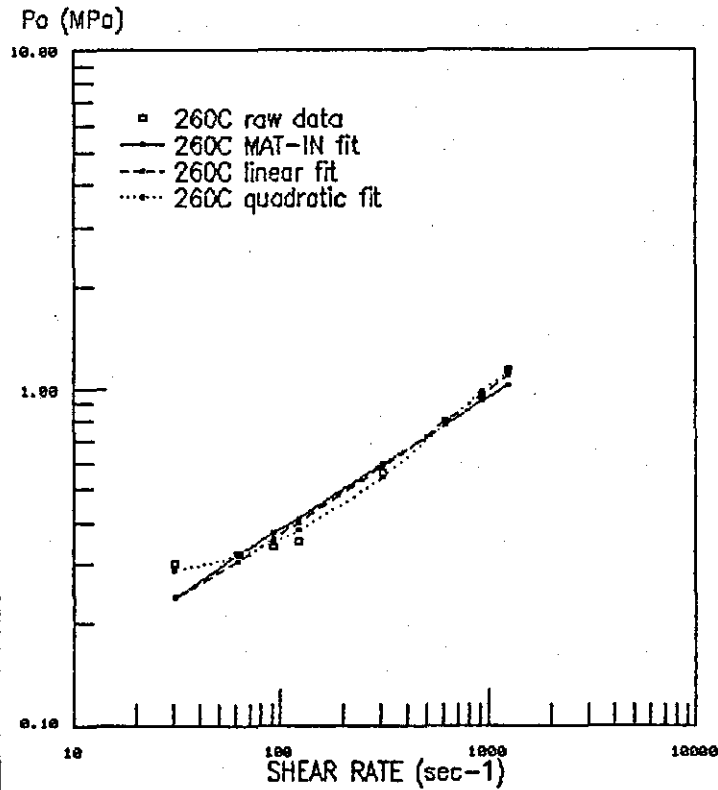
5.4 SIMPOL Simulated Practical Injection Moulding Trials

5.4.1 Introduction To Simulation Trials

The SIMPOL computer simulation program was used to re-run the injection moulding experiments that have been reported in Section 5.2. The machine specification for the Negri-Bossi NB55 (see Table 5.1) was entered into the MAC-IN program. Details of a lay-flat description of the mould used was entered into the CAV-IN program, (see Appendix 11). The materials working files databank contained the modelled rheological data of three materials used.

The mould and melt temperatures were entered into the simulation. The melt temperature was assumed to be the nozzle temperature. The maximum pressure limit (117MPa) and packing pressure (75MPa) were entered. The packing pressure was assumed to be constant for a 6 second packing time.

The injection rates were calculated, assuming a constant displacement rate, using the calculation:

$$\text{injection rate} = \text{cavity volume} \div \text{fill time} \qquad (5.14)$$

All the experimental injection rates were re-run on the simulation.

The effect of packing time and pressure on the simulation was investigated, keeping all other conditions the same.

5.4.2 Results From Simulated Injection Moulding Trials

The SIMPOL simulation provides three screens full of information for each set of conditions entered. The first contains the operating parameters for the trial, the second contains the minimum requirements for the machine specification compared to the machine specification for the Negri-Bossi NB55, the third screen contains cost estimates for the production of parts using the set conditions. Not all the data generated are reported here. The SIMPOL estimated pressure drops and feasibility of moulding are reported below in Figures 5.36-5.38 and Table 5.9.

Table 5.9 shows that SIMPOL predicts that short mouldings are likely to be obtained in most of the trials of processing conditions reported.

Figures 5.36-5.38 show the pressure drop-flow rate relationships,

for the cavity, runner and total pressure drops, for the three polymers used in the injection moulding exercise.

TABLE 5.9 LIKELIHOOD OF SHORT MOULDINGS

Polymer	Mould Temperature (°C)	Melt Temperature (°C)	Injection Rate Range (ml/s)	Likelihood
B90S	10	280	1 - 39	Very Likely
B90S	10	290	1 - 39	Very Likely
B90S	50	280	2 - 39	Very Likely
B90S	50	290	1 - 39	Very Likely
EX167	10	280	5 - 16	Very Likely
EX167	10	290	7 - 22	Very Likely
EX167	50	280	6 - 39	Very Likely
EX167	50	290	2 - 3	Very Likely
EX167	50	290	3 - 5	Possible
EX167	50	290	6 - 8	Very Possible
EX167	50	290	10 - 39	Very Likely
PCTG	10	260	3 - 27	Very Likely
PCTG	10	270	2 - 3	Very Unlikely
PCTG	10	270	3 - 6	No comments
PCTG	10	270	10 - 14	Very Likely
PCTG	10	270	18 - 27	No comments
PCTG	10	270	39	Very Likely
PCTG	50	260	2	Very Unlikely
PCTG	50	260	2 - 3	Possible
PCTG	50	260	6 - 27	Very Likely
PCTG	50	270	2	Very Unlikely
PCTG	50	270	3 - 10	No comments
PCTG	50	270	14	Very Likely
PCTG	50	270	18 - 27	No comments
PCTG	50	270	39	Very Likely

SIMPOL likelihood comments correspond to the pressure drop ranges shown below:

"Very Unlikely"	Up to 58MPa
"Possible"	58-71MPa
"Very Possible"	71-78MPa
"Very Likely"	Greater than 78MPa

FIGURE 5.36: SIMPOL SIMULATED INJECTION
MOULDING TRIALS OF B90S

P (MPa)

280C,10C
280C,50C
290C,10C
290C,50C

TOTAL

RUNNER

CAVITY

Q (ml/s)
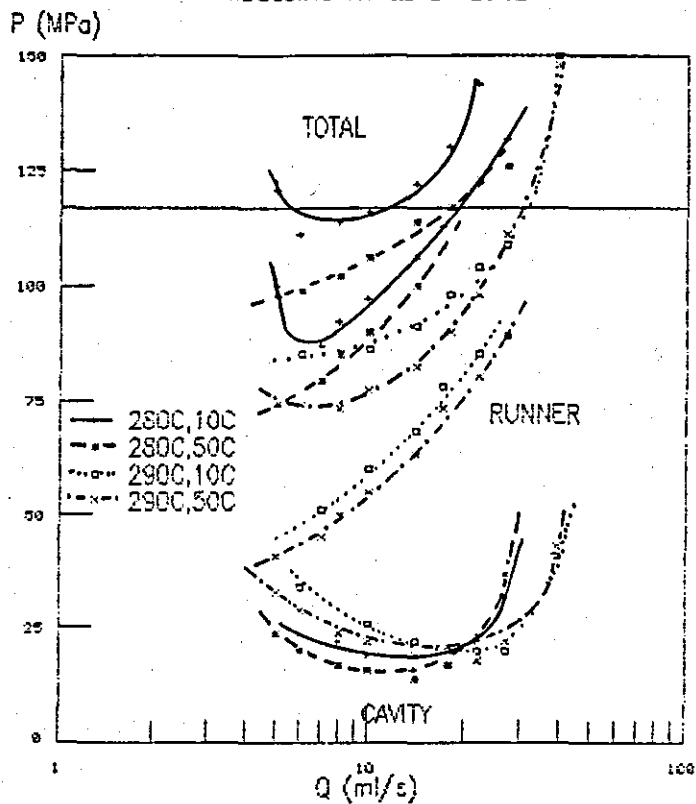
FIGURE 5.37: SIMPOL SIMULATED INJECTION
MOULDING TRIALS OF EX167

P (MPa)

280C,10C
280C,50C
290C,10C
290C,50C

TOTAL

RUNNER

CAVITY

Q (ml/s)

FIGURE 5.38: SIMPOL SIMULATED INJECTION
MOULDING TRIALS OF PCTG COPOLYESTER
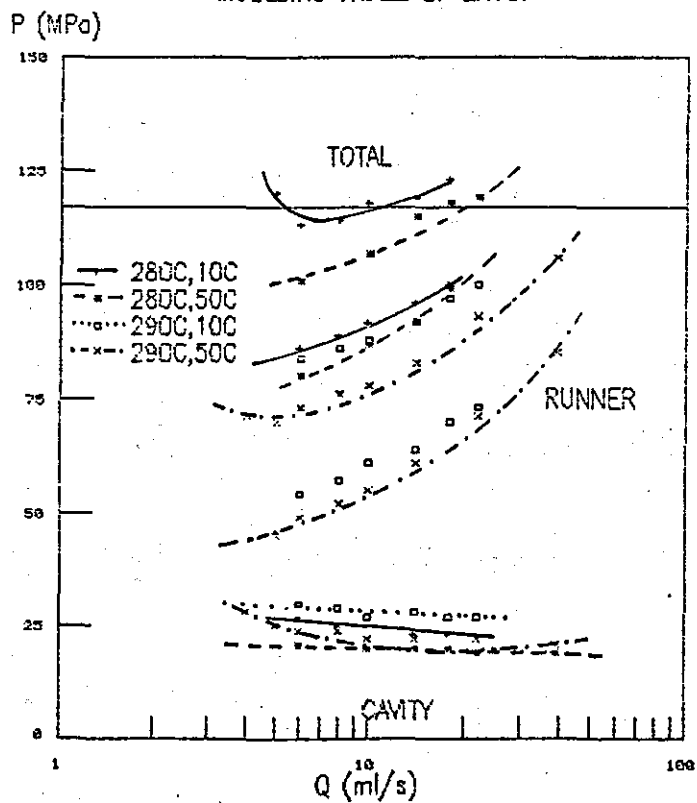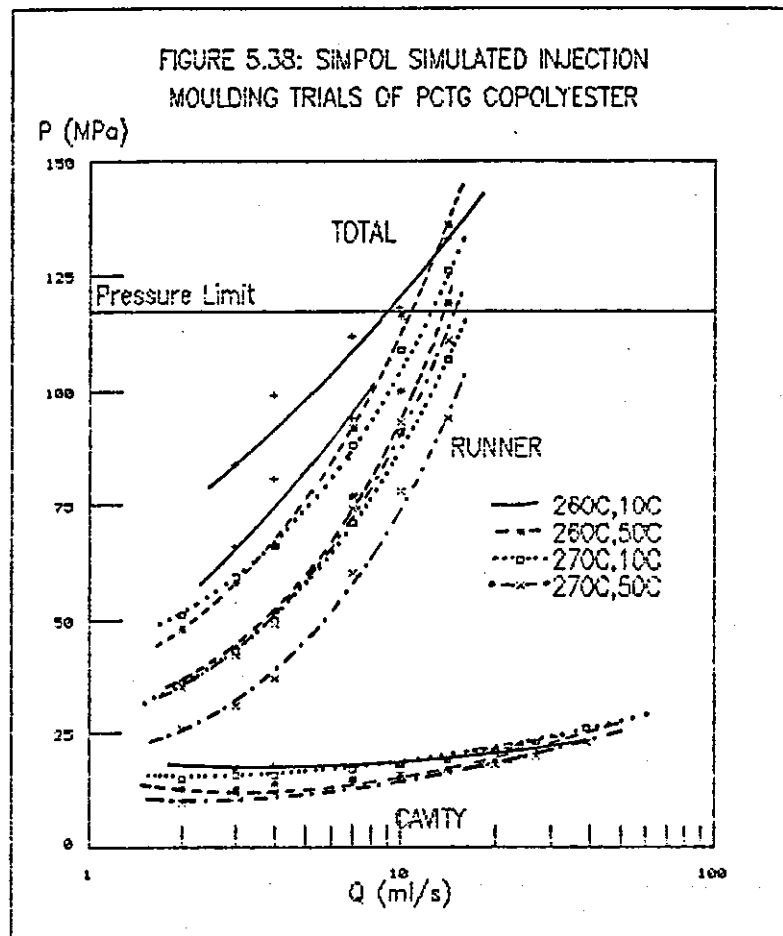
Figure 5.36 shows the results simulated for B90S, the cavity and total pressure drop curves show that a minimum pressure condition exists at a flow rate which will be the optimum flow rate (due to minimum energy required, and minimum stress induced to the melt). The runner pressure drop increased with increasing flow rate. The total pressure drop is the sum of the cavity and runner pressure drops. The effect of temperature on the pressure drops is illustrated in Figure 5.36 as the minimum cavity pressure increases with increasing melt temperature, and decreases with increasing mould temperature. The pressure drop dependence on temperature in the runner system is illustrated by the pressure at a given flow rate increases with decreasing melt temperature and decreasing mould temperature. The temperature dependence of the total pressure drop is illustrated by the minimum pressure decreasing with increasing melt and mould temperatures. The simulation predicts the mould filling pressure to

be close to the machine pressure limit (117MPa) especially for the coolest temperatures case.

Figure 5.37 shows the results simulated for EX167, some of the total pressure drop curves show a minimum pressure point, the others did not span as wide a range of flow rates and the minimum pressure is assumed to occur outside the range tested. The cavity pressure drop curves show decreasing pressure with increasing flow rate. The runner pressure drop curves show increasing pressure with increasing flow rate. The runner pressure drop is much more temperature dependent than the cavity pressure drop. The cavity pressure increases with increasing melt temperature and decreasing mould temperature. The 280°C melt temperature curves of total pressure are close to the machine pressure limit.

Figure 5.38 shows the results simulated for PCTG, no minimum pressure points are shown though the gradient of the curves decreases at lower flow rates. All the pressures increase with increasing flow rate. The runner system pressure drop is more temperature dependent than the cavity pressure. The pressures increase with decreasing mould temperature and decreasing melt temperature. At flow rates close to the minimum pressure points for B90S and EX167, PCTG exceeds the pressure limit of the machine.

The effect of the packing pressure and time on the simulated results was investigated and the results are shown below in Table 5.10.

TABLE 5.10: THE EFFECT OF PACKING PRESSURE AND TIME

Packing Pressure (MPa)	Packing Time (s)	Injection Pressure (MPa)	Minimum Clamping Force (t)	Cycle Time (s)	Likelihood of short mouldings	Total Cost per part (p)
75	8	82,5	22	35	possible	9,6
75	6	82,5	22	35	possible	9,6
75	4	82,5	22	35	possible	9,6
75	2	82,5	22	35	possible	9,6
75	1	82,5	22	35	possible	9,6
50	6	82,5	13	35	possible	9,4
25	6	82,5	3	35	possible	9,3
35	0	82,5	7	35	possible	9,3

It can be seen from Table 5.10 that the packing time does not affect the behaviour predicted by SIMPOL. The packing pressure does not affect the pressure drop estimates, it does affect the estimates of minimum clamping force and costings (machine hour rate and fabrication cost).

5.4.3 Comparison Of Simulated And Experimental Results[103,127-129]

A comparison of Figures 5.39 and 5.40 shows the simulated and experimental results for cavity pressure drop of the B90S polymer. The SIMPOL simulated results give similar curves to those from the experiments on the Negri Bossi injection moulding machine. SIMPOL estimates the minimum pressure to occur at approximately the same flow rate as the experimentally measured minimum. The SIMPOL estimated minimum pressure drops are higher than those measured experimentally on the Negri Bossi injection moulding machine, 14-20MPa and 12-14MPa respectively. The SIMPOL estimated cavity pressure drop increased with a decrease in mould temperature, which agrees with the experimental results shown in Figure 5.39 but disagrees with the results reported by *Johannaber*.[103] The SIMPOL estimated cavity pressure drop increased with an increase in melt temperature, this trend disagrees with the experimental findings shown in Figure 5.39, and those reported by *Johannaber*[103] and *Barrie*.[127-129]

A comparison of Figures 5.41 and 5.42 show the simulated total pressure drop and experimentally measured hydraulic pressure for the B90S polymer. The SIMPOL simulation gave similar curves to those obtained experimentally. The estimates of minimum pressure drop for a melt temperature of 290°C and a mould temperature of 50°C are approximately the same as those measured experimentally. For the other temperatures the simulation estimates a higher value for the minimum pressure drop than was actually measured during the injection moulding experiments. The flow rates at which the minimum pressure occurred are approximately equal for the simulation and the experimentally measured cases. The simulated behaviour predicts a greater temperature dependence of the total pressure drop than that

actually measured from the experiments. The estimated minimum total pressure increased with decreasing temperature, this trend disagrees with that shown in Figure 5.41, but would be expected due to the increased viscosity at lower temperatures.

The simulated and experimentally determined feasibility of moulding of B90S can be compared by referring to Tables 5.3 and 5.9. SIMPOL predicts that short mouldings are "very likely" for all the conditions used, in the experimental exercise short shots only resulted at the slowest flow rate of 1.5ml/s. This difference in results arises partly from the inability of SIMPOL to allow for mould filling during the hold-on stage of the cycle, i.e. under the packing pressure, and probably due to an over-estimation of the frozen layer thickness, by ignoring shear heating.

A comparison of Figures 5.43 and 5.44 shows the simulated cavity pressure drop values for EX167 were higher than the experimental cavity pressure drops. The cavity pressure behaviour from the simulation and the experiments don't agree, the SIMPOL predicted behaviour, Figure 5.44, shows the cavity pressure to be independent or to decrease with increasing flow rate, whereas the experimental results, Figure 5.43, showed a minimum cavity pressure for two curves and the other two curves showed increasing pressure with increasing flow rate.

The simulated results show a lower temperature dependence than the experimental results, this highlights a weakness of SIMPOL with its reliance on generic data, e.g. thermal properties. This leads to the accuracy of the results being dependent on reliable generic data which is widely applicable across the range of polymer grades available for any given generic polymer. This is highlighted by SIMPOL relying on semi-crystalline polymer generic data to model amorphous polymer behaviour which can be very different, e.g. during cooling . The SIMPOL cavity pressure estimations decreased with increasing mould temperature, this agrees with the experimental results reported in Section 5.2.3.2. The cavity pressures decreased with decreasing melt temperature. These trends agreed with the simulated B90S results, shown in Figure 5.40.

FIGURE 5.39: B90S NEGRI BOSSI DATA
FLOW RATE VERSUS CAVITY PRESSURE
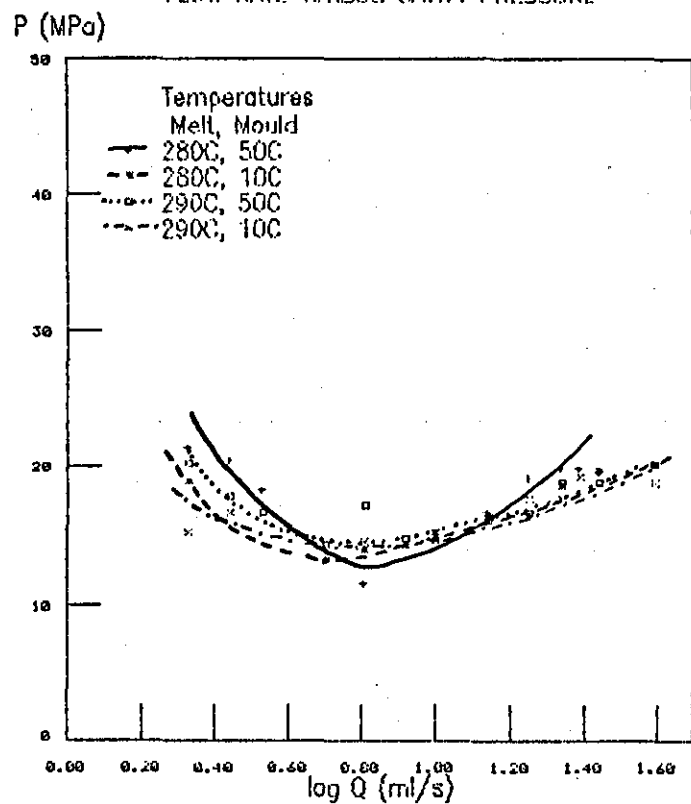
FIGURE 5.40: B90S SIMPOL DATA
FLOW RATE VERSUS CAVITY PRESSURE

FIGURE 5.41: B90S NEGRI BOSSI DATA
FLOW RATE VERSUS HYDRAULIC PRESSURE

FIGURE 5.42: B90S SIMPOL DATA
FLOW RATE VERSUS TOTAL PRESSURE
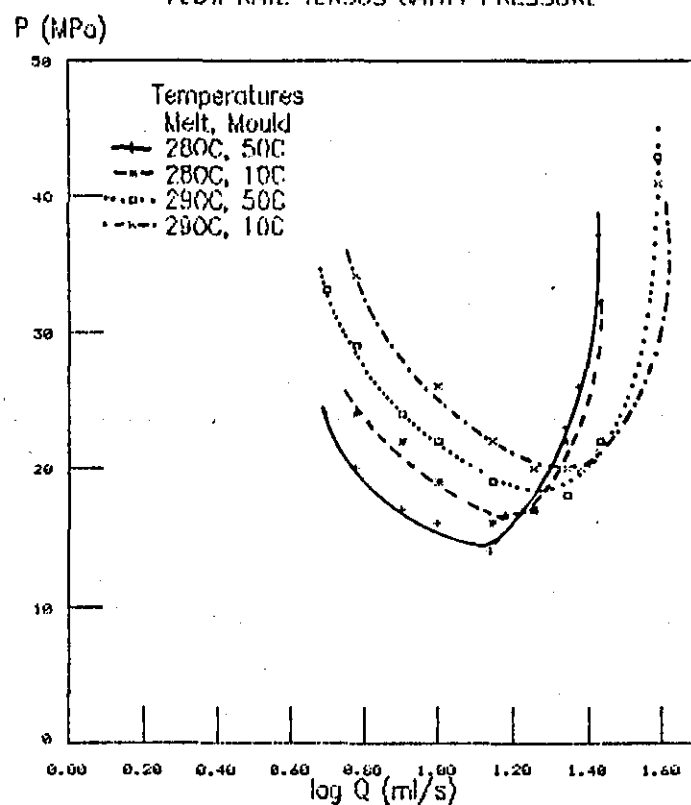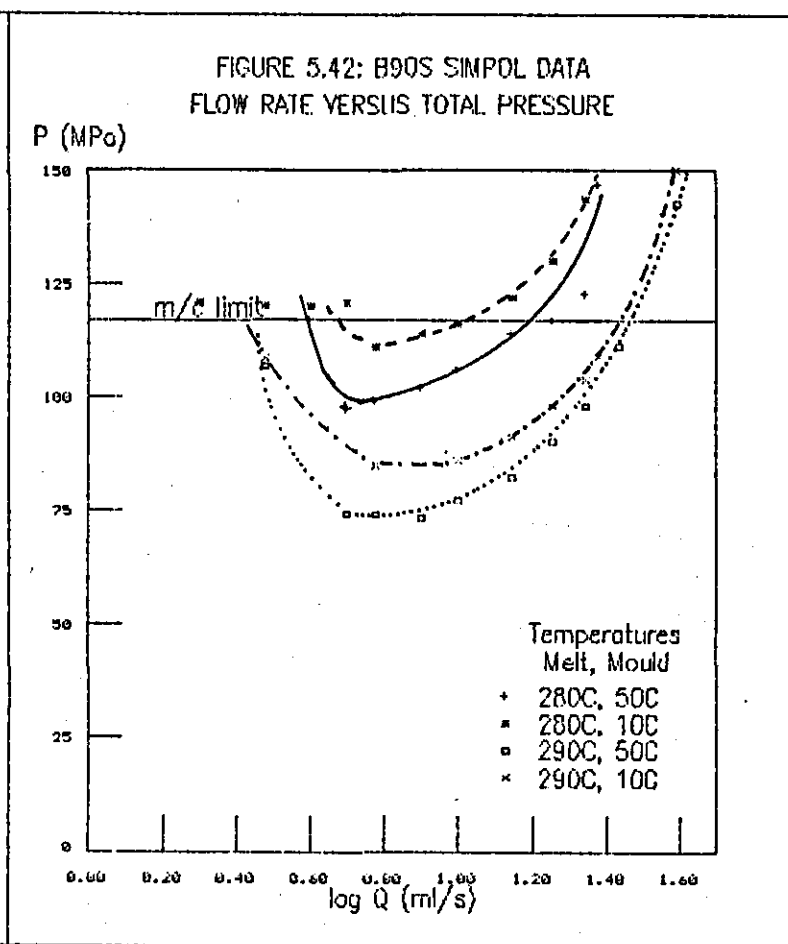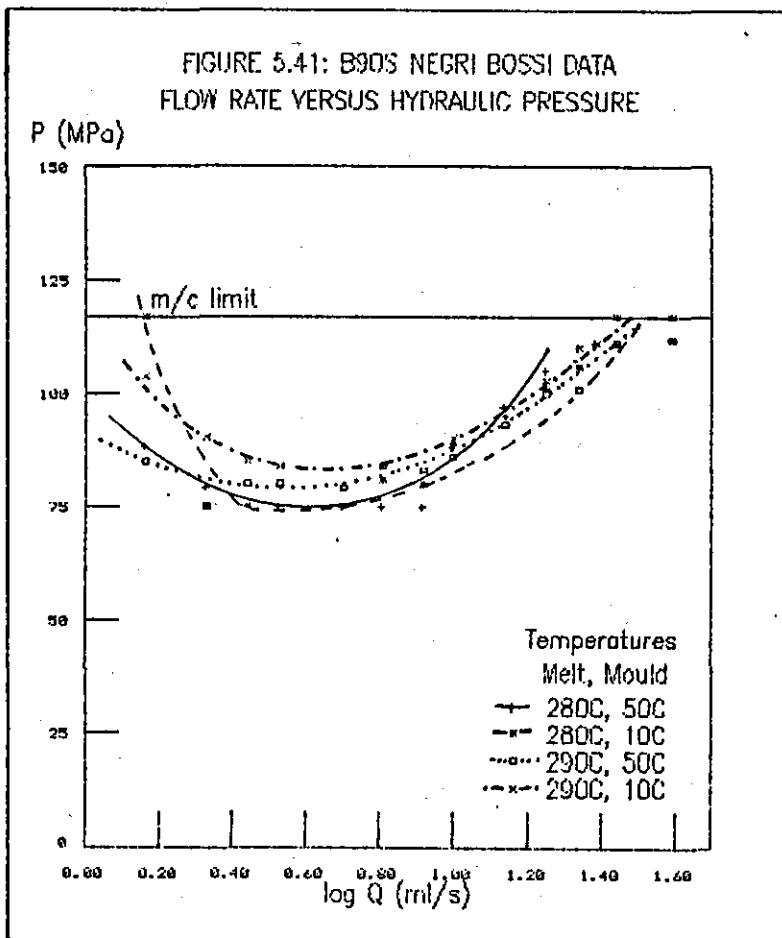
FIGURE 5.43: EX167 NEGRI BOSSI DATA
FLOW RATE VERSUS CAVITY PRESSURE
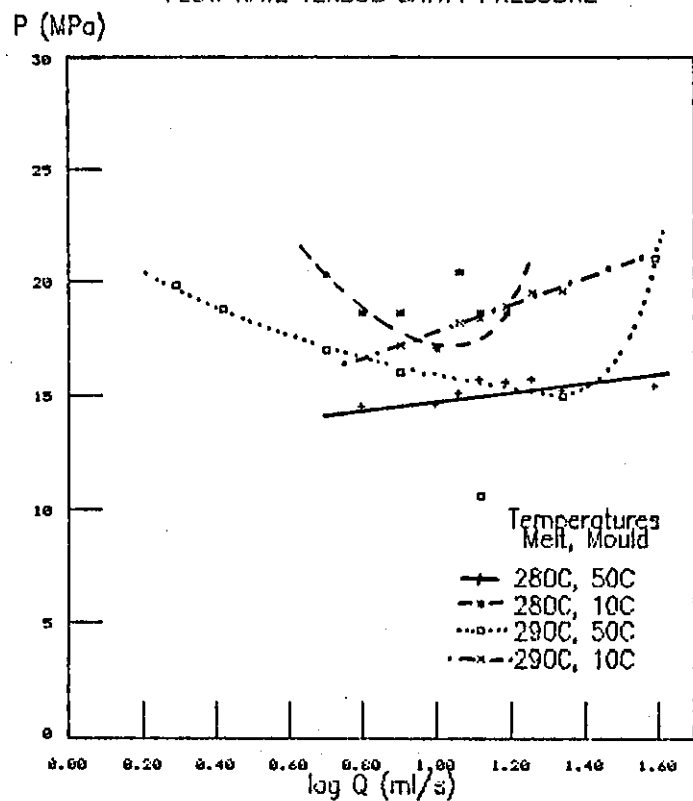
FIGURE 5.44: EX167 SIMPOL DATA
FLOW RATE VERSUS CAVITY PRESSURE
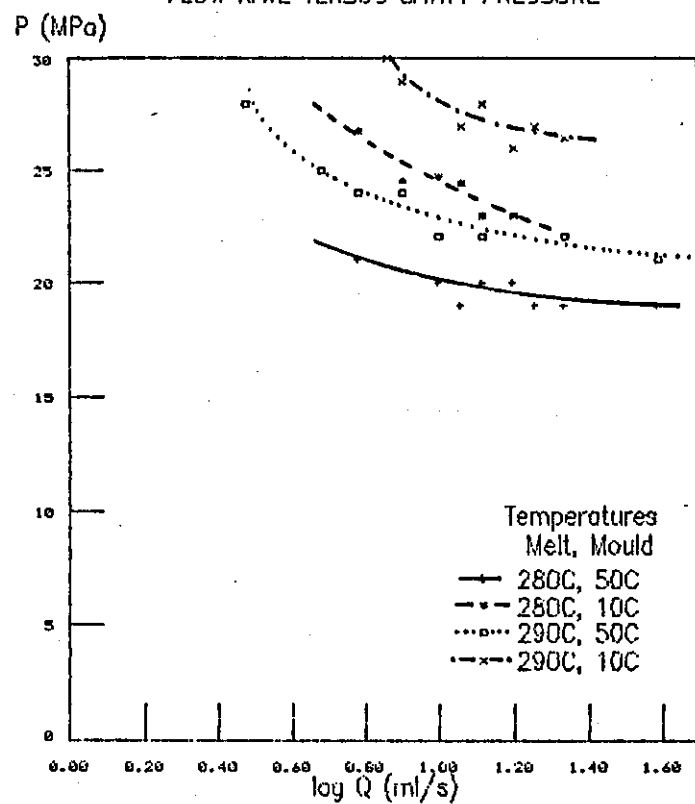
FIGURE 5.45: PCTG NEGRI BOSSI DATA
FLOW RATE VERSUS CAVITY PRESSURE

P (MPa)

Temperatures
Melt, Mould
270C, 50C
270C, 10C
260C, 50C
260C, 10C

log Q (ml/s)
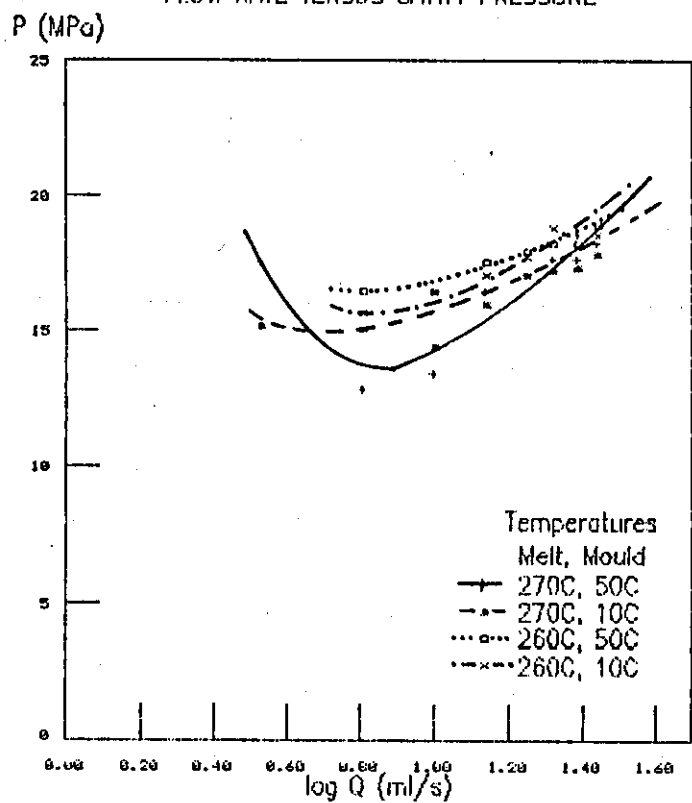
FIGURE 5.46: PCTG SIMPOL DATA
FLOW RATE VERSUS CAVITY PRESSURE

P (MPa)

Temperatures
Melt, Mould
270C, 50C
270C, 10C
260C, 50C
260C, 10C

log Q (ml/s)
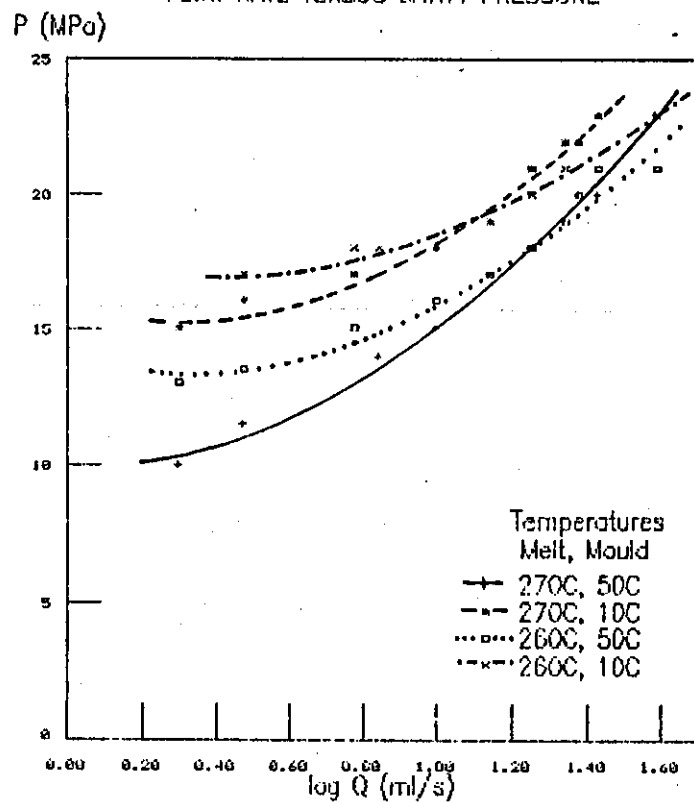
A comparison of the total pressure drop curves in Figure 5.37 and the hydraulic pressure in Figure 5.14 show that two of the simulated curves show similar curves to that in the experimental case, the curves having a minimum pressure point; the other two predicted curves show the total pressure drop increasing with increasing flow rate. The estimated runner pressure drops increased with increasing flow rate. The SIMPOL estimated total pressure drops were lower than the hydraulic pressures measured in the experiments. The estimated runner and total pressure drops increased with decreasing melt and mould temperatures, these trends agree with the results from the experiments.

The SIMPOL simulation predicts that short mouldings are likely for all the conditions tried. For the melt temperature of 290°C and mould temperature of 50°C a range of feasibilities were predicted ranging from short mouldings being "very likely" to "possible". In practice short shots were obtained only in two cases, at 2ml/s for a mould temperature of 50°C and a melt temperature of 290°C; and at 6.4ml/s for a mould temperature of 50°C and a melt temperature of 280°C.

The predicted curves in Figure 5.46 all show increased pressure drop with increasing flow rate, no optimum flow rate is apparent, this does not agree with the experimental results shown in Figures 5.45 and 5.16 where a minimum pressure condition is shown. In Figure 5.46 the cavity pressure curve, for a melt temperature of 260°C and a mould temperature of 50°C, has a different relative position, to the curves for different temperatures, than the curves in Figure 5.45. In Figure 5.45 this curve had the highest pressure drop values, in Figure 5.46 the curve shows lower pressure values than the curves for a 10°C mould temperature and higher values than the curve for a mould temperature of 50°C and a melt temperature of 270°C. Hence the simulation shows the cavity pressure to decrease with increasing mould and melt temperatures. *Barrie*[127-129] and *Johannaber*[103] reported that cavity pressure decreased with increasing melt temperature. The estimated cavity pressure values were similar to those found experimentally and reported in Section 5.2.3.2.

The total pressure drop curves in Figure 5.38 steadily increase with increasing flow rate, this disagrees with the behaviour observed experimentally and shown in Figure 5.16, where the curves of hydraulic pressure show a minimum pressure value at a given flow rate. The SIMPOL estimated values of total pressure drop, below a flow rate of 10ml/s, are lower than those measured experimentally on the Negri Bossi injection moulding machine. At flow rates greater than 10ml/s the shape of the curves in Figures 5.16 and 5.38 are similar though the magnitude of the values are different. The temperature dependence predicted by SIMPOL agrees with the experimental results shown in Figure 5.16. The pressure drop increased with decreasing temperatures, this is the expected trend due to the increased viscosity at lower temperatures.

The SIMPOL simulation predicts that short mouldings are "very likely" for all the flow rates tried for a mould temperature of 10°C and a melt temperature of 260°C, in practice no short shots resulted at these flow rates. For the other temperatures SIMPOL predicted that short mouldings were "very unlikely" at the lowest flow rates, whereas in practice these were the only flow rates at which short shots were obtained. At the other flow rates where SIMPOL predicted that short mouldings were "possible" and "very likely" no short mouldings were found during the experiments.

At low injection rates (below 5ml/s) the SIMPOL simulation gave unrealistic predictions of cooling times, clamping forces and other results, e.g. cooling time of 151s at Q = 5ml/s; cooling time of 30s at Q = 6ml/s, clamping force of −60515 tonnes at Q = 5ml/s; clamping force of 22 tonnes at Q = 6ml/s. This is possibly due to a constant in the calculations being cancelled, but without a true knowledge of the calculations it is impossible to trace this fault.

5.5 A Critical Assessment Of The SIMPOL Simulation Package

5.5.1 Introduction

The SIMPOL simulation of the injection moulding process has been used to run trials on three polymers in the same mould under different conditions, these trials have been compared to experiments carried out on the Negri Bossi NB55 machine. From the trials and the comparison of simulation and experimental results the software package has been assessed below.

The software follows the outlined procedure reported by *Richardson*[105] in the form of the flow chart shown in Figure 5.7. The calculations used in the simulation have been simplified to reduce the computer time needed and to minimise the amount of data needed to run the program. The result is a software package which is easy to use and has good presentation of the data and results. The usefulness of the data depends on its accuracy, but the results predicted, by SIMPOL, would be useful if accurate. The cost of the software and the computer hardware it is designed to run on is very economical compared to competitive packages such as MOLDFLOW.

The accuracy of different estimated parameters varies. The shear rheological properties are modelled to an acceptable degree of error, though the high shear rate viscosity having a power law index approaching zero is a dubious approximation.

The die-entry pressure drop data modelling should be improved, on the evidence from this study. Section 5.3.6 discussed some possible alternative model forms for the die-entry pressure drop. The effectiveness of the die-entry pressure drop modelling was not tested in this study as the mould geometry used did not contain large sections of convergent or divergent flow or pin gated cavities.

From the comparison of results in Section 5.4.3 the feasibility of moulding predictions seem very inaccurate, there are several possible reasons for this: (i) The PET generic datafile in SIMPOL is based on fast-crystallising injection moulding grade PET which has different thermal properties (particularly "no-flow" temperature) to the amorphous PET polymers studied; (ii) the effect of shear heating has

been ignored in SIMPOL, either of these reasons could lead to an over-estimation of the frozen layer thickness and hence predictions of sealed flow channels leading to short mouldings under conditions where complete filling would be achieved in practice. (iii) Modern injection moulding machines can run using various control methods, whereas the SIMPOL model assumes the control to be a constant injection rate method. The practical experiments were carried out using hydraulic pressure control, therefore the SIMPOL estimates of the switchover point could be different to actual practice leading to inaccurate predictions of moulding feasability. SIMPOL neglects to account for flow during the hold-on stage which could allow the mould filling to occur under the packing pressure, this occurred in the practical experiments by the machine prematurely switching over to the packing pressure - this faulty machine setting results in a complete moulding being obtained when a short shot is predicted.

At low injection rates SIMPOL cannot estimate cooling time and clamping force accurately. At very low shear rates the process is dominated by heat transfer. When this happens, the accuracy of the overall model depends on the accuracy of the heat transfer model. This will be different for different polymers (being dependent on the thermal properties, shrinkage away from the mould, crystallisation, etc.). Therefore at low flow rates the general accuracy is more critically related to the type of polymer, the heat transfer process and the accuracy of the data in the generic datafile with respect to the particular grade of polymer being studied.

The pressure drop estimates were similar to those measured experimentally in practice, with some over-estimations and some under-estimations in different cases. The trends of the simulated behaviour as a function of injection rate disagreed with practice, due to the errors in the low injection rate estimations.

The cooling stage is a dominant part of costing estimates and the inability of SIMPOL to account for the detail of the cooling system design more quantitatively must lead to errors in cost estimation.

The feasibility of moulding is limited to predictions of short

shots, whereas the prediction of moulding faults such as jetting, residual strains and orientation are also important in obtaining a "good" moulded part. Other workers[119] have investigated the prediction of these faults.

5.5.2 Possible Enhancement Of SIMPOL

SIMPOL has an empirical basis for many of the calculations used. Other workers[105,124,135] have taken a more analytical approach to the simulation of the injection moulding process, at the cost of higher computing power needed and more data required before the programs can be run. A possible enhancement of SIMPOL would be to allow for some of the effects neglected or assumed constant to be included in the simulation, their relationships with the operating parameters leading to further or more complex calculations. At present SIMPOL has extravagant graphic displays, often with superfluous features, which take up valuable computer memory which could be better used for the proposed extended calculations. The simulation is dominantly based on the injection stage and a full simulation of the process should take more account of the other stages (plasticisation, packing, cooling, ejection), such an approach is reported by *Kamal and Kenig*.[124,135]

Using the same computer hardware any enhancement of the calculations would have to be at the cost of the graphics, or the amount of data presented. The enhancement could be for more detailed calculations of the parameters currently modelled or for further options to be offered as variables.

- An improved die-entry pressure drop model, such as one of those considered in Section 5.3.6, should replace the existing model and would not use up much extra memory.

- The single value estimate of cooling efficiency should be replaced by a calculation of a value based on: the number of cooling channels and effective area per cavity, coolant rate and coolant thermal properties.

- The single value entry of packing pressure and time that SIMPOL currently permits should be replaced to model modern injection moulding machines which usually have a series of packing

pressures and times available. The criteria for modelling the packing stage has been reported by *Greener*.[113]

- *Barrie*[128] assumes the frictional losses to be a constant value for a given machine, the effects of temperature and injection rate on the frictional losses could be accounted for by instrumentation of the injection moulding machine, i.e. fitting a transducer at the nozzle.

If a larger capacity computer was used to run the SIMPOL simulation the more adventurous enhancements could be made.

- The effects of shear heating and pressure could be taken into consideration in the calculations.
- The frozen layer theory, which assumes a constant layer thickness could be modified to model the tapering of the skin reported by *Brydson*[13] or the variable build-up reported by *Ballman and Toor*[110] and *Tanner*.[16]
- A detailed graphic display of the flow path could show the length of short shot mouldings, possibly using the methods reported by *Harry and Parrot*.[122]
- Thermal degradation could be predicted modifying the work of *Berger and Gogos*.[123]
- The single empirical value of freeze-off temperature used in SIMPOL could be replaced by solidification profiles as reported by *Kenig and Kamal*.[137]
- A graphic display showing the mould filling could be incorporated, such as that displayed by MOLDFLOW[139]

5.6 Conclusions

5.6.1 Summary Of Chapter 5

In this chapter the aim of applying the rheological data from Chapters 2 and 3 to the injection moulding process, has been achieved via the SIMPOL simulation system.

The four objectives this experimental programme was designed for have been achieved.

The processability of the three polymers was studied and has been reported in Section 5.2.

The comparison of the MAT-IN modelled rheological data and that from Chapters 2 and 3 has been carried out and reported in Section 5.3.6.

The comparison of the computer simulated processability results with practice has been carried out and reported in Section 5.4.3.

The assessment of SIMPOL and suggested improvements have been reported in Section 5.5.

The study reported in this chapter has several novel features in that:

- the polymer PCTG 5445 copolyester has not been widely studied and its processability has not been published independently.
- The SIMPOL system is a new (1986) commercial package and this is believed to be the first independent study comparing any estimates with practical findings.
- The suggested improvements to the die-entry pressure drop data modelling have not been reported previously.

5.6.2 Conclusions From Chapter 5

- High filling pressures were recorded for all three polymers under all conditions due to the long runner system in the mould used.
- Short shot mouldings were obtained at low injection rates.
- The machine pressure limit (117MPa) was exceeded in several cases under the conditions used.
- There is an optimum flow rate, for a given set of conditions, where the pressure required to fill the cavity is a minimum. Processes should be optimised towards these filling rates.
- Higher mould temperatures lead to higher cavity pressure due to lower pressure loss/drop from the injection unit.
- The pressure drops are generally lower with lower shear viscosity, hence decreased with increased temperatures or a lower degree of cooling.
- EX167 pressure dependence on mould temperature was greater for the lower melt temperature.
- Pressures increase with higher polymer molecular weight.
- B90S showed a lower activation energy than EX167 and PCTG when considering the temperature dependence of pressure at a 10ml/s

flow rate.

- The three polymers can be ranked in order of increasing injection pressure for a given set of conditions as: B90S<EX167<PCTG.

- The reported data is ripe for exploitation by those involved in the new, important PET industry, e.g. for designing moulds for PET bottle preforms etc.

- MAT-IN models PET and PCTG shear rheological data satisfactorily, but the die-entry pressure drop data model shows significant errors.

- Alternative models for die-entry pressure drop data have been proposed, showing improved correlation and less spread of data about the best fit line.

- SIMPOL shows some limitations on estimates of cooling time and clamping force at low injection rates.

- The SIMPOL system predicts the behaviour of PET and PCTG polymers in injection moulding, showing good agreement with practice for pressure drop values, their temperature dependence and their molecular weight dependence; but poor agreement between the feasibility of short mouldings predicted and practice.

- The work reported in the literature could be used to enhance SIMPOL to give improved accuracy and, hence, usefulness of the estimates made.

5.6.3 Further Work Suggestions

Further work that could reinforce the findings of this chapter and could extend the scope of the study could involve:

- The software should be modified to permit new polymer generic files to be created, then files should be created for amorphous PET and the copolyester material and the simulated trials repeated to see if better predictions can be achieved.

- Testing the proposed improvements for die-entry pressure drop modelling, studying the effects on the SIMPOL estimates.

- SIMPOL used with more complex cavity geometries, including converging and diverging flows and pin gates, this would test the effectiveness of the die-entry pressure drop model.

- Further studies comparing SIMPOL simulated behaviour with practical injection moulding behaviour for novel polymers, e.g. blends, copolymers, fibre-filled polymers.
- Optimising conditions for injection moulding using SIMPOL in conjunction with obtaining desired mechanical properties.

Only when such relationships are known can the simulative tool be considered to be relevant and accurate for many groups of modern thermoplastic moulding compounds.

6. Extrusion Blow Moulding

6.1 Introduction

6.1.1 Aims Of Chapter

This chapter describes the experimental programme carried out with the objective of applying the rheological data obtained for various polyester polymers to the extrusion blow moulding process, comparing theoretical predictions of behaviour with experimental measurements from practical processing. The aims of the chapter were:

- to apply rheological data reported in Chapters 2, 3 and 4 to stages of the extrusion blow moulding process;

- to compare the applicability of both converging flow data and uniaxial elongational data to the extrusion blow moulding process;

- to test the conclusions made in Chapters 2, 3 and 4 as to the suitability of the various PET polymers to extrusion blow moulding;

- to compare the theory and practice of parison sagging.

6.1.2 Extrusion Blow Moulding

Extrusion blow moulding is a process used to manufacture hollow articles, such as bottles and other containers including technical mouldings such as automotive petrol tanks and coolant expansion reservoirs. A thick-walled tube of melt known as a 'parison' is extruded, usually vertically downwards and an open mould is positioned either side of the parison. The mould closes and seals off the ends of the parison, one end being clamped around a spigot through which compressed air is pumped to inflate the parison to the shape of the mould. The mould is water-cooled and when the moulding has solidified the mould is opened, the moulding removed and trimmed of any excess material, the cycle then restarts.[151],[152]

The rheology of the process is very complex as the melt preparation by extrusion involves shear flow, the dies are usually of a convergent design and so involve shear and elongational flows, the parison swells due to unconstrained melt elasticity, the parison sags due to low stress uniaxial elongational flow behaviour, the parison

'bounces' due to the elasticity, and the inflation of the parison involves a high stress multiaxial elongational flow. This combination of flows demands a material to have the correct combination of rheological properties both viscous and elastic, in shear and elongation for it to be suitable for the extrusion blow moulding process.

Baron, McChesney and Sinker[5] summarised the shear flow requirements a polymer should possess to be suitable for extrusion blow moulding: the polymer should be shear sensitive, having a high melt viscosity at low shear rates and a low melt viscosity at high shear rates. This characteristic rheology enables the material to form a parison with adequate melt strength, while not requiring excessive power in the extruder or exceeding the critical melt fracturing stress in the die lip. Shear rheology alone is insufficient to differentiate between the processability of polymers in extrusion blow moulding[153,154] the viscous and elastic elongational rheology also need determining.[155] Thus, parison formation should not be considered alone but together with the deformation of the parison resulting from sagging and inflation.[156]

The time scale of the deformation is important; if the formation of the parison and delay before inflation is less than the natural time (equation (6.1)) of the polymer, then the deformation will be primarily elastic; if greater, then viscous deformations will assume major importance.[156]

$$t = \lambda / E \qquad\qquad \text{(s)} \qquad (6.1)$$

where t is the natural time of the polymer, λ is the elongational viscosity and E is the tensile modulus of the polymer.

To predict the wall thickness distribution of the moulded article the process can be divided into three stages each presenting problems for any model, these are parison formation, inflation of the parison clamped at both ends, and the contacting of the inflating parison with the mould.[157] *Schaul et al*[154] stated that:

"the rheological complexity of the problem of predicting parison behaviour arises from the circumstance that is a free-surface problem, involving time-dependent elastic recovery from a complex

flow of a viscoelastic fluid, subject to the force of gravity".

Cogswell et al[158], *Garcia-Rejon et al*[12], *Dutta and Ryan*[159] and *Dealy and Orbey*[160] have published computer models for the extrusion blow moulding process, these models require a large array of data before they can be used to predict the likely behaviour of a polymer during the process. Simpler analyses of different stages of the process have been more widely published.[6,13,15,156]

Parison Formation

The parison formation has been studied for the swelling that occurs due to elastic recovery and the sagging that occurs due to gravitational forces. The swelling of the parison involves the swelling of the thickness of the polymer and the swelling of the diameter of the parison. Several studies have related die-swell data from capillary rheometry to the parison swelling behaviour in extrusion blow moulding.[155,158,161,162] *Dutta and Ryan*[159] concluded that the pure swell behaviour could be easily modelled using exponential functions with experimentally determined rate constants. *Cogswell*[158] reported the relationships for elastic recovery after simple shear and after elongational flows as equations (6.2) and (6.3) respectively.

$$B_{SR}B_{SH} = \tfrac{1}{2}[\ (1+\gamma_R^2)^{1/2}+(1/\gamma_R)\ln\{\gamma_R+(1+\gamma_R^2)^{1/2}\}\ ] \qquad (6.2)$$

where B_{SR} is the diameter swell after shear, B_{SH} is the thickness swell after shear and γ_R is the recoverable shear strain corresponding to the stress at the die exit.

$$B_{ER}B_{EH} = \{\exp(\varepsilon_R)\}^{3/4} \qquad (6.3)$$

where B_{ER} is diameter swell after elongation, B_{EH} is the thickness swell after elongation and ε_R is the recoverable tensile strain corresponding to the stress at the die exit.

The shear and elongational components are not additional, the observed swell being the greater of the two. The relationship between the diameter and thickness swelling is shown in equation (6.4).

$$B_H = B_R^2 \qquad (6.4)$$

Crawford[15] reported a simple equation to estimate the amount of parison sagging that would occur; equation (6.5) accounts for the sum of the viscous strain and the elastic strain.

$$\varepsilon = \rho g L.[(\frac{1}{2}E) + (t/\lambda)] \qquad (6.5)$$

where ε is the total strain, ρ is the melt density, g is the acceleration due to gravity, L is the initial length and t is the deformation time. However, this equation applies only when the deformation time is less than the natural time of the polymer, i.e. with predominantly elastic polymers. *Cogswell*[5] provided four more equations (6.6)-(6.9) for other parameters to be considered when estimating parison sagging.

Maximum stress (at top of parison) $\sigma_{MAX} = L\rho g$ (Pa) (6.6a)

Minimum stress (at bottom of parison) $\sigma_{MIN} = 0$ (Pa) (6.6b)

Between these limits $d\sigma/dx$ is linear.

Strain rate $\dot{\varepsilon} = (\frac{1}{2}L\rho g) \div \lambda$ (s^{-1}) (6.7)

Total strain $\varepsilon_{TOTAL} = (\frac{1}{2}L\rho g t) \div \lambda$ (6.8)

Total deformation $\Delta L = (\frac{1}{2}L^2 \rho g t) \div \lambda$ (m) (6.9)

Another aspect of the parison formation stage is the occurrence of parison 'bounce', which has been modelled by *Cogswell et al*[58] by equation (6.10).

$$\varepsilon_R = \sigma_{INERTIA} \div E \qquad (6.10)$$

where ε_R is the recoverable strain corresponding to the inertial stress $\sigma_{INERTIA}$.

More elaborate analyses have considered the parison as a series of elemental units each having a different strain history. *Dutta and Ryan*[59] concluded from their attempts to model parison sagging that it is not so easily modelled as the pure swell behaviour. *Garcia-Rejon, Dealy and Kamal*[12] used elongational stress growth function data obtained from an elongational rheometer in their model of

parison sagging, whilst, *Dealy and Orbey*[160,161] used the Lodge "rubberlike liquid" model with three relaxation times, using the relaxation modulus corresponding to a relaxation time determined from experimental storage modulus data. As the Rutherford Elongational Rheometer in our own laboratories generates elongational stress growth function data (see Chapter 4) the analysis described by *Garcia-Rejon et al*[2] for HDPE is of particular interest. The analysis considers the parison deformation as consisting of three components: swelling, sagging during extrusion and sagging after complete extrusion. The sagging and swelling during extrusion are determined by equation (6.11):

$$L_{(N+1)} = (V_d(t - N\Delta t)) \div B_{R(\Delta t/2)}B_{H(\Delta t/2)} \quad (6.11)$$

where $L_{(N+1)}$ is the length of parison element $(N+1)$, V_d is the average velocity at the die, t is the extrusion time, Δt is the time interval for extruding each element, B_R and B_H are the swell ratios.

The sagging after extrusion has stopped is considered as the sum of the element deformations, defined by equation (6.12):

$$1/Z_{i(t_i)} = 1/Z_{i(t_i=0)} - \tfrac{1}{2}\rho g(i-1)\int_0^{t_i} dt/\lambda_{(\varepsilon_i, t_i)} \quad (6.12)$$

where Z_i is the length element i would have reached if there were no swell, t_i is the time that has elapsed since element i was completely extruded, and λ is the elongational stress growth function. This deformation can be adjusted to account for swell and added to equation (6.11) to give the total length.

Parison Inflation

The parison is inflated by a predetermined air pressure. The hoop strain is a tensile deformation and has an elastic and a viscous component.[158] The total hoop strain rate is given by equation (6.13).

$$d/dt(\varepsilon_{TOTAL}) = I \div (2\pi R^2 L) \quad (6.13)$$

where I is the volume flow rate of air, and R is the parison radius (assuming no draw-down). The deformation approximates to equation (6.14):

$$I \div (2\pi R^2 L) = 3/4 \{d/dt(\sigma/E) + (\sigma/\lambda)\} \qquad (6.14)$$

The blowing pressure can be calculated from thin-shell theory by equation (6.15):

$$P = \sigma 2H \div R \qquad (6.15)$$

where P is the blowing pressure and H is the half-thickness of the parison assuming no draw-down.

For stable inflation of the parison the viscosity should increase with the increasing stress; this will cause deformation to occur in the least deformed part of the parison. The value of the natural time t for the polymer during the inflation stage should be large, so the polymer will respond elastically to the high blowing pressure. The faster the inflation the more stable will be the deformation, provided the yield stress of the melt is not exceeded. Powell[56] reported a criteria for qualitative stability during inflation, shown as equation (6.16):

$$1/t < 4I \div (3\pi R^2 L) \qquad (6.16)$$

where t is the natural time of the polymer. The natural time for the process t' can be calculated from equation (6.17):

$$t' = (d/dt(\varepsilon)) \div \varepsilon_{TOTAL} \qquad (6.17)$$

If the natural time for the process t' is greater than the natural time of the polymer t then the parison inflation will be stable (and vice versa). If the polymer is tension thinning in a free-surface flow then an uneven wall thickness will be obtained as the thinnest parts of the parison will be deformed during inflation in preference to the thicker parts. A tension stiffening polymer will produce a more even wall thickness as the thinner parts of the parison will offer a greater resistance to deformation than the thicker parts and so the

thicker parts will be preferentially deformed. If the resistance to deformation is constant (i.e. Troutonian behaviour) then the final thickness will be proportional to the blow ratio.[158] This phenomena has an important significance in the blow moulding of irregularly shaped articles.

Mould Contact

The parison is usually assumed to stop deforming on contact with the mould. Depending on the shape of the mould, the blow ratio may vary for different parts of the parison. The final thickness will vary at these different blow ratios dependent on the response of the polymer to multiaxial elongational flow. A polymer that is Troutonian will have thick sections at the lower blow ratios and thin sections at the larger blow ratios. With a tension thinning polymer the thickness variation will be even greater, whilst a tension stiffening polymer will tend to show less thickness variations with different blow ratios.

The cooling is predominantly achieved by thermal diffusion between the melt and the water-cooled mould. The cycle time can be reduced by using chilled air for the inflation and then circulating chilled air inside the moulding.[163]

Summary

From the above description of polymer requirements for extrusion blow moulding, it can be concluded that a good extrusion blow moulding polymer represents a compromise of properties. At high shear rates a low elastic modulus and a low viscosity are necessary to avoid sharkskin; for stable inflation the polymer should have a low modulus and a high viscosity; to minimise parison sag at low stresses a high modulus and a high tensile viscosity are required.[156]

The rheology of linear PET polymers is generally unsuitable for extrusion blow moulding, since they behave as near-Newtonian fluids above the melting temperature and do not usually have sufficient shear sensitivity.[5] However, the advantages of the extrusion blow moulding process - the ease of making complex shapes, handled containers, the basic economy of both capital equipment and conversion costs (extrusion blow moulding moulds are less costly than

those for the injection stretch blow moulding process) - have led to the development of PET polymers for this process. Success in producing extrusion blow mouldable PET polymers has been claimed by developing copolymers and branched PET polymers.[6] The experimental programme described in this chapter tests these claims.

6.2 Experimental Extrusion Blow Moulding

This experimental programme involved the extrusion of parisons of PETG Copolyester and B90S linear PET at two temperatures and two output rates for each polymer. The parison extrusion was filmed using video equipment and measurements of parison sag were made from the video recordings. Some of the equations described in Section 6.1.2 were used to predict the parison sagging and compared to the observed values. Bottle inflation experiments were undertaken studying the effect of the inflation air pressure on the final bottle quality.

6.2.1 Description Of Apparatus

A *Hayssen* Monablow 2070 extrusion blow moulding machine was used for these experiments. The machine specification is shown in Table 6.1. The machine was modified for use with PET polymers by fitting a dehumidifying hopper on top of the existing hopper unit, the existing hopper was flooded with dry nitrogen gas, these measures were necessary to minimise degradation due to hydrolysis and oxidation.

In these experiments no direct swelling measurements were made as the parison sagging was so great and rapid the swell component could not be measured from the video recording. The quenched parisons were too distorted to allow any accurate measurements to be made after cooling. Die swell measurements from Chapter 2 were used to estimate the swelling behaviour during extrusion blow moulding.

Parison Sagging

To study the parison sagging a scale was fixed behind the open mould so that the length could be measured as a function of time, a stop-clock was placed next to the scale. The experiments were filmed using video-tape equipment (*JVC* camera and *Mitsibushi* tape unit), the equipment layout is shown in Figure 6.1. The video recordings enabled

the sagging measurements to made later using the freeze-frame facility. The parisons were quenched in a water bath after being cut-off from the extruder, the quenched parisons were then weighed. Two melt temperatures and two output rates were used for each polymer. The output rate Q (see equation (6.18)) was established by extruding for a given extrusion time, $t_{extrusion}$, then the quenched parison weight W was determined.

$$Q = W \div (\rho . t_{extrusion}) \qquad (6.18)$$

TABLE 6.1: HAYSSEN MONABLOW 2070 EXTRUSION BLOW MOULDER

EXTRUDER
Screw Diameter	45mm
L/D ratio	21:1
Feed Section L/D ratio	8:1
Compression Section L/D ratio	5:1
Metering Section L/D ratio	8:1
Screw Speed	20-100 r.p.m.

DIE
Outside Diameter	20mm
Die Gap	1.5mm

BOTTLE MOULD
Height (to shoulder)	180mm
Overall Height	194mm
Shoulder Diameter	66mm
Waist Diameter	58mm
Base Diameter	68mm
Volume	568ml (1 pint)

FIGURE 6.1: PARISON SAGGING VIDEO EQUIPMENT
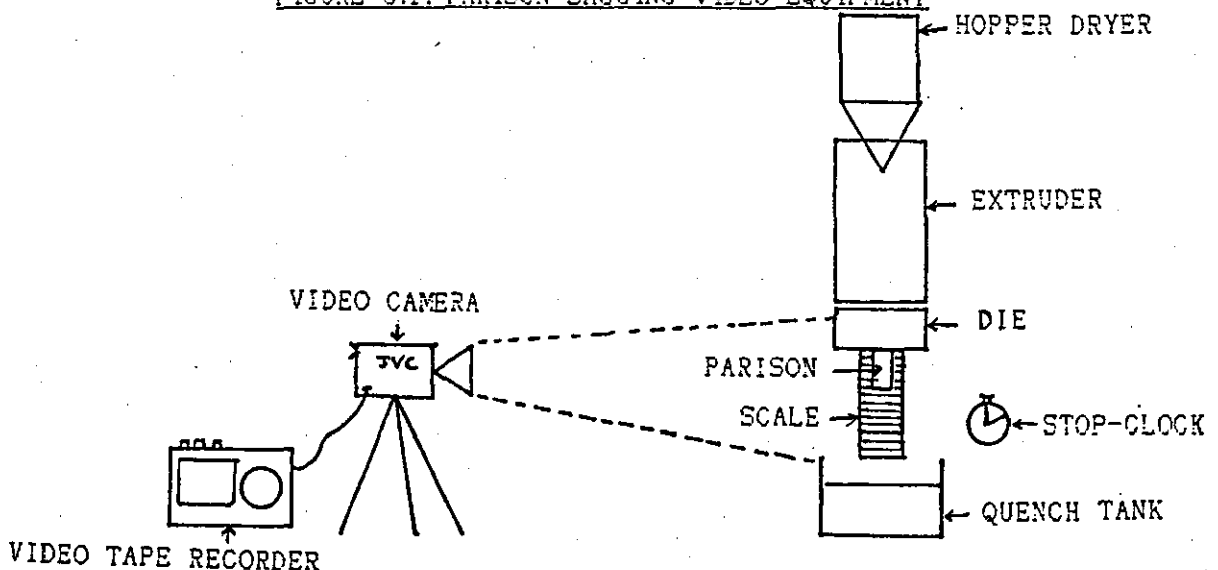
Bottle Inflation

Due to failure to obtain a satisfactory parison for the B90S polymer, only the PETG Copolyester was used for the bottle inflation experiments. A series of inflation pressures were used and the blown bottles were judged to be under-inflated (either by an incomplete bottle shape or undefined ridges formed at the shoulders of bottle), satisfactory, over-inflated (by the presence of thin walled areas) or burst, see Figure 6.2. The operating conditions used for the bottle inflation experiments are shown in Table 6.2.

TABLE 6.2: BOTTLE INFLATION OPERATING CONDIONS

Extruder
Screw Speed   24 r.p.m.
Zone 1 Temperature   174 °C
Zone 2 Temperature   260 °C
Zone 3 Temperature   200 °C
Zone 4 Temperature   200 °C
Zone 5 Temperature   185 °C

Inflation Stage
Pre-blow Air Pressure   68943 N/m² (10 p.s.i.)
Blow Time   8 seconds
Vent Time   3 seconds
Index Time   0.9 seconds
Knife Delay Time   0.05 seconds

FIGURE 6.2: INFLATED BOTTLE QUALITY

UNDER INFLATED   GOOD BOTTLE   BURST BOTTLE

6.3 Results

The results of the parison sagging experiments are shown in Figures 6.3-6.10. Figures 6.3-6.8 show the effect of different extrusion times (i.e. lengths of parisons) on the sagging behaviour.

Figure	Polymer	Temperature	Output Rate
6.3	PETG	170 °C	1.91 kg/h
6.4	PETG	170 °C	2.88 kg/h
6.5	PETG	200 °C	8.17 kg/h
6.6	PETG	200 °C	23.22 kg/h
6.7	B90S	240 °C	12.60 kg/h
6.8	B90S	255 °C	18.00 kg/h

Figures 6.9 and 6.10 show the effects of temperature and output rate on the relative parison length after a 5 second extrusion time, for PETG and B90S respectively.

The results of the bottle inflation experiments are shown in Figure 6.11, the results are shown as a percentage of the bottles blown at each inflation pressure.

FIGURE 6.3: PARISON SAGGING OF PETG AT 170C AND 1.91kg/h
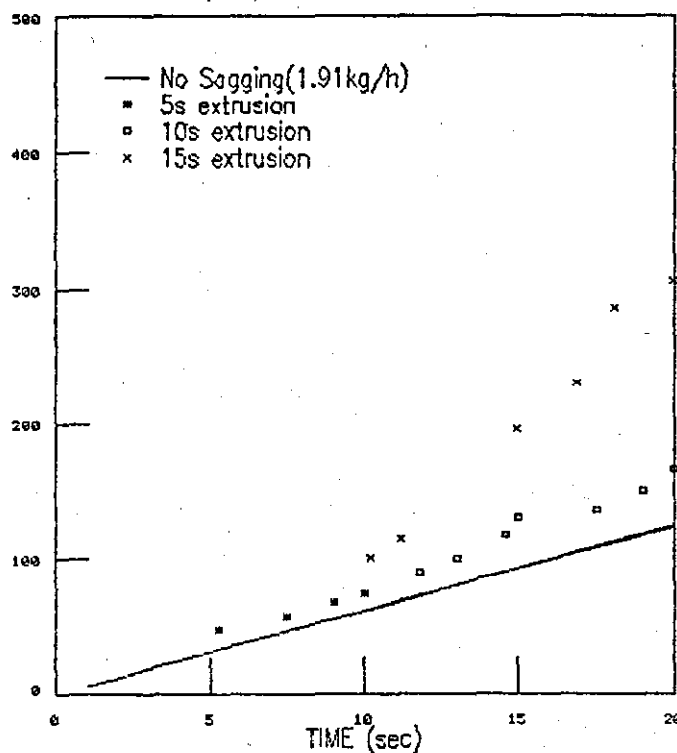
FIGURE 6.4: PARISON SAGGING OF PETG AT 170C AND 2.88kg/h
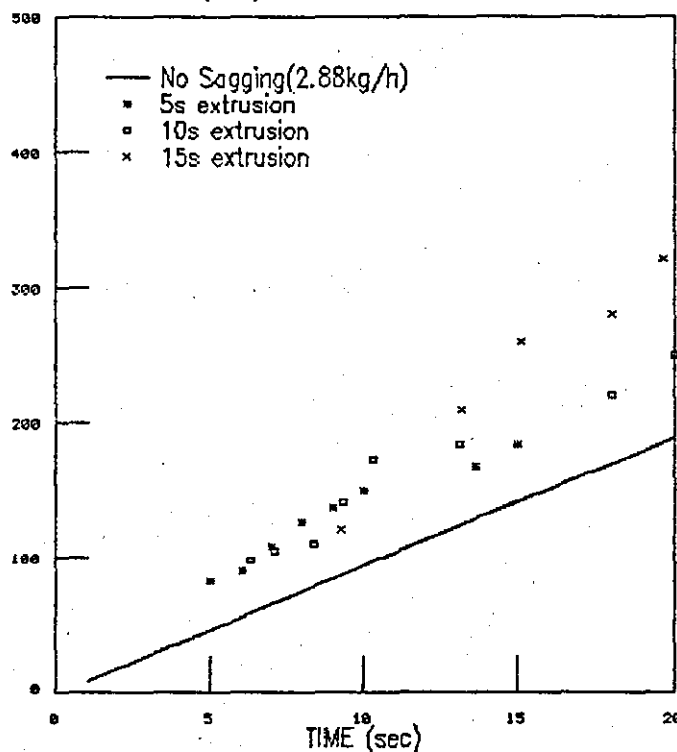
FIGURE 6.5: PARISON SAGGING OF PETG AT 200C AND 8.17kg/h

PARISON LENGTH (mm)

— No Sagging(8.17kg/h)
* 2s extrusion
□ 5s extrusion

TIME (sec)
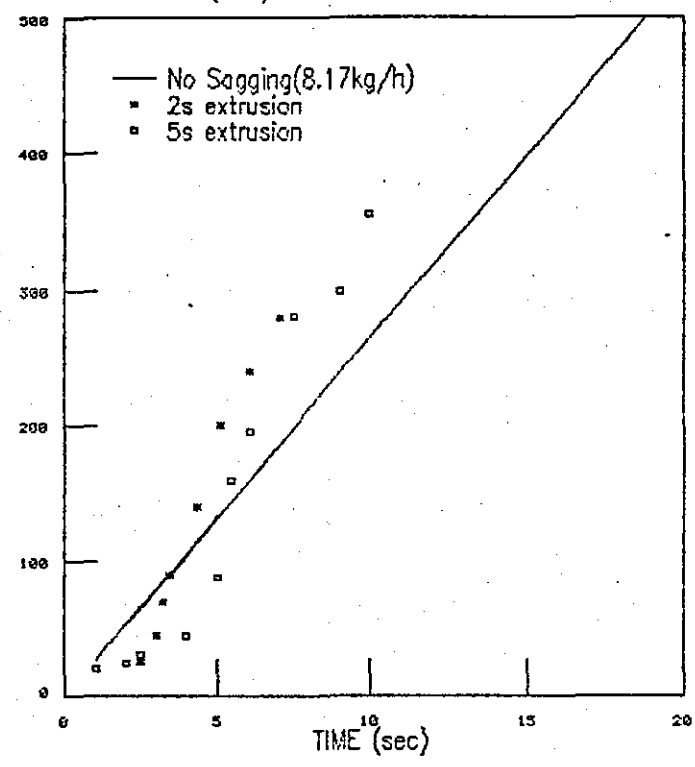
FIGURE 6.6: PARISON SAGGING OF PETG AT 200C AND 23.2kg/h

PARISON LENGTH (mm)

— No Sagging(23.2kg/h)
* 2s extrusion
□ 5s extrusion
× 10s extrusion

TIME (sec)
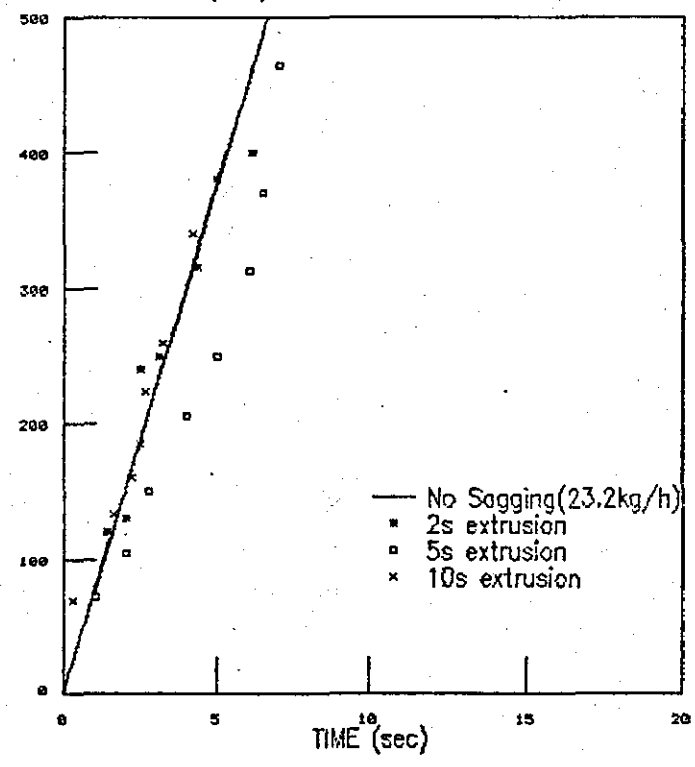
FIGURE 6.7: PARISON SAGGING OF B90S PET AT 240C AND 12.6kg/h
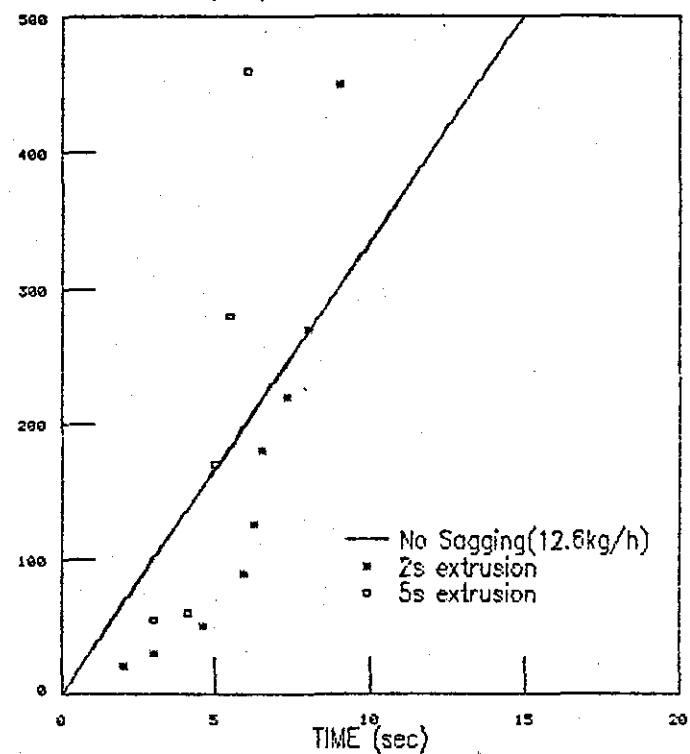
FIGURE 6.8: PARISON SAGGING OF B90S PET AT 255C AND 18kg/h

FIGURE 6.9: PETG PARISON SAGGING
5s EXTRUSION TIME

RELATIVE LENGTH

IDEAL EXTRUSION

+   170C (1.91 kg/h)
*   170C (2.88 kg/h)
□   200C (8.17 kg/h)
×   200C (23.2 kg/h)

TIME (sec)

FIGURE 6.10: B90S PET PARISON SAGGING
5s EXTRUSION TIME

RELATIVE LENGTH

+   240C (12.6kg/h)
*   255C (18 kg/h)

IDEAL EXTRUSION

TIME (sec)
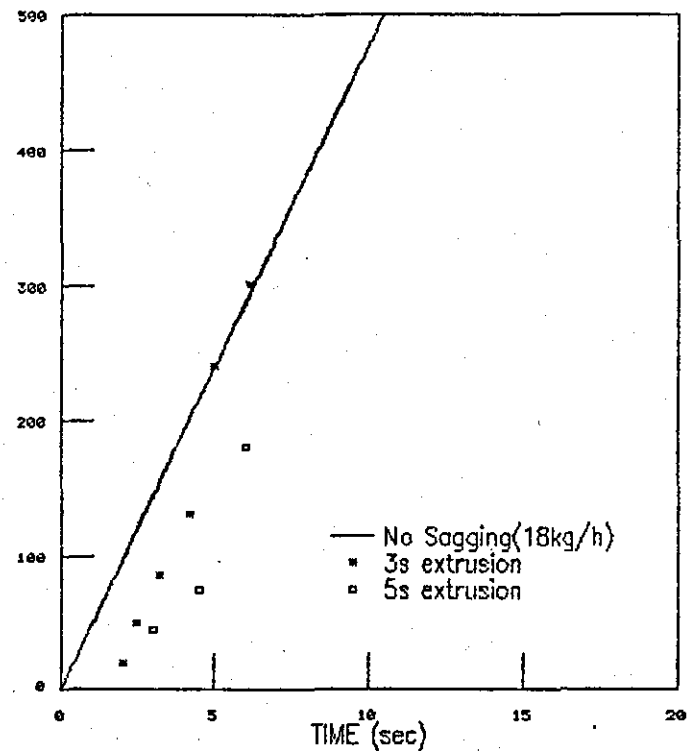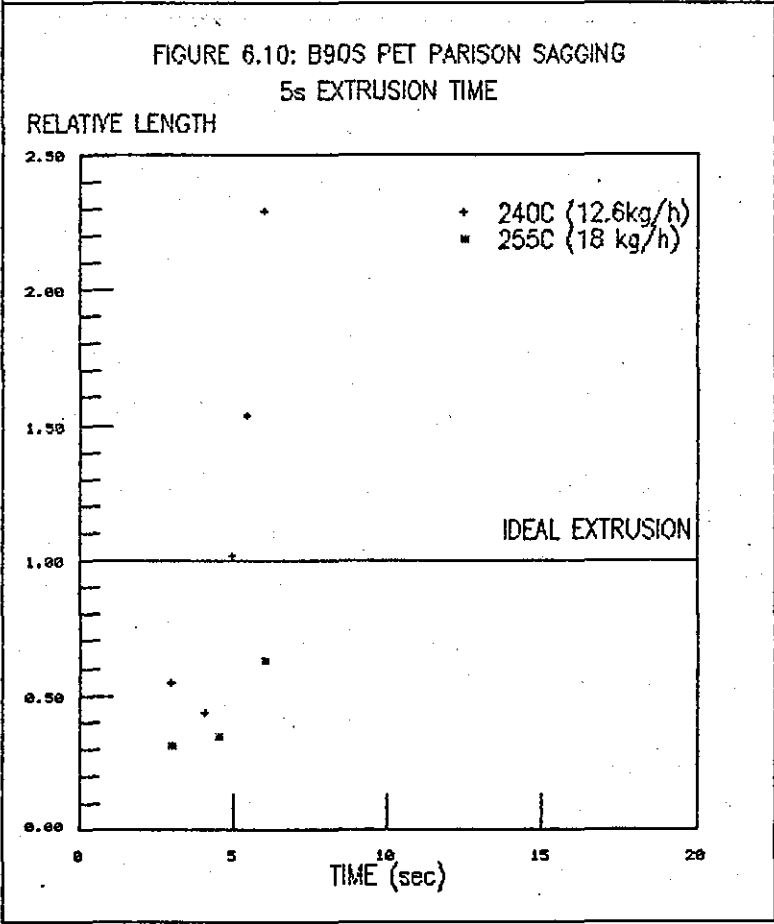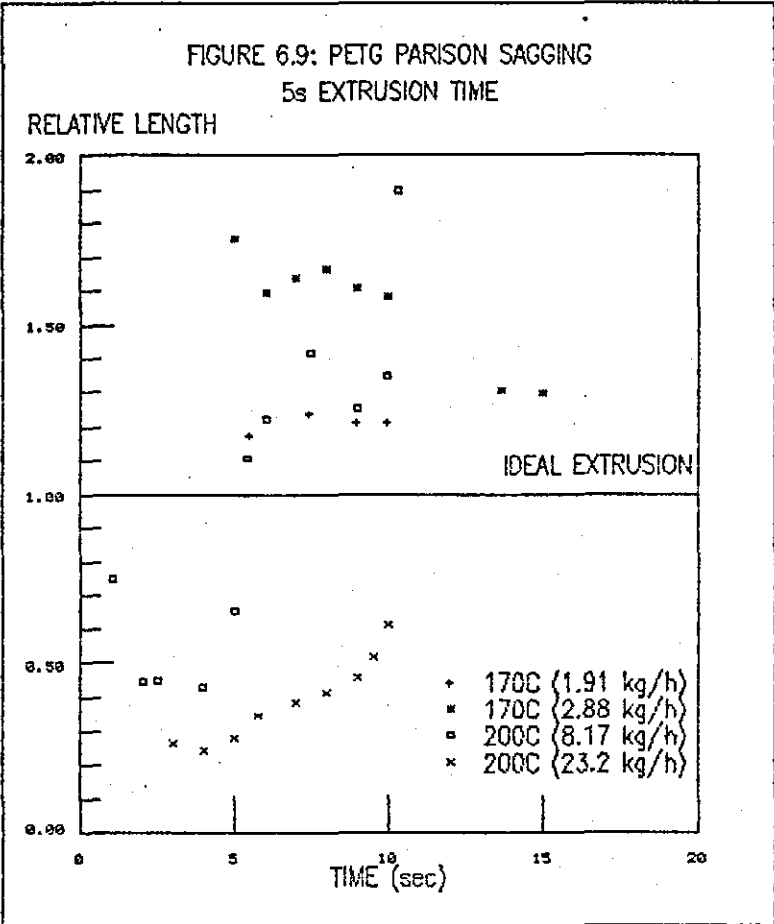
FIGURE 6.11: BOTTLE INFLATION
PETG AT 170C

% OF BOTTLES MADE

UNDER INFLATED
GOOD BOTTLE
THIN SECTIONS
BURST BOTTLE

INFLATION PRESSURE (psi)
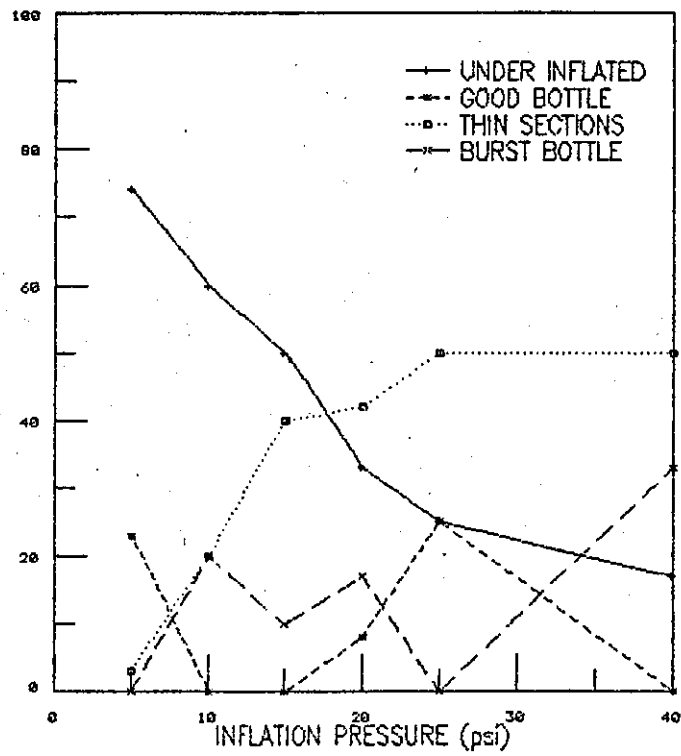
FIGURE 6.12: SHEAR VISCOSITY CURVES

VISCOSITY (Pa.s)

PETG at 170C
PETG at 200C
B90S at 270C

SHEAR STRAIN RATE (sec-1)
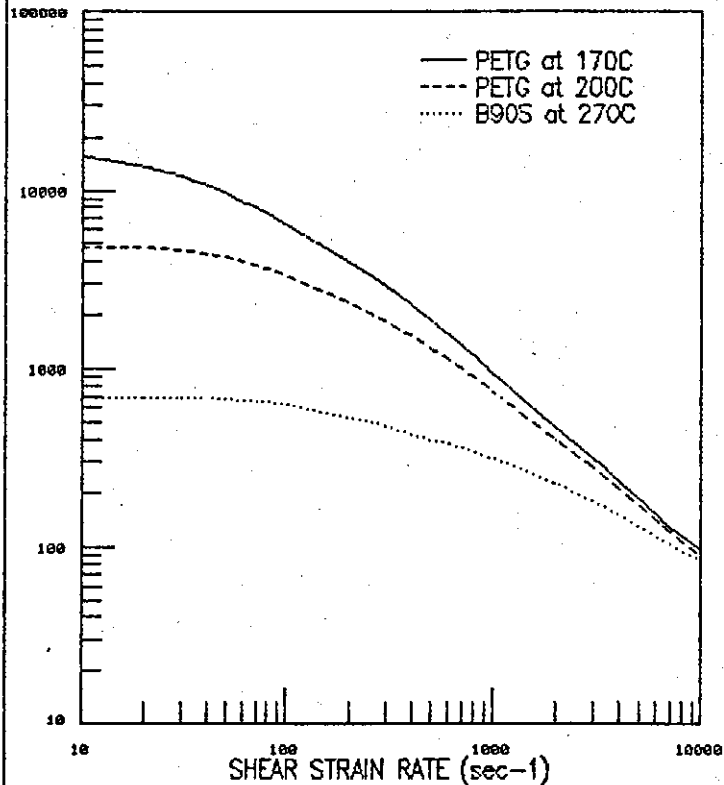
6.4 Discussion

6.4.1 Processing Experiments

<u>Parison Sag</u>

In Figures 6.3-6.6 the ideal behaviour for an incompressible melt is shown by the solid line; this shows the parison length to increase linearly with time at a rate determined by the extrusion velocity. In the early stages the parison length increases almost linearly with time. The lower rate of growth shown in Figures 6.5 and 6.6 are due to parison swelling (as the extrusion rate is constant, any increase in the radial dimensions will be accompanied by a decrease in axial distance). As time increases, the sagging (drawdown due to gravity) becomes dominant as the parison weight increases. This is illustrated by the rapidly increasing rate of growth in parison length. The effect of parison swelling is greater at the higher extrusion rates as the polymer has a shorter residence time in the die and therefore will have had less relaxation time, this results in a greater degree of elastic strain recovery. The shear stress at the die is higher which results in a greater degree of swelling. This behaviour is an increase in die swell with increasing shear strain rate as reported in the literature.[13]

The extruder used was fitted with a HDPE screw and a high restriction head. These are not recommended for PETG use as it "results in high back pressure and excessive melt temperature".[164] A PVC type screw and head are recommended for PETG.[164]

Figures 6.7 and 6.8 show the sagging behaviour for the B90S linear PET polymer, again the change in response from a predominance of the swelling behaviour to the sagging behaviour is shown.

Figures 6.9 and 6.10 show the effects of temperature and output rate on the sagging behaviour for parisons extruded in 5 seconds. The relative length is the ratio of the observed length at a given time divided by the corresponding "ideal extrusion" length. Values greater than one show a predominant sagging behaviour; values of one indicate no overall deformation of the parison; values of less than one indicate predominantly swelling and parison 'bounce' behaviour.

Figure 6.9 shows that for the PETG copolymer at short times after extrusion the swelling behaviour dominates, then the response passes through a minimum before increasing with time to a predominance of parison sagging. The minimum occurs over a period where the sag and swell are balanced. The data for the extrusion at 170°C shows the relative parison length to decrease with time, this is due to the 'bounce' exceeding the sagging at this temperature (i.e. the elastic response is greater than the viscous response). The effect of output rate was different for the two temperatures; the parison sagging increased with output rate at 170°C which suggests a tension thinning behaviour, whilst the sagging decreased with increasing rate at 200°C which suggests tension stiffening behaviour. In Chapter 4 the response of PETG in uniaxial extension was shown to be tension stiffening, see Section 4.7.4. An explanation for the apparent opposite behaviour observed at 170°C is a decreased viscosity due to a longer residence time in the extruder barrel at the lower output rate.

Figure 6.10 shows that for the B90S polymer the response was predominantly parison swelling at early times after extrusion followed by much more rapid sagging, once the viscous response started to dominate.

Bottle Inflation

Figure 6.11 shows the reduction in under-inflated bottles and the increase in observed thin sections and burst bottles with increasing inflation pressure. The occurrence of both under-inflated bottles and thin sections in bottles inflated at the same pressure shows that the process was not really stable enough to claim any optimum conditions. The presence of thin sections of bottles suggests the polymer has shown tension thinning behaviour, preferentially stretching at the weakest points of the bottle. The data obtained in Chapter 3 showed the PETG Copolyester to be tension thinning, but the data in Chapter 4 showed a tension stiffening response. However, as the bottle inflation is a free-surface uniaxial elongational deformation it is modelled more closely by the Rutherford Elongational Rheometer data from Chapter 4, i.e. the expected

behaviour during parison inflation would be a tension stiffening response. An explanation could be that the parison had an uneven parison wall thickness distribution due to the die not being centred properly, this would be more pronounced when a low viscosity melt, such as PET or PETG, is processed.

6.4.2 Comparison With Rheological Data

Parison Sagging

Baron, McChesney and Sinker[5] described the desired shear rheological properties a polymer should possess for it to be suitable for extrusion blow moulding. Figure 6.12 shows the shear rheology of the two polymers studied in these experiments. From Figure 6.12 it can be seen that PETG at 170°C fulfils the criteria laid down by Baron et al[5] better than PETG at 200°C and B90S at 270°C, having a high viscosity at low shear rates and a low viscosity at high shear rates. The criteria are based on the ability to obtain a parison having sufficient melt strength to avoid excessive sagging and to avoid melt fracture during extrusion. Figure 6.9 shows that the PETG at 170°C sags less than PETG at 200°C and B90S at 240°C and 255°C (shown in Figure 6.10). Therefore the criteria laid down by Baron et al[5] agree with the experimental observations for parison sagging. However, they fail to account for the swelling and bounce behaviour of the parison or the inflation of the bottle.

Powell[156] suggested that a comparison of the natural time of the polymer with the time scale of the deformation offers a guide to the polymers suitability for a given process. The elasticity data reported in Chapter 3 provides the natural times (equation (6.1)) for the polymers studied in these experiments:

    PETG at 170°C and 1.91 kg/h, natural time = 0.136s

    PETG at 170°C and 2.88 kg/h, natural time = 0.111s

    PETG at 200°C and 8.17 kg/h, natural time = 0.015s

    PETG at 200°C and 23.22kg/h, natural time = 0.011s

    B90S at 270°C, relaxation time = 0.034s*

(* only shear data available for B90S, Table 2.14)

The time scales involved in the extrusion of the parison and the delay before inflation are greater than all the relaxation times

which implies that viscous deformations will dominate, i.e. parison sagging will occur before the bottle can be inflated, therefore, rapid extrusion is needed; this would also result in an increased shear rate giving, a desired, greater degree of swelling.

This method which takes account of both the elastic and viscous components of the polymers behaviour indicates the likelihood of the problems that were encountered experimentally in trying to extrusion blow mould these materials.

In Section 6.1.2 some simple equations were described which predict parison deformation from a knowledge of elongational viscosity data. Equation (6.5) could not be used with the converging flow data reported in Chapter 3 as the natural time of the polymer exceeded the sag time, invalidating the assumptions used for this equation and those proposed by *Cogswell* (equations (6.6)-(6.9)). By using the stress growth function data reported in Chapter 4 as an apparent elongational viscosity equation (6.9) offered first approximations of the sagging behaviour for PETG at 170°C. An example is shown below:

Case 1

It was assumed that no swelling occurred and that no sagging occurred during extrusion of the parison. The parison was extruded for 5 seconds at an output rate of 2.88kg/hr (9.4mm parison length/second). The parison length at start of sag time was 47mm. From equation (6.6) this corresponds to a maximum initial stress of 451.7N/m². The closest comparison of viscosity data from Figure 4.8 was given by the Hencky strain rate = $0.5s^{-1}$ curve. (At 5s, $\sigma = \acute{\epsilon}.\lambda = 505N/m^{-2}$.)
Therefore: L=0.047m, $\acute{\epsilon}=0.5s^{-1}$, $\rho=980kg/m^3$ and $g=9.81m/s/s$.

Table 6.3 shows the parison sag calculated using equation (6.9) and the experimentally measured sag.

TABLE 6.3: CASE 1 PARISON SAG RESULTS

RUN TIME (s)	SAG TIME (s)	ELONGATIONAL VISCOSITY (Pa.s)	PREDICTED SAG (mm)	EXPERIMENTAL SAG (mm)
6	1	1100	9.7	50
7	2	1200	17.7	80
8	3	1300	24.5	87
9	4	1400*	30.3	101
10	5	1500*	35.4	114

* extrapolated data.

Case 2
Allows for sagging during extrusion of parison by taking the observed parison length at 5s as the length at sag time = 0. L = 0.080m The predicted and observed sag values are shown in Table 6.4.

TABLE 6.4: CASE 2 PARISON SAG RESULTS

RUN TIME (s)	SAG TIME (s)	ELONGATIONAL VISCOSITY (Pa.s)	PREDICTED SAG (mm)	EXPERIMENTAL SAG (mm)
6	1	1100	28	17
7	2	1200	51	47
8	3	1300	71	54
9	4	1400*	88	68
10	5	1500*	103	81

* extrapolated data.

It can be seen from Tables 6.3 and 6.4 that the predicted values respectively under-estimate and over-estimate the experimentally measured sagging. The predicted values in Table 6.4 show the better estimate of the actual values. The estimates shown are not very accurate and so a more rigorous analysis was tested.

Garcia-Rejon, Orbey and Dealy[12] reported a model, see Section 6.1.2, that requires stress growth function data and successfully predicted the parison deformation behaviour of HDPE and PP. As stress growth function data has been obtained for PETG at 170°C from the Rutherford Elongational Rheometer (see Chapter 4) this model has been tested for PETG Copolyester.

Using equation (6.11) the parison sagging occurring with PETG Copolyester at 170°C, during extrusion, has been predicted and compared in Table 6.5 to the observed values from the video recorded practical experiments. The swell ratios were calculated using die swell data from Chapters 2 and 3. The recoverable strain and extension were determined from Figure 2.4 and equation (3.10) respectively:

$$\gamma_R = 1.8$$

$$\varepsilon_R = 0.52$$

Equations (6.2) and (6.3) were used to determine the swell ratio product after shear and elongational flows respectively:

$$B_{SR}B_{SH} = 1.40$$

$$B_{ER}E_{EH} = 1.48$$

The observed swell ratio product was taken as the greater of the two values, i.e. 1.48, for application to equation (6.11).

TABLE 6.5: PARISON SAGGING DURING EXTRUSION

OUTPUT RATE (kg/h)	EXTRUSION TIME (s)	PREDICTED PARISON LENGTH (mm)	OBSERVED PARISON LENGTH (mm)
1.91	5	39	55
1.91	10	80	88
1.91	15	122	188
2.88	5	58	85.5
2.88	10	122	170
2.88	15	184	237

It can be seen from Table 6.5 that the predicted values under-estimate the experimentally observed values of parison length during extrusion, the model tending to under-estimate, probably due to shear heating effects during extrusion reducing the viscosity of the melt and resulting in greater parison sagging.

Using equation (6.12) the parison sagging occurring with PETG Copolyester at 170°C, after extrusion has stopped, has been predicted and added to the predicted length from Table 6.5, these values are compared to the observed experimental values in Table 6.6.

Table 6.6 shows the results using the sum of all the parison elements deformations and also the estimate from using a single element deformation, the first element to be extruded. It can be seen from Table 6.6 that the summation of all the parison elements deformations generally lead to an over-estimation, though a good agreement between the predicted and experimentally observed values was obtained at the faster output rate. By using just the first extruded elements deformation, excellent agreement was obtained for the 1.91kg/h output rate results but an under-estimate was obtained for the 2.88kg/h results.

TABLE 6.6: PARISON SAGGING AFTER EXTRUSION

EXTRUSION TIME (s)	SAG TIME (s)	PREDICTED PARISON LENGTH (mm)	OBSERVED PARISON LENGTH (mm)
OUTPUT RATE = 1.91kg/h			
First element only			
5	1	44.5	44
5	2	51.5	52
5	3	58.4	60
5	4	65.3	67.5
5	5	72.2	75
All elements			
5	1	57.5	44
5	2	77.5	52
5	3	97.3	60
5	4	117.0	67.5
5	5	136.7	75
OUTPUT RATE = 2.88kg/h			
First element only			
5	1	66	97
5	2	77	127
5	3	88	134
5	4	99	148
5	5	110	161
All elements			
5	1	86	97
5	2	116	127
5	3	147	134
5	4	178	148
5	5	209	161

The over-estimation may be due to the parison 'bounce' having been ignored, the elastic recovery in the vertical direction leading to a shorter parison length than that predicted by the model. Also the swell ratio product has been treated simply as being the greater of the two values determined from shear and elongational flows. In extrusion blow moulding dies both types of flow occur and it is possible that some interaction occurs that would increase the overall swell ratio; hence a reduced amount of sagging would be observed compared to that predicted by the model.

The under-estimation obtained for the faster output rate case, considering the first element extruded only, is probably due to a viscosity reduction occurring during extrusion caused by shear

heating in the die, the faster output rate resulting in a greater shear rate and an increase in viscous dissipation.

The model could be refined to account for the parison 'bounce' and shear-heating during extrusion. Though shear-heating may not be such a great problem with the polyolefines for which the model was originally derived and tested.[12]

Bottle Inflation

The hoop stress was calculated from equation (6.19):

$$\sigma_{HOOP} = PD \div 2H \qquad (6.19)$$

where σ_{HOOP} is the hoop stress, P is the inflation pressure and H is the final wall thickness.[15] The final wall thickness was calculated from equation (6.20):

$$H = B_R{}^3 H_d (D_d/D) \qquad (6.20)$$

where B_R is the diameter swell ratio, H_d is the die gap and D_d is the average die diameter.[15]

$$H = 1 \times 1.5 \times (18.5/34) = 0.816mm$$

If the hoop stress exceeds the melt fracture stress then unstable inflation will result. The melt fracture stress for PETG at 170°C was 0.8975MPa. Table 6.7 shows the hoop stresses for the different inflation pressures used in the bottle inflation experiments.

TABLE 6.7: PETG HOOP STRESSES

INFLATION PRESSURE		HOOP STRESS
(psi)	(N/m²)	(MN/m²)
5	34474	0.7182
10	68948	1.4364
15	103421	2.1546
20	137895	2.8728
25	172369	3.5910
40	275790	5.7457

Table 6.7 shows that at inflation pressures greater than 5 p.s.i. the hoop stress exceeds the melt fracture stress for PETG at 170°C. Therefore, the inflation will be unstable at inflation pressures above 5 p.s.i., Figure 6.9 shows that this was the case in the experiments,

both under-inflated bottles and bottles with thin walled sections were obtained at the same inflation pressure.

Powell[156] stated that the stability of inflation is dependent on the ratio of the natural time for the process, see equation (6.17) divided by the natural time of the polymer, see equation (6.1). If the ratio is greater than one then the inflation of the parison will proceed in a stable manner. If the ratio is less than one the inflation will be unstable.

The natural time for the PETG copolyester at an elongational stress of 0.7182MPa is obtained using data reported in Chapter 3:

$$t = 4754 \div 850000 = 0.0056s$$

The natural time for the process is equal to:

$$t' = \dot{\varepsilon}_{HOOP} \div \varepsilon_{HOOP} \qquad (6.17)$$

$$t' = \dot{\varepsilon}_{HOOP} \div 2.4$$

As the inflation time and therefore the hoop strain rate is unknown, estimated values were used to calculate the natural time for the process t' shown in Table 6.8.

TABLE 6.8: NATURAL TIME OF THE PROCESS

(Inflation) Deformation Time (s)	Hoop Strain Rate (s^{-1})	Natural Time (s)
10.0	0.24	0.1
1.0	2.4	1.0
0.1	24.0	10.0
0.01	240.0	100.0

Table 6.8 shows that over an exaggerated time scale range for the time taken for the parison to be inflated and contact the mould, the natural time for the process is always greater than the natural time for the polymer. This indicates that the inflation should have been stable. The experimental observations disagree with this result, possibly due to thin spots occurring on the parison. Therefore, it is concluded that the onset of melt fracture was the limiting factor to the stable inflation of the PETG Copolyester into the bottle mould in this study.

6.5 Conclusions From Chapter 6

6.5.1 Aims And Novelty

The aims of this chapter have all been achieved by the comparison of theoretical predictions and practical observations of the behaviour of the PETG Copolyester and B90S linear PET during extrusion blow moulding.

The rheological data from Chapters 2, 3 and 4 have been applied using various models from the literature and the resulting predictions have been assessed with respect to the processing of the two polymers tested. The converging flow data provided results for the natural time of the polymer which could be compared to the natural time of the process. The Rutherford Elongational Rheometer provided data, which was more applicable than converging flow data for the equations used to model parison sagging. The conclusions made in the earlier chapters as to the suitability of the two polymers to this process were verified by this study and found to be correct.

The study described in this chapter offers rheological explanations why linear PET polymers are not extrusion blow moulded and why PETG Copolyester can be used for this process. The study proves the applicability to processing of the stress growth function data obtained using the Rutherford Elongational Rheometer. The problems of modelling extrusion blow moulding are highlighted by the limited applicability of the equations available and the difficulties in obtaining the appropriate data.

6.5.2 Conclusions

The conclusions that can be made from the work described in this chapter are:

1. Although linear PET polymers are unsuitable for extrusion blow moulding their structure may be modified to increase their processabilty. Copolymers such as PETG and branched PET polymers possess the correct combination of shear and elongational, viscous and elastic properties to be successfully extrusion blow moulded. The desired combination of rheological properties that a polymer should possess for this process are: (i) a high shear

viscosity at low shear rates; (ii) a low shear viscosity at high shear rates; (iii) a high degree of elasticity, a long natural time; (iv) tension stiffening behaviour at both low and high elongation rates in free-surface uniaxial elongational flows. This combination of properties would prevent excessive parison sag and ensure stable inflation and an even thickness distribution.

2. From the parison sagging experiments with both polymers it has been concluded that: the parison length increases with time both during and after the extrusion stage. The draw-down due to gravity (sagging) increases with time, overtaking the swell effects that prevail in the early stages and dominating the parison deformation. The natural time for the PET polymers confirm that viscous deformation will generally be dominant in this situation.

3. The behaviour of the PETG Copolyester was more elastic at 170°C than at 200°C, shown by observations of a lower degree of sagging with time, also shown by greater die swell from the Davenport Capillary Rheometer experiments in Chapter 2 and 3. The tension stiffening response observed in uniaxial extension in Chapter 4, was also observed at 200°C in the parison sagging experiments. PETG Copolyester has rheological properties that permit the polymer to be extrusion blow moulded.

4. The behaviour of the B90S linear PET polymer showed run-away parison sagging, indicating a tension thinning response in uniaxial extension, preventing the polymer from being processed by extrusion blow moulding.

5. The inflation of the PETG parisons into bottles was unstable and defective bottles were obtained at all the inflation pressures used. The predominant defects changed with increasing inflation pressure: the occurrence of under-inflated bottles decreased as the number of bottles with thin wall sections and burst bottles increased. The unstable inflation was not due to the natural time of the polymer being greater than that of the process, but was

due to the hoop stress exceeding the melt fracture stress of the polymer.

6. The criteria proposed by *Baron, McChesney and Sinker*[6] for the shear rheological properties desirable in an extrusion blow mouldable polymer proved to be valid for the polymers tested in this study. However, as the predominant geometry of the flows in extrusion blow moulding are elongational, the appropriate free-surface uniaxial elongational data should be considered in preference to and in addition to the shear rheology criteria.

7. The natural time comparison for the process and the polymer proved to offer a qualitative guide for parison deformation behaviour but fails to account for the melt fracture limitation during bottle inflation.

8. The models tested for parison sagging predictions provided good estimates of the observed behaviour and have demonstrated the applicability of stress growth data to processing. However, for application to thermoplastic polyesters and copolyesters the models could be refined to account for parison 'bounce' and shear-heating effects.

6.5.3 Suggestions For Further Work

The volumetric inflation rate and the hoop strain rate should be determined experimentally, this information could be used to test the calculations for predicting the inflation pressures and inflation stability.

Processing trials should be undertaken for the branched PET polymers and PCCE Copolyester to test the conclusions made in earlier chapters as to their suitability for blow moulding. The similarities between the rheological behaviour of the branched PET polymers with PETG Copolyester suggest that they will be suitable for extrusion blow moulding.

7. Injection Stretch Blow Moulding

7.1 Introduction

7.1.1 Aims Of Chapter 7

This chapter describes an experimental programme designed to study the effect of varying the inflation pressure in injection stretch blow moulding on the final bottle properties. The processing characteristics are compared to the free surface uniaxial deformation study of PET in the thermoelastic region reported in Chapter 4.

The aim of this chapter was to compare the stretching behaviour of PET in the injection stretch blow moulding process and the Rutherford Elongational Rheometer.

7.1.2 Injection Stretch Blow Moulding

Injection stretch blow moulding differs from the conventional methods for producing hollow mouldings in two respects: stretching in axial as well as in radial directions, and the thermal conditioning in which stretching is carried out.

The use of PET in a two-stage bottle forming process comprising injection moulding a preform or parison and subsequently thermally conditioning it for blow orientation has only been practised commercially since 1977[5].

Preforms, much smaller than the finished bottle, are injection moulded. The injection moulding stage of the process has been studied by *Miller*[165], *Schaul*[142] and *Brascome*[143,144] When injection moulding the polymer into tubular preforms prior to blow moulding containers, the preforms are cooled rapidly in the mould cavity which enables the polymer to solidify without recrystallising, leaving the preform in the amorphous (transparent) state. The preforms are reheated to a temperature, just above the glass-transition temperature of the polymer; (90°-95°C) once in the 'rubbery' state, the preforms are blown into moulds of the desired container shape. The stretching of the wall of the preform as it conforms to the geometry of the mould results in biaxial orientation. While uniaxial orientation gives higher stress and modulus in one direction only and has very poor impact strength, biaxial orientation gives a better balance of mechanical

properties, excellent toughness and improved gas barrier properties. The extent of drawing is such that strain-induced crystallisation occurs. Tensile yield strength, impact strength, and creep resistance of the polymer are vastly improved as a direct result of the orientation process. The improved creep resistance of oriented containers made from PET is one of the major factors responsible for the success of these containers for packaging highly pressurised carbonated beverages.

Either a single-stage or a two-stage process can be used. The two processes differ in the way the preforms are further processed.

In the single-stage process the same machine is used to quench preforms, reheat preforms and then blow and stretch the preforms into bottles. This process is more suited to wide-necked containers. As the preform is kept in the same orientation, with respect to the machine, differential heating can be used on different parts of the preform. (This is more difficult to achieve on small containers when using the two-stage process).

In the two-stage process the same procedure is followed, but different machines are used for injection moulding the preforms and blow moulding the bottles. Therefore, the preforms that have been cooled to room temperature must be heated again to the stretch blow moulding temperature. However, the preforms can be stored, between stages.

Both processes employ the same principle for forming the bottle: stretching by means of a stretching rod and radial expansion by means of compressed air. *Miller*[165] observed that as the stretching rod travels downwards, air pressure is introduced blowing the bottle in the hoop direction simultaneous to the axial extension. The rod continues downwards guiding the preform, whilst the air continues to inflate the bottle. The blow pressure is maintained until the preform has been fully blown and cooled. This deformation sequence has been confirmed by *Erwin, Gonzalez and Pollack*[166] and *Cakmak, White and Spruiell*.[167]

The three problem areas in PET preform injection moulding were identified by *Schaul*[142] and *Brascome*[143,144] as acetaldehyde

generation, preform haze and molecular weight reduction. The acetaldehyde generation is a function of the heat history since it is generated as a product of the thermal degradation of PET. It is a product of thermochemical degradation and, to a lesser extent, oxidative degradation. The major chemical reaction involves ester link decomposition with a secondary reaction being the thermal decomposition of the hydroxyethyl end groups (see Figure 7.1).

FIGURE 7.1: CHEMISTRY OF ACETALDEHYDE FORMATION[168]

Ester Link Decomposition

1   ⌁⟨O⟩–C.O.CH₂CH₂.O.C–⟨O⟩⌁⌁⌁

                     ↓

2   ⌁⟨O⟩–C.OH + CH₂=CHOC–⟨O⟩⌁⌁⌁

                                Vinyl Ester End (A)

3   ⌁⟨O⟩–C–O.CH₂CH₂OH + A

                                  ↓

       CH₃CHO ⌁⌁⟨O⟩–C.OCH₂CH₂O.C⟨O⟩⌁

       (AA)   (PET)
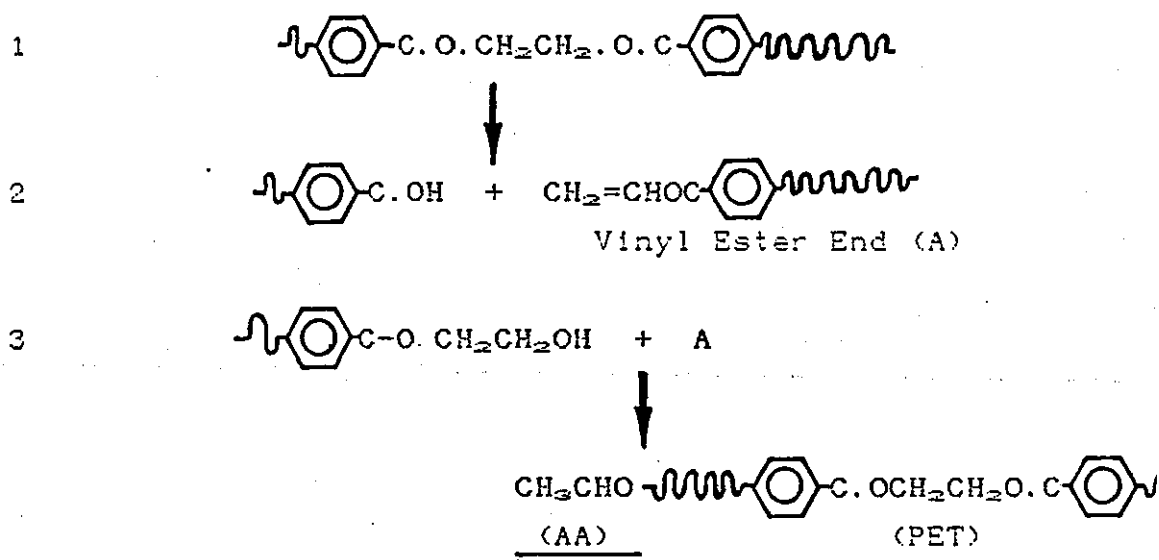
Thermal Decomposition of Hydroxyethyl End Groups

    ⌁⌁⌁⟨O⟩–C.O.CH₂CH₂OH   (PET)

                    →

       ⌁⌁⟨O⟩–C.OH + CH₃CHO   (AA)
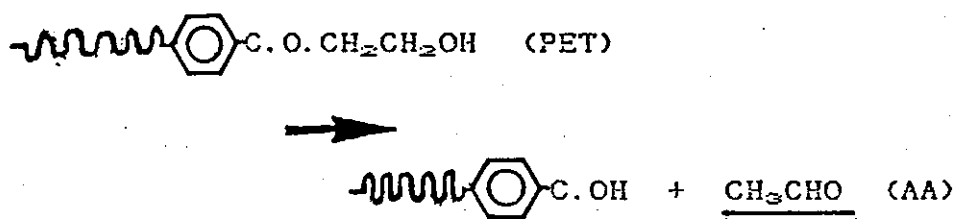
Acetaldehyde causes problems with beverage containers as even trace quantities can taint the taste of the contents which may be disastrous for food applications. It can be reduced by increasing the

injection rate and decreasing the barrel temperature[144] or can be removed at the reheating stage by extending the preheat time.[165] Preform haze is a function of thermal-induced crystallisation (spherulitic-type) which necessitates rapid cooling of the preforms in the injection mould; if a preform lacks clarity it may not be able to achieve the required draw ratio, since the preform has crystallised. This is due to amorphous PET at temperatures above the glass-transition point being more extensible than partly-crystalline PET. Molecular weight drop occurs if the polymer has not been dried sufficiently; in addition, if the barrel temperature and residence time are excessive this can lead to more rapid crystallisation (resulting in haze) and reduced mechanical properties in the bottle.[143]

During the blowing phase the stretch blow moulds are cooled with water. It has been reported that the inflation pressure must be fairly high (12 to 20 bar, 1.2 to 2.0 MN/m^2). Miller[165] reported that the hoop tensile strength of the bottle increases with increasing blow pressure, due to an increased rate of orientation which acts preferentially in the hoop direction. The cooling time in the mould must be chosen so that the finished article does not deform when ejected.

Further improvement in gas barrier properties of PET has been achieved by coating the bottles with a PVdC latex. This allows beer to be packaged with an acceptable shelf life against oxygen ingress.

Improvements in the high-temperature resistance can be made by 'heat setting' the containers, this results in further crystallisation, sufficient to allow hot filling.

The markets for injection stretch blow moulded PET containers include: bottles for carbonated beverages, bottles for beers, table waters, wines and spirits, containers for foods, edible oils, sauces, household chemicals, pharmaceuticals, cosmetics and toiletries.

The injection stretch blow moulding process was described in detail by Fritz.[169]

The high production rates (up to 10000 bottles/hour) are achieved by using the two-stage process with rotating tables which

condition the preforms prior to stretching and then mould the bottles on a continuous basis. The conditioning is achieved using infra-red heating elements which raise the temperature of the preform above the T_g of the polymer so that the rheological and thermal properties are correct for stretching. The rotating table containing the moulds accepts a preform, closes the mould, lowers the push-rod, inflates the bottle, cools the bottle, opens the mould and ejects the bottle.[169]

To enable small volume containers (e.g. half-litre) to be made higher molecular weight polymers are used to achieve acceptable conditioning times, homogeneous biaxial orientation, coupled with reasonable stretching rates.[169]

Leigner[170] determined the natural blow characteristics of various preform designs by free blowing the preforms. The stretch characteristics were related to the preform design allowing bottles having optimum properties to be designed by matching the natural stretch ratio of the preform with the ratio of the blow mould to the bottle preform. As PET stretches, it strain-hardens (crystallisation) thus increasing the stress required for further strain to occur. Stress-whitening and fibrilation occurs above a internal stretch ratio of about 6, demonstrated by the observation of microvoids in the preform wall. The onset of stress-whitening acts as a limiting stretch ratio for the preform design. The hoop stretch ratio and bubble wall thickness were found to be proportional to the preform heat up time, whilst the axial stretch ratio was relatively unaffected. Also, the hoop stretch ratio was proportional to the blow pressure. The limiting blow pressures result in incomplete blowing or ruptured bubbles. It was found to be that the stretch ratio is inversely proportional to the molecular weight of the PET.[170] To prevent local thinning or thickening of PET and to achieve a uniform wall thickness reduction increasingly high surface stretch ratios are necessary as the molecular weight increases.[169]

Miller[165] reported that increased blow pressures cause a slight increase in the hoop tensile strength while the axial tensile strength remains unchanged. The inside stretch ratio was found to be significantly higher than the outside bottle ratios.

Fifer[171] reported that during stretching and blowing, a thickness levelling effect is obtained and a 200% expansion developed the highest tensile strength. *Ola*[172] also observed this effect which is due to the stabilising influence of PET as it crystallises. The oriented crystallites are "stiffer", i.e. more resistant to further deformation.

Chedd and Haworth[173] studied the effects of preform design on final bottle properties including creep under the internal pressure of a carbonated liquid. Greater creep deformation occurred at the label panel area near the base where the wall section was thinnest. The creep compliance (creep strain/tensile stress) was found to increase with hoop stress. A lower creep compliance was obtained by inducing significant crystallisation during stretching.

In designing a pressurised bottle two aspects need to be considered: (1) the retention of gases in the bottle, and (2) the mechanical stability of the bottle.[174] *Wu and Stachurski*[174] described models for predicting the bursting pressure of oriented plastic bottles. They reported that the yield pressure (and bursting pressure) increases with the draw ratio in the hoop direction of a PET bottle and that strain hardening can prevent the bottle from bursting.

Analysis of the deformation that occurs during blowing has been studied by *Erwin, Gonzalez and Pollock*[166] and also by *Cakmak, White and Spruiell*[167] and has been described as a "sausage balloon" geometry, (see Figure 7.2).

FIGURE 7.2: "SAUSAGE BALLOON" DEFORMATION[166]
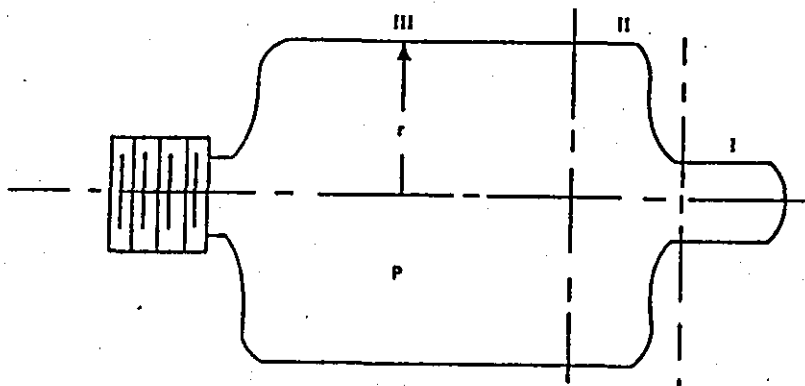
Cakmak et al[67] made direct measurements of the deformation behaviour during stretch blow moulding by using a mould fitted with spring-loaded LVDT transformers in different locations in the mould. A series of inflation pressures were used, the pressure remained constant once it had reached the set level. Membrane theory was applied to the deformation zone. The axial and radial displacement data was used to calculate the hoop and meridional stresses in the deformation zone; the difference between the hoop and meridional stresses as a function of radius showed the dominance of the hoop stress. This observation led them to conclude that the overall stress field causes a higher stretching in the hoop direction than in the axial direction.

Erwin et al[66] used PET stress-elongation data, from a series of film samples stretched on a biaxial film stretcher, to determine a model of the stretch blow moulding process. Using two sets of equations for the hoop and meridional stresses, one set from thin-wall shell theory and the other set from a constitutive relationship based on strain invariants and strain energy, the bottle blowing process was analysed. The axial stretch as a function of hoop stretch in cylindrical geometries was determined as shown in Figure 7.3. The pressure required to achieve a stretch was also determined as shown in Figure 7.4. This shows that a high initial pressure was required to initiate the inflation, but once the 'neck' formed the high pressure was not required to sustain inflation. The curvature of the meridian is approximately equal to the radius of the preform which doubles the radial stress of the preform at a given pressure. This results in a blow propagation pressure about half that of the blow initiation, see Figure 7.5. The natural draw ratio in the hoop direction can be determined as being half the maximum inflation pressure shown in Figure 7.4. The PET in the 'neck' expands until it can support the blowing pressure in a cylindrical geometry. The PET not in the deformation zone will relax until the 'neck' propagates to it, at which time it will expand through non-cylindrical geometries to the free-blow diameter (natural draw ratio in the hoop direction). After all the bottle has expanded to the free-blow diameter then

uniform stable expansion will ensue until rupture.

FIGURE 7.3 BALANCE AS A FUNCTION OF HOOP STRETCH[166]
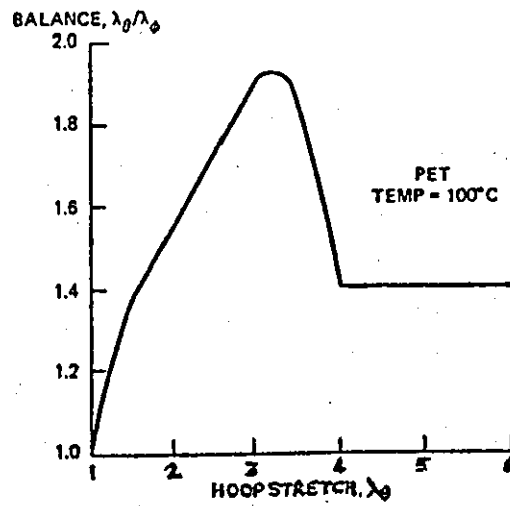
FIGURE 7.4: PRESSURE AS A FUNCTION OF HOOP STRETCH[166]
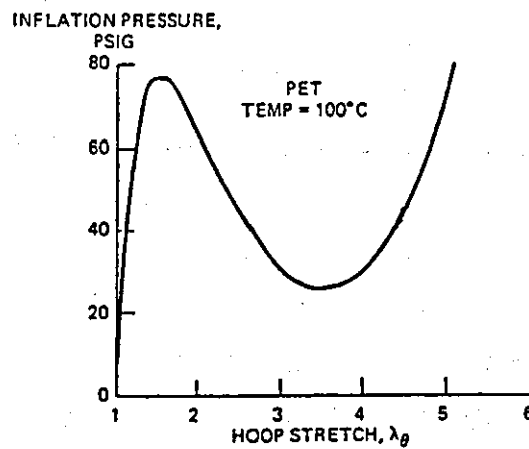
FIGURE 7.5: FREE BLOW PRESSURE AS A FUNCTION OF TIME[166]
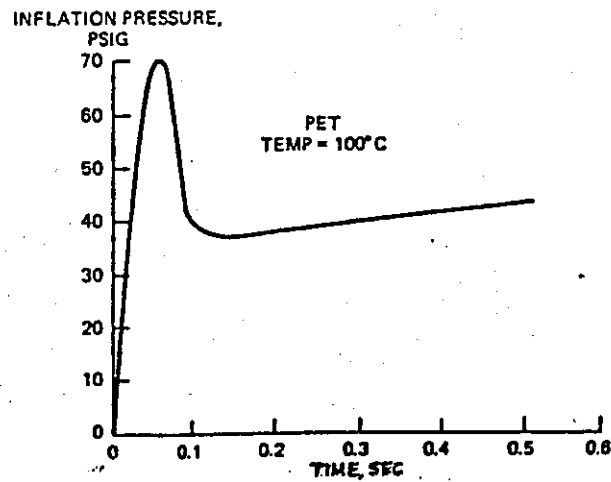
If the bottle diameter at the natural draw ratio is greater than the desired bottle diameter then there will be difficulty in obtaining a uniform wall thickness as the natural process stability will be lost.[166] The overall stress field causes a higher stretching ratio in the hoop direction than in the axial direction.[167]

Cakmak, Spruiell and White[175] investigated the molecular orientation in PET injection stretch blow moulded bottles. The birefringence Δn_{23} (hoop-thickness) (see Figure 7.6) was greater than Δn_{13} (axis-thickness), the Δn_{12} (axis-hoop) birefringence was negative. There is a difference in the draw ratio between the inner surface and outer surface of the bottle; this results in a difference between the inner and outer surface birefringence values, determined using an Abbe Refractometer.[165,175]. The inner Δn_{23} and Δn_{13} were greater than the outer values. Higher inflation pressures resulted in higher Δn_{23} values. The molecular chain axes were concluded to be equi-biaxial, with respect to the developed orientation in the axial and hoop directions. The benzene rings align parallel to the bottle surface.

FIGURE 7.6: BOTTLE AXES FOR BIREFRINGENCE MEASUREMENTS
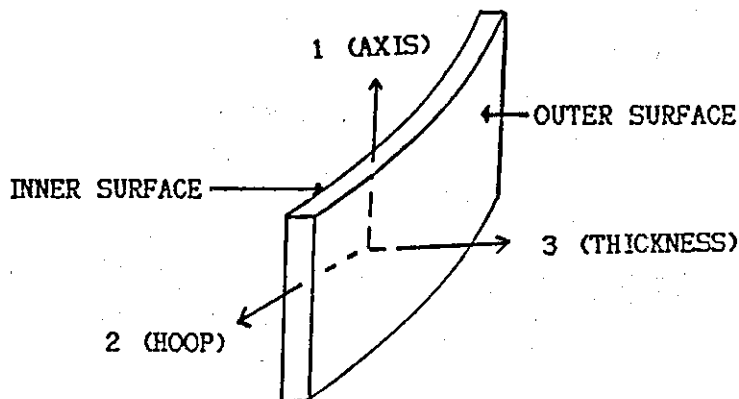
These studies that relate stretching behaviour measurements to a theoretical model form the bridge between the laboratory measurements and processing practice that this chapter is attempting to cross by comparing the stretching behaviour of PET in the Rutherford Elongational Rheometer with practical stretch blow moulding processing.

7.2 Experimental Procedure

7.2.1 Processing Experiments

The injection stretch blow moulding processing experiments were carried out on a commercial production line at Carters Ltd, Long Eaton. The two stage reheat blow process was used, with push-rod axial stretching and air pressure biaxial inflation. Injection moulded preforms, made with 'Melinar' B90S grade PET polymer, were taken from stock and used in the experiments.

A series of 47g preforms were stretch blow moulded on a SIDEL machine into 2 litre bottles. The standard operating conditions are shown in Table 7.1. The inflation pressure was varied as shown in Table 7.2. At an inflation pressure of 0.4 MN/m² incomplete bottles were obtained as shown in Figure 7.7.

TABLE 7.1: STANDARD OPERATING CONDITIONS

Preform Weight	47g
Bottle Size	2 litre
Line Speed	5775 bottles/hour
Temperature Of Air In Oven	128°C
Residence Time In Oven	23.8s
Preform Temperature	92°C
Air Line Pressure	1.5 MN/m²
Individual Mould Pressures	0.8-1.0 MN/m²
Mould Temperature	12°C
Axial Draw Ratio	2.2
Hoop Draw Ratio	3.8

TABLE 7.2: EXPERIMENTAL CONDITIONS

	Line Pressure (MN/m²)	Mould Pressure (MN/m²)
A	0.4	0.2
B	0.8	0.39
C	1.1	0.7
D	1.3	1.03
E	1.5	1.1

FIGURE 7.7: INCOMPLETE BOTTLE BLOWING

COMPLETE   INCOMPLETE
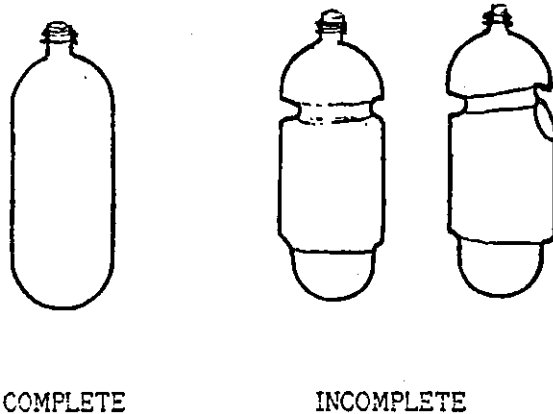
Bottles produced under the different conditions were tested using the manufacturers quality control methods for burst strength, top load strength and thickness distribution. Also, to determine the orientation distribution, the birefringence was measured and thermal shrinkage tests were carried out.

7.2.2 Burst Pressure

The burst strength of five bottles from each inflation pressure were determined using a purpose built piece of equipment (see Figure 7.8) capable of recording the internal pressure at burst. The bottle was filled with water and clamped into the equipment. The internal pressure was increased manually until bursting occurred. The rate of pressure increase was kept approximately constant.

7.2.3 Top Load Strength

The top load strength (resistance to buckling) of five bottles from each inflation pressure was determined using the equipment shown schematically in Figure 7.9. An empty bottle is clamped into the equipment. A compressed air-line applies a pressure to a plunger that makes secure contact with the neck of the bottle. The pressure was increased at a constant rate of 1 p.s.i./second. The pressures at which the bottles buckled were recorded. It is essentially an 'elastic instability' test, done in axial compression.

FIGURE 7.8: BURST PRESSURE EQUIPMENT

PRESSURE GAUGE

TAP

WATER-FILLED PET BOTTLE

SAFETY CABINET

HYDRAULIC PUMP

DRAIN HOLE
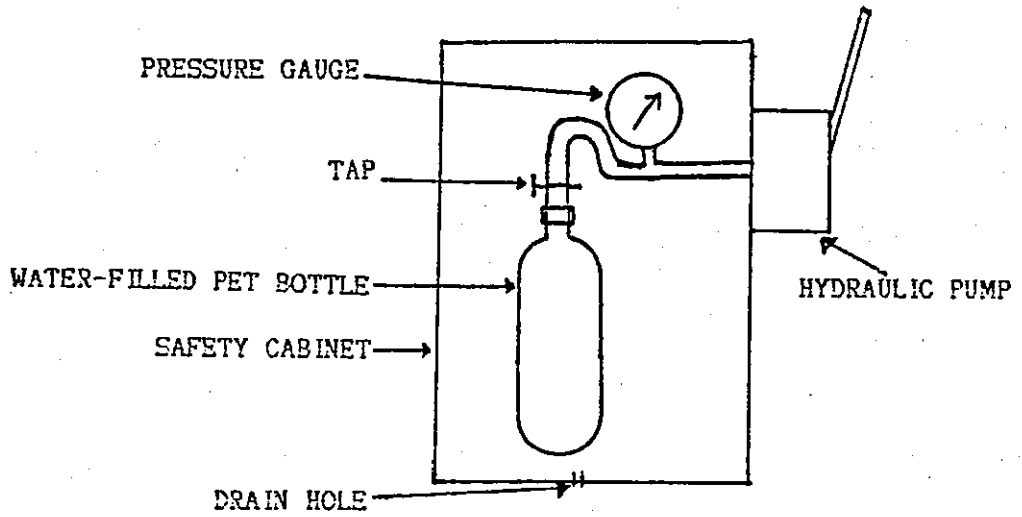
FIGURE 7.9: TOP LOAD STRENGTH EQUIPMENT

PRESSURE GAUGE

COMPRESSED AIR

VALVE

PISTON

PET BOTTLE

BOTTLE STAND
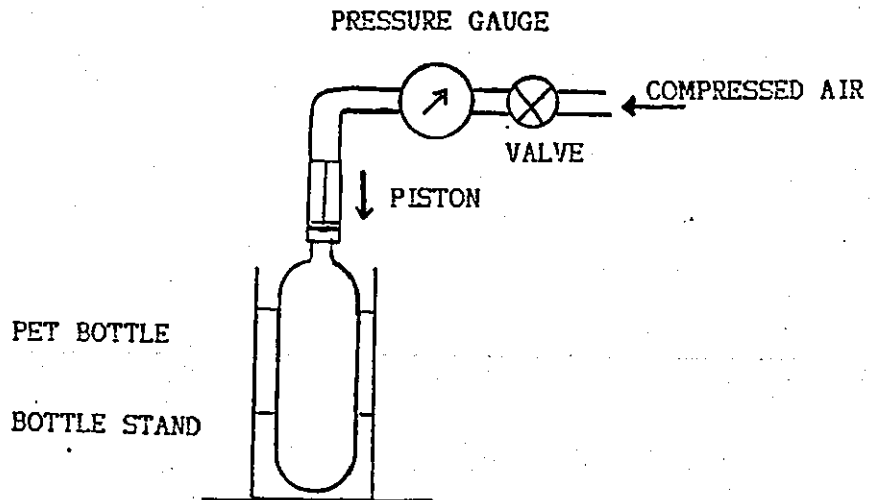
7.2.4 Thickness Distribution

Thickness distributions were obtained for all the bottles included in the analysis using a fully automatic 'Gawis 1100' infra-red measuring device. By rotating the bottle and scanning along the bottle axis, measurements at 80 different position were enabled. An average matrix for each bottle was also produced.

7.2.5 Tensile Strength Measurements

Five dumb-bell specimens were cut in the axial and hoop directions from the label panel of bottles from produced at each inflation pressure. The specimens were tested at 21°C on a JJ Lloyd Instruments Type T5002 tensile testing machine, at a cross-head speed of 10mm/min and using a 500N load cell.

7.2.6 Birefringence Measurements

Ten bottles from each inflation pressure were tested. The difference between the refractive indices in the hoop and the axial directions is the Δn_{12} birefringence. This gives an indication of the inbalance between hoop and axial orientation. Values of Δn_{12} were measured through the label panel of the bottle sidewall using a spectroscopic method.[176] *Chedd and Haworth*[173] tried to measure the other two birefringence values Δn_{13} and Δn_{23}, but were unsuccessful as surface scatter from the sectioned PET prevents any spectroscope trace being obtained.

A sample is cut from the bottle label panel and placed between crossed polars in a KONTRON UVIKON 810 ultra-violet spectrophotometer. With the h-lamp on a wavelength scan was made between 450-800nm. A trace is obtained which has a series of peaks. The peak number was plotted as a function of the reciprocal of the peak wavelength. A tangent was drawn at a wavelength of 546nm, the gradient of the tangent is equal to the optical retardation. Equation (7.1) shows that the optical retardation divided by the sample thickness is equal to the average through-thickness birefringence.

$$\overline{\Delta n} = [m \div (1/\lambda_m)] \div h \qquad (7.1)$$

where **m** is the peak number, λ_m is the peak wavelength and **h** is the sample thickness.

7.2.7 Shrinkage Tests

Samples were cut from the label panel of five bottles from each batch, produced with different inflation pressures, and a 50mm line marked on the sample in both the hoop and axial directions. The samples were then placed in an air oven at 80°C for 15 minutes. Shrinkage occur when oriented amorphous plastics are heated to a temperature above the glass-transition point. After cooling the lines marked on the samples were remeasured and the percentage shrinkage in the hoop and axial directions were calculated.

7.3 Results

Typical tensile stress-strain curves obtained for axial and hoop specimens at each inflation pressure are shown in Figure 7.10. The other results are shown as a function of inflation pressure.

The burst pressure and top load strength results are shown in Figures 7.11 and 7.12 respectively. Table 7.3 shows the thickness distributions at a height of 219mm above the bottle base, this is within the label panel area where the maximum hoop strain occurred. Appendix 12 shows the complete thickness matrices for the bottles included in Table 7.3. Figure 7.13 shows the average wall thickness for all the bottles tested at each inflation pressure; the wall thickness at 219mm above the base is shown.

Figures 7.14-7.16 show the effect of inflation pressure on the ultimate tensile strength, yield strength and tensile modulus in both the hoop and axial directions respectively.

Figure 7.17 shows the Δn_{12} birefringence as a function of inflation pressure. Figure 7.18 shows the results from the shrinkage tests.

TABLE 7.3: ABSOLUTE THICKNESSES 219mm ABOVE THE BASE

PROCESSING CONDITIONS (MN/m^2)										AVERAGE
0.2	Best A	26	25	25	25	25	25	25	26	25
0.2	Worst A	34	24	11	11	11	24	24	22	20
0.39	Best B	24	24	25	25	25	25	24	24	25
0.39	Worst B	27	25	24	23	23	24	27	28	25
0.7	Best C	25	26	25	25	26	25	25	25	25
0.7	Worst C	25	25	27	28	28	26	25	25	26
1.03	Best D	26	26	27	26	26	26	26	26	26
1.03	Worst D	27	27	28	30	32	31	30	28	29
1.1	Best E	28	29	29	30	30	30	29	28	29
1.1	Worst E	28	28	29	31	32	33	28	27	30

FIGURE 7.10(a): TENSILE PROPERTIES OF
0.2 MPa INFLATION PRESSURE BOTTLE
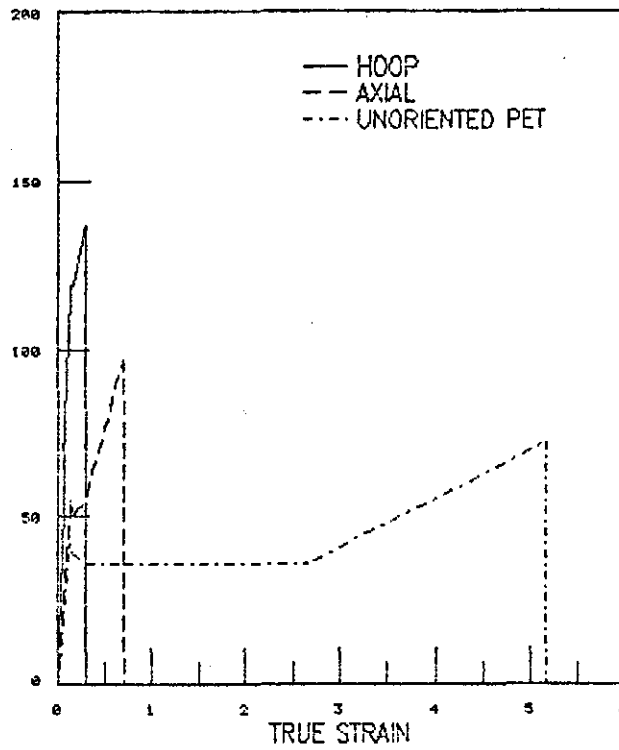
FIGURE 7.10(b): TENSILE PROPERTIES OF
0.39 MPa INFLATION PRESSURE BOTTLE
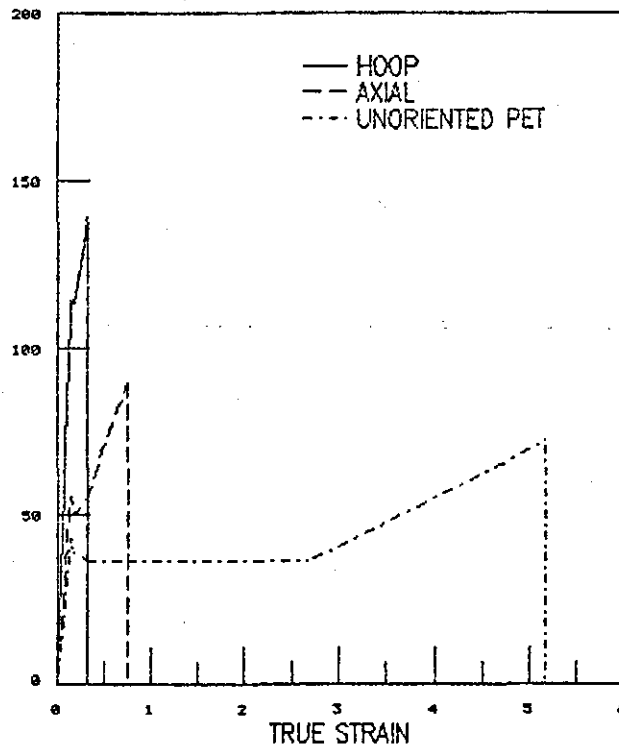
FIGURE 7.10(c): TENSILE PROPERTIES OF
0.7 MPa INFLATION PRESSURE BOTTLE

STRESS (MN/m2)

HOOP
AXIAL
UNORIENTED PET

TRUE STRAIN
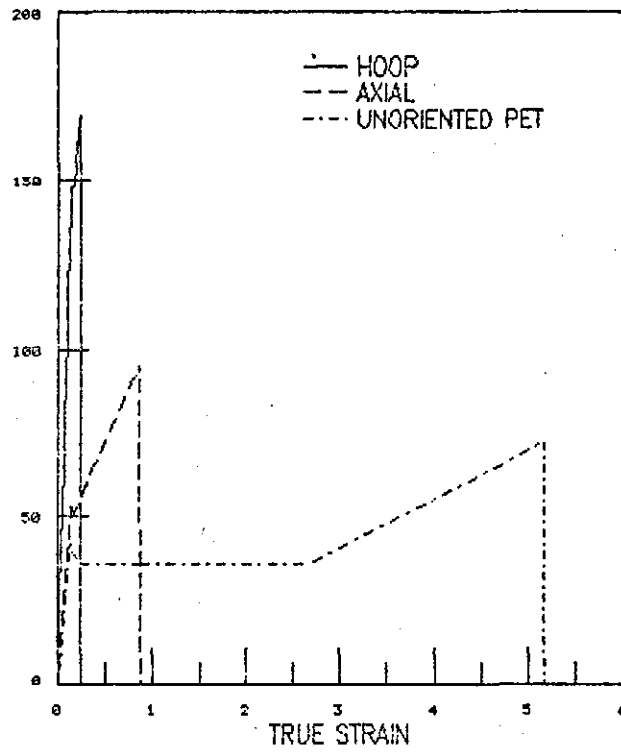
FIGURE 7.10(d): TENSILE PROPERTIES OF
1.03 MPa INFLATION PRESSURE BOTTLE

STRESS (MN/m2)

HOOP
AXIAL
UNORIENTED PET

TRUE STRAIN
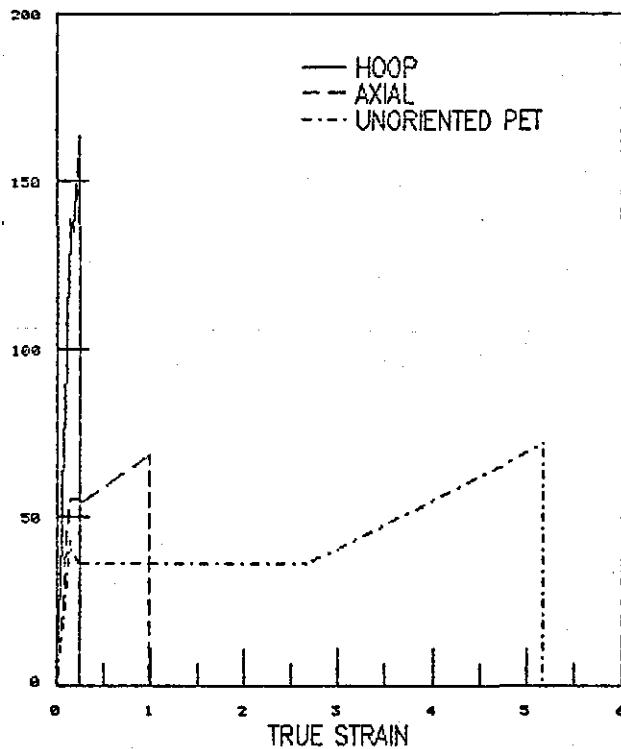
FIGURE 7.10(e): TENSILE PROPERTIES OF
1.1 MPa INFLATION PRESSURE BOTTLE

STRESS (MN/m2)

HOOP
AXIAL
UNORIENTED PET

TRUE STRAIN
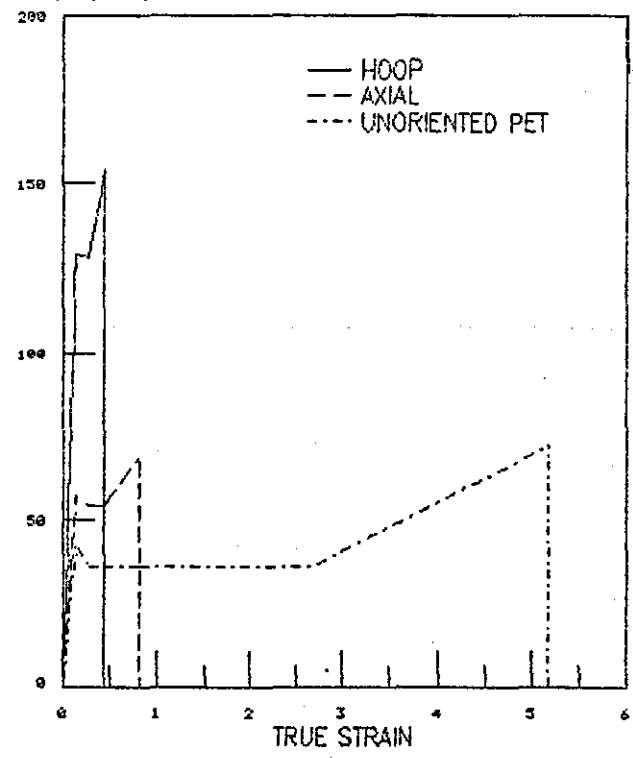
FIGURE 7.11: BURST PRESSURE
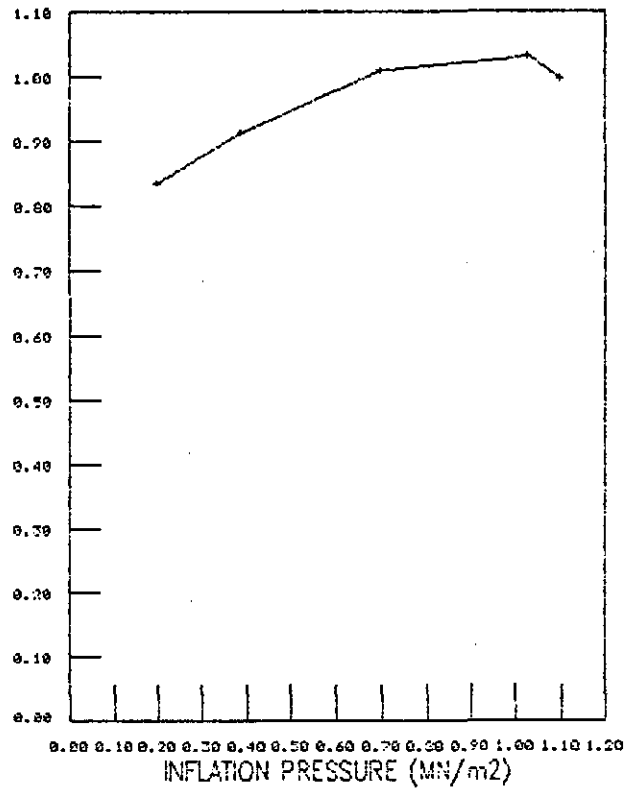
FIGURE 7.12: TOP LOAD STRENGTH
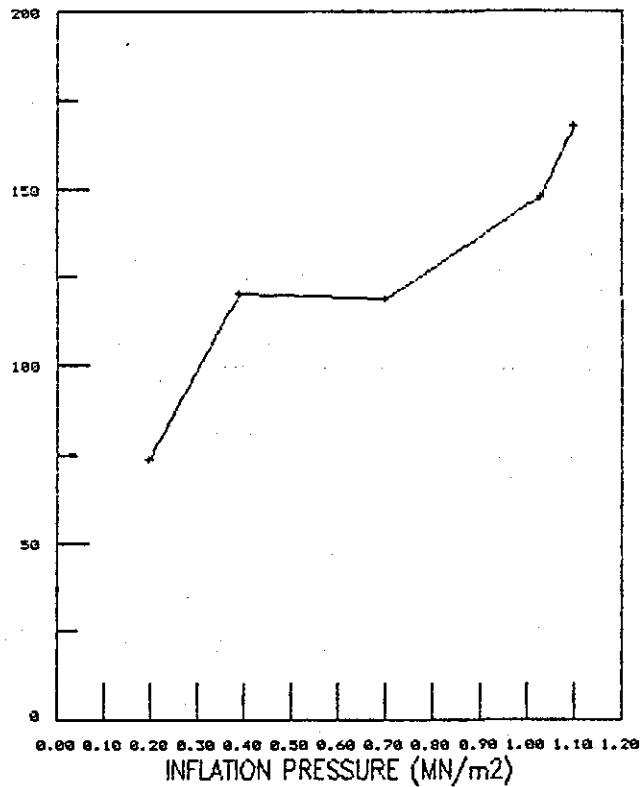
FIGURE 7.13: AVERAGE WALL THICKNESS

THICKNESS (mm)

+S.D.

-S.D.

INFLATION PRESSURE (MN/m2)
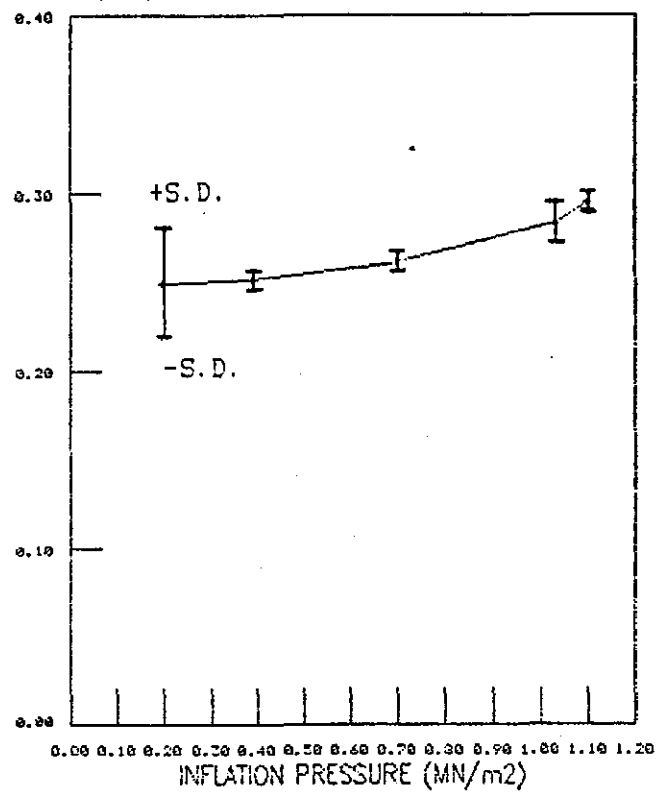
FIGURE 7.14: ULTIMATE TENSILE STRENGTH

UTS (MN/m2)

---- HOOP
···■··· AXIAL

INFLATION PRESSURE (MN/m2)
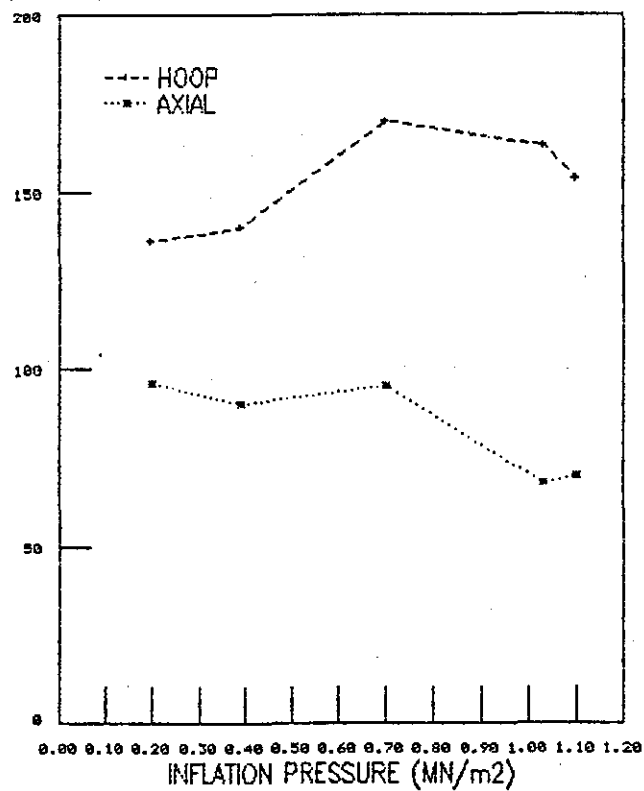
FIGURE 7.15: TENSILE YIELD STRESS

STRESS (MN/m2)

INFLATION PRESSURE (MN/m2)
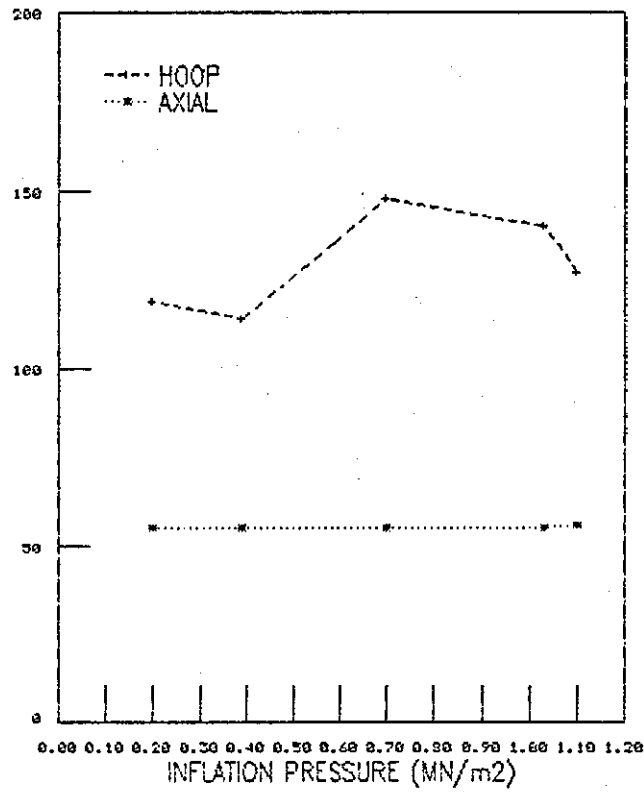
FIGURE 7.16: TENSILE MODULUS

MODULUS (MN/m2)

INFLATION PRESSURE (MN/m2)
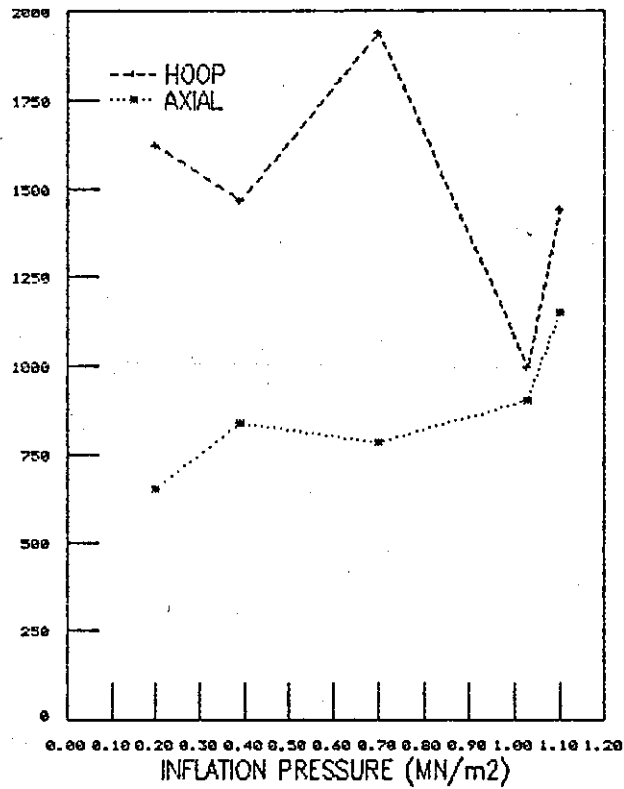
FIGURE 7.17: BIREFRINGENCE

BIREFRINGENCE (x10−3)

INFLATION PRESSURE (MN/m2)
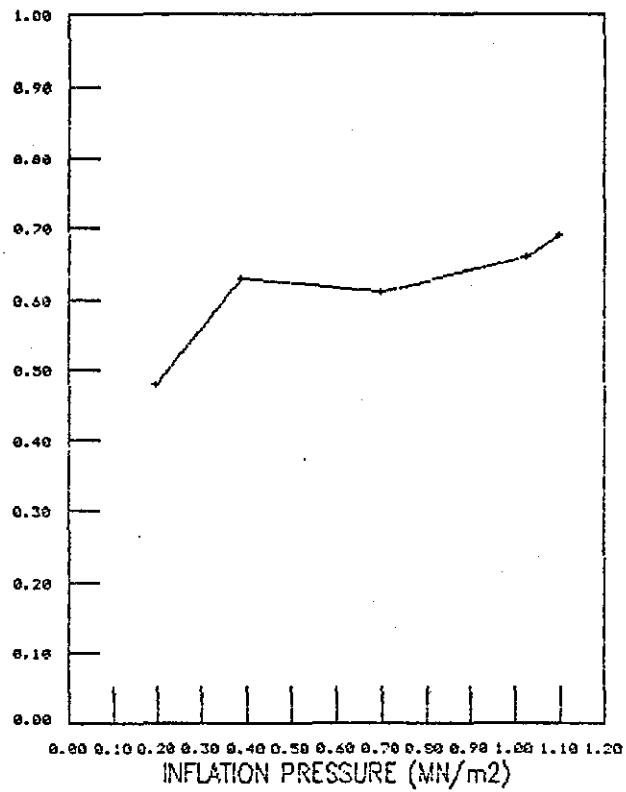
FIGURE 7.18: SHRINKAGE AT 80C

SHRINKAGE (%)

HOOP SHRINKAGE
AXIAL SHRINKAGE

INFLATION PRESSURE (MN/m2)
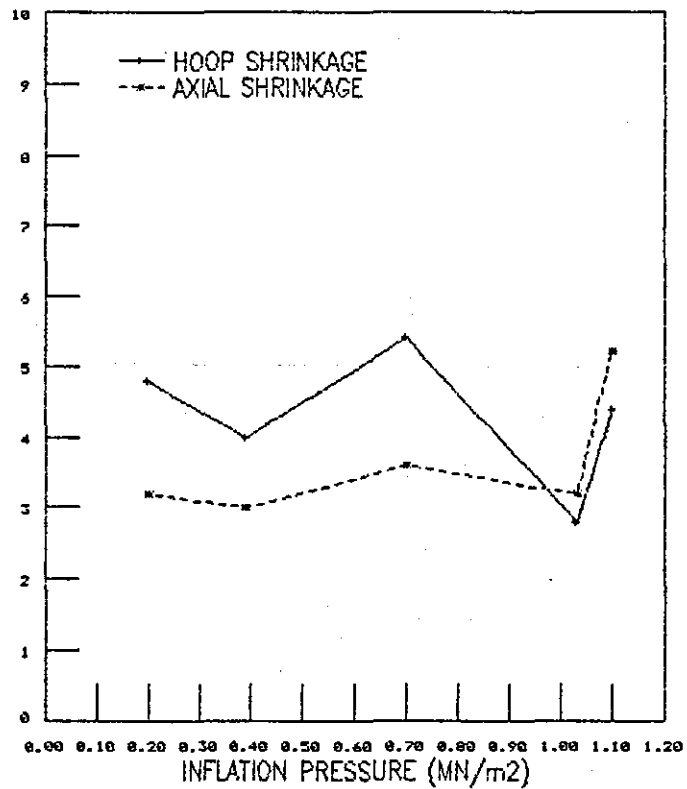
7.4 Discussion Of Results

Figures 7.10(a)-7.10(e) show typical stress-strain curves for different inflation pressures, each plot incorporates a curve for unoriented PET as a reference. From the experimental curves it can be seen that the bottles exhibit tensile properties which are stronger, stiffer but more brittle in the hoop direction compared to the axial direction. This indicates a higher degree of orientation is present in the hoop direction. This result is expected as the hoop draw ratio is greater than the axial draw ratio, 3.8 and 2.2 respectively.

The Effect Of Inflation Pressure

Figure 7.11 shows the burst pressure to increase with inflation pressure. The burst pressure is dependent on the yield stress in the direction of bursting. Comparing Figures 7.11 and 7.15 similar curves were obtained for the burst pressure and the hoop yield stress, indicating that the burst pressure is dependent on the hoop yield stress. Wu and Stachuski[174] reported that the occurrence of strain hardening (strain-induced crystallisation in PET processing) improves bottle burst strength. Therefore, the increased burst pressure at high inflation rates may indicate the occurrence of greater strain-induced crystallisation; shrinkage tests were carried out to test this hypothesis.

Figure 7.12 shows the top load strength to increase with increasing inflation pressure. The top load test is an elastic instability test and is very sensitive to thickness variations. The low value at 0.2 MPa inflation pressure is due to the large thickness variation at this pressure (see Table 7.3). At high inflation pressures a more stable stretching occurs and less thickness variation is observed (see Table 7.3). This may account for some of the observed increase in top load strength. The top load strength is dependent on the axial modulus and a comparison of Figures 7.12 and 7.16 shows that similar curves were obtained for both these properties.

Figure 7.13 shows a slight increase in the average wall thickness

for all the bottles tested for a given inflation pressure, the distribution of average bottle thickness values shows less scatter with increased inflation pressure, possibly due to strain-induced crystallisation stabilising the deformation process. *Chedd and Haworth*[173] reported a large variation in the distribution of bottle wall thickness values from apparently identical processing conditions around the bottle circumference. Table 7.3 shows that for condition A (0.2MN/m² inflation pressure), there was a large variation in the thickness around the bottle circumference; but for the other conditions a much narrower distribution, which was relatively independent of inflation pressure, was observed. The increasing resistance to deformation with time shown in Figure 4.17 results in a stabilised preform stretching process and a more even bottle thickness distribution. The tension thinning response shown in Figure 4.39 results in faster inflation rates being achieved with increasing inflation pressures and the process is known to be more stable at higher strain rates.

Figure 7.14 shows the ultimate tensile strength in the hoop direction increasing and simultaneously the axial strength decreasing with increasing inflation pressure. This indicates an increase in hoop orientation at higher inflation pressures, which would result in a compensating decrease in axial orientation. At the higher pressures the "sausage balloon" deformation[166,167] can result in the inflation occurring ahead of the stretch-rod and hence there would be a shift in the resultant biaxial orientation towards a more dominant hoop orientation. *Miller*[165] reported increased tensile strength in the hoop direction with increased inflation pressure, whilst the axial strength remained unaffected.

Figure 7.15 shows the axial tensile yield stress to be independent of inflation pressure and lower than the hoop tensile yield stress. The hoop tensile yield stress is higher due to the increased orientation as a result of the greater draw ratio in this direction. The increase with inflation pressure may be due to differences in the degree of orientation due to different strain rates.

Figure 7.16 shows the tensile modulus in the hoop and axial directions as a function of the inflation pressure. The modulus in the axial modulus increases with inflation pressure whilst no clear trend can be observed for the hoop modulus. The hoop direction modulus behaviour may be due to the change in deformation mode that occurs as the bottle forms ahead of the stretch-rod at high inflation pressures, the inflation pressure is therefore stretching the bottle in both directions; compared to the lower pressure mode where the stretch-rod induces the axial deformation and the inflation pressure acts in the hoop direction.

Figure 7.17 shows the $\Delta n_{1,2}$ birefringence to marginally increase with increasing inflation pressure. This indicates a shift in the balance of the planar orientation; as the axial orientation, resulting from the stretch-rod action, becomes less significant compared with the hoop direction orientation, resulting from the inflation of the bottle. This result agrees with that observed in the tensile testing experiments, which indicate the shift towards a more dominant hoop orientation with increasing inflation pressure. The values shown are average values as no account was taken of the difference in draw ratios, and hence birefringence, between the inner and outer surfaces.

Figure 7.18 shows the hoop and axial shrinkage that occurred after putting the specimens in an oven at 80°C for 15 minutes. As the oven was above the glass-transition temperature of PET the molecular orientation in the amorphous regions was able to revert to a random configuration. If strain-induced crystallisation occurred during the stretching process then some crystalline molecular orientation would be present which would not revert during the shrinkage test.

In Chapter 4, Figure 4.17 shows the strain hardening response of PET at 90°C occurs at a true strain of between 2.32 and 3.16 dependent on the elongation rate. The true strain in the hoop direction during the bottle blowing was 2.81 (outer surface) and the true strain in the axial direction was 1.24. Therefore, strain hardening could be expected to have occurred in the hoop direction, but possibly not in the axial direction.

The results shown in Figure 7.18 show the hoop shrinkage to be generally greater than the axial shrinkage, this is expected as more orientation has been shown to be present by the tensile tests and the birefringence tests (see Figures 7.14-7.17). However, the hoop shrinkage behaviour .observed at inflation pressures above 1.03 MPa indicates that strain-induced crystallisation occurred at these pressures; the orientation in the amorphous regions reverts whilst in the crystalline regions the structure prevents the molecular movement necessary for reversion to occur.

The onset of stress-induced crystallisation limits the size of a bottle or a preform as further deformation requires a drastic rise in the air pressure.

From the results shown in this chapter and in Chapter 4 some of the effects of PET uniaxial deformation behaviour on the stretch blow moulding performance can be summarised. The strain hardening behaviour of PET shown in Figure 4.17 occurs in the hoop direction during stretch blow moulding and improves the burst strength properties of the bottle. The stress-induced crystallisation that was shown to occur above a critical strain in Chapter 4, is induced in the hoop direction, but not in the axial direction, during stretch blow moulding as shown by the shrinkage measurements. The increasing resistance to deformation with time, shown in Figure 4.17, stabilises the preform stretching and inflation process giving a more even thickness distribution in the bottle. The tension thinning response shown in Figure 4.39 results in faster inflation rates for greater inflation pressures in stretch blow moulding, stabilising the stretching process.

7.5 Conclusions From Chapter 7

The aim of the chapter to compare the stretching behaviour of PET in stretch blow moulding with the stretching data in Chapter 4 has been achieved and the conclusions are shown below:

1.   An increase in burst and top load strengths occurs with

increasing inflation pressure due to strain hardening (stress-induced crystallisation) in the hoop direction and increased molecular orientation. The effect of thickness variations dominate the top load behaviour.

2. A better bottle thickness distribution was achieved with increased inflation pressure indicating more stable stretching as a result of the increasing resistance to deformation with time, reported in Chapter 4.

3. The birefringence results showed a slight increase in hoop direction orientation with respect to axial direction orientation as the inflation pressure increases.

4. The shrinkage results indicate that whilst the axial deformation involves amorphous orientation the deformation in the hoop direction involves strain-induced crystallisation, at the higher inflation pressures, resulting in both oriented amorphous and crystalline regions of which only the amorphous regions shrink.

5. The data reported in Chapter 4 provides information useful for application to stretch blow moulding in form of data on uniaxial deformation behaviour, strain hardening and stress-induced crystallisation.

7.5.1 Suggestions For Further Work

If an extended access to production line time could be arranged with an injection stretch blow moulding company, then the oven temperatures could be varied to study the effects of preheat temperature on bottle properties which could then be compared with the data for PET at different temperatures reported in Chapter 4.

To gain knowledge of the molecular alignment that occurs in the process a more detailed structural investigation on PET would be necessary, similar to that carried out by *Cakmak, Spruiell and White*[175], who used birefringence and wide-angle x-ray diffraction methods to determine the polymer chain orientation with respect to the hoop and axial directions.

8. Conclusions

8.1 General Conclusions

The following sections summarise the main conclusions of the work:

(i) Shear Flow

Linear, branched and copolymer thermoplastic polyesters have been characterised and their rheological properties determined in shear capillary flow. All the polymer melts were pseudoplastic under shear flow over a shear rate range of 10 to $10000s^{-1}$. The branched PET polymers were more pseudoplastic (n=0.6) than the linear PET polymers (n=0.8) and the onset of shear thinning occurred at a lower shear rate.

The shear modulus for branched PET polymers and the three copolyesters increased with increasing shear stress. For the branched PET polymers the shear modulus decreased with increasing molecular weight and broader molecular weight distribution.

The shear rheology and relaxation times of the linear PET and the PCTG copolyester indicate their suitability for injection moulding, whilst branched PET polymers and the PETG copolyester have suitable melt viscosity properties and relaxation times for extrusion blow moulding.

(ii) Converging Flow

Linear, branched and copolymer thermoplastic polyesters have been characterised and their rheological properties determined in shear and elongational flows from converging flow. In converging flow all the polymers behaved in an apparent tension-thinning manner, but the elongational viscosities of the linear PET polymers were relatively independent of temperature and increased with increasing molecular weight. Stress-induced crystallisation occurred at high elongation rates with the linear PET polymers, especially at lower temperatures.

The branched PET polymers were tension thinning below a

critical rate, at which the rate of elongational deformation exceeds the shear disentanglement causing the chain branches to snag. Above the critical rate the branched PET polymers response appoaches rate-independent behaviour. The branched PET polymers showed decreased apparent elongational viscosity with increasing temperature and decreasing molecular weight, the temperature sensitivity increased with increasing elongation rate and molecular weight.

The PETG Copolyester showed a tension thinning response with a deviation towards rate-independent behaviour at high elongation rates, due to either (i) the different phases present in copolymer systems, or (ii) the flow induced molecular orientation causing steric hindrance of the bulky cyclic molecular groups and therefore increasing the resistance to elongational flow.

The PCTG and PCCE Copolyesters are tension thinning polymers, having similar apparent elongational viscosity values to the linear PET polymers in converging flow.

The apparent elongational viscosity of PETG, PCTG and PCCE Copolyesters decreased with increasing temperature.

The PETG and PCCE tensile modulus values increased with increasing elongational stress, whilst the PCTG tensile modulus passed through a minimum. The PETG, PCTG and PCCE tensile modulus values are relatively independent of temperature.

(iii) Rutherford Elongational Rheometer

The Rutherford Elongational Rheometer has been successfully modified to enable operation up to 280°C for polycarbonate melts by replacing the heating elements, silicone oil, and temperature controller.

The Rutherford Elongational Rheometer cannot presently be used to study the elongational flow properties of PET melts as the melt density exceeds the specific gravity of commercially available silicone fluids at the relevant temperatures by an unacceptable margin.

PETG Copolyester melts at 170°C show tension stiffening response when tested at constant Hencky strain rate and constant temperature in free-surface uniaxial elongation, using the Rutherford

Elongational Rheometer.

The data from the Rutherford Elongational Rheometer for PETG Copolyester showed qualitatively opposite trends with respect to elongation rate compared with converging flow data. Therefore, direct comparisons of elongational flow data from different sources should only be made after considering the respective test methods used, and elongational data should only be applied to processing situations involving similar flow environments.

At 110°C the PETG Copolyester is predominantly elastic and the stress growth behaviour obeys the rubber-like network theory. The elongational behaviour is highly time-dependent, the stress decreases above a critical elongation rate as the temporary rubber-like network breaks down. At a critical stress chain slippage occurs and the response becomes stress independent.

The PET polymers show a tension thinning response in the rubbery phase when tested at constant Hencky strain rate and constant temperature using the Rutherford Elongational Rheometer.

The combination of stress growth-time data and stress relaxation data offer supporting evidence for the hypothesis that the deviations from the time-dependent stress growth baseline at a Hencky strain of about 1.3 represent the departure from linear viscoelastic behaviour. The response shows a very rapid increase in the elongational stress growth function after the onset of stress-induced crystallisation.

The elongational stress growth function decreases with increasing temperature, the temperature dependence is greater at low strains. The onset of stress-induced crystallisation occurs at a critical Hencky strain of approximately 1.4 which is relatively insensitive to elongation rate and temperature. The percentage strain recovered decreases with increasing maximum strain and is relatively insensitive to temperature and Hencky strain rate.

(iv) Injection Moulding

Due to the long runner system in the mould used, high filling pressures were recorded for all three polymers (under all conditions) and short shot mouldings were obtained at low injection rates. Under

non-isothermal conditions, there exists an optimum flow rate, for any given set of conditions, where the pressure required to fill the cavity is a minimum.

The pressure drop increases if the melt temperature decreases or the mould temperature decreases or a higher molecular weight polymer is used. The three polymers can be ranked in order of increasing injection pressure for a given set of conditions as: B90S<EX167<PCTG.

The computer simulation models PET and PCTG shear rheological data satisfactorily, but the die-entry pressure drop data model showed significant errors at low shear rates. Alternative models for die-entry pressure drop data have been proposed, showing improved correlation and less data-spread.

The simulation predicts the behaviour of PET and PCTG polymers in injection moulding, showing good agreement with practice for pressure drop values, (and their dependence on temperature and molecular weight). However, the simulation shows some limitations on estimates of cooling time and clamping force at low injection rates and also poor agreement between the feasibility of short mouldings predicted and those observed in experimental processing, due to the simulations restriction in using thermal properties of rapidly crystallising PET rather than using the thermal properties of the various amorphous PET based polymers studied.

(v) Extrusion Blow Moulding

The desired combination of rheological properties that a polymer should possess for the extrusion blow moulding process are:

(i)   A high shear viscosity at low shear rates;

(ii)   A low shear viscosity at high shear rates;

(iii)   A high degree of elasticity and a long natural time;

(iv)   Tension stiffening behaviour at both low and high elongation rates in free-surface uniaxial elongational flows.

This combination of properties would prevent excessive parison sag, ensure stable inflation and an even thickness distribution, as verified by pilot-scale processing trials. Linear PET polymers are

unsuitable for this process, but the branched PET polymers and PETG copolymer possess the correct combination of flow properties to be successfully extrusion blow moulded.

The criteria proposed by *Baron, McChesney and Sinker*[5] for the shear rheological properties desirable in an extrusion blow mouldable polymer are valid for the polymers tested in this study though they fail to consider predominant elongational flows that are present in extrusion blow moulding.

The natural time comparison between the process and the polymer offer a qualitative guide for parison deformation behaviour but fails to account for the melt fracture limitation during bottle inflation.

The models tested for parison sagging predictions provide good estimates of the observed behaviour and demonstrate the applicability of stress growth data to processing. However, for application to thermoplastic polyesters and copolyesters the models could be refined to account for parison 'bounce' and shear-heating effects.

(vi) Stretch Blow Moulding

An increase in burst pressure and top load strength occurs with increasing inflation pressure due to strain hardening in the hoop direction and increased molecular orientation. The birefringence results show an increase in hoop direction orientation with respect to axial direction orientation, also a better bottle thickness distribution is achieved as the inflation pressure increases. The shrinkage results show axial deformation involves amorphous orientation, whilst, the deformation in the hoop direction induces crystallisation resulting in both oriented amorphous and crystalline regions.

The thermoelastic PET Rutherford Elongational Rheometer data provides information useful for application to stretch blow moulding in form of data on uniaxial deformation behaviour, strain hardening and stress-induced crystallisation.

8.2 Recommendations For Further Research

Shear And Converging Flow Rheology Of PET Melts

The branch length and density should be determined for the branched PET polymers. The copolymers should be analysed to determine the second phase content.

Further work to extend the applicability of the shear and converging flow results include the extension of the temperature range over which the flow properties have been studied and the study of molecular weight effects on the three copolyesters.

An investigation into the behaviour of the branched PET polymers to determine the influences of branch length and branch concentration on the elongational behaviour should be carried out.

Molecular engineering could be used to produce a branched PET copolymer which could well be an extrusion blow mouldable PET material.

Rutherford Elongational Rheometer

The branched PET polymers and the PCCE and PCTG copolyesters could be tested if further quantities of material were made available. Other polymers can now be tested using the Rutherford Elongational Rheometer such as polycarbonate and other engineering polymers, PET/PC and other blends, and the new high-barrier thermoforming materials (e.g. PP/EVOH/PP). By 'molecular engineering' new plastics can be produced which can then be tested in this mode to determine if the desired properties have been achieved.

Injection Moulding

The SIMPOL software should be modified to permit the creation of new generic files for new polymers. Generic data files of the thermal properties of amorphous PET and PCTG Copolyester should be set up, to see if a better simulation of preform injection moulding can be obtained than the current system can offer.

The proposed improvements for die-entry pressure drop modelling should be tested, studying the effects on the SIMPOL estimates. Alternatively, the input of die-entry data should be restricted to the linear portion of the data (i.e. pressures greater than 0.5 MPa).

SIMPOL should be tested, against experimental practical

processing results, with more complex cavity geometries; including converging and diverging flows and pin gates, this would test the effectiveness of the die-entry pressure drop model.

Further studies comparing SIMPOL simulated behaviour with practical injection moulding behaviour for novel polymers, e.g. blends, copolymers, fibre-filled polymers should be carried out.

Optimising injection moulding conditions using SIMPOL in conjunction with obtaining the desired mechanical properties in the product should be attempted.

Extrusion Blow Moulding

Processing trials should be undertaken on the branched PET and PCCE Copolyester materials to compare their processability with the rheology results reported here.

Stretch Blow Moulding

The effects of preheat temperature on bottle properties could be studied and compared to the data for PET at different temperatures reported here.

A more detailed structural investigation on the PET bottles could enable the polymer chain orientation with respect to the bottle axes to be determined.

References

1. Gregory, D.R., and Watson, M.T., "Steady-state flow properties of PET melts", *Journal of Polymer Science, Part C*, 30, 399-406, (1970).

2. Gregory, D.R., "Rheological properties of molten poly(ethylene terephthalate)", *Journal of Applied Polymer Science*, 16, 1479-1487, (1972).

3. Boudreaux, E., and Cuculo, J.A., "A comparison of the flow behaviour of linear polyethylene, PBT, and PET", *Journal of Applied Polymer Science*, 27, 301-318, (1982).

4. Gregory, D.R.,and Wampler, F.C., "Errors that result from thermal degradation during shear measurements on some molten polymers", *Polymer Engineering and Science*, 25(6), 362-366, (1985).

5. Baron, J.J., McChesney, C.E., and Sinker, S.M., "Extrusion blow moldable PET", *Proceedings of SPE 39th Antec Conference, May 1981, Boston, USA*, 713-715, (1981).

6. Cogswell, F.N., *"Polymer Melt Rheology"*, Godwin: London, (1981).

7. Gibson, A.G. and Williamson, G.A., "Shear and Extensional Flow of Reinforced Plastics in Injection Molding, I. Effects of Temperature and Shear Rate with Bulk Molding Compound", *Polymer Engineering and Science*, 25(15), 968-979, (1985).

8. Gibson, A.G. and Williamson, G.A., "Shear and Extensional Flow of Reinforced Plastics in Injection Molding, II. Effects of Die Angle and Bore Diameter on Pressure with Bulk Molding Compound", *Polymer Engineering and Science*, 25(15), 980-985, (1985).

9. Smoker, D.G., "A study of the extensional flow behaviour of low density polyethylenes", *Ph.D. thesis, Loughborough University*, (1984).

10. Arif, M.N.Z., "Elongational Flow of PVC", *Ph.D. Thesis, Loughborough University Of Technology*, (1984).

11. Barrie, I.T., "SIMPOL Users' Guide", *Ian Barrie Consultancy, Hertford, England*, (1986).

12. Garcia-Rejon, A., Orbey, N. and Dealy, J.M., "Parison Swell and Drawdown A Fundamental Study", *SPE Technical Papers*, 27, 431-433, (1981).

13. Brydson, J.A., *"Flow Properties of Polymer Melts"*, 2nd. edition, Godwin: London, (1981).

14. Lodge, A.S., *"Elastic Liquids"*, Academic Press: London, (1964).

15. Crawford, R.J., *"Plastics Engineering"*, published by Pergamon Press, Oxford, (1983).

16. LLoyd, L.L., *Polymer Laboratories Ltd.*, private communication, 21st March (1985).

17. Dealy, J.M., *"Rheometers for Molten Polymers"*, Van Nostrand Reinhold, (1982).

18. Walters, K., *"Rheometry"*, Chapman and Hall: London, (1975).

19. Philipoff, W. and Gaskins, F.H., "The capillary experiment in rheology", *Transactions of the Society of Rheology*, II, 263-284, (1958).

20. ASTM, "Rheological properties of thermoplastics with a capillary rheometer", *Standard Test Method D3835-79*, (1979).

21. Bagley, E.B., "End corrections in capillary flow of polyethylene", *Journal of Applied Physics*, 28(5), 624-627, (1957).

22. Kumar, N.G., "Viscosity-molecular weight-temperature-shear rate relationships of polymer melts: a literature review", *Journal of Polymer Science: Macromolecular Reviews*, 15, 255-325, (1980).

23. Bowers, S., "Development of inelastic models for the injection-moulding process", *Progress in Rubber and Plastics Technology*, 2(1), 23-38, (1986).

24. Williams, M.L., Landel, R.F. and Ferry, J.D., "The temperature dependence of relaxation mechanisms in amorphous polymers and other glass-forming liquids", *Journal of the American Chemical Society*, 77, 3701-3706, (1955).

25. Mendelson, R.A., "Polyethylene melt viscosity: shear rate-temperature superposition", *Transactions of the Society of Rheology*, 9(1), 53-63, (1965).

26. Allen, V.R. and Fox, T.G., "Viscosity-molecular weight dependence for short chain polystyrenes", *Journal of Chemical Physics*, 41, 337-343, (1964): *ibid.*, "Dependence of the zero shear melt viscosity and the related friction coefficient and critical chain length on measurable characteristics of chain polymers", 344-352, (1964).

27. Turney, R.J., *Eastman Plastics*, private communication, (1986).

28. Jabarin, S.A. and Lofgren, E.A., "Thermal Stability of Polyethylene Terephthalate", *Polymer Engineering and Science*, 24(13), 1056-1063, (1984).

29. Buchneva,T.M., Kulichikhin, S.G., Gabrielyan, G.A., Artemova, M.N., Anan'Eva, L.A., Malkin, A.Ya., and Rogovin, Z.A., "Viscometric study of some structural features of modified PET", *Polymer Science U.S.S.R.*, 25(4), 931-936, (1983).

30. Munari, A., Pilati, F., Pezzin, G., "A study of the melt viscosity of linear and branched PBT", *Rheologica Acta*, 23, 14-19, (1984).

31. Munari, A., Pilati, F., Pezzin, G., "Linear and branched PBT: activation energy for melt flow", *Rheologica Acta*, 24, 534-536, (1985).

32. Mishra, S.P., and Deopura, B.L., "Rheological behaviour of poly(ethylene terephthalate) and poly(butylene terephthalate) blends", *Rheologica Acta*, 23, 189-194, (1984).

33. Mulla, M. and Haworth, B., unpublished work, M.Sc. project, *Institute of Polymer Technology, Loughborough University of Technology*, (1983).

34. Robinson, T.M. and Haworth, B., unpublished work, M.Sc. project, *Institute of Polymer Technology, Loughborough University of Technology*, (1984).

35. Doughty, D., *Eastman Plastics U.S.A.*, Private communication, April (1987).

36. "PET chemistry yields more high-end resins", *Modern Plastics International*, February 1986, 10, (1986).

37. *Eastman Plastics*, "KODAR PETG Copolyester 6763", Technical datasheet MB-80D, March (1983).

38. *Eastman Plastics*, "Tentative data development PCCE flexible copolyester", Technical datasheet dge/TT72 56g; PSTMC 88-56(LPF) 11-9-83, (1983).

39. *Eastman Plastics*, "KODAR PCTG Copolyester 5445", Technical datasheet MB-94, August (1985).

40. *ASTM*, "Standard test method for dilute solution viscosity of polymers", D2857-70(Reapproved 1977), (1977).

41. Moore, W.R, and Sanderson, D., "Viscosities of dilute solutions of polyethylene terephthalate, *Polymer*, 9, 153-158, (1968).

42. Hergenrother, W.L. and Nelson, C.J., "Viscosity-molecular weight relationship for fractionated poly(ethylene terephthalate)", *Journal of Polymer Science, Polymer Chemistry Edition*, 12, 2905-2915, (1974).

43. *British Standards Institution*, "Standard test method for the determination of dilute solution viscosity", B.S.2782 Part7 Method 730A:1979, (1979).

44. Harrison, M.E., "Melinar technical aspects of injection moulding", *ICI technical datasheet 5*, issued at PRI seminar "Injection stretch blow moulding of PET", NEC, Birmingham, 20th September, (1985).

45. Evans, J.M., "Gel permeation chromatography: a simplified treatment", *RAPRA Members Journal*, 1(8), 198-203, (1973).

46. Evans, J.M., "Gel permeation chromatography: a guide to data interpretation", *RAPRA Bulletin*, 26(11), 334-342, (1972).

47. Billingham, N.C., *"Molar Mass Measurements in Polymer Science"*, Kogan Page, London, (1977).

48. Holding, S., "Gel permeation chromatography", visiting lecturer from RAPRA, lecture presented to The Polymer Society, Institute of Polymer Technology, Loughborough University of Technology, 13th February (1985).

49. Overton, J.R. and Browning, H.L., "Methylene Chloride-Hexafluoroisopropyl Alcohol (70/30), Use in High Performance GPC of PET", *ACS Symposium Series*, Part 245, 219-226, (1984).

50. Paschke, E.E., Bidlingmeyer, B.A. and Bergmann, J.G., "A New Solvent System For GPC Of PET", *Journal Of Polymer Science: Polymer Chemistry Edition*, 15, 983-989, (1977).

51. Jabarin, S.A., and Balduff, D.C., "Gel permeation of polyethylene terephthalate", *Journal of Liquid Chromatography*, 5(10), 1825-1845, (1982).

53. Janca, J., "Polymer analysis by size exclusion chromatography", *Journal of Liquid Chromatography*, 4(suppl. 1), 1-42, (1981).

54. "PLgel Users Guide", *Polymer Laboratories*, (1986).

55. Cogswell, F.N., Chapter 12 "Stretching Flows" in *"Polymer Rheology"*, edited by R.S.Lenk, published by Applied Science Publishers Ltd., London, (1978).

56. Denson, C.D., "Implications of Extensional Flows in Polymer Fabrication Processes", *Polymer Engineering and Science*, 13(2), 125-129, (1973).

57. Trouton, F.T., "On the coefficient of viscous traction and its relation to that of viscosity", *Proceedings of the Royal Society*, A77, 426-440, (1906).

58. Cogswell, F.N., "Measuring the Extensional Rheology of Polymer Melts", *Transactions of the Society of Rheology*, 16(3), 383-403, (1972).

59. Cogswell, F.N., "Polymer melt rheology during elongational flow", in *Fiber and Yarn Processing*, edited by J.L.White, Applied Polymer Symposia 27, 1-27, (1975).

60. Dealy, J.M., "Extensional Rheometers For Molten Polymers; A Review", *Journal of Non-Newtonian Fluid Mechanics*, 4, 9-21, (1978).

61. Meissner, J., "Polymer melt elongation - Methods, results, and recent developments", *Polymer Engineering and Science*, 27(8), 537-546, (1987).

62. Ziabicki, A. and Kedzierska, K., "Studies on the Orientation Phenomena by Fiber Formation from Polymer Melts. III. Effect of Structure on Orientation. Condensation Polymers", *Journal of Applied Polymer Science*, VI(19), 111-119, (1962).

63. Klement, J.J. and Geil, P.H., "Deformation and Annealing Behavior.
    I. Polyethylene Terephthalate Films", *Journal of Macromolecular
    Science - Physics Edition*, B5(3), 505-533, (1971).

64. Hennesey, W.J. and Spatorico, A.L., "Stress-Induced Crystallization
    of Branched PET Films", *Polymer Engineering and Science*, 19(6),
    462-467, (1979).

65. Sasano, H. and Kawai, T., "On the Mechanism of the Flow Process
    of PET", *Makromol. Chem.*, 184, 217-223, (1983).

66. Padibjo, S.R. and Ward, I.M., "A structural study of the tensile
    drawing behaviour of PET", *Polymer*, 24, 1103-1112, (1983).

67. De Vries, A.J., Bonnebat, C. and Beautemps, J., "Uni- and Biaxial
    Orientation of polymer films and sheets", *Journal of Polymer
    Science: Polymer Symposium*, 58, 109-156, (1977).

68. Hill, J.W. and Cuculo, J.A., "Isothermal Elongational Rheology of
    Poly(ethylene Terephthalate)", *Journal of Applied Polymer
    Science: Applied Polymer Symposium*, 33, 3-29, (1978).

69. Crater, D.H. and Cuculo, J.A., "A Visualization Study of
    Poly(ethylene Terephthalate) Flow Using Potential Chain-Ordering
    Die Geometries", *Journal of Polymer Science: Polymer Physics
    Edition*, 21, 2219-2242, (1983).

70. Petrie, C.J.S., "Elongational flows", Pitman, London, (1979).

71. Forsythe, T.H., "Converging flow of polymers", *Polymer and
    Plastics Technology and Engineering*, 6(1), 101-131, (1976).

72. Cogswell, F.N., "Converging flow of polymer melts in extrusion
    dies", *Polymer Engineering and Science*, 12(1), 64-73, (1972).

73. Cogswell, F.N., "Converging Flow and Stretching Flow: A
    Compilation", *Journal of Non-Newtonian Fluid Mechanics*, 4, 23-38,
    (1978).

74. Denn, M.M., "Extensional flows: experiment and theory", in *"The
    Mechanics of Viscoelastic Fluids"* edited by R.S.Rivlin, AMD-
    Volume 22, ASME, New York, 101-125, (1977).

75. Barrie, I.T., "The Rheology of Injection Moulding", Chapter 13 in
    "Polymer Rheology", R.S.Lenk, published by Applied Science
    Publishers, London, (1978).

76. Hurlimann, H.P. and Knappe, W., "Der Zusammenhang zwischen der Dehnspannung von Kunstoffschmelzen im Duseneinlauf und im Schmelzbruch" *Rheologica Acta*, 11, 292-301, (1972).

77. Shroff, R.N., Cancio, L.V. and Shida, M., "Extensional Flow of Polymer Melts", *Transactions of the Society of Rheology*, 21(3), 429-446, (1977).

78. Billmeyer, F.W., "*Textbook of Polymer Science*", 19-20, 2nd. edition, published by Wiley-Interscience, New York, (1971).

79. Cogswell, F.N., private communication, 15th July 1986.

80. Cogswell, F.N., private communication, 21st August 1986.

81. White, J.L. and Ide, Y., "Rheology and dynamics of fiber formation from polymer melts", *Applied Polymer Symposium*, 27, 61-102, (1975).

82. Nazem, F. and Hill, C.T., "Elongational and shear viscosities of a bead-filled thermoplastic", *Transactions of the Society of Rheology*, 18(1), 87-101, (1974).

83. Ballman, R.L., "Extensional flow of polystyrene melt", *Rheologica Acta*, 4, 137-140, (1965).

84. Everage, A.E. and Ballman, R.L., "Extensional viscosity of amorphous polystyrene", *Journal of Applied Polymer Science*, 20, 1137-1141, (1976).

85. Vinagradov, G.V., Fikhman, V.D., Radushkevich, B.V. and Malkin, A.Ya., "Viscoelastic and Relaxation Properties of a Polystyrene Melt in Axial Extension" *Journal of Polymer Science (Physics)*, 8, 657-678, (1970).

86. Meissner, J., "Rheometer zur Untersuchung der deformationsmechanischen Eigenschaften von Kunstoff-Schmelzen unter definierter Zugbeanspruchung", *Rheologica Acta*, 8, 78-88, (1969).

87. Meissner, J., "Development of a universal extensional rheometer for the uniaxial extension of polymer melts", *Transactions of the Society of Rheology*, 16(3), 405-420, (1972).

88. Munstedt, H., "New universal extensional rheometer for polymer melts. Measurements on a polystyrene sample", *Journal of Rheology*, 23(4), 421-436, (1979).

89. Munstedt, H., "Viscoelasticity of polystyrene melts in tensile creep experiments", *Rheologica Acta*, 14, 1077-1088, (1975).

90. Dealy, J.M., "New methods for measuring rheological properties of molten plastics", *Proceedings BSR/PRI Conference "Polymer Rheology and Plastics Processing", Loughborough*, 35-48, (1975).

91. Covas, J., "Processing of uPVC in single and twin screw extruders", *Ph.D. thesis*, Loughborough University Of Technology, (1985).

92. Canevarolo, S.V., unpublished work, I.P.T., (1984).

93. Canevarolo, S.V., unpublished work, I.P.T., (1984).

94. Axtell, F.H., private communication to Dr.Pye, BCL Ltd., 3rd October 1985.

95. Pullen, M., Axtell, F.H. and Haworth, B., unpublished work, B.Sc. project, I.P.T., (1985).

96. Carneiro, O. and Axtell, F.H., unpublished work, I.P.T., (1986).

97. Meissner, J., "Dehnungsverhalten von Polyathylen-Schmelzen", *Rheologica Acta*, 10, 230-242, (1971).

98. Wilkinson, D.M., unpublished work 1986, "Environmental Stress Cracking of injection moulded thermoplastics", *M.Phil. thesis to be submitted, Loughborough University of Technology*, (1988).

99. Pye, R.G.W., *"Injection Mould Design"*, published by G.Godwin, (1978).

100. Harrison, M.E., "Melinar PET Physical Properties", *ICI technical datasheet 1*, issued at PRI seminar "Injection stretch blow moulding of PET", NEC, Birmingham, 20th September, (1985).

101. ASTM *D1505-68 (Reapproved 1979)*, "Standard test method for Density of Plastics by the Density-Gradient Technique", (1979).

102. Rodriguez, F., *"Principles of Polymer Systems"*, 205-206, published by McGraw-Hill, (1970).

103. Johannaber, F., (translated by R.J. Kalh), *"Injection Molding Machines: A User's Guide"*, published by Carl Hanser Verlag, Munich, (1983).

104. Han, C.D., *"Rheology in Polymer Processing"*, published by Academic Press, London, (1976).

105. Richardson, S.M., Chapter 5 "Moulding", in *Computational Analysis of Polymer Processing* edited by J.R.A.Pearson and S.M.Richardson, published by Applied Science Publishers, London, (1983).

106. Kamal, M.R., Patterson, W.I. and Gomes, V.G., "An injection molding study. PartI: melt and barrel temperature dynamics", *Polymer Engineering and Science*, 26(12), 854-866, (1986).

107. Donovan, R.C., Thomas, D.E. and Leversen, L.D., "An experimental study of plasticating in a reciprocating-screw injection moulding machine", *Polymer Engineering and Science*, 11, 353-360, (1971).

108. Malloy, R., University of Lowell "Injection molding study reveals timed filling produces least consistent parts" in *Easy Reading* *Dynisco Pressure and Temperature Instrumentation News*, p.3, Fall (1986).

109. Mavridis, B., Hrymak, A.N. and Vlachopoulos, J., "Deformation and orientation of fluid elements behind an advancing flow front", *Journal of Rheology*, 30(3), 555-563, (1986).

110. Ballman, R.L. and Toor, H.L., "Orientation in injection moulding", *Modern Plastics*, 38(2), 113,114,117,120-122,124&205-207, (1960).

111. Huseby, T.W., "Pressure effects in the spiral mold", *Modern Plastics*, 40(12), 112-116&188, (1962).

112. Darlington, M.W., Scott, A.J. and Smith, A.C., "Pressure losses in the packing stage of injection molding", *Polymer Engineering and Science*, 26(18), 1282-1289, (1986).

113. Greener, J., "General consequences of the packing phase in injection molding", *Polymer Engineering and Science*, 26(12), 886-892, (1986).

114. Allan, P.S. and Bevis, M.J., "The production of void-free thick section thermoplastic and fibre-reinforced thermoplastic mouldings", *P.E.D. Review Meeting, 15-17 April 1985, Loughborough University of Technology*, (1985).

115. Kenig, S. and Kamal, M.R., "Cooling molded parts - a rigorous analysis", *SPE Journal*, 26(7), 50-57, (1970).

116. Filbert, W.C., "Design Nylon 66 for optimum injection moulding performance" *Plastics Technology*, 17(6), 35-38, (1971).

117. Spencer, R.S. and Gilmore, G.D., "Residual strains in injection moulded Polystyrene", *Modern Plastics*, 28(4), 97,98,100,102,104,106&108,155, (1950).

118. Isayev, A.I. and Hieber, C.A., "Toward a viscoelastic modelling of the injection molding of polymers", *Rheologica Acta*, 19, 168-182, (1980).

119. Casale, A., Moroni, A. and Ronzoni, I., "An approach for the processing engineer: rheotechnics", *Polymer Engineering and Science*, 14(9), 651-655, (1974).

120. Donovan, R.C., "A theoretical melting model for a reciprocating-screw injection moulding machine", *Polymer Engineering and Science*, 11, 361-368, (1971).

121. Fenner, R.T., Chapter 4 "Extrusion (Flow in Screw Extruders and Dies)" in *"Computational Analysis of Polymer Processing"* edited by J.R.A.Pearson and S.M.Richardson, published by Applied Science Publishers, London, (1983).

122. Harry, D.H. and Parrott, R.G., "Numerical simulation of injection mold filling", *Polymer Engineering and Science*, 10(4), 209-214, (1972).

123. Berger, J.L. and Gogos, C.G., "A numerical simulation of the cavity filling process with PVC in injection molding", *Polymer Engineering and Science*, 13(2), 102-112, (1973).

124. Kamal, M.R. and Kenig, S., "A complete model for the injection moulding of thermoplastics", *30th SPE ANTEC*, 18, 679-684, (1972).

125. Grinbalt, V.N., "Flow of a polymer melt in the mould in injection moulding", *Soviet Plastics*, (2), 24-28, (1970).

126. Barrie, I.T., "Injection moulding plastics", a paper presented at an IPT short course, (1984).

127. Barrie, I.T., "An application of rheology to the injection moulding of large-area articles", *Plastics and Polymers*, 38, 47-51, (1970).

128. Barrie, I.T., "An analysis of large-area moulding technology", *Plastics and Polymers*, 37, 463-468, (1969).

129. Barrie, I.T., "Understanding how an injection mold fills", *SPE Journal*, 27(8), 64-69, (1971).

130. Vostorgov, B.E. and Kalinchev, E.L., "Pressure transfer in injection mould filling of thermoplastics", *Soviet Plastics*, (4), 19-25, (1971).

131. Filbert, W.C., "Design Nylon 66 for optimum injection moulding performance" *Plastics Technology*, 17(6), 35-38, (1971).

132. Filbert, W.C., "Design Nylon 66 for optimum injection moulding performance" *Plastics Technology*, 17(9), 48-52, (1971).

133. Kamal, M.R., Chu, E., Lafleur, P.G. and Ryan, P.G., "Computer simulation of injection mold filling for viscoelastic melts with fountain flow", *Polymer Engineering and Science*, 26(3), 190-196, (1986).

134. Mavridis, H., Hrymak, A.N. and Vlachopoulos, J., "Finite element simulation of fountain flow in injection molding", *Polymer Engineering and Science*, 26(7), 449-454, (1986).

135. Kamal, M.R. and Kenig, S., "The injection moulding of thermoplastics. Part I: theoretical model", *Polymer Engineering and Science*, 12(4), 294-301, (1972).

136. Kamal, M.R. and Kenig, S., "The injection moulding of thermoplastics. Part II: experimental test of the model", *Polymer Engineering and Science*, 12(4), 302-308, (1972).

137. Kenig, S. and Kamal, M.R., "Heat transfer in the cooling of thermoplastic melts under pressure", *The Canadian Journal of Chemical Engineering*, 49, 210-220, (1971).

138. Tadmor, Z, "Molecular orientation in injection moulding", *Journal of Applied Polymer Science*, 18, 1753-1772, (1974).

139. *Plastics and Rubber Weekly*, No.1097, July 20th, "Computerisation – Special Report", 7-16, (1985).

140. Bernhard, M.G., "Improving production and quality through the Moldcool CAD system", *ANTEC'84, 42nd SPE Annual Technical Conference*, 977-978, (1984).

141. Schauer, K.R., "The Moldcool computer-aided design program", *ANTEC'83, 41st SPE Annual Technical Conference, Chicago May 2-5*, 865-866, (1983).

142. Schaul, J.S., "Drying and injection moulding PET for beverage bottle preforms", *SPE Antec'80, 38th Annual Technical Conference, New York, May 5-8, 1980*, 534-536, (1980).

143. Brascome, L.W., "Processing of PET bottles: effects of selected preform injection molding parameters on preform properties", *SPE Antec'80, 38th Annual Technical Conference, New York, May 5-8, 1980*, 537-539, (1980).

144. Brascome, L.W., "How to handle haze, and acetaldehyde too, in PET blowmolding", *Plastics Engineering*, 36(5), 66-69, (1980).

145. Bier, P.N. and Ong, G.N., "High Performance PET injection moulding resins", *SPE Antec'80, 38th Annual Technical Conference, New York, May 5-8, 1980*, 510-513, (1980).

146. Cox, H.W. and Metzner, C.C, "Injection molding: the effect of fill time on properties", *Polymer Engineering and Science*, 26(7), 488-498, (1986).

147. Dietz, W. and White, J.L., "Ein einfaches Modell zur Berechnung des Druckverlustes wahrend des Werkzeugfullvorganges und der eigefrorenen Orientierung biem Spritzgießen amorpher Kunstoffe", *Rheologica Acta*, 17, 676-692, (1978).

148. Cogswell, F.N. and Lamb, P., "Polymer properties relevant in melt processing", *Plastics and Polymers*, 38, 331-341, (1970).

149. Cogswell, F.N. and Lamb, P., "The mechanism of melt distortion", *Transactions of the Plastics Institute*, 35, 809-813, (1967).

150. Corridan, P., *"AMSTAT 3"* software manual, (1986).

151. Powell, P.C., *"Engineering with Polymers"*, 59-61, published by Chapman and Hall Ltd, London, (1983).

152. Fenner, R.T., *"Principles of polymer processing"*, 13, published by Macmillan Press, London, (1979).

153. Miller, J.C., "A Rheological Product Problem in Blow Molding", *Transactions of the Society of Rheology*, 19(3), 341-350, (1975).

154. Schaul, J.S., Hannon, M.J. and Wissburn, K.F., "Analysis of factors determining parison properties in high shear rate blow molding", *Transactions of the Society of Rheology*, 19(3), 351-370, (1975).

155. Garcia-Rejon, A., Dealy, J.M. and Kamal, M.R., "Rheological comparison of four blow molding resins", *Canadian Journal Of Chemical Engineering*, 59, 76-81, (1981).

156. Powell, P.C. "Processing methods and properties of thermoplastic melts", 205-207, Chapter 11 in *"Thermoplastics properties and design"*, edited by R.M.Orgorkiewicz, published by Wiley-Interscience, London, (1974).

157. Petrie, C.J.S., "Film blowing, blow moulding and thermoforming", 234-240, Chapter 7 in *"Computational Analysis of Polymer Processing"* edited by J.R.A.Pearson and S.M.Richardson, published by Applied Science Publishers, London, (1983).

158. Cogswell, F.N., Webb, P.C., Weeks, J.C., Maskell, S.G. and Rice, P.D.R., "The scientific design of fabrication processes: blow moulding", *Plastics and Polymers*, 39, 340-350, (1971).

159. Dutta, A. and Ryan, M.E., "A study of parison development in extrusion blow molding", *Journal of Non-Newtonian Fluid Mechanics*, 10, 235-256, (1982).

160. Dealy, J.M. and Orbey, N., "A model for parison behaviour in the extrusion blow moulding process", *A.I.Ch.E. Journal*, 31, 807-811, (1985).

161. Orbey, N. and Dealy, J.M., "Isothermal swell of extrudate from annular dies; effects of die geometry, flow rate, and resin characteristics", *Polymer Engineering and Science*, 24(7), 511-518, (1984).

162. Kamal, M.R., Tan, V. and Kaylon, D., "Measurement and calculation of parison dimensions and bottle thickness distribution during blow moulding", *Polymer Engineering and Science*, 21(6), 331-338, (1981).

163. Edwards, M.F., Georghiades, S. and Suvanaphen, P.K., "A study of the cooling of blow moulded objects", *Plastics and Rubber Processing and Applications*, 1(2), 161-165, (1981).

164. Eastman Plastics, "Some Do's and Don'ts for Extrusion Blow Molding KODAR PETG Copolyester 6763", *Technical Literature Publication No. PTP-20*.

165. Miller, B.H., "Reheat Blow Molding of PET Bottles", *Proceedings of the Society of Plastics Engineers 38th Annual Technical Conference "Plastics Progress Through Processing"*, New York, 5-8 May, 1980. ANTEC 80, 540-542, (1980).

166. Erwin, L., Gonzalez, H. and Pollock, M., "Analysis of an experiment in blow moulding of oriented PET bottles", *Proceedings of the Society of Plastics Engineers 41st Annual Technical Conference, "Plastics-Engineering Today For Tomorrow's World"*, Chicago, Ill, 2-5 May, 1983, ANTEC 83, 807-809, (1983).

167. Cakmak, M., White, J.L. and Spruiell, J.E., "Dynamics of Stretch Blow Moulding PET", *Proceedings of the Society of Plastics Engineers 42nd Annual Technical Conference*, ANTEC 84, 920-923, (1984).

168. Harrison, M.E., "Melinar and Acetaldehyde", *ICI technical datasheet 10*, issued at PRI seminar "Injection stretch blow moulding of PET", NEC, Birmingham, 20th September, (1985).

169. Fritz, H.G., "Stretch and injection blow moulding", *German Plastics*, 71(10), 36-42, 1981; translated from *Kunstoffe*, 71(10), 637-699, (1981).

170. Leigner, F.P., "Free-Blown PET Preforms Characterise Blown Bottles", *Plastics Engineering*, 41(6), 47-52, (1985).

171. Fifer, R.L., "PETP Stretch Blow Moulding Experimental Data Showing Container Physical Characteristics Related To A Variable Container Size", *Proceedings of the Society of Plastics Engineers 39th Annual Technical Conference "Creating Value Through Innovation"*, Boston, 4-7 May, 1981, ANTEC 81, 696-699, (1981).

172. Ola, A.O. ,"The Basis Of Thermoforming Poly(ethylene terephthalate) Containers", *Ph.D. Thesis, Loughborough University Of Technology*, (1987).

173. Chedd, P. and Haworth, H., unpublished work, *M.Sc. project, I.P.T., L.U.T.*, (1986).

174. Wu, R.Y. and Stachurski, Z.H., "Prediction of the Bursting Pressure of Oriented Plastic Bottles", *Polymer and Plastics Technology and Engineering*, 24(2), 109-115, (1985).

175. Cakmak, M., Spruiell, J.E. and White, J.L., "A Basic Study Of Orientation in Stretch Blow Moulded Bottles", *Proceedings of the Society of Plastics Engineers 41st Annual Technical Conference "Plastics-Engineering Today For Tomorrow's World", Chicago, Ill, 2-5 May, 1983*, ANTEC 83, 394-396, (1983).

176. Yang, H.H., Chouinard, M.P. and Lingg, W.J., "Birefringence of Highly Oriented Fibers", *Journal of Polymer Science: Polymer Physics*, 20 981-987, (1982).

APPENDIX 1: Method of Conditioning PET in Humid Environments

The linear PET polymers used in the study were 'Melinar' B90S, a standard bottle grade PET polymer (0.74ml/g nominal I.V.) supplied by ICI, a high viscosity (0.9ml/g nominal I.V.) development grade, EX167, supplied by ICI, and a series of four lower viscosity polymers prepared by conditioning B90S in humid environments. The dry B90S was placed in constant environment chambers for a given duration. The polymer was then extruded through the capillary rheometer, where hydrolysis took place causing a reduction in the molecular chain length, and hence lowering the viscosity. Samples of the extrudate were characterised to determine the final molecular properties of the polymer samples.

The humidity level, in the environmental chambers, was established by the presence of a saturated solution of a given salt, (potassium acetate and sodium dichromate were used). [C.R.C. Handbook of Chemistry and Physics 1982-1983, 63rd edition, edited by WEAST, E-43, (1983).] The conditions used are given below in Table A-1.

TABLE A-1: HUMIDITY CONDITIONING OF B90S

SAMPLE CODE	SALT USED	HUMIDITY	DURATION
LIN-A	$KC_2H_3O_2$	20% r.h.	16hours
LIN-B	$KC_2H_3O_2$	20% r.h.	24hours
LIN-C	$KC_2H_3O_2$	20% r.h.	48hours
LIN-D	$Na_2Cr_2O_7$	52% r.h.	24hours

(Referred to on page 26 of thesis.)

APPENDIX 2: GPC System Calibration

The solvents used were reagent grade tetrachloroethane (TCE) (Fisons Ltd), and analytical grade nitrobenzene (NB) (BDH Chemicals Ltd). The GPC eluent (NB-TCE) was 0.5% NB-99.5% TCE by volume at room temperature.

The system was prepared for running on the NB-TCE solvent system, in place of the usual tetrahydrafuran (TFH) solvent, using the column manufacturers recommended procedure.[54] The system was flushed with toluene at a rate of 1ml/min overnight, then the system was flushed for 24 hours with the NB-TCE solvent system. The system was then ready to use.

The system was calibrated using 10 fractionated polystyrene samples (Polymer Laboratories - PS Standards) dissolved in the NB-TCE solvent at a concentration of 0.1%. The fractionated polymers used had molecular weights of 1200; 3770; 9000; 28000; 68000; 173000; 450000; 1030000; 1750000; and 2950000. From the elution times of these standards linear and cubic fit calibration curves were plotted. The cubic fit gave the best correlation and was used in the later analyses of the PET samples. The ratio of monomer mass $M_{PET}/M_{PS} = 1.846$ was applied to the resultant molecular weights derived from the calibration curve. This correction method assumes that both the polymers have the same hydrodynamic volume. The PET distributions are reported in terms of equivalent PS molecular weight, this method was used as the Mark-Houwink constants for the solvent system was unknown for both polystyrene and PET.
(Referred to on page 34 of thesis.)

APPENDIX 3: RAPRA GPC Sample Preparation For Different Batches

For the first batch of samples the preparation technique was as follows: 50ml of hot solvent was added to 250mg of sample and then heated in an oven at 150°C until the sample dissolved. The solutions were shaken regularly.

The second batch included a rerun of one of the first batch samples to act as a reference. The preparation technique used was as follows: 10ml of hot solvent was added to 50mg of sample and heated on a hot plate (not boiling) for 35 minutes. The cooled solutions were reheated on the hot plate for 5 minutes immediately before the chromatography.

The molecular weights are expressed as "polystyrene equivalent".

(Referred to on page 36 of thesis.)

APPENDIX 4: Values Used In Activation Energy Calculations
TABLE A-2: ZERO SHEAR RATE VISCOSITY ESTIMATES

Polymer	Temperature (°C)	'n'value	Shear Rate (sec^{-1})	n_0 estimate (Pa.s)
B90S	270	0.795	10	700
B90S	275	0.979	10	530
B90S	280	0.926	10	360
B90S	285	0.952	10	380
B90S	290	1.0	60	220
EX167	270	0.989	30	1200
EX167	280	0.771	10	600
EX167	270	0.989	30	1200
B90S	270	0.795	10	700
LIN-A	270	0.89	25	190
LIN-B	270	0.865	100	60
LIN-C	270	0.81	100	135
LIN-D	270	0.65	600	57
EX167	280	0.771	10	600
B90S	280	0.926	10	360
LIN-A	280	1.0	25	140
LIN-B	280	0.69	100	20
LIN-C	280	0.77	300	100
LIN-D	280	0.875	600	28.5
BRAN-4	270	0.580	10	4000-5000
BRAN-4	280	0.668	10	2000-3000
BRAN-5	270	0.547	10	4000-5000
BRAN-5	280	0.619	10	1000-3000
BRAN-3	270	0.946	10	1100
BRAN-3	280	0.973	10	1000
BRAN-1	270	0.7	10	760
BRAN-1	280	0.95	10	680
BRAN-2	270	0.96	10	500
BRAN-2	280	0.88	10	480
PETG	170	0.62	10	18000
PETG	200	0.93	10	4900
PETG	220	0.78	10	2500
PETG	240	0.72	10	1400
PETG	260	0.98	10	700
PCTG	240	0.545	30	2900
PCTG	250	0.76	30	1100
PCTG	260	0.761	30	1000
PCCE	230	0.555	30	850
PCCE	245	0.781	50	275
PCCE	260	0.663	100	170

(Referred to on pages 68 and 69 of thesis.)

APPENDIX 5: Diagrams Of Rutherford Heating Element Systems

Old system designed by *Smoker* consisting of three heating elements
wired up parallel with each other.
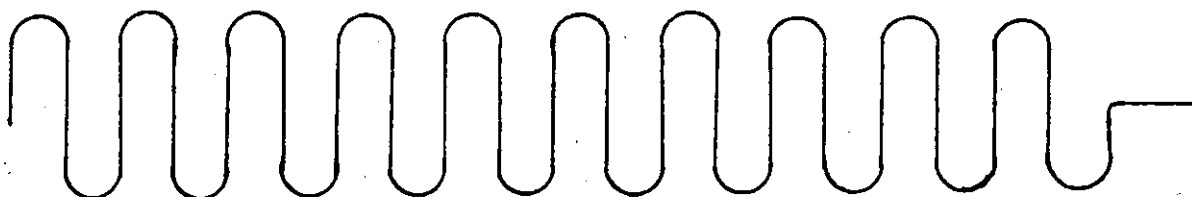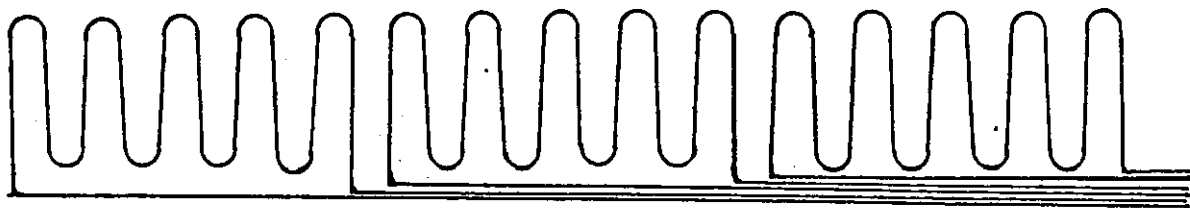
New system, one higher power rated heating element.

(Referred to on page 129 of thesis.)

APPENDIX 6: Diagram Of Temperature Probe Holder

Temperature Probe

Holder

Copper Oil Bath
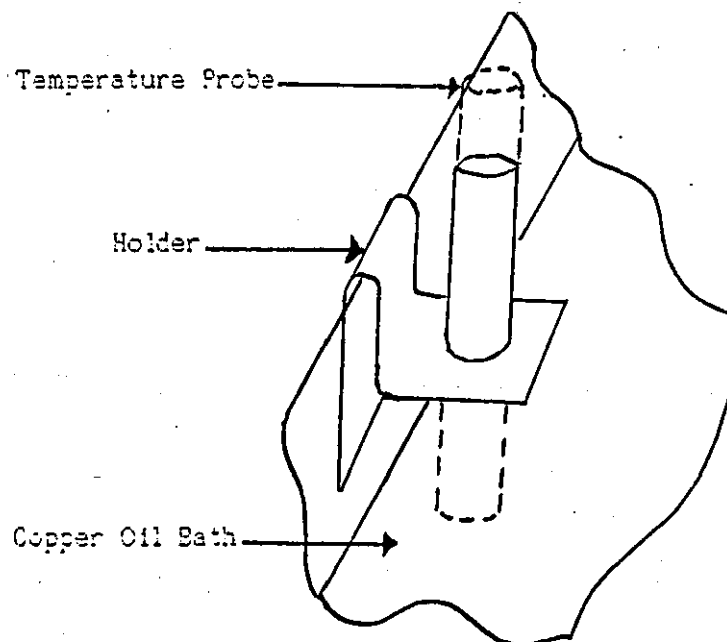
(Referred to on page 130 of thesis.)

APPENDIX 7: Selection Of Heat Transfer Media
Heat Transfer Media
The heat transfer medium was a silicone fluid (ICI F190) which had
a maximum working temperature of 200°C. Two high temperature fluids
were tested for their suitability and the best one was selected, it
is a dimethyl polysiloxane fluid (Dow Corning 210H), which has a
maximum working temperature of 288°C.
Selection of Heat Transfer Medium
Tests of weight loss, gelling behaviour and interaction with the
polymer were carried out on two commercially available fluids. The
two fluids tested were a dimethyl polysiloxane fluid (Dow Corning
210H fluid) and a phenyl methyl polysiloxane fluid (Dow Corning 710
fluid).
Fluid Weight Loss
Samples of the two fluids were heated to 290°C in open and
closed systems for 200 hours. The results are shown below in Table
A-3, the values are quoted as percentage weight loss.

TABLE A-3: PERCENTAGE WEIGHT LOSS OF FLUIDS AT 290°C

Open System	DC 210H	DC 710
50 hours	9.9 %	10.3 %
100 hours	12.7 %	16.8 %
150 hours	16.4 %	21.8 %
200 hours	18.8 %	25.7 %
Closed System		
50 hours	5.7 %	3.5 %
100 hours	7.3 %	3.5 %
150 hours	9.5 %	6.1 %
200 hours	11.7 %	9.0 %

Gelling Behaviour
The viscosity of the fluids as delivered and after 200 hours at
290°C were measured using a Haake RV2 viscometer. The results are
shown below in Table A-4.

TABLE A-4: VISCOSITY OF FLUIDS

Sensor Head MV2 50 scale, DC 210H as delivered:

Speed (rpm)	Deflection (%)	Shear Rate (sec-1)	Viscosity (Pa.s)
36.2	9.5	32.58	0.10946
51.2	14.0	46.08	0.11405
72.4	19.5	65.16	0.11234
90.5	24.5	81.45	0.11292
128.0	34.5	115.20	0.11242
181.0	49.5	162.90	0.11407

Sensor Head SV2 50 scale, DC 210H after 200 hours at 290°C,
Closed System:

Speed (rpm)	Deflection (%)	Shear Rate (sec-1)	Viscosity (Pa.s)
181.0	7.0	161.09	0.14984
256.0	10.0	227.84	0.15134
362.0	14.5	322.18	0.15519
512.0	21.0	455.68	0.15891

Sensor Head SV2 50 scale, DC 210H after 200 hours at 290°C,
Open System:

Speed (rpm)	Deflection (%)	Shear Rate (sec-1)	Viscosity (Pa.s)
181.0	8.0	161.09	0.17124
256.0	12.0	227.84	0.18161
362.0	17.5	322.18	0.18729
512.0	25.0	455.68	0.18918

Sensor Head SV2 50 scale, DC 710 as delivered:

Speed (rpm)	Deflection (%)	Shear Rate (sec-1)	Viscosity (Pa.s)
64.0	9.0	56.96	0.54484
90.5	13.5	80.54	0.57795
128.0	19.5	113.92	0.59024
181.0	28.0	161.09	0.59935
256.0	40.0	227.84	0.60537

Sensor Head SV2 50 scale, DC 710 after 200 hours at 290°C,
Closed System:

Speed (rpm)	Deflection (%)	Shear Rate (sec-1)	Viscosity (Pa.s)
16.0	10.5	14.24	2.54257
22.6	15.0	20.11	2.57150
32.0	22.0	28.48	2.66365
45.2	32.5	40.23	2.78579
64.0	45.5	56.96	2.75445
90.5	65.5	80.55	2.80412

Sensor Head SV2 50 scale, DC 710 after 200 hours at 290°C,
Open System:

Speed (rpm)	Deflection (%)	Shear Rate (sec-1)	Viscosity (Pa.s)
22.6	12.5	20.11	2.14292
32.0	18.0	28.48	2.17935
45.2	26.0	40.23	2.22864
64.0	37.5	56.96	2.27015
90.5	53.5	80.55	2.29039

Interaction with PET

A series of experiments were carried out to investigate any
possible attack on PET by the fluids. The experiments involved were :
- i.   Oil Absorbance
- ii. Retention of Tensile Strength
- iii. Plasticisation
- iv. Attack on Molecular Structure
- v.   Surface Attack

The tests were carried out on injection moulded dumbbell
specimens of a 0.9 I.V. PET material.

Oil Absorbance

The weight of injection moulded PET dumbbell specimens were
measured before and after immersion in the two fluids for 24 hours
at 23°C and 130°C. Dried and undried specimens were tested. Also a
dried specimen was immersed in DC 210H for 21 days at 140°C. The
results are shown below in Table A-5, as percentage weight gain.

TABLE A-5: OIL ABSORBANCE

	DC 210H	DC 710
24 hours immersion		
Undried		
23°C	0.15%	0.64%
130°C	0.06%	0.43%
Dried		
23°C	0.30%	0.53%
130°C	0.20%	0.36%
21 days immersion		
140°C	0.33%	–

Retention of Tensile Properties

The tensile properties of injection moulded PET dumbbell specimens were tested as-moulded and after immersion in the two fluids for 24 hours at 23°C and 150°C. The oil was blotted off rather than driven off by vacuum. The results are shown below in Table A-6, as percentage retention of as-moulded values.

TABLE A-6: RETENTION OF TENSILE PROPERTIES

	DC 210H	DC 710
Immersion at 23°C		
Tensile Strength	85%	86%
Elongation at break	93%	75%
Relative Energy to break	69%	74%
Immersion at 150°C		
Tensile Strength	81%	95%
Elongation at break	71%	65%
Relative Energy to break	48%	73%

Plasticisation

The effect on T_g after 24 hours immersion in the fluids at 23°C and 150°C was measured. A decrease in T_g indicates plasticisation has taken place. The results are shown below in Table A-7.

TABLE A-7: PLASTICISATION OF PET AFTER IMMERSION IN SILICONE FLUIDS

	DC 210H	DC 710
24 hours at 23°C	no change	+2°C
24 hours at 150°C	-7°C	-2°C

Attack on Molecular Structure

A reduction in the intrinsic viscosity(I.V.) of PET after immersion in the silicone fluids is interpreted as a reduction in the molecular chain length due to chemical attack. Values of the reduction in I.V. after immersion in the silicone fluids for 24 hours at 130°C are shown below in Table A-8.

TABLE A-8: REDUCTION IN I.V. AFTER IMMERSION IN SILICONE FLUIDS

	DC 210H	DC 710
As-moulded specimens	-11.65 g/dl	-18.94 g/dl
Dried specimens	-11.22 g/dl	-18.84 g/dl

Surface Attack

Scanning Electron Microscope analysis of the surface of injection moulded PET dumbbells as-moulded and after immersion in the fluids for 24 hours at 130°C, was carried out, signs of etching and blistering were looked for.

Heat Transfer Media Summary

From the results above the DC 210H silicone fluid was selected.

This fluid had the best high temperature lifetime and did not significantly attack the PET samples. However due to the fluid fuming at high temperatures, the rheometer was placed in a fume cupboard.

(Referred to on page 130 of thesis.)

APPENDIX 8: Datalogging Program.

```
5          DIM A(3000) , B(3000)
10         D$= CHR$(4)
20         PRINT D$ ; "BLOAD BUS3.OBJ"
30         POKE 33269,73: CALL 33272
40         HOME
50         INPUT" TIME INTERVAL BETWEEN SAMPLING";TT
60         INPUT" INPUT CHANNEL NO. FOR STRESS"; P1
70         INPUT INPUT CHANNEL NO. FOR LENGTH"; P2
80         P1 = P1+96
90         P2 = P2+96
100        HOME
110        HTAB 12:VTAB 12
120        PRINT"TEST RUNNING"
130        N = N+1
140              FOR I = 1 TO 5
150        POKE 33271,P1: CALL 33448
160        C(I) = PEEK(33013): D(I) = PEEK (33014)
170        C(I) = C(I) - 224
180        IF C(I)<0 THEN E(I) = (C(I)+32)*-1: D(I) = -1 * D(I)
190        IF C(I)>=0 THEN E(I) = C(I)
200        Z(I) = D(I) + 256 * E(I)
210        NEXT I
220        FOR J = 1 TO 5
230        POKE 33271, P2: CALL 33448
240        F(J) = PEEK(33013): G(J) = PEEK(33014)
250        F(J) = F(J) - 224
260        IF F(J) <0 THEN H(J) = (F(J)+32) * -1: G(J) = -1 * G(J)
270        IF F(J) >=0 THEN H(J) = F(J)
280        Y(J) = G(J) + 256 * H(J)
290        NEXT J
300        FOR T = 1 TO 5
310        ZZ = ZZ + Z(T)
320        YY = YY + Y(T)
330        NEXT T
340        A(N) = ZZ/5
350        B(N) = YY/5
360        FOR K = 1 TO (1000*TT): NEXT K
370        T1 = T1 +TT
380        IF A(N-1) - A(N) >1000 THEN 400
390        GOTO 89
400        HOME
410        VTAB 12
420        HTAB 12
430        PRINT "TEST COMPLETE"
```

APPENDIX 9: INJECTION MOULDING CONDITIONS

Conditions set on 55 tonnes Negri Bossi injection moulding machine.

Mould Speeds:	initial close speed	150	(%)
	second close speed	350	(%)
	final close speed	150	(%)
	initial open speed	150	(%)
	second open speed	350	(%)
	final open speed	150	(%)
Mould Pressures:	low close	13	(bar)
	ejection	50	(bar)
	ejection return	25	(bar)
Screw Pressures:	1st injection	140	(bar)
	2nd injection	90	(bar)
	3rd injection	80	(bar)
	4th injection	70	(bar)
	5th injection	60	(bar)
	6th injection	50	(bar)
Mould Strokes:	maximum stroke	750	(%)
	low close	320	(%)
	mould preposition	350	(%)
	fast close	700	(%)
	initial open	500	(%)
	final open	700	(%)
	maximum pressure	999	(%)
Screw Strokes:	2nd injection speed	200	(%)
	3rd injection speed	150	(%)
	4th injection speed	100	(%)
	2nd injection pressure	85	(%)
	shot size	250	(%)
	screw suckback	270	(%)
Timers:	alarm	50	(sec)
	cooling time	35	(sec)
	single cycle restart	0.5	(sec)
	carriage backwards	0.6	(sec)
Hold-on Timer:	hold-on pressure time	6.0	(sec)

APPENDIX 10: Curve Fitting Equations[50]

x, independent variable
y, dependent variable
a, constant
b, constant
c, constant
n, number of data pairs
r, Pearsons Correlation Coefficient

Linear Regression

$$y = a + b.x$$
$$b = \{[n\Sigma xy - \Sigma x\Sigma y] \div [n\Sigma x^2 - (\Sigma x)^2]\}$$
$$a = [y - b.\Sigma x] \div n$$

Polynomial Regression

$$y = a + b.x + c.x^2$$
solve:
$$\Sigma y = n.a + b\Sigma x + c.\Sigma x^2$$
$$\Sigma xy = a.\Sigma x + b.\Sigma x^2 + c.\Sigma x^3$$
$$\Sigma x^2 y = a.\Sigma x^2 + b.\Sigma x^3 + c.\Sigma x^4$$

Pearsons Correlation Coefficient
$$r = (n\Sigma xy - \Sigma x\Sigma y) \div \{[n\Sigma x^2 - (\Sigma x)^2]*[n\Sigma y^2 - (\Sigma y)^2]\}^{\frac{1}{2}}$$

Index of Determination $= r^2$

Standard Deviation S.D. $= \{[\Sigma y^2 - a.\Sigma y - b.\Sigma xy] \div (n-2)\}$

MAT-IN Fit
$$\log(y) = \log(a) - b.\log(x)$$
Linear Transformation Used
$$y = a - b.x^{\frac{1}{2}}$$
Quadratic Fit
$$y = a + b.x + c.x^2$$

APPENDIX 11: Cavity Details in SIMPOL

Area Factor = 1
No. of Impressions = 2
No. of Hot Runner Sections = 0
No. of Cold Runner Sections =7
No. of Cavity Steps = 4

Runner Details

Flow Rate (ml/s)	Initial Diameter (mm)	Final Diameter (mm)	Section Length (mm)	Hot/Cold	Shape Type
40	4.66	6.5	47	C	O
20	6.5	6.5	152	C	D
20	4	5	2	C	T
20	3.65	6.5	2	C	T
20	2.35	8	2	C	T
20	1.7	9.5	2	C	T
20	1.4	11.0	2	C	T

Volume of Cold Runner = 6.6ml

Cavity Details

Flow Rate (ml/s)	Thickness (mm)	Length (mm)	Width (mm)
20	3.25	5	13
20	3.25	25	12.7
20	3.25	189	12.7
20	3.25	190	0

Volume = 21.889ml
Areas: Plan = 47.043
   Projected = 47.043
Flow Ratio = 58
Regrind = 30.2%

APPENDIX 12: Complete Thickness Matrices From Table 7.3

BOTTLE E3

275	31	31	29	29	28	30	29	29
251	33	30	28	28	28	28	29	29
231	28	27	27	28	28	29	28	26
219	28	28	29	31	32	33	28	27
205	29	30	29	28	28	29	30	28
167	30	31	31	31	31	30	32	28
105	27	27	27	25	25	25	27	28
57	23	22	22	22	23	23	24	24

BOTTLE E20

275	30	30	30	30	30	30	30	31
251	30	30	29	29	29	29	30	30
231	28	28	28	29	29	29	28	28
219	28	29	29	30	30	30	29	28
205	30	30	30	29	30	30	30	29
167	32	32	32	32	32	33	32	31
105	28	28	27	27	27	27	27	28
57	23	24	24	24	23	23	23	23

BOTTLE D15

275	30	30	30	28	27	28	28	29
251	32	31	30	28	27	28	28	29
231	28	29	28	28	29	30	28	27
219	27	27	28	30	32	31	30	28
205	28	27	29	30	29	29	29	29
167	30	29	31	32	31	31	31	31
105	27	28	27	25	25	24	26	27
57	24	24	23	22	23	23	23	24

BOTTLE D16

275	23	26	27	27	28	25	24	25
251	29	29	28	28	28	29	29	29
231	26	26	26	26	26	26	26	26
219	26	26	27	26	26	26	26	26
205	30	29	31	31	30	28	28	29
167	30	30	30	30	30	30	29	31
105	26	26	25	24	24	26	26	27
57	22	22	22	22	22	22	22	21

BOTTLE C11

275	16	19	20	19	21	22	17	20
251	27	27	26	25	26	27	28	28
231	25	25	25	26	26	26	25	26
219	25	25	27	28	28	26	25	25
205	27	28	28	28	28	28	27	28
167	28	29	29	29	29	29	28	28
105	26	24	23	22	24	26	26	26
57	24	23	22	22	23	25	25	24

BOTTLE C12
275	23	24	24	23	23	24	23	23
251	27	27	27	27	27	27	27	27
231	25	25	25	25	25	25	25	25
219	25	26	25	25	26	25	25	25
205	28	28	28	28	28	28	28	28
167	28	29	29	29	29	28	28	28
105	25	24	24	24	24	25	25	24
57	23	22	22	23	23	24	23	24

BOTTLE B1
275	26	20	18	18	20	27	27	26
251	26	26	25	25	25	26	26	26
231	24	24	24	24	25	25	24	24
219	24	24	25	25	25	25	24	24
205	27	26	27	27	27	27	27	27
167	27	27	28	28	28	28	27	27
105	24	23	23	23	23	24	24	24
57	23	23	23	22	22	23	24	23

BOTTLE B5
275	32	28	22	20	20	27	30	23
251	24	25	26	26	26	26	25	24
231	25	24	24	24	24	24	25	26
219	27	25	24	23	23	24	27	28
205	26	27	26	26	26	27	27	26
167	28	28	26	26	26	26	29	29
105	22	23	24	25	25	24	23	22
57	22	22	23	24	24	24	22	21

BOTTLE A4
275	16	14	13	4	0	2	17	19
251	24	24	25	26	26	25	25	25
231	23	23	23	23	24	23	23	24
219	26	25	25	25	25	25	25	26
205	25	25	25	25	26	26	25	25
167	24	23	23	24	24	25	26	26
105	22	23	23	23	23	23	23	22
57	25	27	29	29	27	25	24	23

BOTTLE A7
275	191	190	192	189	190	188	191	185
251	27	31	18	21	19	32	23	27
231	24	24	24	24	24	24	24	24
219	34	24	11	11	11	24	24	22
205	16	20	21	20	23	21	19	14
167	25	24	23	23	24	24	24	25
105	22	22	23	23	23	23	23	23
57	23	24	25	26	26	25	25	24